Discovery and characterization of mechanisms that promote the intracellular growth of the pathogen *Francisella tularensis*

Hannah Elizabeth Ledvina

A dissertation

submitted in partial fulfillment of the

requirements for the degree of

Doctor of Philosophy

University of Washington

2020

Reading Committee:

Joseph Mougous, Chair

Joshua Woodward

Lucas Hoffman

Program Authorized to Offer Degree:

Microbiology

University of Washington

Abstract

Discovery and characterization of mechanisms that promote
the intracellular growth of the pathogen *Francisella tularensis*

Hannah Elizabeth Ledvina

Chair of the Supervisory Committee:
Professor, Joseph D. Mougous
Department of Microbiology

The survival of pathogenic intracellular bacteria relies on their ability to establish and maintain a permissive niche. For *Francisella tularensis*, the causative agent of tularemia, this involves both escaping the degradative endocytic pathway and the acquisition of essential nutrients from the host cell once in the cytosol. In this work I investigate mechanisms employed by *F. tularensis* at both stages of intracellular infection. We and others have previously established that escape from endosomes is mediated via the action of a set of effector proteins secreted by the *F. tularensis* subsp. *novicida* pathogenicity island-encoded secretion system. I discovered that a substrate of this secretion system, OpiA, represents a previously undescribed, widespread family of bacterial phosphatidylinositide (PI) 3-kinase enzymes. Through biochemical and cell biology-based assays we were able to demonstrate OpiA is recruited to endocytic membranes and acts on the *Francisella*-containing phagosome to promote bacterial escape into the cytoplasm. Furthermore, I found that the phenotypic consequences of OpiA inactivation are mitigated by arresting endosomal maturation. Once in the cytoplasm, the ability

of *F. tularensis* to grow is dependent upon nutrients derived from the host. Critical amongst these is glutathione (GSH), a tripeptide whose catabolism provides a source of cysteine that *F. tularensis* requires for growth. We performed a highly saturated transposon library screen which uncovered that *F. tularensis* encodes two distinct, yet essential pathways for the utilization of extracellular GSH. Additionally, my data demonstrates a unique role for each of these pathways during the course of infection. Finally, I provide evidence that one of these pathways, the ChaC-pathway, is involved in additional aspect of *F. tularensis* metabolism and stress defense. In total, this work highlights novel mechanisms utilized by *F. tularensis* to both manipulate and exploit host cell pathways to promote bacterial growth.

Table of Contents

List of Figure

Chapter 1

Chapter 2

Chapter 3

Chapter 4

List of Tables

Acknowledgments

The biggest thank you of all goes to my number one support team, my parents, Michael and Jeanne Ledvina. My mom was my first teacher and she instilled in me a thirst for knowledge about of the world around me while providing me with the best role model I could ask for. For helping me stay grounded and for teaching me to cook through the craziness, I have to thank my dad. Their love and support are unwavering and have kept me afloat during graduate school. I also need to thank my husband, Paul Jordan, who joined me on this adventure just four months into graduate school. Paul has been at my side through it all, celebrating every success and mourning every failed experiment. I couldn't ask for a better partner in life.

Dr. V.K. Viswanathan first took a chance on me as a scientist and through his mentorship I discovered my love for microbiology. It was in Dr. Viswanathan's lab I had to honor of working with Dr. John Scott Wilbur who spent countless hours teaching me molecular biology. The support and encouragement of these two outstanding scientists lead me to pursue microbiology as a lifelong career. After I graduated I had the opportunity to work as a research technician in Dr. Jeffery Frelinger's lab. During this time, I worked closely with Dr. Lydia Roberts who taught me countless skills and nurtured my desire to take a more active role. To this day Lydia inspires me to pursue challenging scientific questions.

I consider myself exceptionally lucky to have worked in the Mougous Lab. The fun, supportive and nurturing environment I found myself in everyday was due in large to my fantastic colleagues. I want to thank Kaitlyn LaCourse, Marcos de Moraes, See-Yeun Ting, Brook Peterson, Aria Eshraghi, Dustin Bosche, Benjamin Ross, Marlen Adler, Daniel McLeod, Katherine Kelly, Rachel Kim, Fo Sheng Hsu and Beth Shen. All of you embraced me into your lives and families and for that I am endlessly grateful. I especially value the friendship, advice

and support of Kaitlyn LaCourse, Marcos de Moraes, Aria Eshraghi and Brook Peterson. I am also grateful to two wonderful women, Tenaya Tresko and Catherine Tower, undergraduates who worked with me for several years. The faith you placed in me along with your hard work and dedication mean the world to me.

My work would have been impossible without the help of incredible collaborators. A special thank you to Dr. Jean Celli who taught me immunofluorescence and triggered my interest in host cell biology. I'd also like to thank Dr. Simon Dove and Dr. Kathryn Ramsey for including me in their exciting work.

I would like to thank the entire UW Microbiology department for providing such a collaborative and supportive environment. In particular, I want to thank all the members of the Woodward Lab for all of their help throughout my graduate work. This experience would not have been the same without the incredible women that were my classmates and support network, Hannah Tabakh, Erin Garcia de Jesus, and Arianna Samadapour. A special thanks to Hannah Tabakh (aka "other Hannah") for being there through all the ups and downs.

I immensely value the advice and support I received from my thesis committee members, Peter Greenberg, Lucas Hoffman, Joshua Woodward, Jessica Hammerman and Michelle Reniere. I would especially like to thank the members of my reading committee, Joshua Woodward and Lucas Hoffman.

Finally, an endless thank you to my graduate advisor Joseph Mougous. When I entered graduate school, I was an overexcited, eager to please but slow to question student. Joseph's mentorship has helped shape me into a critical, careful (although likely still overexcited) scientist. He was by my side trouble shooting every breakthrough discovery we had, demonstrating the care and rigor needed to perform the perfect experiment. I cannot thank him

enough for his dedication to his trainees and pursuit of exciting, novel science. I want to thank Joseph for his support outside of work. I have greatly enjoyed being a part of this amazing lab and getting to watch the succuss and exciting discoveries made throughout the years.

Chapter 1: The mechanisms underlying the intracellular lifecycle of *Francisella tularensis*

1.1 Introduction

Francisella tularensis is a Gram-negative bacterium and the etiological agent of the zoonotic disease tularemia. This intracellular pathogen is highly infectious (LD^{50}<10 CFU for certain species) and is capable of causing disease in a large variety of mammals and arthropods [1]. Humans can acquire *F. tularensis* through numerous routes, including direct contact with infected animals or arthropods, ingestion of contaminated substances, and inhalation of aerosolized bacteria. Regardless of the route of infection, the bacteria can disseminate throughout the body, and if left untreated pneumonic tularemia can develop – the most severe form of the disease [2]. The low infectious dose, numerous infectious routes, and ability to cause a life-threatening disease has earned *F. tularensis* the designation of a Category A select Agent by the United States Centers for Infectious Disease Control [3].

To date, four subspecies of *F. tularensis* are recognized: *holarctica (Fth), mediasiatica (Ftm), novicida (Ftn), tularensis (Ftt)* [4]. These organisms differ in host range, geographical origin, natural reservoir and virulence in humans. *F. tularensis* subsp *tularensis* is highly pathogenic to humans and is primarily found in North America, whereas subsp *holarctica* causes a less severe yet similar disease and is located throughout Europe. *F. tularensis* subsp *novicida* is typically avirulent in humans, however, it robustly infects and causes disease in mice [2, 4]. Due to the high degree of sequence conservation across the genome (98%), both *Fth* and *Ftn* are commonly used models for studying the more pathogenic subspecies. Specifically, *Fth* strain LVS is a common surrogate for the *Ftt*. LVS is an attenuated derivative of *Fth* that was developed by the former Soviet Union as a vaccine that was not licensed for use in the United States [3].

Upon entry into a host, *F. tularensis* invades cells without observable extracellular replication [5]. While *F. tularensis* is capable of replicating in a wide range of cell types, phagocytic cells, specifically macrophages, are believed to be the primary mediator of disease [6, 7]. Regardless of the cell type, upon entry into host cells *F. tularensis* initially resides within the phagosomal pathways in a membrane-bound vesicle termed the *Francisella* containing phagosome (FCP). However, unlike some other intracellular

pathogens, *F. tularensis* is unable to grow in this compartment and instead breaks into the cytoplasm where proliferation occurs (Fig. 1.1) [5]. As intracellular growth is essential for infection, much work has been carried out to define the intracellular lifecycle of this pathogen, as well as to discover and characterize the virulence factors required. In this review, we will focus on the key steps of the *F. tularensis* intracellular lifecycle, with an emphasis on the molecular mechanisms employed by the organism to promote disease. As macrophages are believed to be the primarily cell types infected, we will primarily discuss studies using this model; we apologize to our colleagues whose work we were unable to highlight.

1.2 Adherence and uptake into macrophages

F. tularensis internalization is mediated through pseudopod loops, as opposed to traditional receptor mediated phagocytosis [8] (Fig. 1.1). These loops result in a spacious compartment in which the bacteria reside prior to uptake. The receptor(s) utilized for adherence and uptake is dependent on the state of the bacteria upon contact with the macrophage [9]. These differences also have a profound impact on the trafficking of the FCP, the dynamics of bacterial growth intracellularly, and the engagement of downstream signaling pathways. Here we will discuss what is known regarding how *F. tularensis* adheres to and is internalized by macrophages (summarized in Fig. 1.2).

When *F. tularensis* is opsonized in fresh serum prior to infection, adherence and uptake is primarily mediated by the interaction of iC3b on the bacterial surface with the CR3 and CR4 receptors displayed by macrophages [10]. These results have been recapitulated by multiple groups and uptake via this pathway is known to result in immune suppression. Under opsonizing conditions, surface-exposed Ef-Tu on *F. tularensis* has been demonstrated to promote uptake by binding the C-termini of surface-exposed nucleolin (S-EN) on host macrophages [11]. Authors of this study demonstrate blocking the binding sites of both Ef-Tu and CR3 dramatically inhibits bacterial uptake, suggesting these two mechanisms work synergistically to promote uptake. A small but significant role for the uptake of

opsonized bacteria has also been attributed to the mannose receptor (MR); however, as discussed below, this is considered the primary receptor for non-opsonized bacteria [8]. Finally, adherence of opsonized bacteria to macrophages is partially mediated by scavenger receptor A (SR-A) binding to scavenger protein A(SP-A) [12]. In total, internalization of opsonized bacteria appears to occur primarily via CR3 with S-EN and MR playing secondary roles.

Due to contradictory results, the contribution of Fcγ receptor in uptake of fresh serum opsonized bacteria is unclear [12]. One study defined a critical role for this receptor and suggested it works cooperatively with CR3 to mediate uptake, whereas others found no role for the receptor in the uptake of *F. tularensis* [12]. Conflicting findings on the effects of heat-treating the serum suggest this discrepancy may be a result of the serum sources utilized. This is supported by the fact that Geier and Celli demonstrated that uptake of antibody-opsonization *F. tularensis* occurred via Fcγ receptor and that uptake via this route results in unique downstream events (see below) [9]. Therefore, this mechanism of uptake likely occurs under conditions of antibody opsonization; i.e. secondary infection.

Adherence and uptake of non-opsonized *F. tularensis* is primarily through MR binding [13]. The bacterial component responsible for engaging MR remains undefined. While SR-A has also been demonstrated to contribute to the uptake of non-opsonized bacteria, entry through this mechanism results in less bacterial growth when compared to uptake via MR [9]. Optimal adherence to macrophages is dependent on the Type IV Pili; however, this structure played no role in the internalization of the bacteria [14].

Uptake mechanism has significant downstream consequences on the trafficking of bacteria. *F. tularensis* that enter via the MR route are exposed to rapid acidification of the FCP (15-20min), and undergo rapid escape into the cytoplasm (30-60min) [9]. In contrast, uptake of serum-opsonized bacteria results in delayed FCP acidification and considerably slower escape (2-4hrs). These differences further manifest in differential growth rates in the cytoplasm, with non-opsonized *F. tularensis* displaying significantly higher bacterial loads [9]. Antibody-opsonization of the bacteria also results in acidification

and escape delay, but also leads to increased reactive oxygen species within the FCP. The elevated levels of ROS results in significantly reduced rates of escape and cytoplasmic proliferation by *F. tularensis* [9]. These results suggest that uptake via MR is more permissive for *F. tularensis*.

Beyond the receptors necessary for uptake, studies have assessed what other cellular components are necessary for uptake. Caveolin-1-enriched cholesterol containing lipid domains are targeted by *F. tularensis* during entry and are therefore required for optimal uptake [15]. Using a panel of chemical inhibitors, authors demonstrated that optimal internalization of the bacteria requires GPI-anchored proteins and tyrosine kinases. However, the PI3K pathway, which has been shown to play an essential role in the uptake of other intracellular pathogens, is dispensable. Studies have also demonstrated a critical role of the Syk-Erk pathway in uptake of non-opsonized bacteria [16]. The mechanisms underlying the contribution of each of these pathways remains to be determined.

The discrepancy in uptake mechanism and resulting downstream signaling events raises the question, are the bacteria likely to be opsonized upon encounter with macrophages? *F. tularensis* employs multiple mechanisms to avoid opsonization via complement or antibodies [16, 17]. Therefore, it is tempting to speculate that entry via MR is the physiological relevant pathway. However, studies indicating that entry via CR3/4 results in suppression of innate immune pathways, along with the diverse uptake mechanisms utilized by nonphagocytic cells, suggests that *F. tularensis* has evolved multiple mechanisms to facilitate growth following uptake through diverse pathways [18].

1.3 Survival within and escape from the phagosomal system

Upon uptake into macrophages, *F. tularensis* briefly resides within the FCP. These vesicles initially resemble early endosomes, followed by maturation into late endosomal-like vesicles. However, prior to fusion with lysosomes – the normal fate of late phagosomes – *F. tularensis* is capable of escaping out of this degradative compartment to access the host cytoplasm [19-21]. It is within the cytoplasm that *Ft* acquires the nutrients needed to proliferate to high levels (Fig. 1.1). If escape from the FCP is blocked, the bacteria are unable to proliferate, and instead are killed within the phagosomal system [22]. The major

virulence factor responsible for mediating escape is the type VI secretion system subtype ii (T6SS^{ii}) encoded by the *Francisella* pathogenicity island (FPI) [23]. Additionally, several factors have been identified as critical for surviving within the phagosomal compartment [24-27] [28]. In the following sections, we will discuss what is known about the molecular mechanisms underlying these processes and highlight areas that remain to be investigated (Summarized in Fig. 1.3).

1.3.1. *The* Francisella *pathogenicity island*

The FPI is found throughout the *Francisella* genus as well as in closely related bacteria. This island is composed of 17 (*pdpA-C* and *iglA-O*) genes that have distinctly lower G/C-content when compared to the rest of the *F. tularensis* genome, suggesting acquisition through horizontal gene transfer (Fig 1.3A) [23, 29]. The FPI has been recognized as key virulence factors since the late 1990's when the FPI-encoded protein IglC was first found to play a critical role during infection [30, 31]. Over the last two decades, research has revealed that this genetic island is essential for mediating escape from the FCP and thus plays an important role in facilitating the intracellular lifecycle of *F. tularensis* [21, 23, 32]. Through the efforts of numerous groups, we now recognize that the FPI encodes a T6SS^{ii} that delivers a set of effectors proteins into the host cell [32-35]. These effectors not only mediate escape into the cytoplasm but also contribute to the composition and therefore the trafficking of the FCP [36, 37]. Interestingly, this island is found in two identical copies within the genome of many *Francisella* species (*Ftt, Fth, Ftm*), but the consequence of apparent the duplication is unknown. Furthermore, a related but divergent island can be found on the genomes of those species only encoding for a single FPI (*Ftn*) [38].

Based on phylogenetic analyses, three subtypes of the T6SS have been described. Subtypes i and ii are encoded by a wide range of Proteobacteria and Bacteroidetes, respectively [34]. These two systems primarily act to mediate contact-dependent interbacterial antagonism by delivering toxic proteins, called effectors, directly into neighboring bacterial cells [39]. On the contrary, the T6SS^{ii} encoded by *Francisella* has only been found to target eukaryotic host cells (i.e. macrophages and amoeba), suggesting this subtype of the T6SS evolved to mediate interactions specifically with Eukaryotes. Sequence

similarity between the subtypes is low, with only seven and the thirteen core T6SS genes showing significant levels of homology (<40%) [22]. Despite high degrees of sequences divergence, structural studies have revealed a high degree of functional similarity between the systems. Clemens et al recently published an extensive overview of the T6SS^{ii} structure including a detailed comparison with the T6SS^{i} and therefore we will instead focus on the advances in uncovering the proteins delivered by this system and the characterization of how they impact the intracellular life cycle [8].

Work within the T6SS field has revealed that along with the effector proteins, several essential structure components are also released during secretion. In particular, the highly conserved tube protein, Hcp (IglC in *F. tularensis*) and the tip protein, VgrG, are known to be released extracellularly post apparatus contraction [40]. Consistent with this, numerous studies have identified both IglC and VgrG as being secreted by the T6SS^{ii} [22, 41, 42]. Identification of proteins secreted by this system that act solely as effectors was initially limited by the inability to activate the system *in vitro.* Researches therefore had to rely on intracellular studies and while these experiments can be advantageous as they allow for *in vivo* measurements, they are limited to candidate substrates due to the need of engineered genetic fusion [43, 44]. This approach has been highly successful for the identification of effectors delivered by type 3 and type 4 secretion systems, however, genetic and structural studies of the T6SS suggest that large protein fusions to effectors are not tolerated during export. This technical limitation likely underlies the discrepancy and inconsistency in reported substrates of the T6SS^{ii} when genetic fusions were used [43, 44].

To overcome the limitation of studying the T6SS^{ii} *in vitro*, Clemens *et al.* performed a fluorescence-based screen to look for environmental conditions that induce T6SS^{ii} formation in *Ftn* [41]. Using genetic fusions of GFP to the proteins IglA and IglB which are components of the secretion appartatus, authors were able to demonstrate that growth in the presence of 5% potassium chloride (KCl) and growth under a coverslip induced GFP foci formation indicative of apparatus assembly. Further studies using phosphoproteomics revealed that phosphorylation of the structural component IglB underlies the activation of the T6SS^{ii} when grown in the presence of 5% KCl. Using these growth

conditions authors confirmed that VgrG and IglC are secreted in a T6SS^{ii} -dependent manner as predicted from work on other T6SSs.

Our lab took advantage of the then newly-described *in vitro* conditions to perform an unbiased screen for T6SS^{ii} substrates in *Ftn* [22]. The use of *Ftn* was critical, as not only was this strain used in the Clemens et al study, but *Ftn* encodes a single copy of the FPI simplifying downstream analysis. By comparing the extracellular proteome of wild-type and Δ*dotU* (an essential structural component) cultures, we identified eight proteins that were secreted by the T6SS^{ii}, including the structural proteins IglC and VgrG. Our screen identified three other protein encoded within the FPI, PdpA, PdpC, and PdpD. Unexpectedly, the other secreted proteins were not encoded with the in the FPI, FTN_0131, FTN_1069 and FTN_1071 and thus we named them outside the pathogenicity island A (OpiA), OpiB.1, and OpiB.3 respectively. Further structural, *in vitro* and *in vivo* studies revealed PdpA it part of the secretion apparatus, whereas PdpC, PdpD, OpiA and OpiB act solely as effector proteins. Deletion of all the genes encoding effector proteins (*pdpC, pdpD, opiA, opiB.1-3*) rendered the bacteria incapable of phagosomal escape [22] (Fig 1.3A, B). This was the first demonstration that an intact secretion system is not sufficient to mediate escape and instead effector translocation is essential for this process.

PdpA and VgrG are essential for secretion and it therefore complicating interpretations of the role these proteins upon play upon delivery. While the secreted structural protein IglC/Hcp has never been demonstrated to act within the target cells, VgrG proteins from several bacteria have been demonstrated to act as effector proteins [45]. In these cases, the VgrG protein contains a clear C-terminal domain which mediates the effector activity and the VgrG domain plays a structural role that essential for delivery. In *Francisella*, VgrG is markedly truncated when compared to canonical VgrG proteins, and no apparent effector domain can be detected [22]. PdpA interacts with VgrG seemingly compensating for the structural domains that are missing from the *F. tularensis* VgrG [22, 46]. It therefore remains to be determined if VgrG and PdpA play both a structural and effector role during the *F. tularensis* lifecycle, however evidence suggests they act solely as structural components.

The classification of PdpC and PdpD as effectors is consistent with the previous phenotypes attributed to these proteins. Multiple groups have demonstrated that PdpC is required for optimal proliferation using both intracellular growth assays as well as mice infections [22, 37, 47-53]. However, the defect of a Δ*pdpC* was often less severe than that of an *iglC* or *pdpA* mutant strain, which we can now know inactivates the secretion system. In-line with these observations, studies looking at the intracellular localization of the bacteria via immunofluorescence, find that maximal escape from phagosomes requires PdpC, but again this is an intermediate phenotype and a proportion of the bacteria still access the cytoplasm [22, 37]. Less work has been done on PdpD, however genetic screens have revealed that PdpD is non-essential for growth in insects (insect cells and in *Drosophila melanogaster*) yet is required for full virulence in mice [49, 52, 54, 55]. Again, consistent with the classification of PdpD as an effector, the defect in mice is intermediate. The mechanism underlying the contribution of these proteins has yet to be revealed.

The identification of OpiA and OpiB as T6SS^{ii} substrates was unexpected, however substrates of the other T6SSs are often encoded at distal sites from the genes encoding the apparatus. Supporting our classification of these proteins as effector, both the *opiA* and *opiB* genes have been shown to be coregulated with the FPI, by the MglA-SspA master virulence regulator [56]. Additionally, single deletions of the genes encoding these proteins had no impact on intracellular growth, similar to what has been observed for PdpD [22, 37]. OpiB-proteins in *Ftn* are composed of N-terminal cysteine protease domains and C-terminal ankyrin domains. The protease domain, which belongs to the CA clan of cysteine proteases, is conserved in *Francisella* orthologs (61%) and belongs to a previously unrecognized branch of the C58-family [22, 57]. The C58-family includes several other secreted virulence factors suggesting the C58-family of cysteine protease domains is evolutionarily plastic and substrate predication is likely challenging. Ankyrin domains are abundant in eukaryotic cells and typically mediate protein-protein interactions. These domains are less common in bacteria, however when present, they are often associated with proteins known to be secreted by intracellular pathogens and symbionts [58]. It is tempting to speculate that these domains aid in substrate targeting, however this has yet to be determined.

Follow-up studies on OpiA revealed that this effector is the first member of a new family of bacteria proteins, known as the OpiA-family proteins (OFPs) [37]. OFPs possess two conserved motifs and are enriched in host-associate bacteria (ie *Rickettsia*, *Legionella*). These motifs are also found with similar spacing in a subset of the eukaryotic phosphoinositide kinases (PIK) and indeed *in vitro* analysis of OpiA demonstrated that OFPs constitute a novel family of bacterial PI3 kinases (PI3K) that specifically act on phosphoinositol (PI) to generate PI(3)P. The product of OpiA is naturally enriched on the cytoplasmic membrane of early endosomes and has been shown to be critical for membrane trafficking. We found that OpiA generates PI(3)P intracellularly specifically on early and late endosomes. Moreover, prolonged OpiA-dependent PI(3)P existence on the FCP was observed during infection of primary macrophages, in-line with our observation that OpiA can act on late endosomes, where PI(3)P is not typically found. This suggests that OpiA is secreted into the cytoplasm by the T6SS^{ii} during the late phagosomal stage where the enzymes contributes PI(3)P production [37]. Studies in endosomal trafficking have demonstrated that removal of PI(3)P is essential for vesicle maturation and fusion with lysosomes [59, 60]. Consistent with this, we found that the activity of OpiA leads to delayed phagosomal maturation which results in enhanced escape into the cytoplasm [37].

Many of the phenotypes (ie intracellular growth, phagosomal escape) for OpiA were only revealed in a genetic background lacking PdpC [37]. However, as demonstrated extensively in *Legionella*, effectors proteins are often functionally redundant or mask each other's functions [61]. It is important to note that PdpC and OpiA are present on the genome of most *Francisella* spp. and therefore both likely contribute to the fitness of the bacteria. As noted above, PdpC is known to contribute to phagosomal escape and thus is required for full virulence in a mouse model. PdpC is a large, likely multidomain protein that is only found within the *Francisella* genus and the mechanism underlying the contribution of this effector remains unclear.

Beyond PdpC, PdpD, OpiA, and OpiB two other FPI-encoded proteins have been proposed to be secreted and act as effector proteins [42, 52]. These proteins may have been missed in our secretomes analysis due to the stringent cutoff we utilized. One study, again utilizing 5% KCl, investigated the role of

the FPI encoded protein, IglG during secretion. They found this protein behaves similarly to VgrG in that it is secreted yet plays an essential structural role. The authors go on to demonstrate that IglG interacts with IglF, another FPI-encoded protein, and they hypothesize that IglG acts as a linker between IglF and VgrG to mediate the delivery of IglF [42]. However, it remains unclear if IglF is secreted, and if it is, what role it plays during infection. PdpE has also been shown to be secreted, yet in this case the phenotypes attributable to this protein are consistent with the assignment as an effector. This protein was found to be dispensable for full virulence in mice, and several reports demonstrate PdpE plays no role in phagosomal escape [52]. These results are reminiscent of OpiA, which only displayed phenotypes in a background lacking PdpC. It would therefore be interesting to test combinatorial mutants for the predicted effector proteins.

While it has been demonstrated that PdpC and OpiA contribute to phagosomal escape, it remains unknown if the other effectors also act at this stage of infection (Fig 1.3B). It also remains unclear if any of these proteins have a role once the bacteria access the cytoplasm due to inconsistent findings by different groups. Microinjection of *F. tularensis* and mutant strains into the cytoplasm of macrophages suggest there may be a role for certain FPI-encoded proteins in cytoplasmic growth, however these results are inconsistent with our current understanding of the T6SS^{ii} [62]. Biophotonic laser-assisted delivery of the bacteria into the cytoplasm, found that IglC is required for the cytoplasmic stage of growth, suggesting the entire apparatus is needed [63]. In contrast, experiments using a T6SS-inducible strain found that the secretion system is dispensable for cytoplasmic growth [64]. As diverse methods have yielded inconsistent results, it remains unclear what role, if any, the T6SS^{ii} and the secreted effectors play during cytoplasmic growth.

1.3.2. *The* Francisella *containing phagosome*

Vesicles within the phagosomal pathway undergo significant changes during the course of maturation, both in the membrane composition and proteins recruited to this organelle. These changes mediate interactions with other vesicles, such as endosomes and lysosomes, and allow for the containment

of the highly acidic and degradative molecules accumulated during development [65]. Maturation of a phagosome is often broken into three steps – early, late, and phagolysosomes. Upon uptake and membrane closure, the vesicle is referred to as an early phagosome which is characterized by high PI(3)P content, the presence of early endosomal antigen 1(EEA-1), and recruitment of the V-ATPase complex. Through the activity of numerous enzymes as well as fusion with other vesicles, these compartments mature into late phagosomes, which have low levels of PI(3)P, and are characterized by the presence of LAMP1/ 2 and Rab7 [66]. V-ATPase is continuously recruited and active thereby acidifying the compartment throughout the maturation process. Additionally, at late phagosomal stages, hydrolases and NADPH oxidase are recruited making the internal compartment toxic. The final step of maturation is fusion with lysosomes, forming phagolysosomes, where cathepsins, proteases, lysozymes, and lipases act to degrade the contents of the vesicle [67].

The FCP undergoes many hallmarks of phagosomal maturation, particularly at the early stages (Fig 1.3B). In order to characterize these changes, numerous investigators have utilized immunofluorescence to characterize the composition of the FCP at various times post-infection [68] [8, 9] [37]. From this work it has become clear that initially upon uptake, *F. tularensis* colocalizes with EEA-1 and PI(3)P, both of which are known to be enriched on early phagosomes [37, 68] [9]. Rapidly (<15min) there is a loss of EEA-1 and acquisition of LAMP-1, LAMP-2 and Rab7, typical of maturation into late endosomes [9, 68]. However, work on the T6SS^{ii} effector OpiA, demonstrates that PI(3)P is retained on the FCP when they have features of late endosomes, suggesting active modulation of phagosomal maturation at this stage of infection [37]. Cathepsin D and other lysosomal tracers have not been found to colocalize with *F. tularensis*, demonstrating that fusion with lysosomes is limited [9, 68]. Whether the bacteria are simply escaping prior to fusion, or if active inhibition of lysosomal recruitment is occurring, remains unclear.

A major feature of the phagosomal compartment is the rapid acidification of the vesicles due to the recruitment of v-ATPase [69]. v-ATPase has been shown to colocalize with the FCP at early stages of phagosomal maturation, however there are contradictory results on the role this process plays in the *F.*

tularensis lifecycle [70]. One group reported that acidification of the FCP is essential for optimal escape into the cytoplasm whereas others published no role for this process in mediating escape [70]. These differences may be due to the opsonization state of the bacteria used in the experiment as they also observed differential maturation timing. As described in the previous section, the opsonization state of *F. tularensis* prior to infection dramatically alters the downstream infection events [9].

The redox burst within phagosomes is in part mediated by a multiprotein complex called NADPH oxidase which releases reactive oxygen molecules such as superoxide into the lumen of vesicles [71]. It has long been recognized that infection of phagocytic cells with *F. tularensis* does not elicit the strong oxidative burst that is typical of these cell types [72]. Mutational and biochemical assays have revealed that *F. tularensis* employs six acid phosphatases, *acpABCD* and *hapAB*, that act in parallel during infection to directly block NADPH oxidase assembly [27]. Investigators demonstrated that one of these proteins, AcpA, can dephosphorylate essential components of NADPH oxidase. Phosphorylation is an essential step in assembly and thus the Acp enzymes directly blocks the function of this important host complex [73]. It is important to note that it remains unclear how many of the Acp proteins are able to access their substrates as none of the proteins have consistently been reported as secreted. Therefore, the full mechanism underlying this phenomenon remains unclear [5].

F. tularensis also encodes several enzymes which directly detoxify reactive molecules encountered within the FCP. These include *katG* which encodes for a secreted catalase, and the enzymes *sodC* and *sodB* which encode superoxide dismutases of two different families [24] [74] [75] [76]. Additionally, several other genes have been identified as being essential for survival in the phagosome, however the precise mechanism underlying their role remains unclear. For example, GadC is a glutamate transporter which participates in ROS-defense via an unknown mechanism [28]. Finally, the components of the multidrug efflux pumps *erm45* and *silC* have been found to be critical for survival [77 , 78] . In summary, *F. tularensis* encodes numerous, redundant mechanisms to ensure survival within the phagosomal system.

1.4 Cytoplasmic growth

Upon entry into host cell cytoplasm, *F. tularensis* is capable of replicating up to 1000-fold prior induction of programmed cell death pathways and bacterial spread. This remarkable feat involves coordinated efforts to scavenge and utilize host cell metabolites while avoiding premature host cell death or immune detection. Studies have suggested that during intracellular growth nutrient acquisition from the host is more energy-efficient than *de novo* biosynthesis of these molecules [79]. Therefore, numerous pathogens have acquired sophisticated mechanism for nutrient acquisition [80] [81] [79, 82]. *F. tularensis* is no exception, and in fact genome analysis reveals that numerous biosynthesis pathways are non-functional, rendering *F. tularensis* auxotrophic for these metabolites (ie cysteine, asparagine). Through transposon-based mutagenesis screens performed by numerous groups, several metabolic pathways and nutrient uptake systems have been found to be essential for intracellular growth or virulence [83-90]. In particular, amino acid acquisition and assimilation into numerous downstream metabolic pathways (i.e., gluconeogenesis, the TCA cycle, and ROS defense) have been shown to play a critical role during infection [28, 91-94]. In the following section, we will discuss which metabolic pathways are critical during infection as well as the pathways/proteins that are critical for nutrient acquisition.

1.4.1. *Iron scavenging and uptake*

Iron is a limiting yet essential nutrient in nature and is therefore an important component of host-pathogen interactions. As part of the innate immune response, iron is decreased extracellularly and within macrophages, iron is initially concentrated within the phagosomal compartment where it contributes to the damaging Fenton reactions. After this initial burst, iron levels are lowered intracellularly to restrict pathogen growth. Consistent with this, studies using mammalian hosts have demonstrated that the concentration of iron decreases in both the plasma and extracellular fluids during *F. tularensis* infection [95]. Additionally, Nramp, which modulates phagosomal levels of iron, has been shown to play an important role during in *F. tularensis* growth [96, 97]. To combat these immune defenses, *F. tularensis*

has evolved diverse mechanisms to obtain iron from the host and to date, two iron acquisition pathways have been described in *F. tularensis* (Summarized in Fig 1.4).

Ferric Iron Uptake: the Siderophore Pathway. Ferric iron (Fe^{3+}) is the more abundant form of this metal, however, as it is nonsoluble and highly reactive, Fe^{3+} is kept in complex with host proteins. In order to scavenge Fe^{3+}, Gram-negative bacteria commonly use siderophores which are secreted proteins that chelate ferric iron from the surrounding environment and are then taken back up into cells through a dedicated uptake pathway [98]. The fsl operon of *F. tularensis* mediates biosynthesis, secretion and uptake of the siderophore rhizoferrin that mediates Fe^{3+} acquisition for this pathogen [99]. All genes within the operon have been attributed to a role in this pathway except for *fslF*, which remains unlinked to iron acquisition and will not be discussed further.

fslA and *fslC* were initially hypothesized to generate rhizoferrin due to their homology with related biosynthetic genes and indeed, strains lacking either of these genes fail to produce siderophores, as measured by a CAS activity assay [99, 100]. More recently, biochemical studies utilizing radiolabeled substrates confirmed that FslA and FslC indeed are the enzymes responsible for generation of rhizoferrin from citrate and ornithine [101]. *fslB* and *fslD* are required for optimal proliferation in limited Fe^{3+} conditions and are predicted to encode for inner membrane transporters [102, 103]. Optimal extracellular siderophore concentrations are reliant on FslB, thus this protein is predicted to transport rhizoferrin from the cytoplasm to the periplasm [103]. On the other hand, FslD is dispensable for siderophore production and essential for uptake of radiolabeled iron, suggesting this protein acts to deliver iron-bound rhizoferrin to the cytoplasm [102]. Finally, *fslE* has been shown to be necessary for siderophore-mediated uptake of Fe^{3+} consistent with the hypothesis that FslE is a rhizoferrin receptor/transporter [104]. This is further supported by the structural similarities between FslE and siderophore receptors in other Gram-negative bacteria as well as FslE being identified in the outer membrane fraction of Schu S4 and LVS [105].

In most Gram-negative bacteria, import of siderophores into the periplasm by receptor proteins requires energy derived from the proton motive force (PMF) [98]. This energy is transduced across the

periplasm by the TonB complex [98]. The *F. tularensis* genome does not encode homologs of the TonB complex, however experiments utilizing radiolabeled Fe^{3+} have shown that iron uptake is dependent on energy from the PMF [104] [106]. It therefore remains unclear what powers acquisition of rhizoferrin by *F. tularensis*. Interestingly, *Legionella*, which also produces rhizoferrin, is similarly lacking a *tonB* homolog suggesting uptake of this siderophore may be mediate through a previously unrecognize mechanism [98].

Ferrous Iron Uptake: the Feo Pathway. While less abundant in nature, ferrous iron (Fe^{2+}) can enter Gram-negative periplasms through diffusion and non-specific porin proteins. Transport of this molecule to the cytoplasm is mediated by the FeoA/B complex which localizes to the inner membrane. This complex is highly conserved throughout Gram-negative bacteria and, consistent with the predicted role of this pathway, a Δ*feoB* mutant of *F. tularensis* is unable to utilize extracellular Fe^{2+} [100] [107] [108]. Under certain conditions, active uptake of Fe^{2+} into the periplasm can be critical for survival and therefore, *F. tularensis* encodes a predicted energy dependent Fe^{2+} transporter, FupA [102] . This outer membrane protein shares a high degree of homology with FslE and is therefore thought to be function in a similar manner. ^{55}Fe uptake assays demonstrate that maximal Fe^{2+} acquisition is dependent on FupA and therefore it has been hypothesized that under limiting ferrous iron conditions, FupA transports Fe^{2+} into the periplasm where FeoA/B then can transport the iron to the cytoplasm [104].

The biochemical mechanism behind FupA mediated transport remains unclear as does the precise role of this protein. Due to the high homology with FslE, and the fact that FslE transports a small molecule bound to iron, it is unclear how FupA transports Fe^{2+}, which is typically not in complex with other molecules. Complicating interpretation of the role of FupA is the fact that in LVS, but not other *Fth* strains, *fupA* and *fupB* contain large deletions and have been shown to produce a fusion protein [109]. This fusion protein is proposed to act as the siderophore receptor in LVS as FslE but not FupA/B was shown to be required for siderophore uptake [109] How this fusion protein changes substrate specificity is unclear, especially as *fupB* has been shows to be dispensable for iron acquisition in other species of *F.*

tularensis. In *Ftn*, FupA is hypothesized to play a role in membrane stability with a strain lacking *fupA* showing enrichment of putative cytosolic, periplasmic and membrane proteins into the culture supernatant [110]. Consistent with this, author found that a Δ*fupA* mutant was more sensitive to polymyxin B (PMB) [110]. Finally, it has been observed that deletion of *fupA* in SchuS4 results in upregulation of the *fsl* operon even under conditions of high iron [111]. It therefore likely that the full function of FupA has yet to be uncovered.

The two pathways for iron uptake act in parallel, and often phenotypes are only observed when both uptake mechanisms are disrupted. Although a great deal of work has been done to identify the proteins involved in both pathways, many things are still unknown about the mechanisms for both pathways. It currently remains unclear how the rhizoferrin is transported from the periplasm to the extracellular environment. As stated previously, the *F. tularensis* genome does not encode a TonB homolog, so it remains unclear how the PMF is coupled to ferric iron acquisition. Additionally, little work has been done to biochemically characterize the proteins involved in *F. tularensis* and the most functions have been proposed based off homology with proteins characterized in other Gram-negative bacteria. Further investigation into the mechanisms and structures of these proteins is necessary.

1.4.2. *Utilization of host-derived amino acids*

One of the first host metabolites shown to be utilized by *F. tularensis* during cytoplasmic growth is the tripeptide glutathione (GSH; Glu-Cys-Gly) [112]. This stable thiol can be found at low millimolar concentration within host cytoplasm and plays numerous roles in both host and bacterial physiology [113]. Gamma glutamyl transferase (GGT) enzymes are a well-studied family of proteins that are known to degrade GSH into Cys-Gly and Glu. GGT homologs are found throughout the *Francisella* genus and been found to play a critical role in cytoplasmic proliferation [84, 112, 114]. Through a series of growth curve and infection assays, authors have demonstrated that GGT catabolism of GSH liberates an essential source of cysteine, for which *F. tularensis* is auxotrophic, during infection. Therefore, the necessity of

GGT can be overcome by the addition of exogenous cysteine to host cells during infection (Fig.1.5) [84, 112].

GGT has been repeatedly identified in several genetic screens performed in diverse subspecies of *F. tularensis*, confirming the essential role of GSH degradation during infection [85, 90]. Supporting this, a recent screen utilizing a highly saturated transposon library in *Fth*, revealed additional components of the GGT-pathway, as well as identified a secondary GSH-catabolizing enzyme, ChaC [84]. In this work, authors demonstrate that a proton-dependent oligopeptide transporter (POT), DptA, is responsible for transporting Cys-Gly, a byproduct of GGT, from the periplasm into the cytoplasm. Once in the cytoplasm Cys-Gly is further degraded by peptidases and the amino acids can be utilized in numerous metabolic pathways. Consistent with the role of the pathway in cysteine acquisition, the essential role of DptA can be overcome by adding an excess of exogenous cysteine (Fig. 1.5). This was the first demonstration of a POT-family protein contributing to virulence in bacteria.

As mentioned above, the protein ChaC was also found to contribute to GSH-catabolism and intracellular proliferation [84]. This protein has previously been identified in numerous screens as playing a critical role in infection, however the activity of this enzymes remained unclear [85, 90, 115]. *In silico* analysis followed by growth curve studies revealed that ChaC is a member of the gamma-glutamyl cyclotransferase (GGCT) family of enzymes that specifically act on GSH, known as the ChaC-family [36]. These enzymes have been characterized in Eukaryotic cells, yet little is known about the role of these enzymes in bacteria and it is interesting to note that the *F. tularensis* ChaC is uniquely localized to the periplasm [36, 116, 117]. Interestingly, the growth defect of a Δ*chaC* mutant strain in macrophages is not rescued by the addition of exogenous cysteine demonstrating non-redundant roles for the two GSH-catabolizing pathways [84]. While more work needs to be done to uncover the role of ChaC during infection, this work highlights the important role of host-GSH during intracellular growth.

Four peptide transporters beyond DptA - all identified through multiple genome-wide screens - have been shown to play critical roles during infection [28, 93, 118, 119] (AnsP, IleP, GadC and ArgP) (Fig. 1.5). AnsP belongs to the major facilitator superfamily (MFS) of transporters and is required for

optimal cytoplasmic growth. Authors found that addition of excess asparagine, asparagine-containing dipeptides, or aspartic acid and ammonium together recovered the growth defect of a Δ*ansP* strain demonstrating this transporter contributes to asparagine acquisition [118]. IleP, which also belongs to the MFS family, was found to be an isoleucine transporter required for optimal escape from phagosomes [93]. This work suggests that certain nutrients are required either for survival within this compartment or for mediating escape, however in the case if IleP the mechanism underlying this defect is unclear.

The glutamate transporter GadC, which belongs to the amino acid/polyamine/organocation (APC)-family of transporters, has been shown to contribute to survival within the phagosomes [28]. The defect of a Δ*gadC* strain is partially rescued in cells unable to mount a reactive burst, suggesting a role for glutamate in oxidative stress response. Indeed, a strain lacking GadC, thereby unable to efficiently transporter glutamate, was sensitive to hydrogen peroxide specifically under conditions with excess glutamate. While this defect could be recovered by supplementing cells with succinate, the link between the oxidative stress response and the TCA-cycle, remains unclear[28]. Finally, ArgP, which also belongs to the APC-family, has been demonstrated to be a high affinity arginine transporter required for optimal escape into, as well as growth in the cytoplasm. *F. tularensis* is auxotrophic for arginine and thus the existence of a dedicated arginine transporter is not surprising[119].

In support of this, *F. tularensis* has been demonstrated to manipulate the host in order to increase the availability of host-derived amino acids. For example, early after infection the levels of branched amino acids in the cytoplasm of host cells increases, however the mechanism underlying this remains unclear [93]. Importantly this increase is not significant in cells infect with a T6SS^{ii} mutant that is unable to access the cytoplasm [93]. Additionally, studies have reported an upregulation of the host cell amino acid uptake transporter, SLC1A5, post infection with LVS. This upregulation is important for maximal bacterial growth and when SLC1A5 expression is inhibited, bacterial proliferation is hindered [118].

One of the more striking demonstrations of host manipulation for nutrients is the induction of autophagy by *F. tularensis* at later stages of infections [120]. While this pathway normally functions to inhibit invading pathogens, evidence suggests that activation of this autophagy is required for optimal

bacterial growth. Furthermore, if infected host cells are treated with drugs that inhibit this process, or if the host cells are genetically unable to perform autophagy, significantly reduced bacteria burdens are observed - a phenotype that can be rescued by the addition of an excess of amino acids. Authors went on to demonstrate, using radiolabeled molecules, that *F. tularensis* acquires and utilizes the amino acids generated by the autophagosomes. These amino acids were primarily fed into the TCA cycle as opposed to new protein synthesis suggesting the major growth limitation when autophagy is inhibited is a lack of an energy source. Interestingly, while SchuS4 induces an ATG5-independent non-canonical autophagy to harvest nutrients, LVS induces canonical autophagy for the same purpose[120]. The mechanisms and consequences of these differences has yet to be determined.

1.4.3. *Metabolic pathways that contribute to intracellular growth*

Purine biosynthesis was one of the first pathways shown to be essential during infection. This pathway is composed of 13 genes, all of which were recently identified in a Tn-Seq screen as being critical for intracellular growth [84, 121, 122]. Furthermore, mutants that rendered *F. tularensis* a purine auxotroph are attenuated for intracellular growth as well as virulence in mice. Growth within macrophages can be recovered through the addition of excess purines highlighting the limited availability of these molecules in the cytoplasm of host cells [121, 122]. Pyrimidine biosynthesis has also been shown to be important for growth in macrophages but interestingly, this pathway was dispensable for virulence in a chicken embryo and mouse model [123]. Authors went on to demonstrate that pyrimidine biosynthesis is not required for growth in other cell types such as fibroblasts and show that in a mouse model of infection pyrimidine auxotrophs preferentially grow in non-phagocytic cell types [123]. This work demonstrates the adaptability of *F. tularensis* as well as shows the unique metabolic requirements for growth in different cell types.

F. tularensis in unable to obtain all necessary amino acids from the host and therefore relies on biosynthetic pathways to generate them. Tryptophan biosynthesis is one such pathway as the host limits the availability of this amino acid during infection. Consistent with this, the biosynthetic genes for

tryptophan are required for growth for virulence in mice [124]. The glycine cleavage system (GCS), which is part of the serine biosynthesis pathway, is also critical for virulence. This phenotype is only apparent in intracellular growth assay when the host cells are grown in serine limited media, suggesting that, if available, *F. tularensis* will uptake serine from the host [125]. However, serine levels are likely limited *in vivo* and therefore the bacterial rely on the GCS for serine generation.

F. tularensis is capable of utilizing glucose as a carbon source (glycolysis) during intracellular growth, however multiple groups have found this process to be dispensable for virulence [91, 92, 126]. Instead, gluconeogenesis has been shown repeatedly to be the critical pathway for energy generation during growth [91, 92]. Mutational studies revealed that the preferred carbon source in this pathway depends on the model utilized [91]. However, authors went on to show that a strain unable to uptake glycerol mirrored a mutant deficient in gluconeogenesis suggesting this is may be the primary source of energy. Furthermore, if host cell lipolysis, which is required for storing excess glycerol, is inhibited bacterial growth is restricted [91].

While much progress has been made in defining the metabolic pathways critical for intracellular growth, numerous aspects of this process are unclear. More detailed biochemical studies are needed to clearly define the contribution of various proteins to their proposed metabolic pathway. In addition, several important differences have been identified between the different subspecies of *F. tularensis,* particularly in regard to metabolism that we currently do not understand. For examples, studies have demonstrated that the different subspecies contain variable levels of intracellular iron and that this directly contribute to the pathogenicity of that strain [109]. However, the mechanisms underlying this difference have not been defined. Further studies are needed to under the role of various metabolic pathways in mediating virulence.

1.5 Bacterial spread

Following extensive growth in the cytoplasm of infected cells, *F. tularensis* must escape out of the host cell in order to further disseminate (Fig. 1.1). This is in part mediated by bacterial release after host cell death including apoptosis and pyroptosis [127-134]. Additionally, Steele et al have recently described the direct cell-cell transfer of *F. tularensis* via merocytophagy (partial cell eating) and provide evidence that this pathway of bacterial spread is advantageous for the bacteria [64, 135]. In the following section we will briefly review the mechanisms of cell spread. While the authors acknowledge the important aspect of the immune response in this stage of infection, due to the scope of this review this topic will only be cursorily discussed.

1.5.1. Host cell death

For many years the key mechanism of bacterial dissemination was believed to be via bacterial release post host cell death. The form of host cell death following *F. tularensis* infection is either apoptosis or pyroptosis depending on the species of *F. tularensis* employed [127-134, 136]. These two pathways have dramatically different consequences on infection as pyroptosis is a highly inflammatory form of cell death [137]. In fact, only *Ftn*, a non-human adapted strain, is known to induce pyroptosis, contributing to the lower infectivity of this strain [134, 138]. It is critical that the bacteria do not induce host cell death too early during infection and indeed numerous groups have reported that *F. tularensis* is capable of suppressing apoptosis during the early stages of infection [128]. At later stages, high levels of caspase-3 activation as well as elevated levels of apoptosis has been observed both in tissue culture infections and in tissues collected from infected mice, demonstrating this is the primary mechanism of host cell death during infection [136].

1.5.2. Merocytophagy

In 2016 Steele et al published the first description of direct cell to cell spread of *F. tularensis* [135]. The authors hypothesized that the exceptionally fast rate of *F. tularensis* dissemination through a host was due to direct cell-cell spread without the bacteria beings exposed to the extracellular environment. Indeed, through fluorescent labeling experiments authors were able to observe the direct exchange of not only the bacteria but also cytosolic material and membrane components into neighboring macrophages. Direct cell contact was required for this process to occur, and follow-up studies demonstrated that neighboring macrophages are capable of phagocytosing portions of infected cells, termed merocytophagy.

A hallmark of bacterial spread via merocytophagy is the appearance of numerous bacteria within the same phagosome, whereas when bacteria are phagocytosed from the extracellular environment there is a typically single bacterium per FCP [64]. By examining lungs cells from mice collected post infection, authors were able to identify host cells in which multiple *F. tularensis* were within the same FCP. This provides evidence that merocytophagy occurs within the host and is not an artifact of tissue culture infection. In order to investigate the contribution of spread through merocytophagy authors exposed uninfected cells to extracellular bacteria or an equivalent number of bacteria already infecting macrophages. CFU counts, as well as microscopy methods, demonstrate that uninfected cells more efficiently acquire the bacteria through direct cell-cell transfer as opposed to phagocytosis of free bacteria. This is not due to altered dynamics of escape from the phagosome and in total this work demonstrates that merocytophagy is beneficial mechanism for *F. tularensis* dissemination to adjacent cells [64].

1.6 Conclusions

Over the last decade significant advances have been made in our understanding of the *F. tularensis* lifecycle. The employment of numerous genome-wide screens has allowed for the identification of many novel virulence mechanisms utilized by this intracellular pathogen. In particular,

we have gained significant insight into the contribution of the FPI-encoded T6SS[ii] in mediating phagosomal escape. We now know the identity of the effectors secreted by this system, allowing for more targeted studies on the molecule mechanisms underlying this process. Additionally, the work of several groups has revealed the critical role for nutrient acquisition and host-metabolism manipulation by *F. tularensis* to promote cytoplasmic growth. It is now clear that host-derived amino acids in particular play an essential role in supporting proliferation.

Despite the advances made, there are still numerous outstanding questions in this field. There is an apparent lack of mechanistic studies on the virulence factors utilized by *F. tularensis,* with only indirect evidence often presented to support important claims. Furthermore, we need a better understanding of the mechanisms underlying the virulence levels of the different subspecies. This will aid in determining which pathways are critical for causing a robust infection thereby identifying novel drug targets.

1.7 Figures

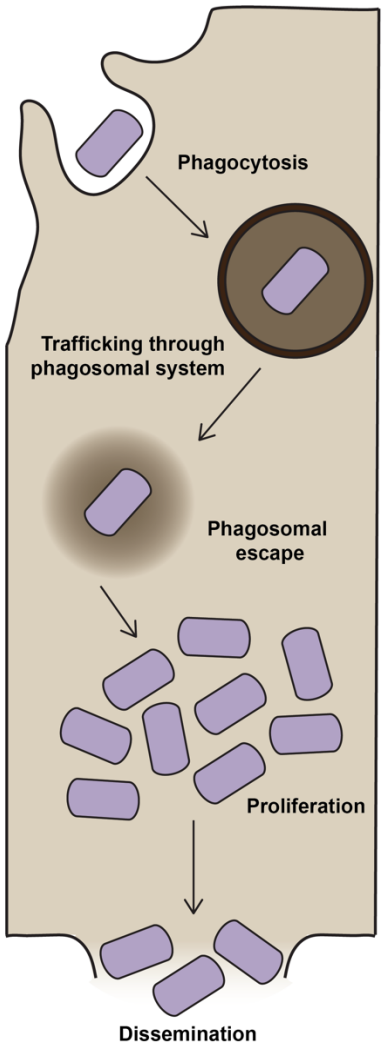

Figure 1.1. Overview of the *F. tularensis* lifecycle.
Model depicting the essential steps of the *F. tularensis* intracellular lifecycle.

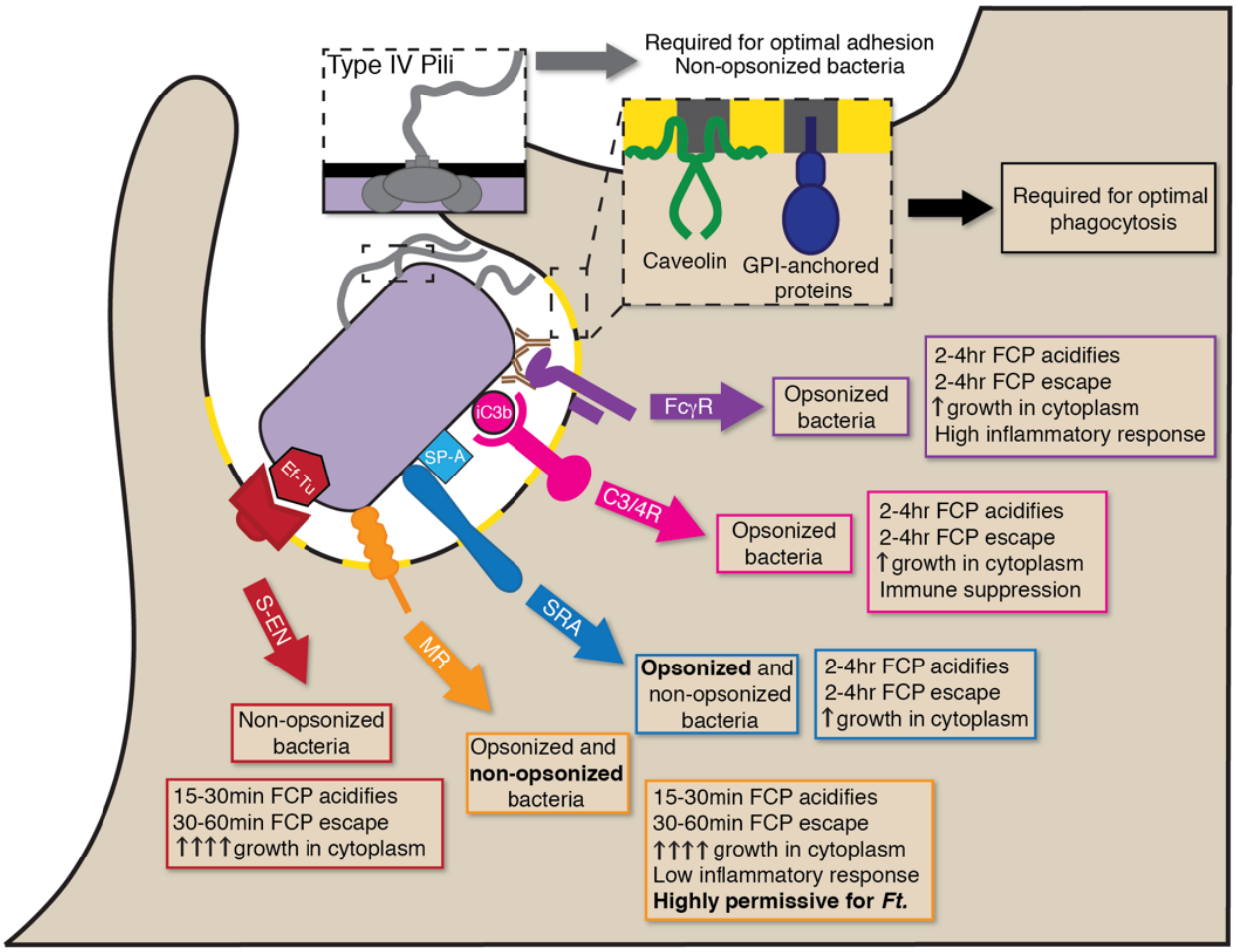

Figure 1.2. Numerous proteins contribute to the uptake of *F. tularensis*.
Model depicting the proteins the contribute to the adherence to and uptake into macrophages. The downstream consequences of uptake through the various pathways are highlighted.

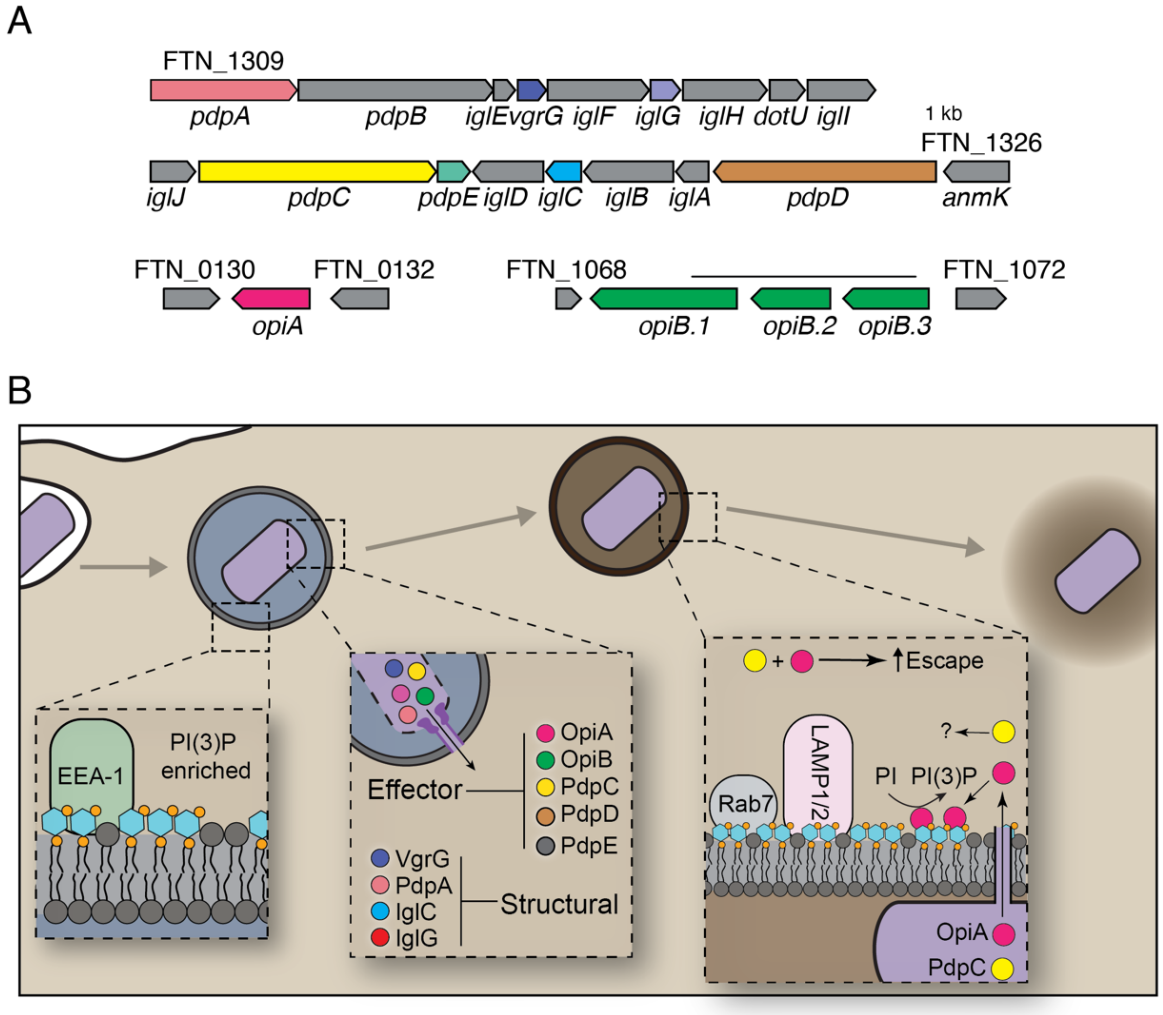

Figure 1.3. The FPI-encoded T6SS^{ii} mediates phagosomal escape.
(**A**) Cartoon depiction of the FPI and the Opi-protein genetic composition. FTN numbers are indicated. Colors correspond to the model in (B). (**B**) Overview of the phagosomal stage of the *F. tularensis* life cycle. Proteins involved in trafficking and escape are depicted as well as an overview of the T6SS^{ii} substrates.

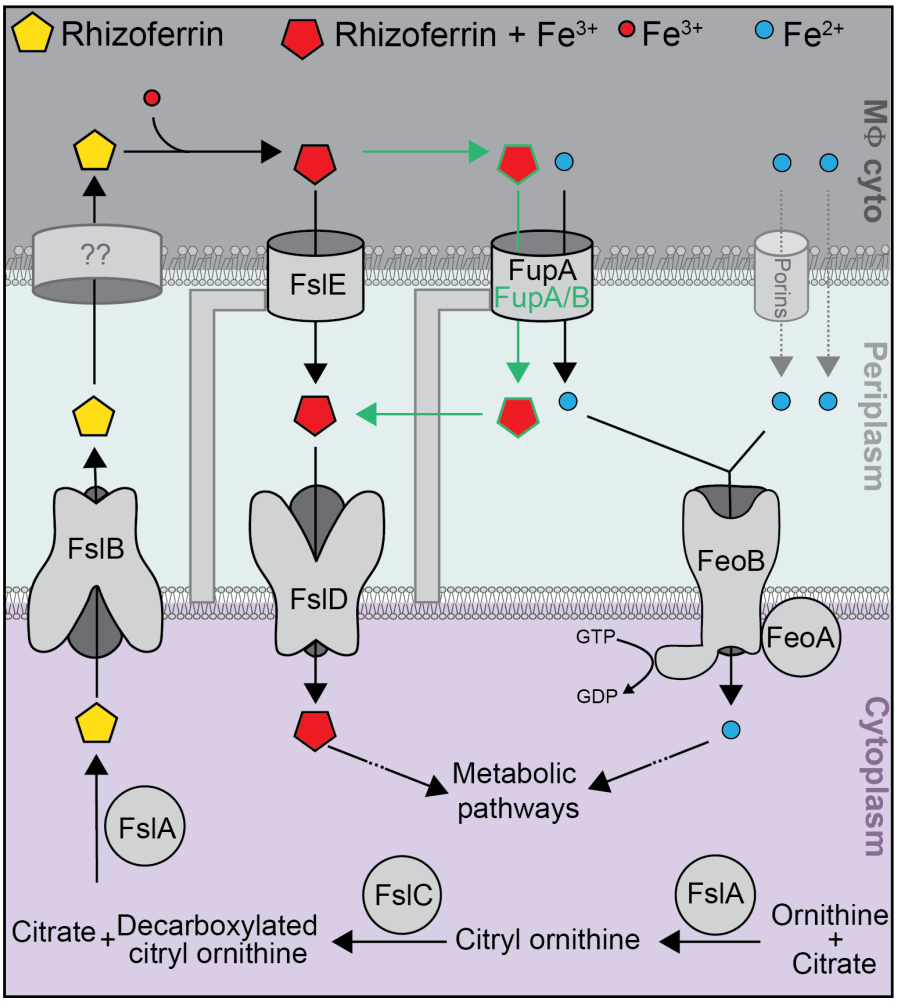

Figure 1.4. *F. tularensis* encodes for two iron uptake pathways.
Model depicting the proteins that contribute to iron acquisition. The proteins that have been found to play a unique role in LVS are highlighted (green).

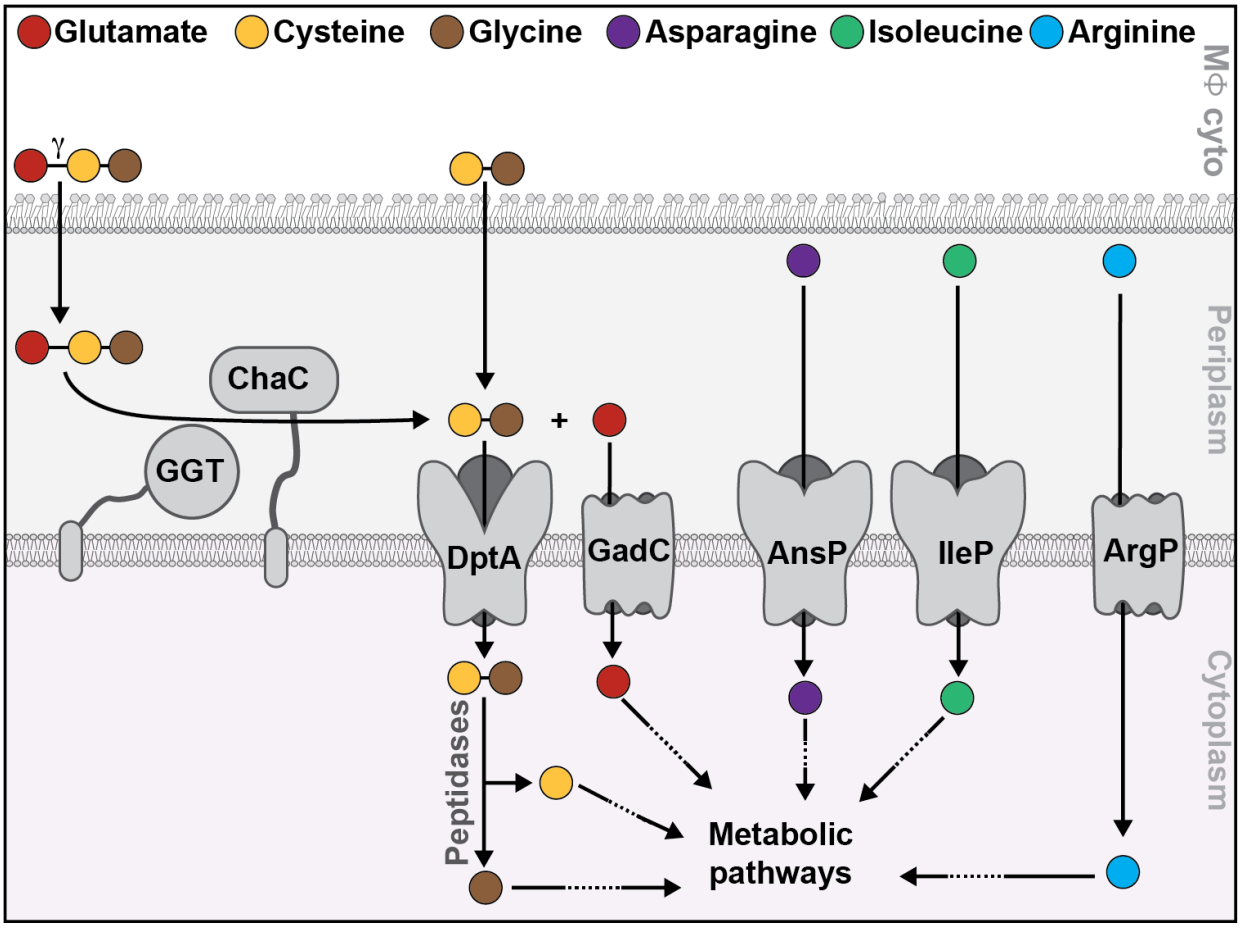

Figure 1.5. *F. tularensis* utilizes several host-derived metabolites during infection.
Model depicting the enzymes and transporters that contribute to utilization of host-derived molecules. Glutathione (GSH) is depicted as entering the periplasm through unknown porins. For asparagine, isoleucine, and arginine, the precise form of the molecules transported is unknown.

Chapter 2: A phosphatidylinositol 3-kinase effector alters phagosomal maturation to promote intracellular growth of *Francisella*

Published as: Ledvina H.E., Kelly K.A., Eshraghi A., Plemel R.L., Peterson S.B., Lee B., Steele S., Adler M., Kawula T.H., Merz A.J., Skerrett S.J., Celli J., and Mougous J.D. (2018). *Cell Host & Microbe,* 24: 285-95.

2.1 Abstract

Many pathogenic intracellular bacteria manipulate the host phago-endosomal system to establish and maintain a permissive niche. The fate and identity of these intracellular compartments is controlled by phosphoinositide lipids. By mechanisms that have remained undefined, a *Francisella* pathogenicity island-encoded secretion system allows phagosomal escape and replication of bacteria within host cell cytoplasm. Here, we report the discovery that a substrate of this system, OpiA, represents a family of wortmannin-resistant bacterial phosphatidylinositol (PI) 3-kinase enzymes with members found in a wide range of intracellular pathogens, including *Rickettsia* and *Legionella* spp. We show that OpiA acts on the *Francisella*-containing phagosome and promotes bacterial escape into the cytoplasm. Furthermore, we demonstrate that the phenotypic consequences of OpiA inactivation are mitigated by endosomal maturation arrest. Our findings suggest that *Francisella*, and likely other intracellular bacteria, override the finely-tuned dynamics of phagosomal PI(3)P in order to promote intracellular survival and pathogenesis.

2.2 Introduction

The success of most bacterial pathogens relies on their capacity to actively override host immune defense pathways. Those that replicate intracellularly face the additional requirement of manipulating cellular trafficking to reach and maintain an inhabitable niche [139, 140. These feats are often accomplished by effector proteins that are delivered directly to host cells by specialized secretion systems, including the well characterized type III and IV secretion systems (T3SS, T4SS){Galan, 2006 #587, 141, 142].

Francisella tularensis is an intracellular Gram-negative pathogen and the etiological agent of tularemia, a zoonotic infection that can be fatal if untreated [1]. Subsequent to internalization, this bacterium escapes the *Francisella*-containing phagosome (FCP) and replicates in the cytoplasm. The molecular mechanisms enabling the intracellular lifestyle of *F. tularensis* remain unknown. However,

studies indicate that a type VI secretion subtype 2 (T6SS^{ii}) pathway encoded on the *Francisella* pathogenicity island (FPI) is required for this bacterium to establish a productive intracellular niche [22, 23, 32, 43, 143, 144]. On the basis of phylogenetic analyses, three T6SS subtypes have been defined: T6SS^{i} and T6SS^{iii} are widely distributed in the phyla Proteobacteria and Bacteroidetes, respectively, and are generally involved in interbacterial antagonism via the delivery of toxins to recipient bacterial cells [34, 39]. On the contrary, the T6SS^{ii} pathway appears to be restricted to *Francisella* and closely related host-associated bacteria, suggesting that this T6SS subtype evolved to mediate interactions with eukaryotic cells.

To begin to understand how the FPI-encoded T6SS^{ii} facilitates intracellular proliferation of *F. tularensis*, we recently performed a proteome-wide search for its substrates [22]. This work identified four T6SS^{ii}-exported effector proteins and several additional proteins that transit the T6SS^{ii} pathway to support core function of the apparatus. A surprising finding to emerge from this work was that two T6SS^{ii} effector proteins, OpiA (outside pathogenicity island A) and OpiB, are encoded by loci distal to the FPI in *F. tularensis* genomes [22]. Macrophage infection assays demonstrated that these proteins contribute to *F. tularensis* subspecies *novicida* (*F. novicida*) intracellular growth; however, their mechanism of action was not defined.

F. tularensis cells defective in T6SS^{ii} activity fail to escape the FCP and instead are shuttled to lysosomes and killed, suggesting that the pathway is important for modulating the trafficking of bacteria within cells [32]. Phosphoinositide (PI) molecules are a family of dynamic signaling lipids that define the identity and fate of many eukaryotic vesicular compartments, including those within the phago-endosomal system [145]. As such, these molecules are frequently manipulated by intracellular pathogens [146, 147]. For example, *Legionella pneumophila* utilizes its Dot/Icm T4SS to deliver PI 3-phosphatases and a PI 4-kinase to the cytoplasm of infected phagocytes [148-150]. The concerted action of these proteins causes the accumulation of PI(4)-phosphate (PI(4)P) on the Legionella containing vacuole (LCV), which leads to the binding of additional *Legionella* effectors and likely promotes the recruitment of endoplasmic reticulum-derived vesicles {Weber, 2006 #1589.

It has been over 15 years since genetic screens first implicated the FPI in the pathogenesis of *F. tularensis* {Gray, 2002 #642}. Despite this, the molecular mechanisms underlying its requirement for intracellular growth remain elusive. Here, we show that the T6SS^{ii} effector protein OpiA belongs to a previously unrecognized bacterial PI 3-kinase (PI3K) family. We provide biochemical and genetic evidence that OpiA enforces high PI(3)-phosphate (PI(3)P) levels on the FCP, leading to delayed maturation of this compartment and efficient escape of bacteria into the cytoplasm.

2.3 Results

2.3.1 *OpiA family proteins share motifs with eukaryotic phosphoinositide kinases*

OpiA is present in the majority of *Francisella* spp., including all subspecies of *F. tularensis* [22] (Fig. 2.1). However, database searches failed to reveal characterized proteins with homology to OpiA beyond this group of organisms. To gain insight into the function of OpiA, we therefore turned to a hidden Markov model-based approach, which can identify small sequence elements conserved between functionally related proteins [151]. This analysis identified a constellation of amino acids that is conserved among all *Francisella* OpiA orthologs and between a group of otherwise non-homologous bacterial proteins (Fig. 2.1). We subsequently refer to the latter as OpiA family proteins (OFPs). These residues constitute two consensus motifs, DxHxxN and IDH, separated by 14 amino acids in OpiA. Interestingly, OFPs are enriched in host-associated bacteria, including species belonging to the genera *Legionella*, *Vibrio* and *Rickettsia* (Fig. 2.2 and 2.3). Moreover, an OFP encoded by *Legionella pneumophila*, previously designated LegA5, was shown to transit the Dot/Icm T4SS [152]. Although the activity of the protein was not investigated, subsequent high-throughput studies further demonstrated that LegA5 is toxic and membrane-associated when expressed in yeast [153, 154].

Literature searches revealed that the sequence and relative positions of the motifs shared among the OFPs closely resemble elements conserved between a subset of phosphoinositide kinases. Specifically, the catalytic and activation loops of phosphoinositide 3-kinases (PI3Ks) and certain

phosphoinositide 4-kinases PI4Ks possess DxHxxN and IDF consensus sequences, respectively, with spacing similar to that found in OFPs (Fig. 2.3) [155]. However, outside of these motifs, OFPs bear no clear similarity with these proteins. For instance, OFPs lack lipid binding and protein interaction domains typical of this subset of eukaryotic PI kinases [156]. Together, our sequence analyses suggested that OFPs may represent a previously unrecognized and unique family of bacterial phosphoinositide kinases that act in eukaryotic cells as effector proteins.

2.3.2 *OpiA and LegA5 are phosphoinositide 3-kinase enzymes*

Despite the divergence between OpiA and eukaryotic PI kinases, we tested whether the effector synthesizes phosphatidylinositol phosphate(s) *in vitro*. *F. novicida* OpiA was heterologously expressed, purified, and incubated with PI- or PI(4,5)P_2-containing liposomes in the presence of [γ^{32}P]-ATP (Figure 2.3A). These molecules were chosen based on the substrate preferences of eukaryotic OFP-related lipid kinase enzymes. PI3Ks of this group act on PI (class I-III) or PI(4,5)P (class III) to generate PI(3)P or PI(3,4,5)P_3, respectively, whereas PI4Ks of this group (class III) act on PI to generate PI(4)P [157]. Separation of products by thin layer chromatography revealed a species consistent with the retention factor of PIP generated in the OpiA reaction (Fig. 2.3A). This product was not observed in a similar reaction prepared using OpiA bearing a substitution of the predicted catalytic histidine residue it shares with characterized PI3K and PI4K enzymes (OpiA^{H261A}) (Fig. 2.3A, 2.4A). In contrast to the class I PI3K p100α, OpiA did not act on PIP_2. We next purified the *L. pneumophila* OFP LegA5, and similarly examined its PI kinase activity. Like OpiA, LegA5 generated PIP from PI and displayed no detectable activity against PIP_2 (Fig. 2.3B, 2.4B).

Our data to this point indicated that OpiA produces PIP; however, it did not identify the position of the phosphate on the inositol moiety. To determine the specific PIP produced by OpiA, we utilized a competitive ELISA strategy that exploits the high selectivity of PI(3)P and PI(4)P binding domains. PI(5)P is produced *in vivo* by the action of phosphatases and is not produced directly by PI

kinases; thus, we did not test for the capacity of OpiA to generate this molecule [156]. The results of these assays indicated that the action of OpiA on PI leads exclusively to the production of PI(3)P (Fig. 2.3C). Moreover, the efficiency of PI(3)P production by OpiA approaches that of p110α, suggesting that this is a physiologically relevant product of the enzyme. This assay additionally confirmed that PIP_2 is not a substrate for OpiA.

The capacity of OpiA to phosphorylate PI and not PIP_2 places its substrate specificity within PI3Ks belonging to classes II and III [157]. Class II and III PI3Ks can be further separated by the ability of the former to act on PI(4)P, generating $PI(3,4)P_2$. We were unable to detect activity against PI(4)P by OpiA, indicating that, biochemically, the effector is most reminiscent of eukaryotic class III PI3K enzymes (Fig. 2.4C).

2.3.3 *OpiA PI3K activity contributes to* F. novicida *growth* in vivo

In the course of our studies, we noted that OpiA over-expression is toxic to *Saccharomyces cerevisiae* (Fig. 2.5A). Given the catalytic activity of the enzyme *in vitro*, we reasoned that this is due to excess PI(3)P production. Consistent with this, $OpiA^{H261A}$ did not inhibit *S. cerevisiae* growth. To further interrogate the activity of OpiA *in vivo*, we examined its toxicity in *S. cerevisiae vps34*Δ. Vps34 is a class III PI3K and is the only enzyme known to generate PI(3)P in *S. cerevisiae* [158]. Deletion of this gene, but not the deletion of *vps30* (a component of the Vps34 complex that is dispensable for PI(3)P production), significantly suppressed the toxicity of OpiA (Fig. 2.5A). The suppression of the OpiA phenotype by Vps34 inactivation is specific, as the expression of another toxic protein (Mcm1) was similarly inhibitory to both *S. cerevisiae* wild-type and *vps34*Δ (Fig. 2.5B) [159].

Motivated by the toxicity of OpiA to yeast, we next asked whether OpiA promotes *F. novicida* pathogenesis. However, macrophage infection assays showed that inactivating *opiA* in wild-type *F. novicida* does not attenuate intracellular proliferation (Fig. 2.5C). In the close relative of *F. novicida*, *L. pneumophila*, it is commonplace for the activity of an effector protein to mask that of another in infection

models [160, 161]. For example, the deletion of genes encoding the effector pairs WipB and LidA, MavP and LidA or WipB and LegC8 leads to intracellular replication defects, while inactivation of any of these effectors individually has no effect on *in vivo* growth [162]. We reasoned this may explain the lack of a discernable phenotype for Δ*opiA* in the wild-type *F. novicida* background. To test this, we performed infection assays with *F. novicida* strains containing Δ*opiA* in combination with deletions in genes encoding each of the T6SS^{ii} effectors previously identified by our group [22]. This analysis uncovered a significant growth phenotype attributable to OpiA specifically in a strain lacking the FPI-encoded effector PdpC (Fig. 2.5D). Genetic complementation of this phenotype was achieved by expressing OpiA from a neutral chromosomal site under the control of its native promoter. OpiA^{H261A} failed to restore growth despite expression and secretion at levels similar to the wild-type protein, suggesting that the PI3K activity of OpiA is critical for its role *in vivo* (Fig. 2.5E , F).

Next, we used an aerosol delivery-based murine model to determine if the cell culture phenotype of Δ*opiA* extends to an animal infection [163]. As observed in our macrophage infection assays, inactivation of *opiA* in the wild-type background did not yield a detectable mouse infection phenotype (Fig. 2.6B). Previous studies have demonstrated that inactivation of *pdpC* attenuates bacterial growth and virulence in mice [49, 52]. We found that deletion of *opiA* further diminished the *in vivo* growth of *F. novicida* Δ*pdpC* and led to an additional decrease in morbidity compared to that exhibited by mice infected with *F. novicida* Δ*pdpC* (Fig. 2.5G, 2.6B). In summary, these data show that the PI3K activity of OpiA can play an important role in the pathogenesis of *F. novicida*.

2.3.4 *OpiA generates PI(3)P on endosomes*

Our observation that the contribution of OpiA to *F. novicida* intramacrophage growth is apparent specifically in strains lacking PdpC led us to hypothesize that these two proteins function in a common pathway. An alternative explanation is that the absence of PdpC cripples *F. novicida in vivo* and non-specifically sensitizes the bacterium to the loss of additional effectors. However, a strain containing deletions of *opiB* and *pdpC* does not have an intracellular growth defect beyond that of one lacking only

pdpC (Fig. 2.6C). Sequence-based algorithms fail to identify candidate functions for PdpC, although recent experimental data implicate the protein in the escape of *F. tularensis* from phagosomes [53]. While wild-type cells typically reach the cytoplasm within two hours, cells lacking PdpC remain co-localized with endosomal markers for an extended period and a large proportion are killed in lysosomes. Notably, PI(3)P – the product of OpiA – accumulates on early endosomes and is a key regulator of their trafficking [157]. These observations lend credence to the hypothesis that PdpC and OpiA promote *F. novicida* pathogenesis by influencing related cellular processes.

To probe the effects of OpiA on cellular PI(3)P, we utilized a well described PI(3)P fluorescent probe that is based on tandem FYVE domains (2xFYVE-mCherry) [164, 165]. Confocal microscopy was used to examine the co-localization of this probe with markers of major cellular compartments in control HeLa cells and those transfected with an *opiA* expression plasmid (Fig. 2.7A, 2.7B and 2.8A). Consistent with the known association of PI(3)P with early endosomes, the probe displayed strong co-localization specifically with EEA1-positive vesicles in control cells. OpiA-expressing cells possessed a similar pattern of 2xFYVE-mCherry localization, with the exception that in these cells the probe showed significantly greater co-localization with LAMP1-positive vesicles, representing late endosomes and lysosomes. These data suggest that OpiA-catalyzed PI(3)P production is limited to sites in the endosomal pathway. However, due to the background of endogenous PI(3)P on early endosomes, they do not distinguish whether OpiA acts on these vesicles or exclusively on membranes derived from later stages of the endosomal pathway.

The potential overlap between the site of OpiA-catalyzed PI(3)P production and the localization of this phosphoinositide in unperturbed cells prompted us to pursue a means to selectively inhibit endogenous PI3K activity. Wortmannin is a fungal-derived natural product that displays potent inhibitory activity against all previously described classes of PI3Ks [166]. The mechanism of inhibition by wortmannin relies on the formation of a covalent adduct between the molecule and the sidechain of a conserved lysine residue present in the active site of target kinases (Lys802 of p110α) [167]. Given the high degree of sequence divergence between OpiA and known PI3K enzymes, we hypothesized that

wortmannin may not efficiently inhibit the bacterial protein. *In vitro* inhibition studies confirmed the capacity of wortmannin to significantly inhibit p110α at concentrations below 10 nM; however, no inhibition of OpiA was observed at wortmannin concentrations exceeding 10 μM (Fig. 2.7C, 2.8B , and 2.8C). Likewise, a high concentration of wortmannin had no detectable impact on Legionella OFP LegA5 activity (Fig. 2.7D). From these data, we conclude that OpiA, and likely the OFPs more generally, are resistant to inhibition by wortmannin.

The selectivity of wortmannin for endogenous PI3Ks allowed us to specifically define the site(s) of PI(3)P production by OpiA. As previously observed, 2xFYVE-GFP appeared diffusely localized in cells treated with wortmannin (Fig. 2.7E , F) [168]. On the contrary, the probe clearly localized to vesicular structures resembling endosomes in wortmannin-treated cells expressing OpiA. This pattern was not observed in wortmannin-treated cells expressing catalytically inactive OpiA. Co-localization analyses indicated that OpiA-catalyzed PI(3)P is significantly enriched on both early and late endosomal compartments (Fig. 2.7A, B; + wort). This localization pattern does not simply reflect the distribution of the substrate of OpiA – PI can be found on many cellular membranes [169]. Therefore, these data strongly suggest that OpiA acts in a site-selective manner *in vivo*.

2.3.5 *OpiA is a selective PI(3)P-binding protein*

The apparent selectivity of OpiA for the endosomal pathway suggested that the protein may be specifically recruited to these vesicles. In immunoprecipitation studies we were unable to identify OpiA-binding proteins that could mediate this recruitment. Accordingly, we tested if OpiA-lipid interactions could be responsible. Using a lipid overlay assay, we found that OpiA exhibited selective binding to its product, PI(3)P (Fig. 2.9A). Based on the distribution of PI(3)P in cells, we posited that similar to several early endosomal proteins (e.g. EEA1 and PIKFYVE), binding to this lipid could facilitate the recruitment of OpiA to endosomes [170, 171].

Using bio-layer interferometry coupled with synthetic streptavidin-conjugated PI(3)P, we determined that the interaction between the lipid and OpiA is likely of sufficient strength (K_d = 190 nM) to target the protein *in vivo* (Fig. 2.9B). The active sites of kinases, like those of other enzymes, can possess some affinity for their products; however, the strength of the OpiA–PI(3)P interaction strongly suggests that binding occurs at a distal site on the protein. Although OpiA lacks canonical PI(3)P binding domains, it is a basic protein (pI = 10.0) with short polycationic motifs that are analogous to those previously shown to mediate specific interactions between eukaryotic proteins and phosphoinositide species [172] A tight association between OpiA and PI(3)P is in-line with our data demonstrating that OpiA-produced PI(3)P is localized to early endosomes in the presence of the pan PI3K inhibitor wortmannin. Whereas *de novo* synthesis of PI(3)P is inhibited by wortmannin, during endocytosis the enzyme inositol polyphosphate-4-phosphatase (INPP4A/B) acts on plasma membrane $PI(3,4)P_2$ to generate an initial, small pool of early endosomal PI(3)P [173, 174].

We sought to determine if PI(3)P binding is a common feature of OFPs. Lipid overlay assays indicated that LegA5 exhibits only weak binding to PI(3)P and preferentially associates with phosphatidylserine (Fig. 2.9C). Together, these findings show that OpiA binds PI(3)P in a selective and high-affinity manner. Furthermore, they suggest PI(3)P binding serves as a mechanism for the specific recruitment of OpiA to endosomal membranes.

2.3.6 *OpiA contributes to PI(3)P production on* Francisella*-containing phagosomes*

Our data to this point were consistent with a feed-forward model to explain the behavior of OpiA (Fig. 2.10A). Upon delivery via the $T6SS^{ii}$ pathway, OpiA binds the FCP via the PI(3)P present on the cytoplasmic face of this early endosome-like vacuole. The effector generates additional PI(3)P, which promotes a positive feedback mechanism for the continued production of PI(3)P on the FCP. This process leads to a departure from the normal localization pattern of PI(3)P on maturing endosomes; OpiA maintains PI(3)P on the FCP even as the vacuole matures to resemble a late endosome.

We interrogated this model *in vivo* by following the co-localization of *F. novicida* wild-type versus Δ*opiA* with PI(3)P during the infection of murine bone marrow-derived primary macrophages (BMDMs). As expected, we observed *F. novicida* within PI(3)P-containing vacuoles at high frequency (>70%) immediately following phagocytosis (Fig. 2.10B). The frequency of co-localization then decreased over the next 30 minutes, consistent with the known dynamics of phagosome maturation. In macrophages infected with Δ*opiA* cells, co-localization of PI(3)P with FCPs continued to decrease until reaching baseline by 40 minutes post-infection. In contrast, infection with wild-type *F. novicida* was associated with prolonged FCP–PI(3)P co-localization, up to 50 minutes post-infection. Inactivation of *pdpC* had no impact on these dynamics in either the wild-type or Δ*opiA* backgrounds (Fig. 2.10B, C). Prior studies show that 40-50 minutes post-infection corresponds to the time during which wild-type *Francisella* are beginning to escape the FCP [19]. Therefore, this finding strongly suggests that, as predicted by our model, OpiA activity promotes PI(3)P accumulation on FCPs that have acquired late endosomal characteristics.

Studies suggest that *Francisella* escape from late endosome-like compartments before beginning replication within the cytoplasm [175]. Based on our data indicating that the product of OpiA is present on this compartment at the approximate time of bacterial exit, we posited that OpiA-generated PI(3)P promotes endosomal escape. We reasoned that retardation of this process could explain why a Δ*opiA*-dependent *in vivo* growth defect is specifically observed in the Δ*pdpC* background, as PdpC is thought to also participate in endosomal escape. To evaluate phagosomal escape, we tracked the co-localization of *F. novicida* with LAMP1 during initial stages of BMDM infection. This assay confirmed the previously established phenotype of Δ*pdpC*, and moreover it revealed that a significant OpiA-dependent contribution to escape is observable in the absence of PpdC (Fig. 2.10D, F). As expected, the escape defect of Δ*opiA* cells was concomitant with a delay in replication (Fig. 2.10E, F).

While PI(3)P is required for early phagosome biogenesis, recent reports suggest that prolonging its presence inhibits maturation of these vesicles [59, 60]. We reasoned that if OpiA-catalyzed PI(3)P accumulation promotes bacterial escape by delaying endosomal maturation, then the impact of *opiA*

inactivation should be minimized in cells wherein this process is interrupted. To test this, we examined the effect of arresting endosome maturation on a panel of *F. novicida* strains. Rab7 is a small GTPase that is required for the progression of early to late endosomes and expression of a dominant negative allele of this protein ($Rab7^{T22N}$) leads to well characterized defects in endosomal maturation in HeLa cells [176, 177]. Remarkably, we found that $Rab7^{T22N}$ restores the intracellular proliferation of Δ*pdpC* Δ*opiA* to the level of Δ*pdpC* in HeLa cells (Fig. 2.10G). The effect of endosomal maturation arrest was specific to the Δ*opiA* genetic background, as neither the growth of Δ*dotU* nor Δ*pdpC* strains was enhanced by this allele. In total, these data strongly suggest that OpiA-catalyzed accumulation of PI(3)P on the FCP enhances *Francisella* intracellular survival by promoting timely escape from late endosomes.

2.4 Discussion

We have shown that the FPI-encoded $T6SS^{ii}$ pathway substrate OpiA belongs to a previously unreported family of bacterial PI3K enzymes. As might be expected based on the phylogenetic distribution of PI, OFPs are found primarily in bacteria that associate intimately with eukaryotic cells. The *Rickettsia* and bacteria belonging to the related genus *Orientia* are particularly replete with genes encoding OFPs. These bacteria are obligate intracellular parasites and cause a wide range of diseases in human [178]. Like *Francisella*, the intracellular lifecycle of *Rickettsia* and *Orientia* spp requires their escape from the endosomal pathway into the cytoplasm [178]. Little is understood mechanistically about the factors required for phagosomal escape by Rickettsia. However, it is conceivable that despite their sequence divergence, OpiA and the OFPs of these bacteria function in a conserved manner to support escape.

Our biochemical analyses demonstrate that the *L. pneumophila* Dot/Icm T4SS effector LegA5 catalyzes the production of PI(3)P. Intracellular growth of *L. pneumophila* occurs within the Legionella containing vacuole (LCV), a compartment with a PI content that is highly orchestrated by the bacterium. At least four effector proteins delivered by *L. pneumophila* are direct PI-processing enzymes and an additional three effectors specifically bind PI(3)P [148-150, 179-182]. An effector central to the

coordinated action of these proteins is LepB, a PI4K that generates PI(3,4)P_2 from PI(3)P [148]. SidF then acts downstream of LepB as a PI 3-phosphatase to generate PI(4)P [149]. The latter is the apparent end product of the pathway and plays an important role in the recruitment of other *L. pneumophila* effectors to the LCV and in the acquisition of ER-derived material necessary to support growth [183]. Interestingly, the source of PI(3)P that LepB phosphorylates during LCV maturation in unknown[148]. Work has demonstrated that *L. pneumophila* actively inhibits endosome fusion with the LCV, thus it is unlikely that the substrate of LepB is produced by a host enzyme [180]. It is tempting to speculate that LegA5 is the enzyme responsible for the generation of PI(3)P on the LCV. Our data suggesting that LegA5 preferentially interacts with phosphatidylserine lends additional credence to this possibility. This phospholipid is enriched on the plasma membrane, the structure from which the LCV derives[184]. Although phosphatidylserine is depleted from the LCV by six hours post-infection, this is after the accumulation of PI(4)P and hence also subsequent to the proposed action of LegA5 [149, 184].

Our data show that in the absence of PdpC, OpiA contributes to the intracellular growth of *F. novicida* by promoting bacterial escape into the cytoplasm. Since PdpC and OpiA are both present in the genomes of most *Francisella* spp., it is likely that each protein independently contributes to the fitness of the bacterium. We posit that the apparent functional redundancy in these proteins represents a limitation in the restrictiveness and relevance of the tissue culture and animal models commonly employed to study *Francisella*. It is therefore possible that, if examined in additional models, an OpiA phenotype may become apparent. Nevertheless, when taken together with our biochemical and cell biological data, the apparent functional overlap between OpiA and PdpC strongly implicate OpiA in the endosomal phase of cellular infection by *F. novicida*. Recent reports wherein individual endosomes were tracked during maturation demonstrate that PI(3)P levels are more dynamic than previously appreciated [185]. Moreover, fine-tuned temporal regulation of PI(3)P levels appears to be important for the progression of early endosomes to lysosomes. For instance, deletions in negative regulators of Vps34 activity, WDR81 and WDR91, markedly delay phagosomal and endosomal maturation [59, 60]. By generating PI(3)P through a positive feedback mechanism, OpiA could override the natural dynamics of PI(3)P, in turn allowing

additional time for other factors to mediate bacterial escape. This model is supported by our finding that cells with arrested phagosomal maturation are permissive to replication of *F. novicida* lacking OpiA.

The *opiA* genes in *F. tularensis* subsp *tularensis* and *holarctica* are split into two open reading frames and, in the case of *F. holarctica,* the N-terminal portion of the gene is truncated (Fig. 1A). Despite these differences, the proteins encoded at these loci share >97% amino acid identity and critical catalytic residues are preserved. This conservation could indicate that the function of OpiA during infection is conserved across *F. tularensis* subsp. However, it is also possible that subspecies-specific differences in OpiA sequence have an impact on protein function. If this is the case, OpiA may be a factor that contributes to the variable host ranges of *F. tularensis* subsp [1]. Work to define the role of OpiA during infection by other *F. tularensis* subsp. is ongoing.

Phosphoinositides are key regulators for a wide range of cell processes, including membrane trafficking, cellular proliferation, and autophagy. These phospholipids act in a spatiotemporal manner, which makes their functional dissection challenging. We demonstrate that OFPs are recalcitrant to inhibition by wortmannin, a potent inhibitor of virtually all known PI3K enzymes. This property of OFP enzymes could afford the opportunity to study the generation of PI(3)P in specific cellular compartments dictated by the unique intracellular biology of the bacterium from which they derive. Therefore, OFPs may provide a tool to study the role of phosphoinositides in eukaryotic cell biology.

2.5 Materials and Methods

Experimental Model and Subject Details

Francisella novicida. *F. novicida* strains U112 and MFN245 were grown in tryptic soy broth or agar supplemented with 0.1% (w/v) cysteine (TSBC or TSAC). For macrophage infections*, F. novicida* and all derived strains were grown in Chamberlain's defined media (CDM). All strains were grown at 37°C while shaking. All strains were stored at -80°C in TSBC supplemented with 40% (v/v) glycerol.

Escherichia coli. *E. coli* strains DH5α and BL21 Rosetta 2 DE3 were utilized for cloning and expression, respectively. All strains were routinely grown in Lysogeny broth (LB) at 37°C while shaking. All strains were stored at -80°C in LB supplemented with 20% (v/v) glycerol.

Saccharomyces cerevisiae. *S. cerevisiae* strain BY4742 MATalpha his3Δ1 leu2Δ0 lys2Δ0 ura3Δ0 was grown at 30°C in yeast extract peptone dextrose broth or agar (YPD). Mutant strains (*vps34*Δ and *vps30*Δ*,* Yeast Knockout Collection) were grown at 25˚C on YPD. Mutations were confirmed by PCR. Strains carrying the inducible expression plasmid pCM190 were grown at 25˚C on synthetic drop out media lacking uracil (C-ura) containing 1μg mL^{-1} doxycycline. All strains were stored at -80°C in YPD supplemented with 20% (v/v) glycerol.

Cell lines. All cell lines were authenticated by microscopic morphologic evaluation. RAW264.7 and HeLa cells were maintained at 37˚C in the presence of 5% CO2. All cells were cultured in supplemented Dulbecco's Modified Eagle's Medium (DMEM; supplemented with 10% (v/v) heat inactivated fetal bovine serum (FBS; Atlanta biologicals), 4.5 g L^{-1} glucose, 2 mM glutamine, 110 mg L^{-1} sodium pyruvate, 100 U mL^{-1} penicillin, 100 μg mL^{-1} streptomycin, and 0.05 mM beta-mercaptoethanol). Human embryonic kidney 293T cells (HEK293T/17) were grown in DMEM (4.5 g/l glucose and sodium pyruvate) supplemented with 10% (v/v) heat-inactivated FBS (Gibco, Life Technologies) and 4 mM L-glutamine at 37 °C and 10% CO_2. Murine bone marrow-derived macrophages (BMDMs) were generated from bone marrow cells collected from female 6-12 week-old C57BL/6NHsd mice (Envigo) and differentiated into macrophages for 5 days at 37°C and 10% CO_2 in 1g/L glucose DMEM (with L-glutamine, and sodium pyruvate) supplemented with 10% (v/v) FBS (Invitrogen) and 20% (v/v) L-929 mouse fibroblasts-conditioned medium in non tissue culture-treated Petri dishes. After 5 days, loosely adherent BMMs were washed with PBS, harvested by incubation in chilled cation-free PBS supplemented with 1g/l D-glucose on ice for 10 min, resuspended in complete medium and replated in 24-well tissue culture treated plates at a density of $5x10^4$ cell/well. BMMs were further incubated at 37°C under 10% CO_2 atmosphere for 72 h, replenishing with complete medium 48 and 24 h before infection.

Mice. Female C57BL/6 mice were purchased from Jackson Laboratories (Bar Harbor, ME) and were 8-10 weeks of age when enrolled in experiments. Animals were group-housed according to experimental group in HEPA-filtered laminar flow cages with cage enrichment and unrestricted access to sterile food and water in the vivarium of Harborview Medical Center. The vivarium is managed by the University of Washington Department of Comparative Medicine in compliance with all policies and regulations of the Office of Laboratory Animal Welfare of the Public Health Service. The facility is fully accredited by the American Association for Laboratory Animal Care. All experimental procedures were approved in advance by the University of Washington Institutional Animal Care and Use Committee.

Construction of Expression Plasmids. Heterologous expression in *E. coli* employed plasmid pET28b. To enable IPTG-inducible expression of *opiA* in this plasmid, the open reading frame of the gene was amplified using primers #5 and #6 (see supplemental table 1) from *F. novicida* genomic DNA and cloned into the NcoI and XhoI sites. The open reading frame of *legA5* was amplified from *L. pneumophilia* subsp *pneumophilla* genomic DNA using primers #9 and #10 and cloned into the NdeI and XhoI sites of pET28b. The H178A mutation of *legA5* was generated using SOE (primers #11 and #12).

The doxycycline repressible plasmid pCM190 was employed for yeast expression experiments [186]. The *opiA* reading frame was amplified from *F. novicida* genomic DNA using primers #13 and #14, and the control gene *mcm1* was amplified from *S. cerevisiae* genomic DNA using primers #15 and #16. Both genes were cloned separately into the NotI and BamHI sites of the plasmid. To generate the OpiA mammalian expression vector, the open reading frame of *opiA* was cloned in the XhoI and EcoRI sites of pMSCVpuro (Clontech) using primers #17 and #18. The H261A point mutation in OpiA was generated by SOE using primers #7 and #8, and was then cloned into *E. coli,* yeast and mammalian expression vectors using the same primers employed for the wild-type *opiA* allele.

Construction of Genetically Modified *F. novicida* Strains. For complementation or expression of GFP

in *F. novicida*, a miniTn7 system was used to integrate constructs ectopically, downstream of *glmS.* For complementation of OpiA, the *opiA* open reading frame plus the intergenic regions upstream (containing the native promoter for the gene) and downstream of the gene were amplified by PCR and cloned into the HindIII and BamHI sites of the mini-Tn7 integration vector pMP749 using primers #1 and #2 (Table S1) [187]. To generate GFP positive bacteria, the super-folder GFP open reading frame was cloned into pMP749. Subsequently, the constitutively active *bfr* promoter was cloned upstream of sfGFP [188].

To generate strains containing mini-Tn7 insertions, pMP749 constructs were first transformed into the plasmid compatible strain *F. novicida* MFN245 carrying the helper plasmid pMP720 [187]. Competent cells were prepared by growing overnight cultures of *F. novicida*, back-diluting 1:100 in 2 mLs TSBC, growing for 3hrs at 37˚C with shaking, harvesting by centrifugation and resuspending in 1mL Francisella transformation buffer (per liter; L-arginine. 0.4 g; L-aspartic acid 0.4 g; L-histidine, 0.2 g, DL-methionine, 0.4g; spermine phosphate, 0.04 g; sodium chloride, 15.8 g, calcium chloride, 2.94g; tris(hydroxymethyl) aminomethane 6.05g). 10 μg of the appropriate pMP749 vectors were added to prepared competent *F. novicida* MFN245 (pMP720), and the bacterial suspensions were then grown at 37˚C with shaking for 30min. Transformed cells were recovered by adding 2 mLs TSBC and followed by incubation at 37˚C with shaking for 3 hrs. Transformants were selected by plating on TSAC + 15 μg mL^{-1} kanamycin. Colonies were screen by PCR using primers #3 and #4. To move chromosomal insertions from *F. novicida* MFN245 to *F. novicida* U112, genomic DNA was prepared from appropriate MFN245 strains and 10 ng was used to transform competent U112, prepared as described above.

To generate deletion strains, previously generated deletion constructions [22] were transformed into competent U112 strains as described above. Resulting merodiploids were grown overnight in non-selective TSBC, diluted 1:100 into CDM containing 0.1% p-chlorophenylalanine (w/v) and allowed to grow to stationary phase. These cultures were streaked onto non-selective TSAC and resulting kanamycin sensitive colonies were screened for deletions by colony PCR.

Bioinformatic identification of OpiA Family Proteins. The protein sequence of OpiA was submitted to the EMBL-EBI HMMMER server Jackhmmer (https://www.ebi.ac.uk/Tools/hmmer/search/jackhmmer) for iterative BLAST searches against the Uniprot protein database [151]. Six iterations of hidden markov model BLASTs were performed. All identified bacterial proteins were then analyzed to determine if they contain the DxHxxN---IDH/F motif. In order to be considered an OFP, the two amino acid constellations had to be less than 25 residues apart; this criterion distinguished between OFPs and homologs of HipA, a protein kinase that contains the DxHxxN sequence but lacks a recognizable IDH/F [189].

Protein Expression and Purification. For protein expression, *E. coli* BL21 cells carrying pET28b expression plasmids were back diluted in 2xYT broth and grown at 37°C until the optical density at 600nM (OD_{600}) was equal to 0.5. Expression was induced by the addition of 1 mM IPTG and cultures were incubated for 18 hours at 18 °C with shaking. Cells were harvested post induction by centrifugation at 7,000 x g for 15 min and resuspended in buffer containing 20 mM Tris-HCl pH 7.5, 500 mM NaCl, 5mM imidazole, 1 mM AEBSF, 10 mM leupeptin, 1 mM pepstatin, 1 mM lysozome and 1mU benzonase. Cells were disrupted by sonication and cellular debris was removed by centrifugation at 45,000 x g for 45 min. His-tagged proteins were purified from lysates using a 1 mL HisTrap FF NI-TA cartridge on an AKTA FPLC purification system. Bound proteins were eluted using a linear imidazole gradient from 5 mM to 500 mM. The purity of each protein sample was assessed by SDS-PAGE and Coomassie brilliant blue staining, and fractions with high purity were used in biochemical and lipid binding assays.

Lipid Kinase Assays. Lipid kinase activity was measured using autoradiography to detect transfer of ^{32}P from [$\gamma^{32}P$]-ATP to phosphoinositide species in liposomes, separated by thin layer chromatography

(TLC). Liposomes were composed of either PI or PI(4,5)P_2 and phosphatidylserine (1:3, Promega V1711, V1701). In PI kinase activity and qualitative wortmannin inhibition screens, we employed 10 nM P110α, and 100 nM PIP5K1C, OpiA, OpiA^{H261A}, LegA5 and LegA5^{H170A}. In quantitative wortmannin inhibition assays, 1 nM P110α and 2 nM OpiA were employed. Reactions were started by the addition of ATP (subnanomolar [γ^{32}P]-ATP and 50 nM ATP) and $MgCl_2$ (2 mM). Kinase reactions were incubated at 25˚C for 20 or 10min, for qualitative or wortmannin titration experiments respectively, and then terminated by the addition 1M hydrochloric acid and at least 4x volume of a 1:1 solution of methanol and chloroform. For the wortmannin titration assays, wortmannin or an equivalent volume of DMSO was added to the protein and liposomes prior to the addition of ATP. Subsequent to reaction termination, a fraction of the non-aqueous portion of each sample was spotted on silica gel 60 TLC plates pretreated with oxylate. Lipid species were resolved in n-propanol:2M acetic acid (65:35) and the TLC plates were exposed to a phosphoscreen. Signal derived from [γ^{32}P]-labeled products was imaged with a Typhoon 9400 scanner. Densitometry analysis of the obtained images (ImageJ) was used to determine the percentage inhibition by wortmannin. Each kinase assay was repeated independently three times, with the exception of the wortmannin titration assay which was repeated twice.

PIP ELISA Assay. Assays were purchased from Echelon (K-3000, K-4000K, K1000s) and performed according to protocols supplied by the manufacturer. For the detection of PI(3)P, KBZ buffer was used during the kinase reaction (Echelon). Proteins were added at the following concentrations: p110α, 20 nM; PI4KB, 2nM; OpiA in the K-3000 assay, 100 μM; OpiA in the K-4000K and K1000s assays, 1 mM; OpiA^{H261A}, 1 mM. Absorbance at 405 nM was read using a Synergy H1 Hybrid Reader (Biotek). Two biological replicates, each with three technical replicates were performed for each assay. Measurements were initially normalized to protein concentration followed by normalization to the activity of the positive control (set to 100% relative activity). Data presented are the average of the two biological replicates.

Yeast Transformations. Plasmids were transformed into *S. cerevisiae* using the Lazy Bone transformation method [190] and plated on C-ura + 1 μg mL^{-1} doxycycline to repress expression of genes carried on pCM190 [186]. Plates were incubated at 25˚C for a minimum of 3 days before use in growth assays.

Yeast Growth Assay. Fresh transformants of *S. cerevisiae* were collect from C-ura + doxycycline plates and re-suspended in sterile water. Density of the suspensions was normalized to OD_{600}=1 and 10-fold dilutions generated in sterile water were plated on C-ura with and without 1 μg mL^{-1} doxycycline for repressing and inducing conditions, respectively. Plates were incubated at 25˚C and imaged after 5 days using a FluoroChemQ. Growth assays were repeated independently 3 times, each performed in duplicate.

Intramacrophage growth assays. 5 x 10^5 RAW264.7 cells were seeded without antibiotic in 24-well plates and incubated overnight at 37˚C. After ~16 hrs, the cells were washed and exposed to mid-log phase *F. novicida* at a multiplicity of infection (MOI) of 0.1. The infection was synchronized by centrifugation at 800 x g at 25˚C for 15 min followed by a 45 min incubation at 37°C. Following this incubation, cells were washed to remove extracellular bacteria, treated with gentamycin for 30 min, rinsed again and returned to 37˚C. At selected time points, cells were lysed by the addition of 0.1% (v/v) Triton X100 in PBS, then serially diluted in PBS and plated on TSAC for CFU enumeration. CFU counts from later time points were normalized to the number of CFUs obtained immediately post-infection. Additionally, averaged data from 2-3 biological replicates for each mutant strain were normalized to the average level of wild-type growth (set to 100%).

Secretion Assays. Overnight cultures of *F. novicida* grown in TSBC were washed and diluted to an OD_{600} of 0.1 in TSBC + 5% (w/v) potassium chloride to stimulate $T6SS^{ii}$ activity [41]. Cultures were grown at 37°C until OD_{600}=1 and then pelleted by centrifugation at 8,000 x g for 10 min. Supernatants were collected and centrifuged for a further 10min at 10,000 x g to remove any remaining bacterial cells. Proteins in resulting supernatant samples were concentrated using a 30kDa cutoff centrifugal filter unit (EMD Millipore) and then mixed 1:2 with SDS-PAGE sample loading buffer. Cell fractions were generated by re-suspending cells in buffer containing 500 mM $NaCl_2$, 50 mM Tris pH 7.5 and 10% (v/v) glycerol followed by mixing 1:2 with SDS-PAGE sample loading buffer. Secretion assays were repeated independently 3 times.

Western Blotting. Anti-OpiA serum was generated by injecting rabbits with purified OpiA-6xHis, and polyclonal anti-OpiA antibodies were purified by antigen affinity (GenScript). To detect α-OpiA, an anti-rabbit antibody conjugated to horse radish peroxidase (HRP, Sigma Aldrich, 1:5000) was employed. α-His-HRP conjugated primary (Qiagen, 1:2000) was used to detect purified LegA5-6xHis. Bacterial cell lysates were generated as described above for secretion assays. Samples in SDS-loading buffer were boiled at 95°C for 15 min, loaded at equal volumes to resolve using SDS-PAGE, then transferred to nitrocellulose membranes. Membranes were blocked in TBST (10 mM Tris-base pH 7.6, 150mM $NaCl_2$, and 0.1% w/v Tween-20) with 3% (w/v) bovine serum albumin (BSA) for 30 min at 24°C, followed by incubation with primary antibodies diluted in blocking buffer for 2hrs at 24°C. The blots were developed using Radiance HRP substrate (Azure Biosystems) and visualized using the Azure Biosystems c600. Representative images were assembled using Adobe Illustrator CC 2015.

Mouse infections. Mice were exposed to aerosolized bacteria in a whole-body aerosol exposure chamber, as described [191]. Briefly, stocks of each bacterial strain were grown to stationary phase at 37 °C in TSBC, diluted in 20% (v/v) glycerol, aliquoted, and stored at -80 °C. The post-freeze titer of each stock

was determined to be >6 x 10^8 CFU/ml when cultured on TSAC. For each experiment, aliquots of bacteria were thawed and diluted in PBS to 10^8 CFU/ml prior to nebulization. Cohorts of mice were exposed to aerosolized bacteria in a whole animal exposure chamber with a computer interface to control pressures and flows (Biaera Technologies, Hagerstown, MD). Bacterial aerosols were generated by mini-Heart nebulizers with a flow rate of 8 L/min at 40 psi. Dilution air was regulated at 11.5 L/min to maintain total chamber flow at 19.5 L/min during a 10-minute exposure. Actual bacterial deposition in each experiment was determined by quantitative culture of the homogenized left lungs of three sentinel mice euthanized immediately after completion of the aerosol exposure. The remaining mice were returned to their cages. Mice were observed and weighed daily. At serial time points after infection, mice were euthanized with pentobarbital, exsanguinated by cardiac puncture, and left lungs were harvested and homogenized in 1mL PBS. Serial dilutions were generated in PBS then plated on TSAC for quantification. N=10 mice per bacterial strain per time point were used over two independent experiments.

Lipid-binding assays. PIP Strips (Echelon) were utilized in lipid overlay assays according to the protocol supplied by the manufacturer. Briefly, membranes containing spotted lipid species were blocked for 1 hr with 3% (w/v) BSA in TBST. 10 μg of purified protein (either OpiA-6xHis or LegA5-6xHis) was added to the membrane in blocking buffer and incubated at 25 ˚C for 1 hr. Membranes were then washed 3x for 10 min in TBST and then incubated with α-His-HRP (Qiagen, 1:2000) for 1 hr. Membranes were again washed 3x prior to addition of Radiance HRP substrate (Azure Biosystems) and imaged using the Azure Biosystems c600. Each binding assays was independently performed twice for each protein.

Bio-layer interferometry. Binding of proteins to phosphoinositol species was measured and analyzed using Bio-layer interferometry with an Octet Red 96. Streptavidin biosensors (ForteBio) were equilibrated

in running buffer (500 mM NaCl, 50 mM Tris pH 7.5, 1 mM Tris(2-carboxyethyl) phosphine hydrochloride (TCEP), 0.05% Tween-20 (v/v) and loaded with 200 nM of biotin-labeled PI(3)P (Echelon). A duplicate sensor was run in buffer without lipid as a background binding control subtracted from experimental measurements. Binding assays were conducted at 30°C with shaking at 1000 rpm. The K_d of OpiA for PI(3)P was calculated by determining the kinetic fit of on and off rates for four protein concentrations (333, 111, 37, 12 nM) simultaneously using a 1:1 fit model. Data shown are a representative graph from one of two independent experiments.

Transfection and Immunofluorescence Staining of HeLa cells. $5x10^4$ HeLa cells were seeded on 12 mm coverslips, incubated 16hrs at 37°C, then transfected with pBABE-2xFYVE-mCherry [164], the appropriate pMSCVpuro vector, and pEGFP-mt target (in cells to be used for mitochondrial staining) using Lipofectamine 3000 according to the instructions from the manufacturer. 24hrs post-transfection, cells were gently washed x3 in PBS and fixed for 10min in 3% paraformaldehyde (v/v) in PBS at 37°C. Following fixation, coverslips were washed 3 additional times in PBS then incubated with 50 mM NH_4Cl in PBS for 10min to quench free aldehyde groups. Fixed cells were blocked and permeabilized in 10% (v/v) donkey or goat serum and 0.1% (v/v) saponin in PBS for 30min. Labeling was accomplished by inverting coverslips onto drops of the appropriate primary antibody diluted in blocking buffer and incubating at 25°C for 1 hour. Primary antibodies used were mouse α-Lamp1 (Abcam, 1:100), mouse α -EEA1 (Abcam, 1:50), rabbit α -calnexin (Cell Signaling Technologies, 1:50), rabbit α -pmp70 (Thermo Fisher, 1:100), and rabbit α -tgn46 (Abcam, 1:100). Samples were then incubated with a 1:500 dilution of the appropriate Alexa 488-conjugated secondary antibody (Invitrogen) for 45min in the dark. Coverslips were then washed twice with PBS + 0.1% (v/v) saponin, twice with PBS, and once in H_2O followed by mounting onto slides using ProLong Diamond Antifade Moutant with DAPI. For wortmannin treatment, 24hr post-transfection cells were incubated 2x for 20min with fresh complete DMEM + 800 nM wortmannin. Samples were then washed and processed

for immunofluorescence staining as described above. Confocal fluorescence microscopy was performed using a Leica TCS SP8X Microscope. Representative fluorescent confocal micrographs were acquired as 1024 x 1024 pixels images using a 63x/1.4 NA HC PL APO objective and assembled using ImageJ. To determine Pearson's correlation coefficients, confocal micrographs were acquired as 3064 x 3064 pixels images using a 40x/1.24 HC PL APO objective and Leica analysis software was utilized to analyze a minimum of 75 individual cells over three independent replicates.

Intracellular growth assays in transfected HeLa cells. 2 x 10^5 HeLa cells were seeded without antibiotic in 24-well plates, incubated at 37°C for ~16hrs, then transfected with either pCDNA3-eGFP-rab7_T22N or pCDNA3 (generated by cutting the rab7T22N plasmid with SalI and religating the empty vector) using Lipofectamine 3000 according to the instructions from the manufacturer [192]. 24hrs-post transfection, cells were washed and exposed to mid-log phase *F. novicida* at an MOI of ~10. Infections were otherwise conducted as described above in the intramacrophage growth assay section.

Lentivirus Transduction. Lentiviral transductions of BMDMs were performed using pLenti_CMV_neo-mCherry-2xFYVE [193] and the packaging plasmids pCMVdeltaR8.2 and pMD2.G (plasmids 12263 and 12259; Addgene) which were gifts from D. Trono (EPFL, Lausanne, France). Lentiviral supernatants were generated as follows: 2x10^6 HEK 293T/17 cells were seeded in 10 cm tissue culture dishes in 20ml medium and transfected after 24 h with a mix of 800 µl DMEM, 16 µg DNA (1:1:1 molar ratio of plasmids), and 48 µl FuGene® 6 following the manufacturer's protocol and incubated for 48 h prior to collection. Lentiviral supernatants filtered through a 0.45 µm filter were added to BMMs (2:5 ratio v/v), and lentiviral transduction proceeded for 72 h before BMM infections were performed.

Infection and Fluorescence microscopy of Primary Murine BMDMs. For BMDM infections, *F. novicida* strains were grown in Chamberlain's modified medium at 37 °C under shaking to an OD_{600} of

0.3-0.5, washed once in DMEM by centrifugation for 5 min at 6,000 x *g* at 15 °C, diluted to an MOI of 100 in complete medium and added to ice-chilled BMDMs in 24-well plates. Bacteria were centrifuged onto BMDMs at 400 x *g* for 10 min at 4°C and plates were immediately placed on a 37 °C water tray in a CO_2 incubator to rapidly initiate synchronized uptake. Samples were collected at indicated times post-infection for immunofluorescence analysis. For time points later than 30 min post infection, extracellular bacteria were removed at 30 min post-infection by 3 washings in pre-warmed DMEM followed by replenishing with complete medium, in order to avoid continued, asynchronous bacterial uptake.

mCherry-2xFYVE-expressing BMDMs seeded onto 12 mm glass coverslips and infected with GFP-expressing *F. novicida* strains were washed 3 times in 1 x PBS at specific times post infection and fixed in 3% (v/v) paraformaldehyde (EMD) in 1 x PBS for 10 min at 37°C. For LAMP1 staining, coverslips were processed as described above. Coverslips were then washed 3 times in 1 x PBS, rinsed in distilled H_2O, and mounted on glass slides in Mowiol (Calbiochem). Samples were viewed with a Leica DM4000 epifluorescence upright microscope for quantitative analysis or a Leica SP8 confocal laser-scanning microscope for image acquisition. Representative confocal micrographs of 1024 x 1024 pixels were acquired and assembled using Adobe Photoshop CS6. Data shown represent the average of three biological repeats.

Quantitative and Statistical Analysis. Statistical analysis was performed using GraphPad Prism 7 software. Results are presented as means ± standard deviation, except for Pearson correlation coefficients which are presented as means ± standard measure of error. Statistical significance between treatment groups was determined using either an unpaired, two-tailed Student's *t*-test, or for group analysis, using either two-way analysis of variance (ANOVA, on log-transformed data) with Tukey's multiple-comparison test or one-way ANOVA with Dunnett's multiple-comparison test. The values for N and the definition of N for each experiment is provided in the relevant methods section; statistical analyses performed for each experiment is indicated in appropriate figure legends. No particular method was used to determine whether the data met assumptions of the statistical approach.

2.6 Figures

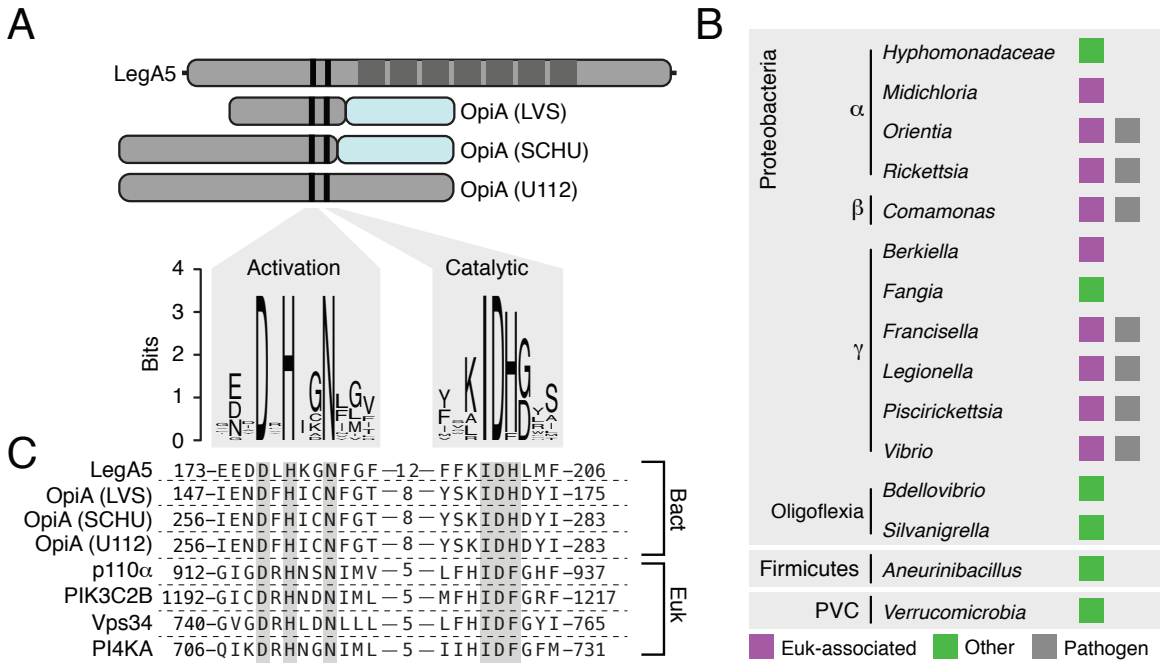

Figure 2.1. OpiA and related bacterial proteins share conserved motifs with eukaryotic PI kinases. (**A**) Overview of conserved sequence motifs found in OFPs. Graphical representations of OpiA orthologous proteins from *F. tularensis* subsp *novicida, tularensis* and *holarctica,* and the *Legionella pneumophila* OFP LegA5. Conserved residues (black), portions of the gene encode by a separate ORF (blue) and ankyrin repeats in LegA5 (dark grey) are highlighted. Sequence logo indicates conserved catalytic motifs derived from an alignment of OFP sequences from bacterial species representative of the genera shown in panel B (alignment shown in Figure 2.2). (**B**) Bacterial genera found to contain OFPs, grouped by class and phylum and with lifestyle indicated by box colors (eukaryotic-associated, purple; pathogen, grey; other, green). (**C**) Alignment depicting the residues shared between OFPs and the indicated human PI3K and PI4K enzymes (Bact, bacterial; Euk, eukaryotic).

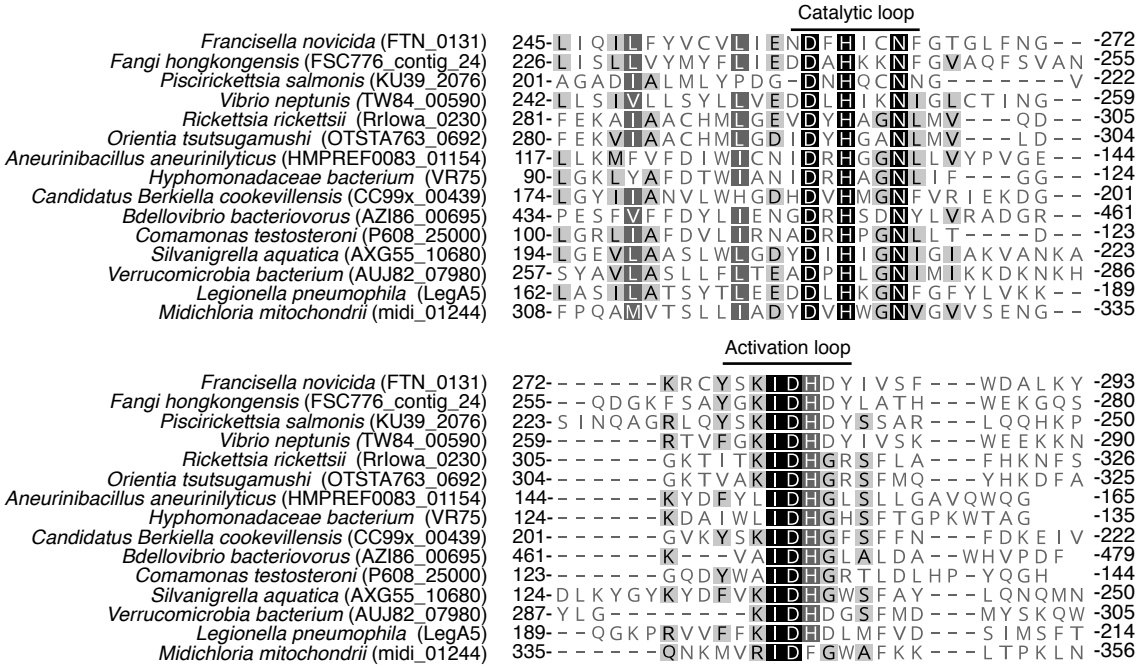

Figure 2.2. OFPs possess two conserved amino acid motifs.
Partial alignment of OFP sequences from species representative of each OFP-containing genus, highlighting the two conserved motifs (perfectly conserved residues, black; highly conserved residues, dark grey; conserved residues, light grey).

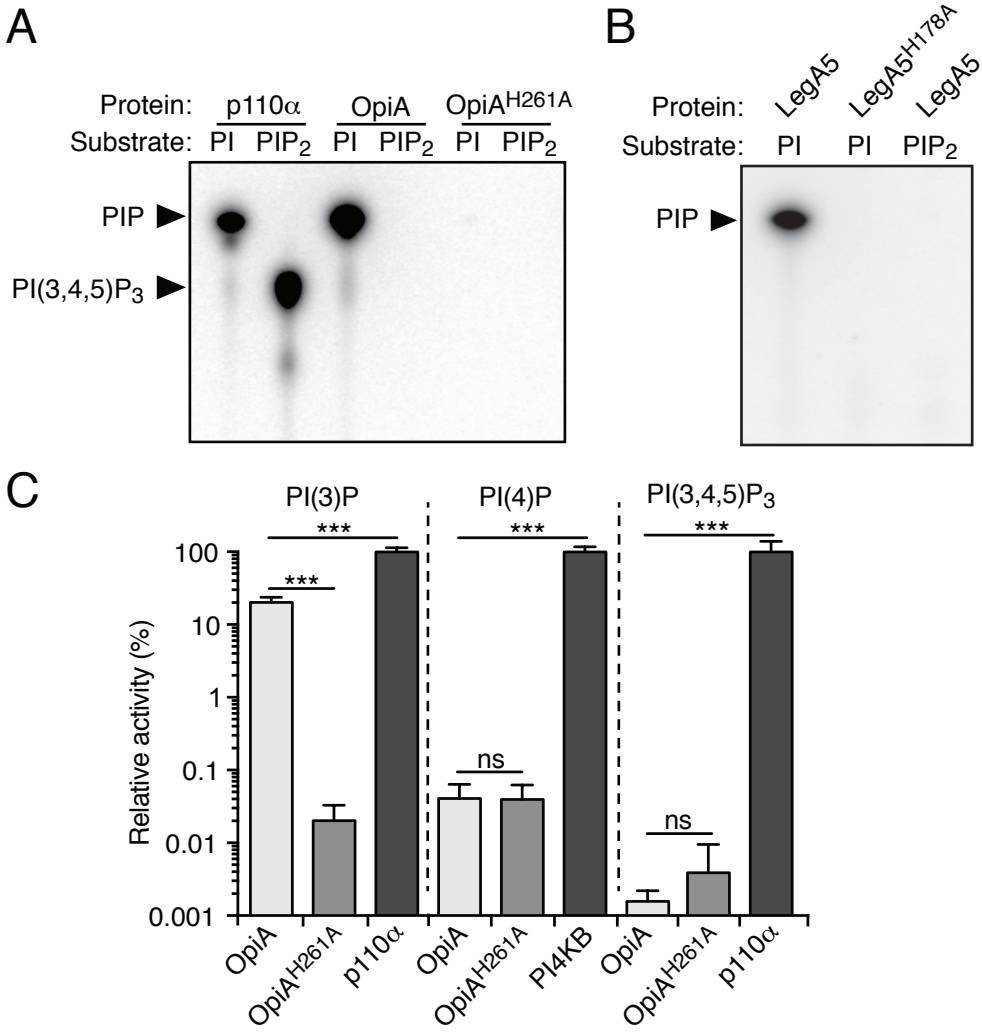

Figure 2.3. OpiA and LegA5 are class III-like phosphatidylinositol 3-kinase enzymes.
(**A and B**) Autoradiographs of thin layer chromatography (TLC)-separated lipid products produced by incubating the denoted proteins with [γ^{32}P]-ATP and the indicated lipid substrates. (**C**) Quantification of PIP species generated from incubating the indicated proteins with solubilized derivatives of PI (left and middle panels) and PIP_2 (right), normalized to activity of control proteins for each reaction (dark grey). Data presented as mean values ± s.d. Asterisks represent statistically significant differences (Student's t-test; ***$p \leq 0.0001$).

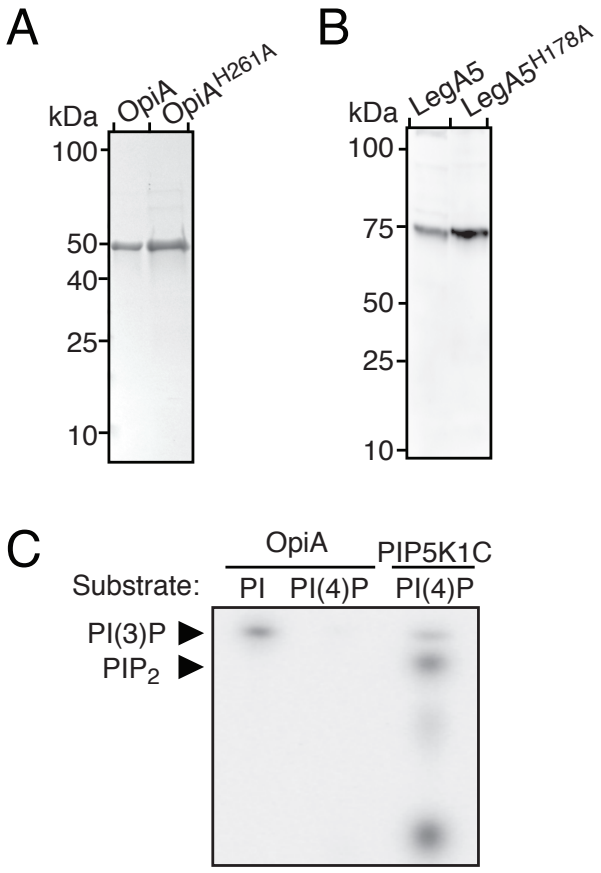

Figure 2.4. Catalytic point mutations do not destabilize OpiA and LegA5 and OpiA does not phosphorylate PI(4)P lipid substrate.
(**A**) Coomassie brilliant blue staining of purified OpiA and OpiA^{H261A}. (**B**) Western blot analysis of purified LegA5 and LegA5^{H178A}. (**C**) Autoradiograph of TLC analysis of the lipid products produced by incubating the indicated proteins with [γ^{32}]-ATP and the indicated lipid substrate.

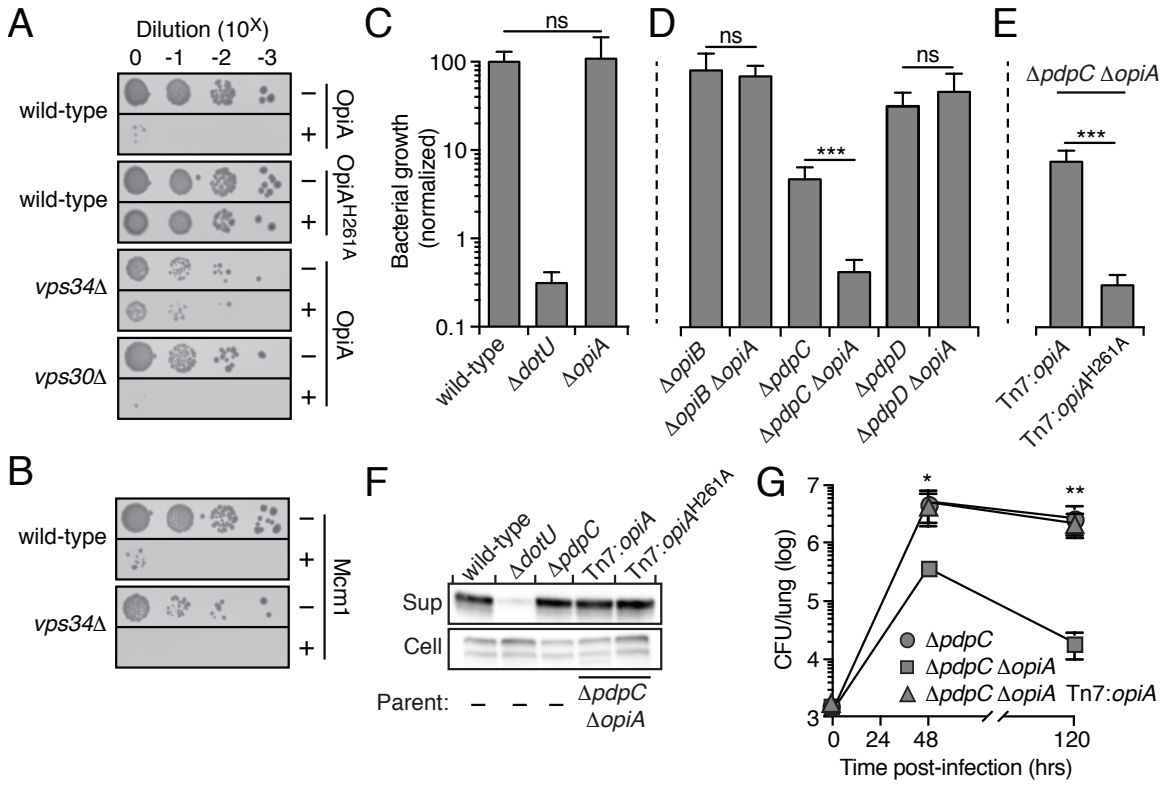

Figure 2.5. The PI3K activity of OpiA leads to toxicity when expressed in yeast and contributes to *F. novicida* growth *in vivo.*

(**A and B**) Growth resulting from serial dilution of the indicated yeast strains carrying plasmids to express the noted OpiA alleles (**A**) or Mcm1 (**B**) plated on inducing (+) or non-inducing (-) media (**C-E**) Growth at 24hrs of the indicated strains of *F. novicida* in RAW 264.7 cells, normalized to level of growth by the wild-type strain (100%). Data are shown as the mean ± s.d. Asterisks represent statistically significant differences (Student's t-test; ***p ≤ 0.0001). (**F**) Western blot analysis of OpiA or OpiA^{H261A} in the supernatant (sup) and cellular (cell) fractions of the indicated strains of *F. novicida* grown in the presence of 5% (w/v) potassium chloride. (**G**) Quantification of the bacterial burden in the lungs of mice infected via aerosolization with the indicated strains of *F. novicida.* Data are shown as the mean ± s.d. and asterisks represent statically significant differences (ANOVA; *p ≤ 0.05, **p ≤ 0.001).

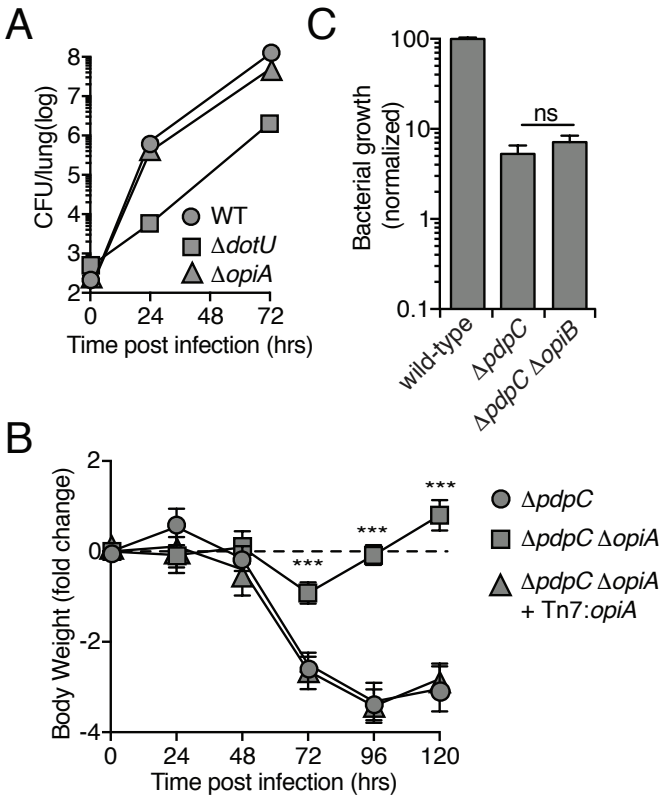

Figure 2.6. Phenotypic characterization of selected *F. novicida* mutants containing deletions of genes encoded secreted effectors.
(**A**) Bacterial burden in the lungs of mice infected via the aerosol route with the indicated strains of *F. novicida.* (**B**) Change in body weight over time of mice infected by the aerosol route with indicated strains of *F. novicida*. (**C**) Growth at 24hrs of the indicated strains of *F. novicida* in RAW 264.7 cells, normalized to level of growth by the wild-type strain (100%). Data in A-C is shown as the mean ± s.d. and asterisks represent statically significant differences (Student's t-test; ***$p \leq 0.0001$).

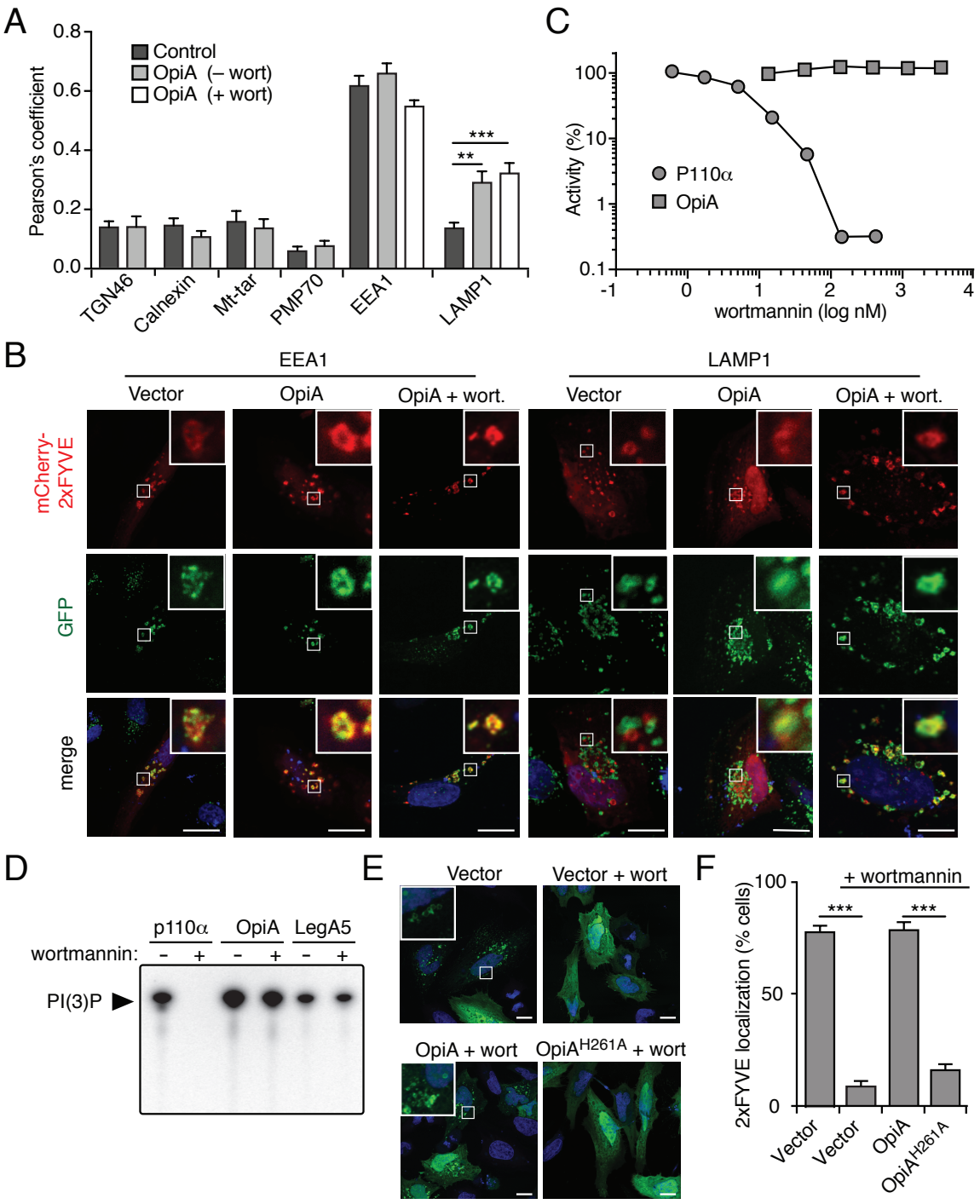

Figure 2.7. OpiA is a wortmannin-insensitive PI3K that generates PI(3)P on endosomes.
(**A**) Pearson correlation coefficients indicating degree of co-localization between PI(3)P probe 2xFYVE-mCherry and markers for the Golgi network (TGN46), endoplasmic reticulum (calnexin), mitochondria (Mt-tar), and peroxisomes (PMP70) in HeLa cells co-transfected with an empty plasmid or a plasmid expressing OpiA, with or without wortmannin (wort) treatment (mitochondria: cells co-transfected to express GFP-labeled mitochondrial targeting sequence (Mt-tar); all other compartments: immunofluorescence with antibodies for indicated proteins). Data are shown as the mean ± SEM and

asterisks represent statically significant differences (Student's t-test; **p ≤ 0.001, ***p ≤ 0.0001). (**B**) Representative immunofluorescence fluorescent images of HeLa cells expressing 2xFYVE-mCherry, cotransfected with vectors expressing OpiA (or empty vector control) and stained for EEA1 or LAMP1(green), with or without wortmannin treatment. Insets depict 6-fold magnification of boxed regions. Scale bar, 10 μm. (**C**) Quantification of the PI3K activity of p110α and OpiA treated with the indicated concentration of wortmannin. Activity normalized to non-wortmannin treated samples (set to 100% relative activity). (**D**) Autoradiographs of thin layer chromatography (TLC)-separated lipid products produced by incubating the denoted proteins with [γ^{32}P]-ATP, PI, and 300 nM wortmannin (+) or DMSO (-). (**E**) Representative fluorescence images of HeLa cells co-transfected with plasmids expressing GFP-2xFYVE and the indicated genes (or empty vector control) for 24hrs followed by treatment with 800 nM wortmannin or a DMSO control for 40min. Insets represent 6-fold magnification of boxed regions. (**F**) Proportion of HeLa cells transfected with the indicated plasmids in which GFP-2xFYVE localized to vesicle-like structures. A minimum of 100 cells over two biological replicates were imaged for quantification and the data are shown as the mean ± s.d. Asterisks represent statistically significant differences (Student's t-test; ***p ≤ 0.0001).

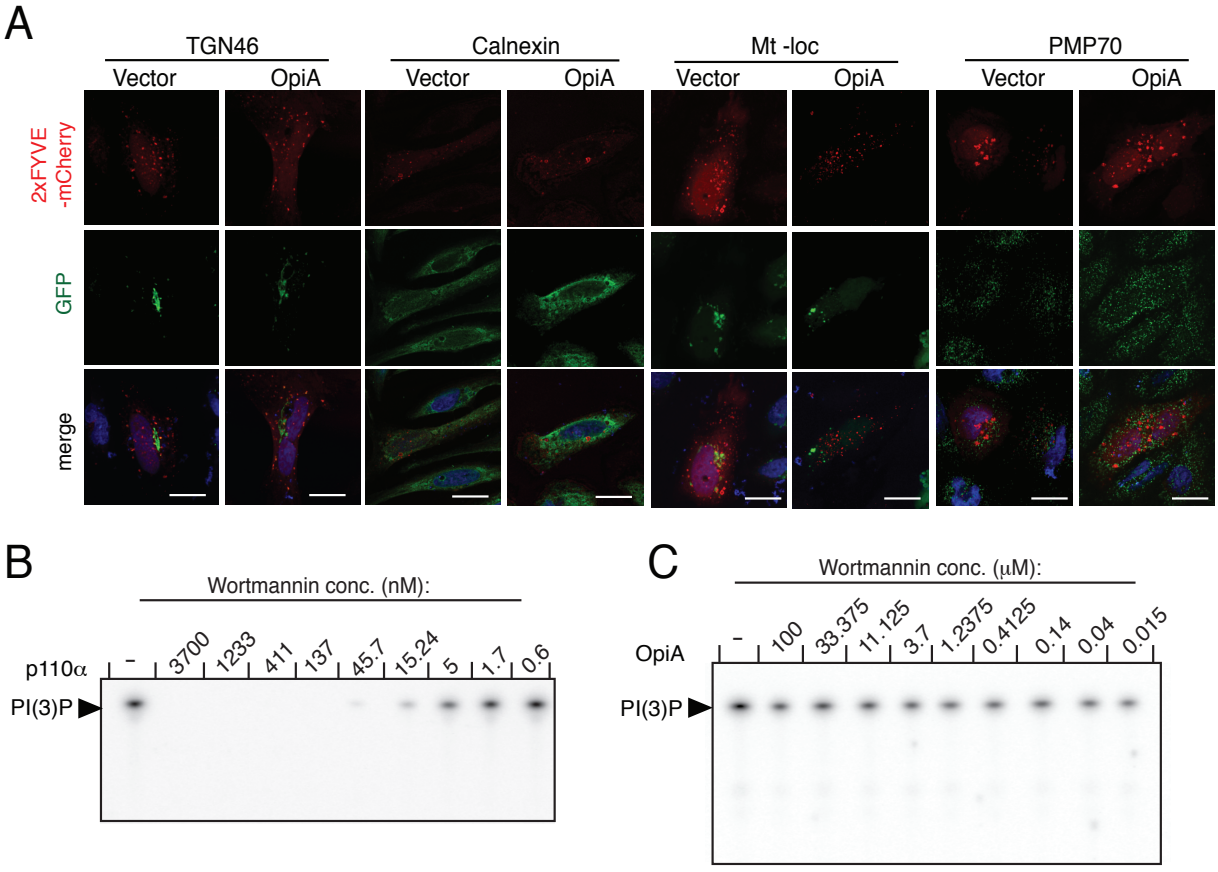

Figure 2.8. Further evidence OpiA is a wortmannin-insensitive PI3K that generates PI(3)P on endosomes.
(**A**) Representative fluorescent images of HeLa cells expressing mCherry-2xFYVE, cotransfected with vectors expressing the indicated proteins and stained (green) for the indicated markers (TGN46, Calnexin and PMP70, immunofloursence; mitochondria, co-transfection to express GFP-labeled mitochondrial targeting sequence). Scale bar, 10 μM. (**B and C**) Autoradiograph of TLC analysis of the lipid products produced by incubating the indicated proteins with [γ32]-ATP, PI-containing liposomes and wortmannin at the designated concentrations.

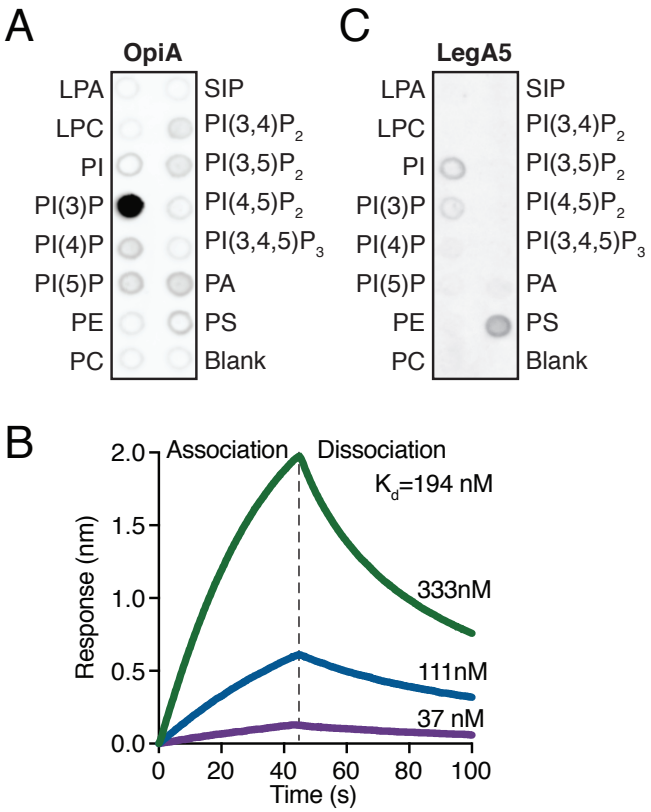

Figure 2.9. OpiA binds PI(3)P specifically and with high affinity.
(**A**) Measurement of the specific lipid binding capacity of purified OpiA-His_6, determined by a lipid-overlay assay and α-His detection of the protein. (**B**) Bio-layer interferometry (BLI)-based quantification of the PI(3)P binding capacity of OpiA. The binding kinetics for three concentrations of OpiA with PI(3)P are shown (333nM, green; 111 nM, blue; 37 nM, purple). (**C**) Measurement of the specific lipid binding capacity of purified His_6-LegA5, determined by a lipid-overlay assay and α-His detection of the protein.

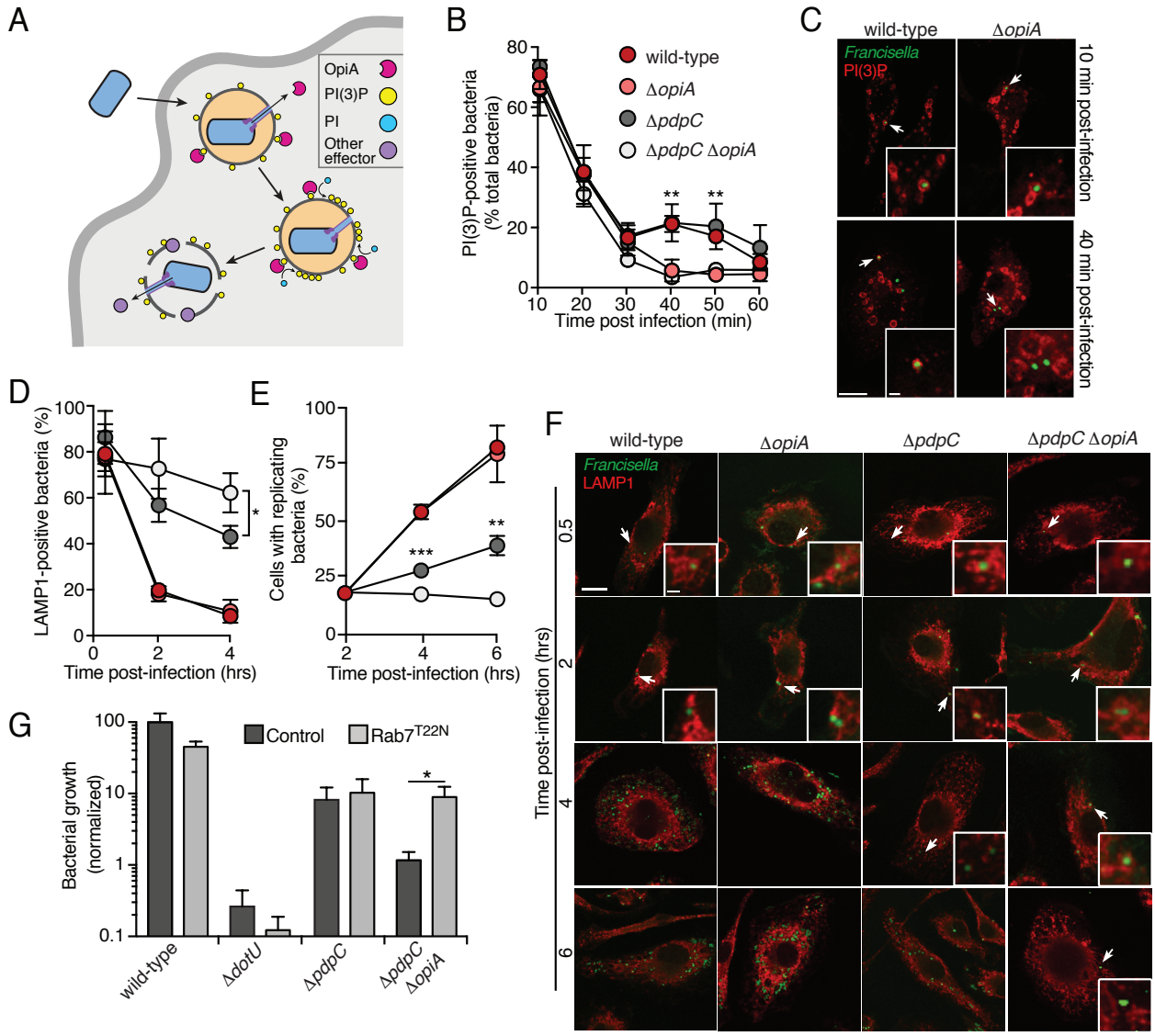

Figure 2.10. OpiA-mediated alterations to phagosomal trafficking contributes to intracellular growth of *F. novicida.*

(**A**) Model depicting localization and hypothesized role of OpiA during intracellular replication. OpiA exported by the T6SS^{ii} binds to PI(3)P on the cytosolic face of the FCP, and facilitates accumulation of additional PI(3)P through phosphorylation of PI. We speculate that FCP lysis is then promoted by additional effectors secreted by the T6SS^{ii}. (**B**) Proportion of *F. novicida* cells that co-localize with the PI(3)P probe mCherry-2xFYVE at the indicate times post infection of primary murine BMDMs. Data represent means ± s.d. of three independent experiments. Asterisks represent statistically significant differences (Two-way ANOVA with Sidak's correction for multiple comparisons; **p ≤ 0.001). (**C**) Representative images acquired at 10 and 40 min post-infection of the experiment described in (B) (PI(3)P, (red); GFP-expressing bacteria, green). Insets represent 2.3-fold magnification of the regions indicated by arrows. Scale bars, 10 μm and 1 μm (insets). (**D**) Proportion of *F. novicida* cells that co-localize with the late endosomal marker LAMP1 at the indicated times post infection of primary murine BMDMs. Colors indicate strains tested as in panel B. Data represent means ± s.d. of three independent experiments. Asterisks represent statistically significant differences (One-way ANOVA with Tukey's correction for multiple comparisons; *p < 0.05). (**E**) Proportion of infected macrophages that contained

replicating bacteria (greater than 5 bacteria/cell) at the indicated times post-infection of primary murine BMDMs. Colors indicate strains tested as in panel B. Data represent means ± s.d. of three independent experiments. Asterisks represent statistically significant differences (One-way ANOVA with Tukey's correction for multiple comparisons; **$p \leq 0.001$, *** $p \leq 0.0001$). (**F**) Representative images acquired at indicated time post-infection of the experiment described in (D) and (E) (PI(3)P, (red); GFP-expressing bacteria, green). Insets represent 3-fold magnification of the regions indicated by arrows. When >5 bacteria present in cytosol, insets are not included. Scale bars, 10 μm and 1 μm (insets). (**G**) Intracellular growth (16hrs post-infection) of the indicated *F. novicida* strains infecting HeLa cells transfected with empty vector or a construct to express $Rab7^{T22N}$. Data represent means ± s.d. Asterisks indicate statistically greater replication in experimental treatments compared to vector-only controls (Student's t-test; *$p \leq 0.05$).

Oligonucleotides		
#1: 5’-AGCATCACGTAAGCTTAGCTTAATTTTATAAGAATGTTTTCTGGATTTG-3’	This paper	N/A
#2: 5’-TCAGTAACGGATCCTCCTAGTGGTATGTCTTATAAATAAGATTATAG-3’	This paper	N/A
#3: 5’-GATAATAGTATTGTGCTAGAGTTAGATGCAGGAC-3’	This paper	N/A
#4: 5’CATAAGTCCACAAAGAACTTGGATGCTTATTTCC-3’	This paper	N/A
#5: 5’-TCAGTAACCCATGGGCAAAAATTTTGAAGTAATACGCAAAGATTTTC-3’	This paper	N/A
#6: 5’-TCAGAAATCTCGAGATTCAACAAATTACACAAATGAGAAAATC-3’	This paper	N/A
#7: 5’-GTACCAAAATTACAGATAGCAAAATCATTTTCTATTAACACACAAACATAAAATAAAATTTGTATTAGTC-3’	This paper	N/A
#8: 5’-GTTAATAGAAAATGATTTTGCTATCTGTAATTTTGGTACAGGACTATTTAATGGAAAG-3’	This paper	N/A
#9: 5’ TCAAGTACTACATATGCCTAGAGTTTATAATCTTAAAGATATTTATCTGG-3’	This paper	N/A
#10: 5’-TCAGTAACCTCGAGTTAGATTTTATTCTTTGATAGTGATATATCCAAAAAGACATTATCC-3’	This paper	N/A
#11: 5’-TCCCTTTAGCCAAATCGTCTTCTTCCAAAG-3’	This paper	N/A
#12: 5’-AGACGATTTGGCTAAAGGGAATTTTGGTTTTTATTTG-3’	This paper	N/A
#13: 5’-TCAGTAACGGATCCATGAAAAATTTTGAAGTAATACGCAAAGATTTTC-3’	This paper	N/A
#14: 5’-TCAGAAATGCGGCCGCTCAATTCAACAAATTACACAAATGAGAAAATC-3’	This paper	N/A
#15: 5’-AGAATCAGTGGATCCATGTCAGACATCGAAGAAGGTACGC-3’	This paper	N/A
#16: 5’-CTGAAAGATAGCGGCCGCTTAGTATTGGCCTTGTTGCGGTTC-3’	This paper	N/A
#17 5’-ACATGATGCCTCGAGGCCACCATGAAAAATTTTGAAGTAATACGCAAAGATTTTC-3’	This paper	N/A
#18: 5’CTACCCGGTAGAATTCTTAATTCAACAAATTACACAAATGAGAAAATC-3’	This paper	N/A

Table 2.1. Oligonucleotides used in this study.

Chapter 3: Tn-Seq reveals hidden complexity in the utilization of host-derived glutathione in *Francisella tularensis*

Published as: Ramsey K.M.[†], Ledvina H.E.[†], Tresko T.M., Wandzilak J.M., Tower C.A., Tallo T., Schramm C.E., Peterson S.B., Skerrett S.J., Mougous J.D. and Dove S.L. (2020). *PLoS Pathogens,* 16(6): e1008566.

[†]Authors contributed equally to this work

3.1 Abstract

Host-derived glutathione (GSH) is an essential source of cysteine for the intracellular pathogen *Francisella tularensis*. In a comprehensive transposon insertion sequencing screen, we identified several *F. tularensis* genes that play central and previously unappreciated roles in the utilization of GSH during the growth of the bacterium in macrophages. We show that one of these, a gene we named *dptA*, encodes a proton-dependent oligopeptide transporter that enables growth of the organism on the dipeptide Cys-Gly, a key breakdown product of GSH generated by the enzyme γ-glutamyltranspeptidase (GGT). Although GGT was thought to be the principal enzyme involved in GSH breakdown in *F. tularensis*, our screen identified a second enzyme, referred to as ChaC, that is also involved in the utilization of exogenous GSH. However, unlike GGT and DptA, we show that the importance of ChaC in supporting intramacrophage growth extends beyond cysteine acquisition. Taken together, our findings provide a compendium of *F. tularensis* genes required for intracellular growth and identify new players in the metabolism of GSH that could be attractive targets for therapeutic intervention.

3.2 Introduction

Francisella tularensis is a facultative intracellular pathogen and the etiological agent of the disease tularemia, which can be fatal if left untreated [1]. Four subspecies of *F. tularensis* have been recognized (*tularensis*, *holarctica*, *mediasiatica* and *novicida*) which possess differential host ranges and cause disease with varying degrees of morbidity and mortality [2, 4]. While *F. tularensis* is capable of replicating in a variety of cell types, growth within macrophages is believed to be the primary mediator of disease [6, 7]. However, the precise virulence mechanisms employed for intracellular proliferation are largely uncharacterized.

F. tularensis initially enters cells through the endosomal pathway but must escape this degradative compartment to replicate within the cytoplasm. Perhaps the best characterized virulence factor utilized by *F. tularensis* is the type VI secretion system subtype 2 (T6SS^{ii}) pathway encoded by

genes present on the so-called *Francisella* pathogenicity island (FPI) [23, 143]. This system has been demonstrated to secrete a set of effector proteins which mediate escape into the cytoplasm [22, 43, 194]. Additional factors known to be important for growth in host cells include many metabolic pathways, including those involved in purine biosynthesis and branched-amino acid utilization [195, 196].

One host-derived metabolite that is essential for the intramacrophage growth of Francisella is the low molecular weight thiol glutathione (GSH; γGlu-Cys-Gly). *Francisella* is a cysteine auxotroph and GSH is a necessary source of cysteine for intracellular replication [112, 180]. This molecule is found at high concentrations (1-10 mM) in the cytoplasm of macrophages, as well as many other eukaryotic cells [113, 180]. Existing literature suggests that the principal enzyme responsible for initiating degradation of GSH in *Francisella* is γ-glutamyl transpeptidase (GGT), which cleaves this tripeptide into glutamate and the dipeptide Cys-Gly [112, 114]. However, this is only the presumed first step of GSH utilization and the role of other factors that work in concert with GGT to facilitate GSH utilization has not been addressed. Moreover, *Francisella* encodes a member of the ChaC family of proteins which have been shown to contribute to the breakdown of GSH in eukaryotes [36, 116, 117]. Whether *Francisella* employs enzymes that act in parallel with GGT to breakdown GSH was not known.

While several screens have been employed to identify genes important for the intracellular replication of multiple *F. tularensis* subspecies [83, 85-90, 197-200], a comprehensive description of genes that are specifically required for the intramacrophage growth of this organism has been lacking. Here, we used transposon insertion sequencing (Tn-Seq) to identify the genes that are required for the intracellular growth of the live vaccine strain of *F. tularensis* (LVS). We leveraged the hits of our screen to define a unique pathway for the catabolism of GSH in Francisella. This pathway includes a promiscuous proton-dependent dipeptide transporter responsible for the import of Cys–Gly and a ChaC-family enzyme that can function alongside GGT to scavenge cysteine from GSH. Our work reveals unexpected complexity in the utilization of GSH by *Francisella* and provides a comprehensive catalog of genes required for the intracellular growth of this pathogen.

3.3 Results

3.3.1 *Characterization of a highly saturated transposon insertion library for Tn-Seq*

The ability of *F. tularensis* to cause disease is dependent principally upon its ability to grow within macrophages (reviewed in [2, 3, 53]). Although a number of genetic screens have been performed in several subspecies to identity genes required for this function [83, 85, 87, 88, 90], a consensus as to the bacterial requirements for intramacrophage growth remains lacking. To comprehensively identify *Francisella* genes critical for growth and survival within macrophages, as well as for growth *in vitro*, we created a saturated library of transposon insertion mutants in the live vaccine strain of *F. tularensis* (LVS) for use in transposon insertion sequencing (Tn-Seq) experiments. In order to use the insertion sequencing (INSeq) method of transposon insertion identification [201], we modified a previously used mariner transposon, which specifically inserts into TA dinucleotides [202]. Using the modified transposon encoding kanamycin resistance, we mutagenized LVS six independent times and combined approximately 800,000 kanamycin-resistant colonies into a single library.

We determined which genes are critical for *in vitro* growth by growing cells of the transposon mutant library on solid media and using extracted genomic DNA to specifically amplify bacterial transposon-chromosome junctions. Through this approach we identified 155,565 unique insertion events in our mutant library, corresponding to 74.6% of all the potential TA insertion sites (208,625) and one insertion event approximately every 12 bp (Fig 3.1A). To assess saturation of the mutant library at the individual gene level, we determined the percentage of TA sites in each gene with identified insertions. About 20% of genes had insertions in fewer than 10% of TA sites, suggesting these genes are essential under these growth conditions. In contrast, we could identify insertions in 90% or more of the TA sites for the majority of genes (73%), as would be expected for nonessential genes. The strong bimodal distribution of the percentage of TA sites disrupted per gene indicates that the library is highly saturated, as this distribution provides evidence that TA sites only lack an insertion when a transposon at that site would disrupt an essential function (Fig. 3.2B). In comparison, the prior most saturated transposon library

used to screen for genes important for the intracellular replication of *Francisella* contained ~15,000 mutant clones (approximately one-tenth of the number of unique insertions in our mutant library) and use of the transposon site hybridization (TraSH) methodology precluded an assessment of the total number of unique insertions [198]. We used ARTIST, which determines essential genetic regions using a hidden Markov model [203], to identify 481 essential genes as well as 61 genes specifying proteins with both essential and non-essential domains (Fig. 3.2A and Appendix 1).

3.3.2 *Tn-Seq identifies genes and pathways critical for intramacrophage replication*

In order to define LVS genes critical for intramacrophage growth, we infected J774A.1 murine macrophage-like cells with our transposon mutant library (with macrophages in ~80-fold excess of the complexity of our mutant library). After twenty-four hours, macrophages were lysed, and bacterial genomic DNA was extracted for library construction. Using Con-ARTIST [203] to compare a sample of the inoculum to the mutants that survived within macrophages, we identified 142 genes that were important for intramacrophage survival (Fig. 3.1C and Appendix 2). Several lines of evidence indicate that our Tn-Seq-based screen for genes important for intramacrophage growth was unbiased and comprehensive.

With regard to bias, if our infection conditions, isolation of bacterial genomic DNA from macrophages, or sequencing depth of recovered bacterial DNA generated a bottleneck, we would expect stochastic loss of transposon insertions in genes non-essential for intramacrophage growth. However, we did not identify a shift in insertion saturation in non-essential genes following growth of our mutant library in macrophages, strongly suggesting the lack of a bottleneck (Fig. 3.2B). Instead, the TA insertion saturation remained strongly bimodal, consistent with recovery of essentially all mutants that were not defective for growth in macrophage. The comprehensive nature of our screen is highlighted by our identification of all thirteen genes encoding purine biosynthesis enzymes as either critical for survival *in vitro* or critical for growth or survival within macrophages (Fig. 3.3). Purine biosynthesis is critical for *F. tularensis* intramacrophage survival, yet prior screens had individually identified only up to eight genes in

this pathway as important for the process [83, 85-90, 197-200]. In addition, the gene encoding PigR, a transcription regulator critical for intramacrophage growth and virulence [202], was a strong hit in our screen despite its small size (336bp) and previous lack of identification in other unbiased screens for factors important for intramacrophage growth or virulence (Fig. 3.1C, Appendix 2). Finally, our screen identified ~68% of the genes previously ascribed importance for growth in the J774 murine macrophage cell line [83] while also revealing 89 additional genes as being critical for this process.

The ability of *F. tularensis* to grow within macrophages is dependent upon several nutrients that are derived from the host [91, 194, 204]. Prominent amongst these is GSH, a tripeptide whose catabolism provides a source of cysteine that *F. tularensis* requires for growth [112] [13]. Consistent with previous findings, our screen identified ggt, which encodes a γ-glutamyl transpeptidase, as important for intramacrophage growth (Fig. 3.1C, E and Appendix 2) [112]. The GGT enzyme mediates the first step in the breakdown of GSH, generating glutamate and the dipeptide Cys-Gly [28]. The *F. tularensis* enzyme contains a strongly predicted Sec signal sequence, suggesting that it localizes to the periplasm (Fig. 3.4). We therefore reasoned that utilization of Cys-Gly as a source of cysteine may require the action of a transporter that shuttles Cys-Gly from the periplasm to the bacterial cytoplasm where Cys-Gly could be broken down further to individual amino acid components. Moreover, we reasoned that the gene specifying a Cys-Gly peptide transporter would be amongst those we identified as essential for intramacrophage growth using Tn-Seq (Appendix 2).

3.3.3 *Identification of a putative Cys-Gly transporter*

A top hit from our *in vivo* Tn-Seq screen was FTL_1251, which encodes a putative proton-dependent oligopeptide transporter (POT) (Fig. 3.1D, 3.5A, Fig 3.6A and Appendix 2). This group of transporters are part of the major facilitator superfamily and are characterized by the presence of 12-14 transmembrane domains, a signature motif of charged proton-binding residues within a transmembrane domain (ExxERF), and two PTR2 domains [205]. Each of these motifs was identified in FTL_1251 (residues 24-32, 72-96, and 153-167, respectively) and this protein contains 14 predicted transmembrane

domains (Fig. 3.5B). POT proteins often transport multiple peptides across the inner membrane, though these are generally related in sequence and chemical properties [206-208]. LVS is predicted to encode eight POT proteins; however, only FTL_1251, henceforth referred to as DptA, was hit in our screen (Appendix 2). As no other putative peptide transporters were hit in our screen, we hypothesized DptA contributes to intracellular growth of *F. tularanesis* by acting within the GGT pathway for GSH catabolism.

As a first step toward characterizing DptA, we probed its contribution to colonization of mice following infection by the aerosol route. Consistent with our Tn-Seq screen, disruption of *dptA* resulted in significantly reduced proliferation within the lungs, as well as lowered dissemination to distal organs (Fig. 3.5C, D). The observed in vivo defects could be complemented by ectopic expression of *dptA* from the Tn7 attachment site on the LVS chromosome. With the confirmation that the predicted transporter contributes to virulence, we set out to determine if DptA plays a role in GSH metabolism.

To evaluate the contribution of DptA to GSH metabolism, we measured the growth of the LVS *dptA*(-) strain in Chamberlain's defined media (CDM) containing a panel of cysteine-containing peptides. We also tested a strain of LVS in which we deleted the gene encoding GGT (LVS Δ*ggt*), which was previously shown to be essential for the growth of LVS with GSH provided as a sole source of cysteine [112]. Indeed, we found that in LVS, GGT is required for growth on GSH and γGlu-Cys, but not on cysteine or Cys-Gly (Fig. 3.5E-G). Moreover, as expected, the in vitro growth defects of the LVS Δ*ggt* mutant strain in media supplemented with either GSH or γGlu-Cys could be complemented by ectopic expression of *ggt* from the Tn7 attachment site on the LVS chromosome (Fig 3.5E-G). On the contrary, cells lacking DptA show no detectable growth on GSH or Cys-Gly and proliferate similarly to cells of the wild-type strain in the presence of γGlu-Cys (Fig. 3.5E-G and Fig. 3.6A, B). Furthermore, the *in vitro* growth defects of the LVS *dptA* mutant strain in media supplemented with either GSH or Cys-Gly could be complemented by ectopic expression of *dptA* from the Tn7 attachment site (Fig. 3.5 E-G). These data suggest that DptA is required for the transport of Cys-Gly. Further, they suggest that under the conditions

of our *in vitro* growth assays, GGT and DptA constitute the single pathway for GSH degradation as well as transport of the resulting Cys-Gly breakdown product.

3.3.4 *DptA is a promiscuous transporter that aids in cysteine acquisition during intramacrophage growth*

To more definitively characterize the role of DptA in LVS, we turned to assays measuring the cellular uptake of radiolabeled GSH (^{3}H-glycine GSH (^{3}H-GSH)). Cells of the LVS Δ*ggt* mutant strain unable to break down GSH displayed low levels of intracellular radiolabel, consistent with previous findings that LVS is unable to harness GSH as a source of cysteine (Fig. 3.7A) [112]. Disruption of *dptA* likewise dramatically reduced intracellular radiolabel accumulation, supporting our hypothesis that DptA transports Cys-Gly, the product of GGT activity on GSH. Treatment of wild-type cells with CCCP, which dissipates the proton motive force, inhibited accumulation to the levels of the *dptA* mutant strain, in-line with our assignment of DptA to the POT family (Fig. 3.7B). Moreover, this result suggests that DptA accounts for all detectable proton motive force-driven transport of GSH derivatives. Additional metabolic labeling experiments using ^{35}S-cysteine-containing GSH confirmed that GSH-derived cysteine is utilized for protein biogenesis (Fig. 3.7C, D).

We next sought to determine the specificity of DptA. Competition for the uptake of ^{3}H-GSH-derived species by various di- and tri-peptides revealed that dipeptides with a C-terminal Gly are preferred substrates. Dipeptides with small, nonpolar C-terminal residues and a tripeptide composed entirely of Gly displayed detectable competition with ^{3}H-GSH derivatives; however, their efficiency was significantly lower relative to Cys-Gly. Other tripeptides and dipeptides containing a bulky C-terminal residue were unable to compete with ^{3}H-GSH products for uptake at the concentrations tested (Fig. 3.7E). These results support our hypothesis that DptA is a key transporter of the Cys-Gly dipeptide in LVS.

Our *in vitro* results led us to a model in which GGT acts on GSH to generate Glu and Cys-Gly. These products are then transported into the cytoplasm via GadC and DptA, respectively, where they feed into general metabolism and to the production of cytosolic GSH (Fig. 3.8A). If our model is correct, one

would predict that the role of DptA during infection is cysteine acquisition, as has been shown for GGT [112]. Therefore, we tested the ability of a strain lacking DptA to grow in J774 macrophages with and without cysteine supplementation (Fig. 3.8B). As expected, based on our Tn-Seq findings, the *dptA* (-) strain displayed a significant intracellular growth defect without cysteine supplementation; however, addition of exogenous cysteine allowed this strain to proliferate to levels indistinguishable from the wild-type (Fig 3.8B). Taken together with our peptide uptake assays, these findings provide an explanation for our Tn-Seq data; DptA plays a critical role for LVS *in vivo* by transporting Cys-Gly, the breakdown product of host-derived GSH, which the cell requires for protein synthesis.

3.3.5 *Identification of a second GSH-metabolizing enzyme, ChaC*

In the course of our efforts to understand GSH metabolism in *Francisella*, we tested several mutants within *F. tularensis* subsp. *novicida* U112 in parallel with those generated in the LVS background. Surprisingly, we found that – in contrast to our results in LVS – GGT is dispensable for the growth of U112 in media containing GSH as a sole source of cysteine. The U112 Δ*ggt* strain failed to grow on γGlu-Cys as a sole cysteine source, indicating that the GGT protein of this species is synthesized and active (Fig. 3.9A, B and Fig 3.6C, D).

One explanation for the capacity of U112 Δ*ggt* to utilize GSH is that cells of this strain encode a second GGT protein. To address this possibility, we compared γ-glutamyl hydrolase activity in cell lysates prepared from wild-type and Δ*ggt* mutant backgrounds of LVS and U112. In both organisms, *ggt* disruption diminished γ-glutamyl hydrolase activity to background levels, suggesting that GGT may be the sole enzyme capable of hydrolyzing g-glutamyl-containing peptides in these organisms (Fig. 3.9C). However, it is worth noting that the substrate used in this assay, L-γ-glutamyl-p-nitroanilide, is not a natural substrate of GGT and related enzymes. Thus, from these data we could not rule out the possibility that other γ-glutamyl-targeting peptidases are present in LVS and U112. Nevertheless, these findings suggest that U112 possesses multiple pathways for accessing cysteine derived from extracellular GSH.

In eukaryotes, GGT-independent catabolism of cytosolic GSH occurs through the action of γ-glutamyl-cyclotransferase (GGCT) enzymes [209]. This family of proteins acts on a wide range of γ -glutamyl-conjugated peptides, and while the majority of GGCT proteins cannot degrade GSH, one group of these enzymes, those termed ChaC proteins, specifically catabolize GSH into 5-oxoproline and Cys-Gly [36, 210, 211]. ChaC proteins are poorly characterized in prokaryotes; the only such protein from bacteria that has been studied in detail is RipAY, a secreted virulence factor encoded by the plant pathogen *Ralstonia solanacearum* [212, 213]. Therefore, whether ChaC participates in GSH metabolism in bacteria in unclear. Nevertheless, we speculated that a second pathway for catabolism of extracellular GSH in U112 may involve the ChaC protein and searched its genome for sequences that could encode such an enzyme. These sequence searches, in conjunction with *in silico* structural analyses, defined FTN_0599 as the highest probability GGCT-family protein encoded by U112. Henceforth we refer to this protein as ChaC. Notably, ChaC contains an N-terminal transmembrane domain and a prior study demonstrated that the catalytic domain of its ortholog in LVS (98% amino acid identity) – one of the top hits in our Tn-Seq screen (Fig. 3.11F, 3.9D and Appendix 2) – resides in the periplasm and requires DsbA for proper folding [115]. We confirm that, like GGT, ChaC localizes to this compartment and is associated with cellular membranes (Fig 3.10A, B).

We hypothesized that in U112, ChaC accounts for growth in GSH-containing media in the absence of GGT. To test this hypothesis, we generated an in-frame deletion of *chaC* in the wild-type and Δggt backgrounds of U112 and monitored growth on GSH. As expected, deletions of *ggt* or *chaC* alone had no effect on growth; however, a strain bearing mutations in both genes displayed markedly attenuated growth on GSH as the sole cysteine source. This phenotype was genetically complemented by expressing either gene ectopically from the chromosome (Fig. 3.9A, B and Fig. 3.6C, D). These findings suggest that in U112, ChaC can liberate GSH-derived species that support *in vitro* growth in media lacking free cysteine. Notably, this does not contradict our γ -glutamyl hydrolase activity assays, as ChaC enzymes are known to act with high specificity and are not predicted to tolerate the non-native substrate L- γ -

glutamyl-p-nitroanilide. At this time, we lack an explanation for the differential contribution of ChaC to the *in vitro* growth of U112 and LVS on GSH. Western blot analyses ruled out expression as a simple explanation for our observations (Fig. 3.10C, D).

While ChaC is not required for the growth of LVS on GSH *in vitro*, as previously mentioned, ChaC was a top hit in our Tn-Seq screen performed in this strain (Fig. 3.1F, 3.9D and Appendix 2), suggesting this protein is important for growth in vivo and that its role is not entirely redundant with GGT. Intramacrophage growth assays confirmed the growth deficiency of LVS Δ*chaC* in this context. However, contrary to our results in the Δ*ggt* strain, exogenous cysteine did not complement the intramacrophage growth defect of LVS Δ*chaC* (Fig. 3.9E). Thus, the role of ChaC within macrophages appears not restricted to generating metabolizable cysteine from GSH. In total, these data highlight the existence of a previously unrecognized GGT-independent pathway capable of the catabolism of GSH by *F. tularensis*, but suggest the importance of ChaC in supporting intramacrophage growth extends beyond cysteine acquisition.

3.4 Discussion

Using Tn-Seq we have identified genes that are specifically required for the intramacrophage growth of *F. tularensis*. For many of the genes in this catalog the mechanistic basis for their role in intramacrophage growth is poorly understood. Utilization of host-derived GSH is essential for *Francisella* intramacrophage growth and we show that one of the genes from our compendium encodes a peptide transporter that plays a key role in transporting the GSH breakdown product Cys-Gly from the periplasm into the bacterial cytoplasm. In addition, we present evidence that another gene specifies a member of the ChaC family of proteins that is involved in the breakdown of exogenous GSH in *Francisella*.

Our Tn-Seq analyses were conducted with LVS, which is an attenuated derivative of a strain of *F. tularensis* subsp. *holarctica*, a type B strain. Recently a Tn-Seq study was performed to define genes essential for rat colonization of the highly virulent type A strain *F. tularensis* subsp. *tularensis* SCHU S4 [85] {Ren, 2014 #1267}. In principle, this screen should define genes important for multiple aspects of

infection, including bacterial uptake, immune evasion, and intracellular proliferation. Nevertheless, comparative analysis between the results obtained in the present study with those generated by Ireland *et al* demonstrate a high degree of overlap, suggesting that many of the genes important for infection in the host are involved in intramacrophage growth. In relation to genes important for the utilization of host-derived GSH, *ggt*, *dptA* and *chaC* were found to play critical roles during infection of the rat with SCHU S4 as assessed by Tn-Seq [85]. Thus, the proteins that play central roles in the metabolism of GSH, which are highly conserved amongst different subspecies of F. tularensis, are important for the intramacrophage growth of LVS as well as for the fitness of SCHU S4 in the host. We note that GGT has previously been shown to be important for the virulence of both LVS and SCHU S4 in mice [85, 112] [115], and that ChaC (i.e. FTL_1548) has been shown to be important for the virulence of LVS in mice [213].

Many bacteria possess transporters for the uptake of intact exogenous GSH, thereby providing an alternative mechanism for the acquisition of GSH-byproducts [144, 214, 215]. Of note, there are no genes that specify predicted GSH-transporters present on the genome of F. tularensis and our in vitro findings utilizing ^{3}H- and ^{35}S-GSH support this observation. Therefore, *F. tularensis* relies on proteins present in the periplasm to first degrade GSH, before the resulting breakdown products are transported into the cytoplasm for subsequent further breakdown or utilization (Fig. 4A).

Previous work demonstrated a critical role for GGT in the acquisition of cysteine, however, it has remained unclear how the products of this typically periplasmic or extracellular enzyme are transported into the cytoplasm for use in downstream pathways [112, 114]. In fact, in the majority of bacteria it remains unclear how GGT-breakdown products reach the cytoplasm. One exception is the pathogen *Campylobacter jejuni*, which has been demonstrated to transport Cys-Gly into the cytoplasm via the oligopeptide transporter (OPT) CptA [216]. The OPT family of transporters is widespread in bacteria and primarily transports oligopeptides 3-8aa long. However, homologs of CptA are restricted to a small subset of bacteria found in the oral and intestinal microbiota of mammals. Of note, CptA was found to be non-essential during infection suggesting *C. jejuni* possess alternative mechanisms for obtaining the breakdown products of GSH [216].

The results from our saturated Tn-Seq screen led to the identification and characterization of the Cys-Gly transporter, DptA. As a member of the POT-family, DptA is powered by the PMF and is capable of transporting multiple di- and tri-peptides with varying affinities. Our results suggest that this protein constitutes the sole mechanism for the transport of Cys-Gly across the inner membrane, making DptA an attractive target for novel therapeutics (Fig. 4A). Interestingly, DptA also represents the first member of the POT protein family to be implicated in bacterial pathogenesis.

For many years GGT was believed to be the sole enzyme capable of catabolizing GSH; however, within the last decade, two additional proteins families have been implicated in the breakdown of this molecule. Members of one of these families, termed the Dug2p/3p complex, are restricted to fungi [217, 218] whereas members of the other, ChaC family proteins, belong to the γ -glutamyl cyclotransferase family of proteins and degrade GSH into 5-oxoproline and Cys-Gly [36]. The majority of studies on ChaC proteins have focused on representatives from mice and humans; however, ChaC-homologs can be found in both prokaryotes and yeast [36, 116, 117]. Multicellular organisms encode two unique copies of ChaC [116]. ChaC1, which participates in the initiation of apoptosis via the unfolded protein response, rapidly catalyzes GSH breakdown in vitro (Kcat = 225.2±15 min^{-1}) [17, 18]. On the other hand, ChaC2 is constitutively expressed and displays much slower GSH turnover (Kcat=15.9± 1 min^{-1}). These results led to the hypothesis that ChaC2 functions to catabolize GSH at a low basal rate, whereas ChaC1 functions in response to stress [116]. However, a recent study using an embryonic stem cell model proposed that ChaC2 maintains GSH homeostasis through competitive binding with ChaC1. The authors demonstrate that ChaC2 was capable of inhibiting ChaC1 degradation of GSH in a dose dependent manner, which was important for embryonic stem cell regeneration [219]. Whether this model for the role of ChaC2 is conserved in other cell types was not addressed. Prior to this work, the physiological function of bacterial ChaC proteins had not been investigated; however, in vitro studies of *Escherichia coli* ChaC revealed its catalytic properties mirror that of mammalian ChaC2 (K_{cat}=13±0.27 min^{-1}) [116].

Here we identify a ChaC homolog in *F. tularensis* and show this protein acts in a GGT-independent pathway to mediate GSH catabolism. To our knowledge, this is the first demonstration that a

bacterial ChaC enzyme contributes to the metabolism of GSH. It is unclear why *F. tularensis* contains two distinct periplasmic enzymes for the catabolism of GSH. We established cysteine acquisition as the critical function of GGT in intramacrophage growth, yet the intramacrophage growth defect of cells lacking the ChaC enzyme, which can also liberate metabolizable form(s) of cysteine from GSH, cannot be complemented by the addition of exogenous cysteine. Therefore, it could be that ChaC catabolizes GSH, but that cysteine is not the only important product for the cell. Indeed, a study from Charbit and colleagues demonstrated that glutamate acquisition, through the action of the transporter GadC, is essential during infection for defense against reactive oxygen species [119]. The glycine cleavage system is also known to play an important role during murine infection [125]. It is tempting to speculate that ChaC functions to liberate these important metabolites from GSH, perhaps under conditions not conducive to GGT activity, or in a manner coordinated with the machinery necessary for their uptake. However, we cannot rule out the formal possibility that ChaC influences intramacrophage growth in a manner unrelated to its ability to catabolize GSH.

Although this work clearly implicates ChaC in GSH metabolism, precisely how the protein benefits *Francisella* during infection remains to be defined. Our efforts to understand ChaC in *Francisella* may also shed light on the role of the protein in other bacteria. However, bacterial ChaC family proteins are diverse, not restricted to host-associated organisms, and most are not predicted to localize to the periplasm. This suggests that ChaC proteins may serve myriad roles in GSH metabolism idiosyncratic to the lifestyles and physiological needs of bacteria harboring it.

3.5 Materials and Methods

Ethics Statement. Animal studies were conducted in compliance with the National Research Council Guide for the Care and Use of Laboratory Animals. All experimental procedures were specifically approved in advance by the University of Washington Institutional Animal Care and Use Committee, under protocol number 2671-06. Animals were group-housed according to experimental group in HEPA-filtered laminar flow cages with cage enrichment and unrestricted access to sterile food and water. The

vivarium is managed by the University of Washington Department of Comparative Medicine in compliance with all policies and regulations of the Office of Laboratory Animal Welfare of the Public Health Service. The facility is fully accredited by the American Association for Laboratory Animal Care.

Bacterial strains and growth conditions. Except where otherwise noted, *F. tularensis* subsp. *holarctica* LVS and derivatives were grown aerobically at 37°C in either liquid Mueller-Hinton broth (Difco) supplemented with glucose (0.1%), ferric pyrophosphate (0.025%), and Isovitalex (2%) (MHB) or on cystine heart agar (Difco) supplemented with 1% hemoglobin (CHAH). *F. tularensis* subsp. *novicida* strains U112, MFN245 and derivatives were grown aerobically at 37°C in tryptic soy broth or agar supplemented with 0.1% (w/v) cysteine (TSBC or TSAC). *Escherichia coli* strains XL1-blue (Stratagene) or DH5a were used in vector construction. For selection, antibiotics were used at the following concentrations: kanamycin 5 μg mL^{-1} (LVS), 15 μg mL^{-1} (U112) or 50 μg mL^{-1} (*E. coli*), nourseothricin 5 μg mL^{-1}, hygromycin 200 μg mL^{-1}, and carbenicillin 150 μg mL^{-1}.

Transposon mutant library construction and growth *in vitro*. The mariner transposon delivery plasmid pSD26 [202]{Goodman, 2011 #636} [34] was modified to facilitate use of the INSeq protocol [60]. The intermediate plasmid pKL84 was created by amplifying the kanamycin resistance cassette (the *F. tularensis* LVS *groES* promoter driving the kanamycin resistance gene [*aphA1*]) from pSD26. The 5′primer included DNA specifying EcoRV and MfeI sites and the 3′primer included DNA specifying NcoI, NheI, and EcoRV sites. The resulting fragment was digested with EcoRV. The mariner transposon delivery plasmid pSAM_Bt [201], which contains MmeI sites within the transposon inverted repeat sequences, was digested with MfeI and XbaI and treated with Klenow large fragment to fill in overhanging 5′ ends. The digested DNAs were ligated together to create the pKL84 plasmid, which contains an MfeI site on the 5′ end of the kanamycin resistance cassette and NcoI, NheI, and the non-unique XbaI sites on the 3′end. To optimize transposase production for LVS, the promoter for rpoD of *Bacteroides thetaiotaomicron* was replaced by the 209 bp fragment of DNA upstream of the transposase in pSD26. The promoter-containing fragment was amplified from pSD26 using a 5′ primer that included

DNA specifying a BamHI site and a 3′ primer that included DNA specifying an optimal RBS (AGGAGG) followed by a NdeI site and ligated into pKL84 digested with BamHI and NdeI, resulting in the final transposon delivery plasmid pKL91.

To construct the transposon mutant libraries, one microgram of transposon delivery plasmid pKL91 was used to transform *F. tularensis* LVS (essentially as described in [220]) in six independent electroporations and cells were plated on CHAH with 5 μg mL^{-1} kanamycin. After two days, the resulting kanamycin-resistant colonies, approximately 800,000, were combined into a single library and frozen. For all Tn-Seq experiments, single aliquots of the library were removed, spread on CHAH with 5 mg mL^{-1} kanamycin, and grown overnight as a confluent lawn.

Separate aliquots were grown and used as the inocula for growth in MHB, intramacrophage growth, or to assess mutants viable on solid media. To screen for mutants deficient in growth in liquid media, transposon mutant library cells were diluted to an OD_{600} of 0.005 in 50 mL MHB and grown for ~17 hours (~6.2 doublings) prior to gDNA extraction.

Transposon mutant library screen in macrophages. Approximately $1x10^7$ of the murine macrophage-like J774A.1 cells were plated on six 150 mm tissue culture plates (~$6x10^7$ cells total) in DMEM (Invitrogen) supplemented with 10% fetal bovine serum (Gemini Bio-Products) (DMEM-F) and incubated overnight at 37°C with 5% CO2. Macrophage were infected with the LVS transposon mutant library resuspended in DMEM-F at a MOI of approximately 1700. After 2 hours, cells were washed twice with PBS and covered with DMEM containing 10 μg mL^{-1} gentamycin. Cells were incubated at 37°C with 5% CO2 for 24 hours then washed twice with PBS and lysed with 1% saponin in PBS for 30 minutes. Lysates were combined and a small aliquot was removed for bacterial enumeration on CHAH. Bacterial cells were pelleted, and genomic DNA was directly extracted from pellets (Epicentre MasterPure Complete DNA and RNA Purification Kit).

INSeq library construction and sequencing. Sequencing libraries were created from 5 samples: (1) input sample for mutants grown in liquid MHB, (2) mutants grown on solid media and not subjected to additional screening, (3) input sample for mutants grown in macrophage (4) output sample for mutants grown in liquid MHB, (5) output sample for mutants grown in macrophage. Libraries were generated from isolated gDNA as in [221], starting with linear PCR using 2 μg DNA per reaction. Libraries were pooled and sequenced using single-end 50 bp sequencing with a single read cluster kit using two lanes of an Illumina HiSeq2500 at 15 pM and 10 pM densities with 20% PhiX and no indexing read. Sequencing reads and processed data files have been deposited at GEO with the accession number GSE138658.

Tn-Seq data analysis. Sequencing libraries from distinct samples were demultiplexed and trimmed using cutadapt (version 1.16; [222]). Reads were mapped to the LVS genome (NC_007880) using bowtie (version 1.2; [223]) with a seed length of 16 and zero mismatches allowed. Custom scripts were used to identify reads corresponding to insertions in TA sites and tally only those insertions with reads mapping from both ends of the transposon. Datasets were normalized for positional bias and analyzed using EL-ARTIST [203] to identify genes essential for in vitro growth using the combined data from all samples grown on solid media. Hidden Markov model analysis resulted in gene classifications ("critical," "non-essential," and "both non-essential and critical domains") after the following sliding window training parameters: 4 TA sites, $P < 0.03$. CON-ARTIST [203] was used to identify genes critical for growth in liquid media and in vivo by comparing inoculum samples to the samples recovered after growth in both MHB and macrophage, respectively. We considered those genes with insertions in at least 4 TA sites, an average fold change of two-fold or more, and with a p-value of less than or equal to 0.05 to be important for survival in a given condition.

***Francisella* mutant and complementation strain construction.** The 3′ end of *dptA* is very close to an *isftu*2 repetitive element, making a deletion using allelic exchange difficult. Therefore, we disrupted this gene by plasmid integration. Briefly, the plasmid pEX_*dptA*-frag was created by modification of pKL02 [224], a suicide plasmid which confers resistance to kanamycin. A 441 bp fragment of the dptA gene,

including DNA specifying a KpnI site, DNA corresponding to amino acids 51 – 197, a stop codon after amino acid 197, and DNA specifying an EcoRI site, was introduced into pKL02 that had been digested with KpnI and EcoRI. The plasmid pEX_*dptA*-frag was then electroporated into LVS cells and cells in which the plasmid pEX_*dptA*-frag integrated though a single homologous recombination event were selected on CHAH with 5 μg mL^{-1} kanamycin.

In-frame deletion mutations in LVS and U112 were generated via allelic exchange. For LVS, the vector pEX18Kan was employed to make the in-frame deletions of *ggt* and *chaC*, as described previously [225]. To generate deletion vectors for allelic exchange in U112, 1000bp of flanking regions of *ggt* and *chaC* were cloned into the BamHI and PstI sites of the vector pEX18-pheS-km [22]. U112 deletion strains were then generated as previously described [22]. For all mutants, strains containing the modified genetic region of interested were confirmed by colony PCR and sequencing of PCR products generated from genomic DNA.

The miniTn7 system vector pMP749 was utilized for genetic complementation in both LVS and U112 [226]. For *ggt* and *chaC* from LVS, the open reading frame plus the intergenic regions upstream (including the native promoter region) and downstream of the gene were amplified by PCR and cloned into the HindIII and BamHI sites of pMP749. For *dptA*, pMP749 was modified using Gibson assembly to replace the kanamycin resistance cassette for one that encodes nourseothricin resistance. The open reading frame plus the intergenic regions upstream (including the native promoter region) and downstream of *dptA* were amplified by PCR and cloned into the HindIII and BamHI sites of pMP749-nourseothricin. Complementation strains were then generated using these vectors as described in [226]. Briefly, parental strains were initially transformed with the helper plasmid pMP720. Hygromycin resistant colonies were then transformed with the appropriate pMP749-based vector. Kanamycin or nourseothricin resistant colonies were then passage in the absence of hygromycin to cure the bacteria of pMP720. Integration downstream of the *glmS* gene was confirmed by colony PCR. For the complementation of *ggt* and *chaC* in U112, the genes were cloned into pMP749 downstream of the

constitutively active *bfr* promoter, and complemented strains were generated as previously described [187]. For localization of ChaC and GGT in U112, the genes encoding ggt and chaC were cloned downstream of the *bfr* promoter with either a N-terminal VSV-G epitope tag or *phoA* (from *E. coli*) gene fusions into the HindIII and BamHI sites of pMP749, and the strains were generated as described above for LVS or U112. As controls for protein localization, full length *phoA* and *phoA* lacking the associated Sec signaling sequence were cloned into the same sites of pMP749. For expression studies in U112 and LVS, the genes encoding ggt and chaC were cloned with their native promoter regions and a N-terminal vsvG eptitope tag into the HindIII and BamHI sites of pMP749, and the strains were generated as described above for LVS or U112.

Mouse infections. Female C57BL/6 mice were purchased from Jackson Laboratories (Bar Harbor, ME) and were 8-10 weeks of age when enrolled in experiments. Mice were exposed to aerosolized bacteria in a whole-body aerosol exposure chamber, as described previously [37]. Briefly, stocks of each bacterial strain were grown to stationary phase at 37 °C in supplemented Mueller-Hinton broth diluted in 20% glycerol, aliquoted, and stored at -80 °C. For each experiment, aliquots of each strain of bacteria were thawed, streaked onto chocolate agar and incubated at 37 °C for 24h. Colonies were harvested and suspended in PBS to a concentration of approximately 3 x 10^9 CFU/mL, as estimated by optical density and confirmed by quantitative culture. Cohorts of mice were exposed to aerosolized bacteria in a whole animal exposure chamber with a computer interface to control pressures and flows (Biaera Technologies, Hagerstown, MD). Bacterial aerosols were generated by mini-Heart nebulizers with a flow rate of 8 L/min at 40 psi. Dilution air was regulated at 11.5 L/min to maintain total chamber flow at 19.5 L/min during a 10-minute exposure. Actual bacterial deposition was determined by quantitative culture of the homogenized left lungs of four sentinel mice euthanized immediately after completion of the aerosol exposure. The remaining mice were returned to their cages. Mice were observed and weighed daily. At serial time points after infection, mice were euthanized with pentobarbital, exsanguinated by cardiac puncture, and left lungs were harvested and homogenized for quantitative culture on chocolate agar.

Growth curves. To assess bacterial growth on different cysteine sources, the indicated strains of *Francisella* were grown overnight in Chamberlain's defined media (CDM) [227] with 1 mM cysteine at 37ºC with shaking. After ~16hrs of growth, the cells were washed three times and resuspended in CDM lacking cysteine. The bacteria were cysteine starved for 2 hrs at 37ºC with shaking to allow the cells to metabolize any remaining cysteine. The OD_{600} of the cultures was then measured and the bacteria were diluted to an OD_{600}= 0.01 in CDM with the indicated potential cysteine source at 100 μM. For U112, cultures were transferred in triplicate to a 96-well plate and the OD_{600} of the cultures was monitored for 36hrs in a plate reader. For LVS, 3 mL cultures inoculated as described above were grown at 37ºC and the OD_{600} was determined at the indicated time points.

GGT activity assays. GGT activity in the indicated strains of LVS and U112 was determined using the γ-Glutamyltransferase (GGT) Activity Colorimetric Assay Kit (Sigma Aldrich). To prepare bacteria for the assay, cells were grown overnight on CDM containing cysteine, then washed x3 in CDM lacking cysteine. The OD_{600} of the cells was determined and cultures were normalized to an OD_{600}=1 (~10^8 cells) in 1 mL CDM lacking cysteine. Cells were pelleted and resuspended in 100 mL of assay buffer provided in the kit. Cells were lysed by incubating at 50ºC for 3 min and cellular debris was removed by centrifugation at max speed for 10 min. The assay was then conducted per the manufacture's specifications. Activity was measured by reading the absorbance at 480 nM in a plate reader pre-warmed to 37ºC.

GSH uptake assays. The indicated strains of LVS were grown for 16 hrs at 37ºC in CDM supplemented with 1 mM cysteine. Cells were spun down, washed three times in uptake buffer (25 mM Tris pH7.5, 150 mM NaCl, 5mM Glucose), then concentrated 20-fold. The OD_{600} was measured and normalized to OD_{600}=10. Each reaction contained 20 mL cells, 5mL 100 mM GSH + 0.5 mCi ^{3}H-GSH, and 25mL uptake buffer or competitor substrate at the indicated concentrations (made in uptake buffer). Uptake was allowed to occur for 45 min at 37ºC followed by quenching with 1 mL ice cold uptake buffer. Cells were

pelleted and washed three times in 1 mL cold uptake buffer, followed by resuspension in 50 mL uptake buffer. Cells were then added to scintillation fluid and counts were measure over 1 minute.

Macrophage replication assays. Macrophage replication assays for LVS and derivative strains were performed as in [228]. Briefly, approximately 2 x 10^4 murine macrophage-like J774A.1 cells were infected with LVS or derivative strains at an MOI of 5-10. Culture media containing extracellular bacteria was removed after 2 hours of infection and replaced with DMEM-F containing 10 mg/mL gentamycin. After 2 or 24 hours of infection, macrophages were lysed for 30 minutes in 1% saponin in 1X PBS and plated for enumeration. For assays including cysteine, 5 mM cysteine was added when macrophages were seeded and this concentration was maintained throughout the experiment.

^{35}S-Cysteine Metabolic labeling. The indicated strains of LVS were grown for 16 hrs in CDM, diluted 1:100 into fresh CDM and grown to mid-log phase (OD_{600}= ~0.5-0.7). Cells were then pelleted, washed three times and resuspended in CDM lacking cysteine. The bacteria were cysteine starved for 2 hrs at 37ºC with shaking to allow the cells to metabolize any remaining cysteine. The OD_{600} was then normalized to 0.5 in 3mL cultures of CDM lacking cysteine. Each strain was then supplemented with 100uM GSH spiked with 5mCi ^{35}S-GSH and grown for 16hrs at 37ºC with shaking. Finally, equal amounts of cells were spun down, resuspended in SDS-PAGE loading buffer, and incubated at 95°C for 10 min. Equal volumes of each sample were loaded in duplicate for separation by SDS-PAGE utilizing an 8-16%-SDS-polyacrylamide gels. One set of samples were stained with Coomassie-blue for total protein visualization, while the other half were fixed in 50% methanol, 10% acetic acid and 40% water. The fixed gel was then vacuum-dried and exposed to a phosphoscreen and ^{35}S-labeled proteins were visualized on an Azure Sapphire scanner.

PhoA-activity assays. U112 strains expressing *chaC*- and *ggt*-phoA fusions from the Tn7 insertion site (*aatB*), along with several controls (no *phoA*, full length *phoA*, and *phoA* lacking the SecA signal sequence), were grown overnight at 37ºC with shaking in CDM media lacking cysteine and supplemented

with 100mM GSH. The OD_{600} of each culture was measured and cells were spun down and resuspended in 1 M Tris-HCl (pH 8.0), 1 mM $ZnCl_2$, 0.01% sodium dodecyl sulfate, and 5% chloroform and incubated for 5min at 37ºC to permeabilize cells as previously described [229]. 200µL of 0.4% p-nitrophenyl phosphate dissolved in 1M Tris-HCl pH 8.0 was added to 1mL permeabilized cells, which were then incubated 8hrs at 37ºC. The resulting mixture was spun down and both the OD_{420} and OD_{550} of the supernatant was determined using a plate reader. The PhoA-activity of each strain was calculated as 1,000 x (OD_{420}-OD_{550})/(min x OD_{600} x mL of culture volume).

Protein localization and expression level measurements. To determine if ChaC is membrane anchored, U112 strains expressing ChaC-vsvG and ChaC-vsvG lacking the predicted transmembrane domain (residues 2-22) were grown overnight at 37ºC with shaking in CDM. 50mL of the cultures were pelleted and resuspended in 10mL 500 mM NaCl, 50 mM Tris pH 7.5 and 10% (v/v) glycerol followed by lysis via sonication. The membrane fraction was separated by centrifuging the lysed cells at 87,207 x g for 2hrs. The resulting pellet was resuspended in 200uL of buffer containing 500 mM NaCl, 50 mM Tris pH 7.5 and 10% (v/v) glycerol followed by mixing 1:2 with SDS-PAGE sample loading buffer. The supernatant, corresponding to the soluble fraction, was concentrated 5-fold using a 5kD cutoff, and was mixed 1:2 with SDS-PAGE sample loading buffer. All samples were then boiled at 95°C for 10 min and processed for Western blotting as described below.

For expression studies LVS and U112 strains expressing either GGT-vsvG or ChaC-vsvG were grown overnight on CDM agar plates. Cells were then back diluted into CDM lacking cysteine supplemented with 100mM GSH at an OD_{600}=0.1. Cells were grown to OD_{600}=0.6-0.8 followed by normalization to OD_{600}=0.5. Bacterial cell lysates were generated by re-suspending cells in buffer containing 500 mM NaCl, 50 mM Tris pH 7.5 and 10% (v/v) glycerol followed by mixing 1:2 with SDS-PAGE sample loading buffer.

For both expression and protein localization studies, extracted protein samples in SDS-PAGE sample buffer were boiled at 95°C for 10 min and loaded at equal volumes to resolve using SDS-PAGE. Proteins were then transferred onto nitrocellulose membranes which were subsequently blocked in TBST (10 mM Tris-base pH 7.6, 150mM NaCl, and 0.1% w/v Tween-20) with 3% (w/v) bovine serum albumin (BSA) for 30 min at 24°C. This was followed by incubation with a monoclonal α-vsv-G antibody (Sigma Aldrich diluted 1:5000), α-Tul4 antibody (BEI diluted 1:3000), α-opiA antibody ([37] diluted 1:5000) or α-GroEL antibody (Sigma diluted 1:15000 provided by Karsten Hazlett, Albany Medical College, Albany, New York, United States) in blocking buffer for 2hrs at 24°C. Following three washes in TBST, blots were incubated for 45min in TBST with an α-Rabbit HRP-conjugated secondary antibody (Sigma Aldrich diluted 1:5000) or α-Mouse HRP-conjugated secondary antibody (Millipore diluted 1:5000). The blots were developed using Radiance HRP substrate (Azure Biosystems), visualized using the Azure Biosystems c600, and densitometry analysis was performed using Image J. Density of the proteins corresponding to GGT and ChaC were normalized to the density of the loading control protein GroEL for each sample. Samples were generated and analyzed by western blot three independent times. Representative images were assembled using Adobe Illustrator CC 2015.

3.6 Figures

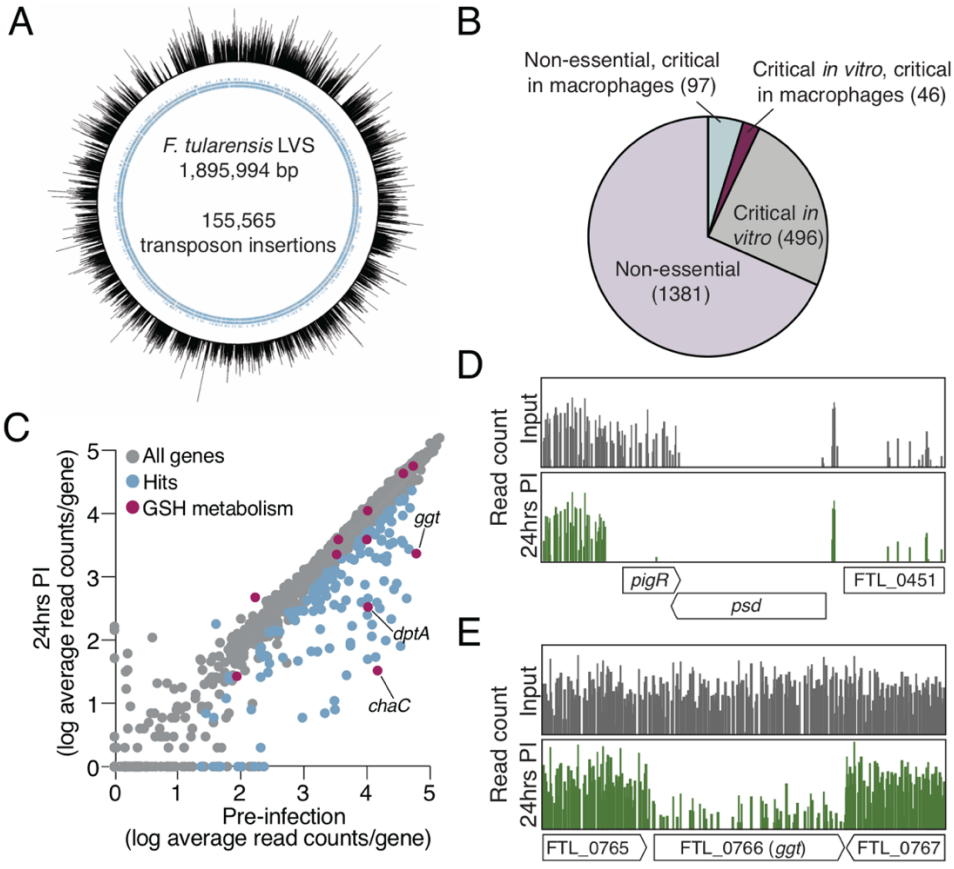

Figure 3.1. Highly saturated Tn-Seq screen in *F. tularensis* LVS to identify genes required for intramacrophage growth.

(**A**) Map of transposon insertions across the *F. tularensis* genome. Of all the potential transposon insertion sites (TA dinucleotides) genome-wide, 75% contain a transposon insertion. Each line corresponds to one mutant with a single insertion; the line height corresponds to the relative abundance of sequencing reads identified for each individual insertion. Blue inner circle represents genes. (**B**) EL-ARTIST and Con-ARTIST analysis of Tn-Seq screen reveals genes that are non-essential under any tested condition (lavender), critical *in vitro* (grey), critical *in vitro* and in macrophages (maroon), and those that are non-essential *in vitro* but critical in macrophages (blue). (**C**) The relative abundance of mutations in each gene (average read count per gene) in the mutant pool used to infect J774A.1 cells (pre-infection) and in mutants recovered after 24 hours of infection. Genes significantly more or less abundant after infection (at least 2-fold changed, with 4 or more informative insertion sites, $p \leq 0.05$) are colored in blue. Genes involved in GSH metabolism are highlighted in purple. (**D-E**) Transposon insertion profiles for the indicated genetic regions from the input library (grey) and 24hrs post infection (green). Line height represents the relative abundance of sequencing reads at that position on a log scale.

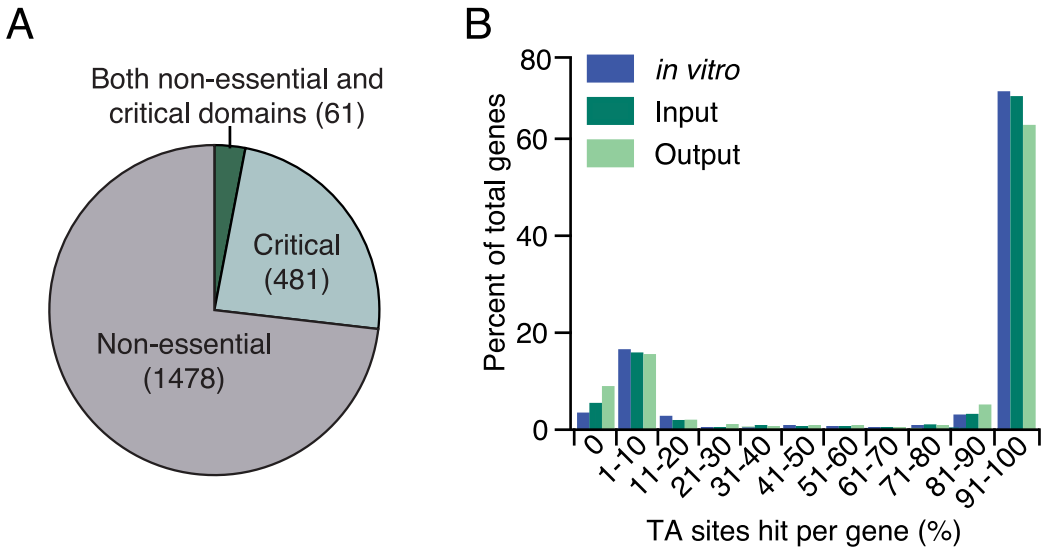

Figure 3.2. Characterization of a highly saturated transposon library generated in LVS.

(**A**) HMM analysis using ARTIST [35] identified which of the 2020 annotated genes that are critical, encode critical and non-critical protein regions, or are non-essential *in vitro*. (**B**) Percentage of potential transposon insertion sites (TA dinucleotides) per gene with a detected transposon insertion for the mutant library grown *in vitro* (blue), the mutant library used to infect macrophage (dark green), and the transposon insertion mutant library recovered after intramacrophage growth (light green). Each bin represents 10% except for the first bin which is 0%.

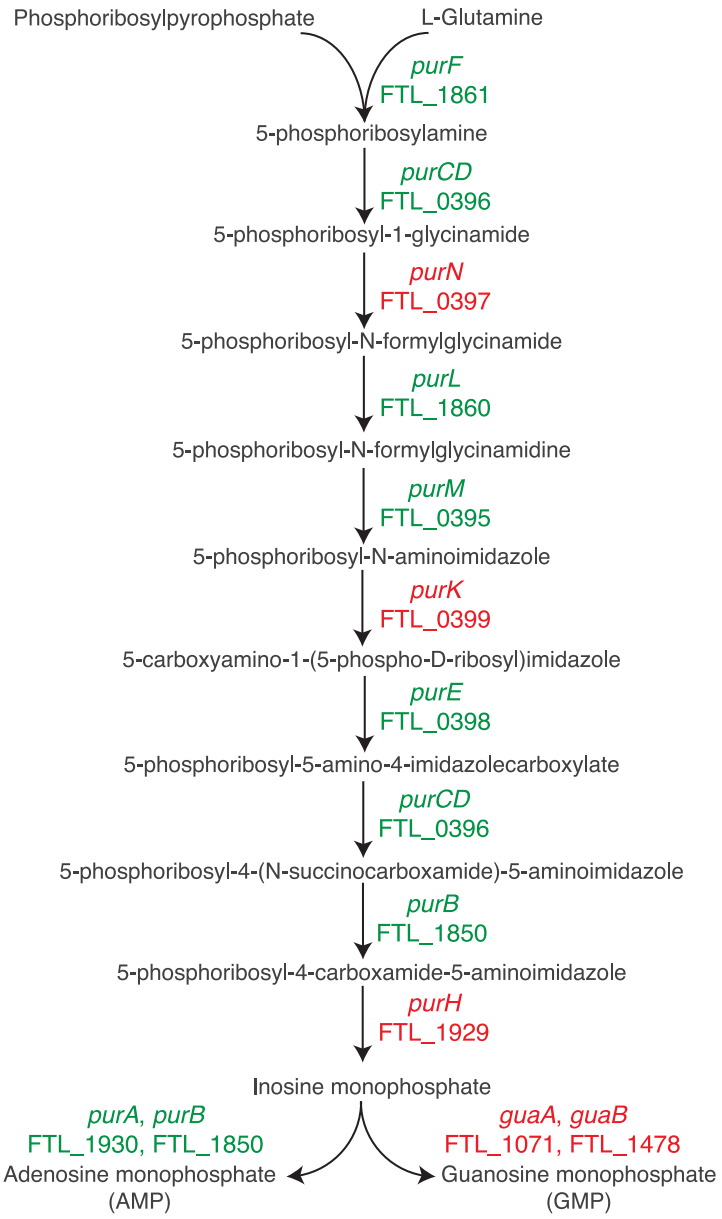

Figure 3.3. The purine biosynthesis pathway is critical during macrophage infection by *F. tularensis.*

The purine biosynthesis pathway of F. tularensis [11] is depicted with the gene encoding the enzyme responsible for each step listed and colored according to the environment in which they were found to be essential (green, essential *in vitro*; red, dispensable *in vitro* but essential in macrophages).

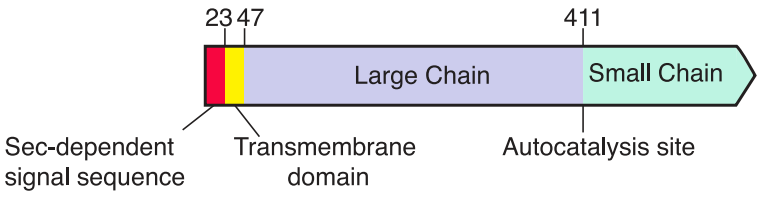

Figure 3.4. GGT is predicted to localize to the periplasm in *F. tularensis*.

Graphical representation of the GGT protein with predicted important features of the protein highlighted. Predictions were based on well-characterized homologs of GGT.

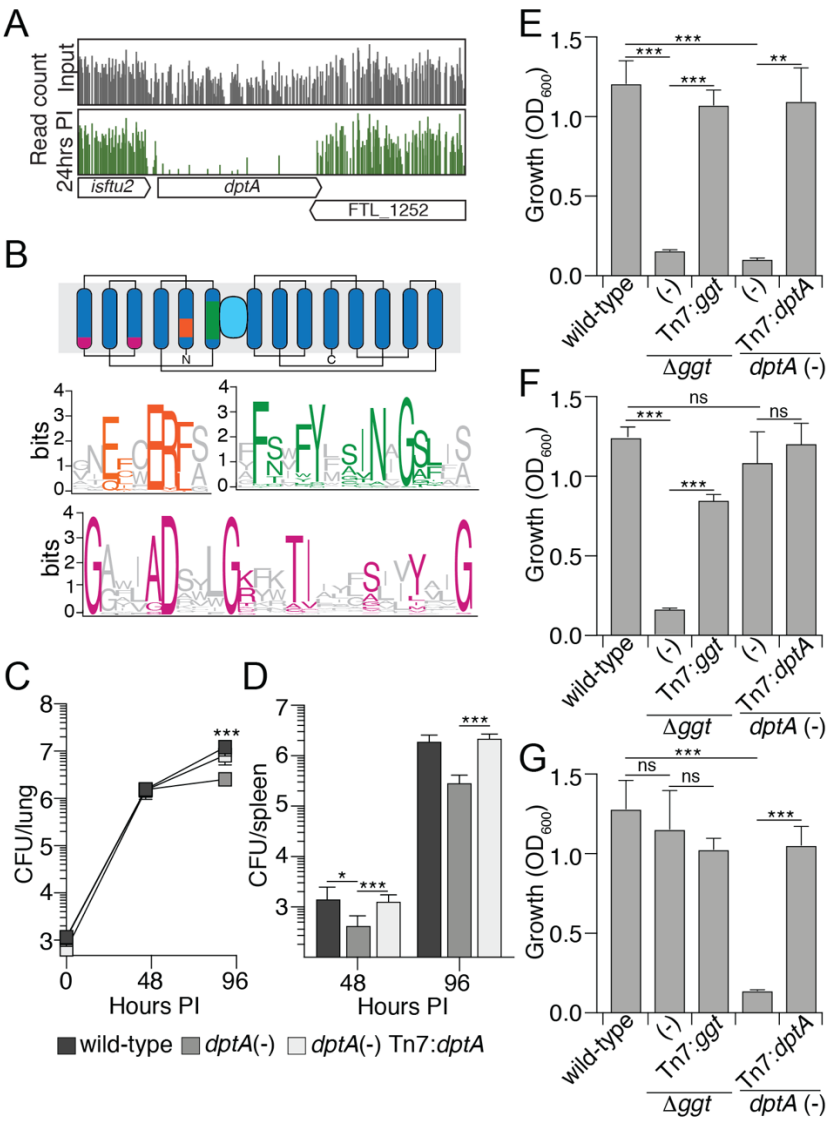

Figure 3.5. DptA is a POT that contributes to GSH utilization by LVS.

(**A**) Transposon insertion profiles for the genetic region encompassing *dptA* from the input library (grey) and 24hr post infection (green). Line height represents the relative abundance of sequencing reads at that position on a log scale. (**B**) Graphical representation of the predicted topology of DptA with conserved sequences motifs found in POT proteins highlighted (proton binding motif, orange; PTR2 domain 1, green; PTR2 domain 2, pink; peptide binding region, light blue). Sequence logo indicates motifs conserved in the POT family derived from an alignment of representative POT proteins. (**C**) Quantification of the bacterial burdens in the lungs of mice infected via aerosolization with the indicated strains of LVS. (**D**) Quantification of the bacterial dissemination to, and burdens within the spleens of mice infected via aerosolization with the indicated strains of LVS. (**E-G**) OD_{600} measurements of the indicated strains of LVS after 16hrs of growth in CDM with glutathione (E), γGlu-Cys (F) or Cys-Gly (G). Data in (C-G) are shown as mean ± s.d. Asterisks represent statistically significant differences (Student's t test; ***p≤0.0005, **p≤0.005, *p≤0.05, ns, not significant).

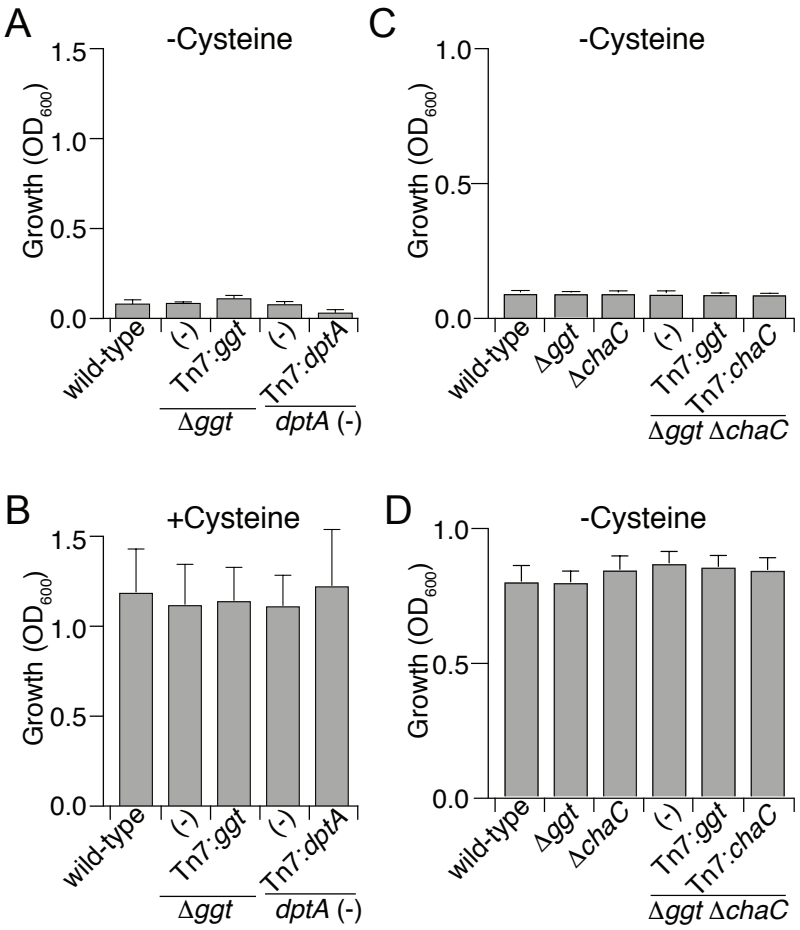

Figure 3.6. Genes involved in GSH catabolism do not play a role in free cysteine utilization.

(**A-B**) OD_{600} measurements of the indicated strains of LVS after 16hrs of growth in CDM without (A) or with (B) free cysteine added. (**C-D**) OD_{600} measurements of the indicated strains of U112 after 36hrs of growth in CDM without (C) or with (D) free cysteine added. Data in A-D are shown as the mean ± s.d.

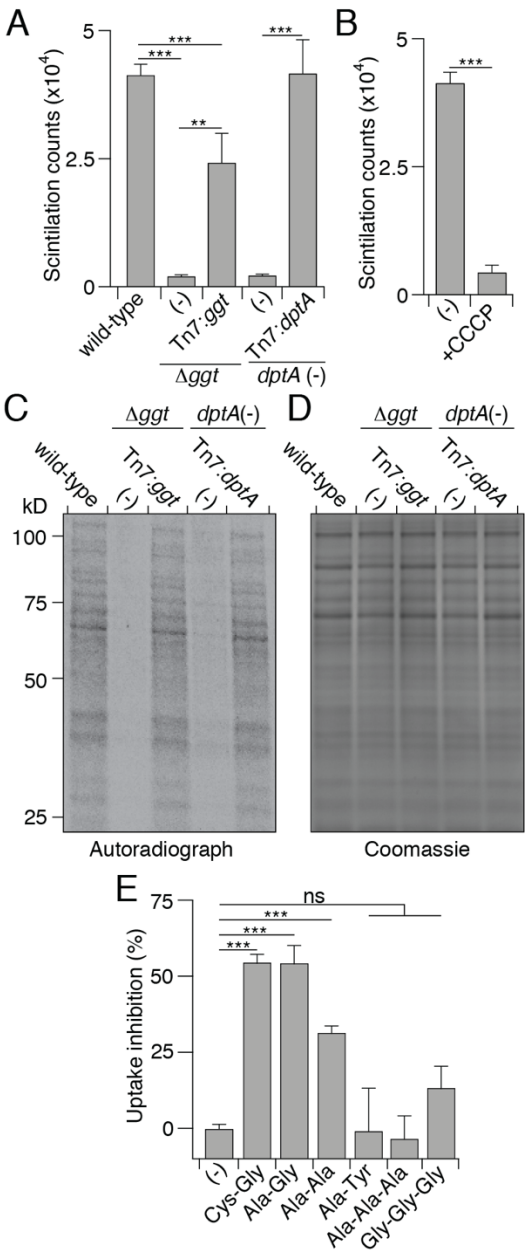

Figure 3.7. DptA is the sole Cys-Gly transporter in LVS.

(**A-B**) Quantification of the intracellular levels of ^{3}H-GSH byproducts after 45 min incubation with the labeled substrate in the indicated strains of LVS (A) or wild-type LVS with and without CCCP (B). (**C**) Autoradiograph of SDS-PAGE separated proteins produced by growing the indicated strains of LVS in CDM lacking cysteine supplemented with ^{35}S-Cysteine containing GSH. (**D**) Coomassie-blue staining of proteins generated as described in (C). (**E**) Percent of ^{3}H-GSH uptake that was inhibited by addition 100mM of the indicated di- or tripeptides. Data in (A-C) are shown as the mean ± s.d. Asterisks represent statistically significant differences (Student's t test; ***p≤0.0005, **p≤0.005, ns, not significant).

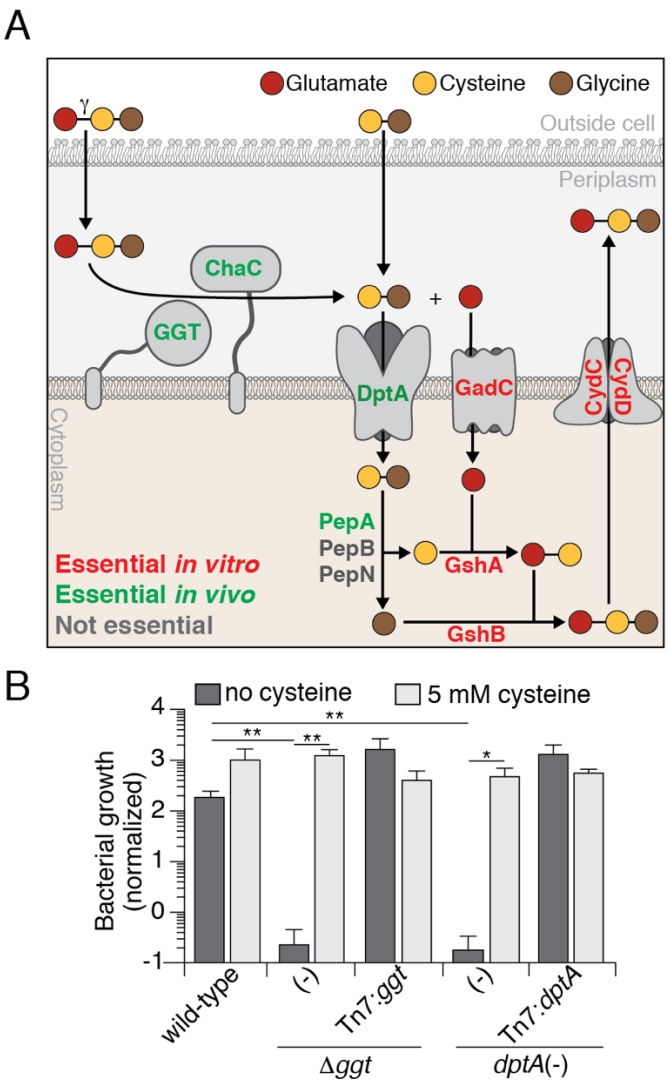

Figure 3.8. DptA and GGT are essential for *Francisella* growth in vivo in the absence of exogenous cysteine.

(**A**) Model depicting the localization and role of the indicated enzymes and transporters in the metabolism of GSH by *F. tularensis*. The color of the name text indicates the essentiality of that protein based on our Tn-Seq screen in J774 macrophages; essential for growth in MH broth, red; essential for growth in J774 macrophages, green; non-essential in the tested conditions, grey. (**B**) Growth of the indicated strains of LVS in J774 cells, normalized to bacterial counts at 2hrs post infection. J774 cells were either left untreated or treated with 5mM cysteine prior to and during the infection. Data are shown as the mean ± s.d. Asterisks represent statistically significant differences (Student's t test; **p≤0.005, *p≤0.05).

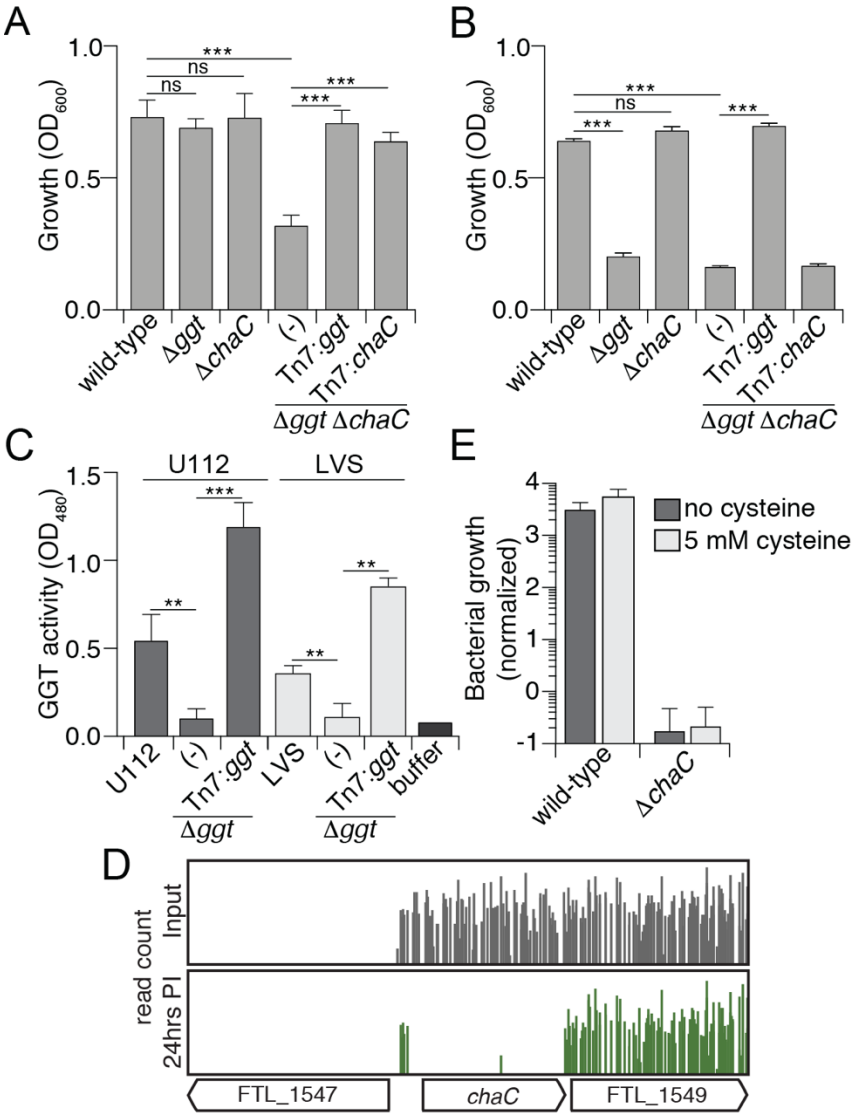

Figure 3.9. Identification of a second GGT-independent pathway in *Francisella* for GSH catabolism mediated by ChaC.

(**A-B**) OD_{600} measurements of the indicated strains of U112 after 36hrs of growth in CDM with GSH (A) and γGlu-Cys (B). Data are shown as the mean ± s.d. (**C**) GGT activity in the indicated strains of U112 and LVS determined via enzyme activity on the substrate L-γ-glutamyl-p-nitroanilide. Data are shown as the mean ± s.d. (**D**) Transposon insertion profiles from the Tn-Seq screen in J774 cells for the genetic region encompassing *chaC* from the input library (grey) and 24hrs post infection (green). Line height represents the relative abundance of sequencing reads at that position on a log scale. (**E**) Growth of the indicated strains of LVS in J774 cells, normalized to bacterial counts at 2hrs post infection. J774 cells were either left untreated or treated with 5mM cysteine prior to and during the infection. Data are shown as the mean ± s.d. Asterisks represent statistically significant differences (Student's t test; ***p≤0.0005, **p≤0.005, ns, not significant).

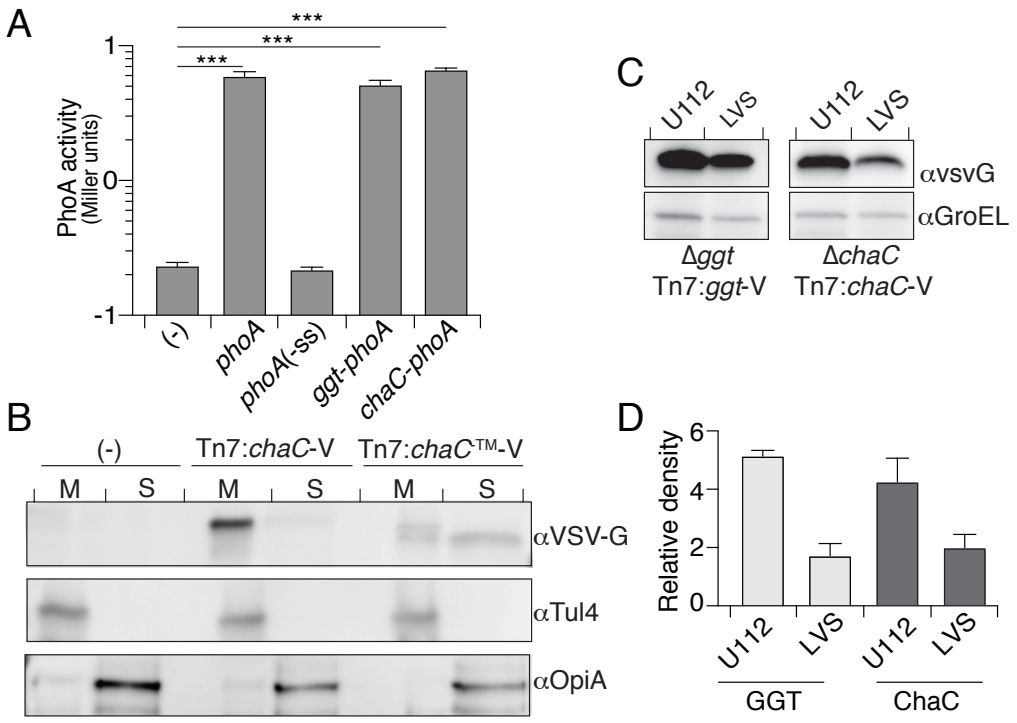

Figure 3.10. GGT and ChaC act within the periplasm and the proteins are expressed in both LVS and U112 under *in vitro* conditions.

(**A**) PhoA-activity of U112 expressing the indicated protein or protein-fusion. Data are shown as the mean ± s.d. of the cumulative results of two biological replicates performed in triplicate. Asterisks represent statistically significant differences (Student's t test; ***$p \leq 0.0005$). (**B**) Western blot analysis of the localization of ChaC in the indicated strains of U112. Tul4 and OpiA were used as controls for the membrane and soluble fractions respectively. (**C**) Western blot analysis of ChaC and GGT abundance in the indicated strains of U112 and LVS grown in CDM where GSH is the sole cysteine source. GroEL was utilized as a loading control. (**D**) Densitometry analysis of ChaC and GGT expression levels from triplicate Western blot analyses as that shown in (C). Data are shown as the mean ± s.d. of three biological replicates.

Chapter 4: GSH-catabolism plays diverse roles in *Francisella tularensis* physiology

4.1 Abstract

Catabolism of host-derived glutathione (GSH) is an essential metabolic process for the success of the intracellular pathogen *Francisella tularensis.* We previously leveraged the results of a highly saturated transposon screen to uncover two unique pathways for GSH-catabolism mediated by the enzymes GGT and ChaC. Here, we further investigate the contribution of the two GSH-catabolism pathways encoded by *F. tularensis* subsp. *novicida* and provide evidence that they differentially contribute to bacterial physiology. We show that ChaC activity contributes to defense against reactive oxygen species and that this function is linked to the outer-membrane protein FupA, with which ChaC interacts. Additionally, we provide a catalog of genes critical for GSH-catabolism in diverse genetic backgrounds. Our findings not only demonstrate a new role for GSH-catabolism in *F. tularensis*, they also highlight the complex and redundant nature of this important metabolic process.

4.2 Introduction

Francisella tularensis is a Gram-negative intracellular pathogen and the etiological agent of the disease tularemia [1]. During infection, *F. tularensis* enters host cells, primarily macrophages, through the phagosomal pathway where its briefly resides prior to escape into the cytoplasm. Within the cytoplasm *F. tularensis* proliferates robustly (~1000-fold), followed by dissemination into neighboring cells via induction of host cell death or merocytophagy [5, 64]. *F. tularensis* is auxotrophic for several important metabolites, such as cysteine, and is therefore reliant on host-derived molecules to support proliferation. In particular, *F. tularensis* has been repeatedly shown to utilize host-derived amino acids and peptides as both energy sources and in new protein synthesis [28, 84, 91, 119, 120].

We recently utilized a highly saturated transposon library to determine which *F. tularensis* genes are essential for intracellular growth [84]. This screen highlighted the important role for GSH catabolism by *F. tularensis.* GSH, which is composed of γGlu–Cys–Gly, is a low molecular weight thiol found at high concentrations (1-10mM) within host cells. Several studies have demonstrated an important function

for this molecule in *F. tularensis* pathogenesis, specifically in its role as a cysteine source [112-114]. Prior to this work, GSH catabolism was thought to be mediated primarily by γ-glutamyl transferase (GGT), which cleaves the γ-glutamyl bond in the tripeptide thereby liberating glutamate and the dipeptide Cys–Gly [112]. Our analysis revealed that *F. tularensis* encodes a second enzyme belonging to the ChaC-family of enzymes which is capable of degrading GSH, but unlike GGT, this protein is predicted to generate glutamate cyclized into 5-oxoproline (pyroglutamic acid) [36, 116, 117, 230]. Our screen additionally uncovered a Cys–Gly transporter belonging to the proton-dependent oligopeptide transporter family (POT), DptA, that is required for utilization of GSH as a cysteine source [84].

Several lines of evidence suggest that the GGT and ChaC pathways have different physiological roles. By supplementing host cells with free cysteine, we and others have demonstrated that GGT-mediated GSH catabolism facilitates cysteine acquisition and incorporation into proteins [84, 112]. However, we found that similar treatment to cells infected with a strain lacking ChaC did not recover growth levels, suggesting an alternative role for ChaC-mediated GSH degradation. Additionally, we found that *F. tularensis* subsp *holarctica* and subsp *novicida* differentially utilize these pathways *in vitro* [84]. Here we further investigate the mechanisms and physiological roles of the two GSH catabolism pathways. We focused our attention on *F. tularensis* subsp *novicida*, (*F. novicida*), as we have found both enzymes to be active *in vitro,* thereby allowing us to individually probe the role of each pathway. Through this work we reveal additional components in the GGT pathway and find that ChaC activity contributes to defense against reactive oxygen species. We provide evidence that ChaC interacts with numerous inner-membrane complexes as well as the outer membrane protein FupA. Finally, we report the results from an unbiased genetic screen which reveals the complex nature of GSH catabolism in *F. novicida*.

4.3 Results

4.3.1 *ChaC and GGT form two distinct pathways for GSH catabolism*

Our previous results suggested that ChaC and GGT act interchangeably in GSH catabolism during *in vitro* growth of *F. novicida* [84]. If both enzymes generate the same product, Cys–Gly, then we predicted that the Cys–Gly transporter we previously identified, DptA, should be required for growth on GSH as a sole cysteine source in this strain. However, we found that a *F. novicida* mutant lacking DptA grew similarly to wild-type when supplied with GSH as a sole cysteine source (Fig. 4.1A). Therefore, we tested the contribution of DptA to growth in conditions with Cys–Gly as the sole cysteine source. This analysis revealed that a strain lacking DptA remains capable of moderate levels of growth under these conditions (Fig. 4.1B).

These results led us to hypothesize that *F. novicida* encodes a second, potentially lower affinity, Cys–Gly transporter. All subspecies of *F. tularensis* encode 8 POT-family members that possess little (<50%) homology with each other, likely contributing to diverse substrate specificities. As substrate specificity is dictated by residues within the POT, we deleted the gene encoding the POT-protein with the highest homology to *dptA*, FTN_1272, which we will refer to as DptB. Deletion of *dptB* alone had no effect on growth when Cys–Gly was provided as the sole cysteine source. However, when both *dptA* and *dptB* were absent, growth on Cys–Gly was abrogated (Fig 4.1B). These phenotypes could be complemented by expressing *dptA* or *dptB* from an ectopic site on the chromosome.

While a Δ*dptA* Δ*dptB* strain is unable to utilize Cys–Gly to support growth, proliferation in conditions where GSH is the sole cysteine source is unaffected (Fig 4.1A). This result is inconsistent with the hypothesis that ChaC and GGT are both predicted to generate Cys–Gly from GSH. We therefore tested the requirement of ChaC and GGT during growth on GSH in a background lacking *dptA* and *dptB*. While deletion of *ggt* did not impact growth dynamics in this background, deletion of *chaC* in combination with *dptA* and *dptB* significantly reduced proliferation (Fig. 4.1A). Of note, the Δ*chaC* Δ*ggt* and Δ*chaC* Δ*dptA* Δ*dptB* strains behave almost identically when grown under conditions wtih GSH as the

sole cysteine source (Fig 4.1A, C). This suggests that while DptA and DptB act as part of the GGT-pathway, ChaC forms part of a unique pathway for GSH catabolism that does not rely on these transporters.

4.3.2 *ChaC enzymes have a unique substrate binding motif and can be found throughout bacteria*

GGT-enzymes are well characterized, and we therefore focused our attention on ChaC to better understand GSH-catabolism in *F. tularensis*. ChaC enzymes have primarily been studied in eukaryotes, and while homologs have been identified in *Escherichia coli* and *F. tularensis*, the distribution of these proteins throughout bacteria has not been examined [36, 116, 117, 230]. There is currently no *in silico* approach for determining if a gamma glutamyl cyclotransferase (GGCT) enzyme will be specific for GSH and therefore fall within the ChaC family. In order to perform phylogenetic analysis of the distribution of ChaC, we sought to define a ChaC domain. GGCT enzymes are defined by the presence of a conserved substrate binding motif and a downstream conserved glutamate that mediates the enzymatic reaction [36, 116, 117, 230].. Comparison of characterized ChaC and non-ChaC GGCT proteins revealed that the substrate binding motif of ChaC is two amino acids longer than that of non-ChaC GGCT enzymes (xYGSx→GYGSL). Additionally, all characterized ChaC enzymes have a conserved arginine immediately upstream of the active glutamate. Therefore, we propose that the ChaC domain is GYGSL…RE where the two amino acid motifs are 60-90 amino acids apart (average ~70) (Fig. 4.2A, 4.3).

Consistent with our assignment of ChaC to this family of enzymes, mutation of either the predicted substrate binding motif (residues 72-75) or the enzymatic glutamate (E144) mimic a *chaC* deletion (Fig. 4.1C). Using our new ChaC domain, we were able to find ChaC enzymes throughout eukaryotes and prokaryotes (Fig 4.2B). When we looked specifically within bacteria, we were able to identify ChaC-enzymes in a diverse array of organisms ranging from Gram-positive to Gram-negative, with an enrichment found within γ–proteobacteria. Whether the role of ChaC is analogous in all

organisms remains unclear, although work on human ChaC enzymes suggest these proteins can have unique impacts on GSH catabolism [36, 116, 117, 230]..

4.3.3 *ChaC contributes to H_2O_2 tolerance*

GSH contributes to numerous processes within cells, but it may be most notorious for its role as a potent antioxidant [113]. While *F. tularensis* encodes several mechanisms to combat reactive oxygen and nitrogen species (ROS, NOS), the role of GSH in redox stress has not been determined [24, 28, 74-76]. We therefore tested the role of ChaC and GGT in resistance to a common ROS, hydrogen peroxide (H_2O_2). While GGT was not required for ROS-resistance, a strain lacking *chaC* displayed dramatically increased sensitivity to H_2O_2 (Fig. 4.4A). The increased sensitivity of a Δ*chaC* strain could be observed over a wide range of H_2O_2 concentrations and importantly, we could complement this defect by expressing *chaC* from an ectopic site on the chromosome (Fig. 4.4A, B).

We next asked if the increased sensitivity was due to altered levels of intracellular GSH, by supplementing the cells with excess GSH prior to H_2O_2 exposure. Addition of GSH did not affect the survival of either the wild-type or Δ*chaC* strains despite the fact GSH was added at significantly higher concentration than the H_2O_2 (Fig. 4.4C). As GSH levels did not contribute to the survival rates of a Δ*chaC* strain, we hypothesized that the role of this protein was independent of its catalytic activity. We therefore tested a strain expressing the catalytically inactive form of ChaC (E144Q) from the native site on the chromosome. Surprisingly, this strain mimics a Δ*chaC* strain and displays increased sensitivity to H_2O_2 (Fig. 4.4A). Therefore, while the catalytic activity of ChaC is required for H_2O_2 tolerance, the mechanism underlying this remains unclear.

4.3.4 *ChaC possesses the core GGCT-fold but is enzymatically inactive in vitro*

To gain insight into the mechanism of ChaC, we determined the X-ray crystal structure of ChaC encoded by *F. novicida*. This periplasmic protein possesses a transmembrane (TM) domain and therefore

in order to obtain soluble protein we utilized a variant lacking the TM domain but fused to the PhoA signal sequence. Using this protein crystalized alone or in the presence of GSH we were able to obtain structures of ChaC in an apo state (not shown) as well as in complex with the GSH-byproduct 5-oxoproline at a resolution of 1.7 Å and 1.45 Å respectively (Fig. 4.6A, Table 4.1). Phases were experimentally obtained using selenomethionine-substituted proteins and molecular replacement was used to solve the structure of the native crystals in the P2 space group.

These structures reveal that ChaC adopts the BtrG/GGCT-fold previously described by Oakely et al which is the characteristic fold of the ChaC-family (GGCT paper and ChaC papers showing same fold). These proteins adopt a mixed α/β topology with the N-terminal region primarily composed of packed β-sheets and the C-terminal region of α-helices (Fig. 4.6A). Furthermore, superimposition with the ChaC-homolog encoded by *Saccharomyces cerevisiae* or the human GGCT C7orf24, demonstrates a high degree of structure similarity specifically in the active site pocket (Fig. 4.6B, C) [116, 231]. The C-terminal region displays lower degrees of overlap, with the yeast protein containing an α-helix between β-sheets 5 and 6 that is not present in the *F. novicida* or human proteins (Fig. 4.2A, 4.6B). Additionally, the majority of the C-terminal α-helices of the *F. novicida* protein do not superimpose with either of the other proteins (Fig. 4.6B, C). Whether this simply reflects the flexible nature of this region or is indicative of important biological differences remains to be determined.

We were excited to see 5-oxoproline in the crystal formed in the presence of GSH (Fig. 4.6A, D). Upon closer examination we were able to confirm that the product of ChaC was present in the active pocket in close proximity to the catalytic glutamate (Fig. 4.6D). This finding supports the predicted enzymatic activity of ChaC and is the first time a ChaC structure has included a by-product. In order to further characterize the enzymatic activity, we utilized purified ChaC in enzymatic assays that monitor the formation of Cys–Gly (ref papers). In parallel we also tested the catalytically inactive form of the protein, along with the ChaC homolog encoded by *E. coli* (^{Ec}ChaC) (Fig. 4.5B). While we were able to measure Cys–Gly generation by ^{Ec}ChaC, we were unable to find conditions under which ChaC from *F.*

novicida (^{Ftn}ChaC) generated this product (Fig. 4.6E). In order to determine if ^{Ftn}ChaC is generating a unique by-product, or if the purified protein is unable to act on GSH, we heat treated the ^{Ftn}ChaC-reactions and exposed the resulting products to ^{Ec}ChaC. We then determined the levels of Cys–Gly generated pre and post addition of the ^{Ec}ChaC. ^{Ec}ChaC-treatment resulted in Cys-Gly levels equivalent to our negative control sample, demonstrating that under the conditions tested, ^{Ftn}ChaC is unable to act on GSH (Fig. 4.6F). Therefore, while we were able to see generation of 5-oxoproline in the X-ray crystal structure, these results suggest that additional factors may be required for optimal ^{Ftn}ChaC activity.

4.3.5 *The transmembrane domain of ChaC facilitates interactions with numerous protein complexes*

The lack of apparent enzymatic activity *in vitro* prompted us to test if ChaC interacts with other proteins that may be required for activity. To this end, we generated a strain of *F. novicida* that expresses a C-terminally vsv-G tagged ChaC, along with an analogous strain expressing vsv-G tagged GGT. Growth assays as well as H_2O_2 sensitivity assays confirm that the epitope tag does not interfere with either function of ChaC (Fig. 4.7A, B). We therefore utilized these strains in immunoprecipitation assays under conditions where GSH is the sole cysteine source. The resulting protein profiles were visualized via Coomassie brilliant blue staining and by comparing our experimental samples with a control strain lacking a vsv-G tag we were able to confirm enrichment for either ChaC or GGT (Fig. 4.7C). Excitingly, we found that additional proteins were immunoprecipitated specifically in the *chaC*-vsv-G samples.

To determine the identity of these proteins, we analyzed the samples via mass spectrometry. Comparison with the control strain revealed that numerous inner-membrane protein complexes (i.e. the T6SS^{ii}, the type IV pili and, the nuo-complex) as well as over 50 other proteins were enriched in the ChaC samples (Fig. 4.7D, Appendix 3). This large list made it challenging to determine which, if any, of the proteins identified contribute to the activity of ChaC. We have previously demonstrated that ChaC possesses a TM domain that anchors the protein in the inner-membrane [84]. We therefore hypothesized that the localization of ChaC may contribute to the large quantity of proteins identified. To test this, we generated a strain of *F. novicida* that expresses ChaC lacking the TM domain, but that is still localized to

the periplasm via a signal sequence (ChaC^{-TM}). Indeed, we found that ChaC^{-TM} co-immunoprecipitated with significantly fewer proteins and that no inner-membrane complexes were identified (Fig. 4.7E, F). This decrease in interacting partners lead us to ask if the TM domain of ChaC is essential for its role in bacterial physiology. Through growth curve analysis as well as H_2O_2 sensitivity assays we found that the TM domain is dispensable for activity thereby demonstrating that the interactions with the inner-membrane complexes are nonessential for ChaC function (Fig. 4.7A, B).

4.3.6 *FupA coimmunoprecipitates with ChaC and contributes to GSH catabolism*

Both full length ChaC and ChaC^{-TM} co-immunoprecipitates with the protein FTN_0444 (FupA, also referred to as FopA) (Fig. 4.7D, E). FupA is an outer-membrane protein that has been demonstrated to play a role in iron acquisition and membrane stability [104, 110, 232]. To test the role of this protein in ChaC-linked phenotypes, we generated strains in which *fupA* was deleted alone or in combination with *ggt* or *chaC*. We next utilized these strains in growth assays where GSH is the sole cysteine source. This analysis demonstrates that FupA is required for optimal growth on GSH, independent of the genetic background (Fig. 4.8A). To further investigate the role of FupA in GSH catabolism, we monitored growth where Cys–Gly is the sole cysteine source. Again, strains lacking *fupA* were attenuated with minimal proliferation observed (Fig. 4.8B). It is important to note that FupA is dispensable for growth when free cysteine is supplied (data not shown). These results suggest that FupA plays a critical role in GSH catabolism independent of its interaction with ChaC.

As stated above, FupA has been linked to iron acquisition and therefore to levels of intracellular iron. Iron is a highly reactive molecule that when exposed to ROS contributes to damaging Fenton chemistry [109]. Therefore, we tested whether FupA contributes to H_2O_2 tolerance, alone or in combination with ChaC. We found that deletion of *fupA* alone leads to survival equivalent to that of wild-type *F. novicida* (Fig 4.8C). However, deletion of *fupA* in combination with *chaC* alleviated the H_2O_2 sensitivity of the ChaC-depleted strain, and that this phenotype can be complemented by expressing *fupA* from an ectopic site on the chromosome (Fig. 4.8C). This suggests that FupA contributes to the increased

sensitivity of a Δ*chaC* strain, potentially linking ChaC to iron metabolism. In contrast with the predicted role of FupA, we found that the concentration of iron present during H_2O_2 exposure did not affect the survival rates of any of the strains tested (Fig. 4.8C). Taken together, these data suggest that FupA plays a previously unrecognized role in *F. tularensis* metabolism and stress response.

4.3.7 *Transposon-based screen highlights the complex nature of GSH-catabolism in U112*

The results thus far support a model in which *F. novicida* encodes two pathways for the catabolism of GSH, both of which require FupA (Fig. 4.9). DptA, and to a lesser extent DptB, transport the GGT by-product Cys-Gly, but do not contribute to the ChaC pathway. While both pathways contribute to the utilization of GSH as a cysteine source, the ChaC pathway uniquely plays a role in ROS tolerance, although the mechanism underlying this are unclear. Numerous components of the GSH-catabolism pathways have yet to be identified, including the transporters for the ChaC by-products. Therefore, we set out to perform an unbiased, genome-wide screen to better understand this important metabolic process (Fig. 4.9). Due to the redundant nature of these pathways, transposon libraries were generated in the wild-type, Δ*ggt*, Δ*chaC*, and Δ*dtptA* Δ*dptB* genetic backgrounds of *F. novicida* for use in transposon insertion sequencing (Tn-Seq) experiments.

Using the transposon previously described, we mutagenized each of the indicated genetic backgrounds resulting in 100,000-300,000 single colonies per library [84]. We then subjected these libraries to growth under conditions of Cys-HCl or GSH as sole cysteine sources and used high throughput sequencing to identify transposon mutants selectively depleted under each condition. The results from this screen recapitulated several phenotypes from our early experiments. For example, the gene encoding FupA was required for growth in all genetic backgrounds with GSH as the sole cysteine source (Fig 4.10). Additionally, *chaC* was critical for growth on GSH specifically in the Δ*ggt* and Δ*dptA*Δ*dptB* samples. Analysis of the wild-type library revealed few genes as critical for growth on GSH, underscoring the redundant nature of the GSH-utilization pathways. In contrast, a significant number of genes were found to contribute to growth on GSH when either the GGT or ChaC pathway is disrupted

(Fig 4.10). While extensive follow-up of this screen is outside the scope of this work, we believe these results highlight the complex nature of GSH catabolism in *F. tularensis* and provide insight on additional components of the ChaC pathway.

4.4 Discussion

The results from our *in vitro* growth assays revealed the existence of a second Cys–Gly transporter, DptB, that contributes to the GGT pathway of GSH catabolism. Of note, a homolog of *dptB* is present on the genome of all species of *F. tularensis* including LVS (FTL_0691), for which we presiouvly found DptA to be the sole Cys–Gly transporter. This finding, along with the differential role of ChaC in different species, highlights the unique utilization of these proteins under *in vitro* conditions. Due to the intermediate phenotype of a Δ*dptA* strain when grown under conditions where Cys–Gly is the sole cysteine source, we speculate that DptB has lower affinity for this dipeptide. Thus, in the absence of *dptA*, DptB can only support growth when high concentrations of Cys–Gly are present, and when concentrations drop, proliferation is limited. Supporting this, we also see the a Δ*chaC* Δ*dptA* strains has an intermediate phenotype when grown under conditions where GSH is the sole cysteine source.

The ChaC family of enzymes belongs to the GGCT superfamily of proteins which are known to cleave γ-glutamyl bonds releasing the attached amino acid(s) and 5-oxoproline [36, 116, 117]. ChaC enzymes solely act on GSH, whereas other members of the GGCT family are unable to catabolize GSH and instead act on other γ-glutamyl containing molecules [36, 84, 116, 117]. Here we report small differences in the substrate binding motif that allow for differentiating ChaC-family proteins, and we therefore propose a new ChaC-domain. We next set out to determine the distribution of these proteins and found ChaC homologs through eukaryotes and prokaryotes. Within bacteria, ChaC-family members are found throughout Gram-positive and Gram-negative organisms. We did not find an enrichment for host-associated bacteria and instead identified organisms from diverse environments. However, we found that only the ChaC homologs encoded by *F. tularensis, Legionella pneumophila* and *Klebsiella oxytoca* – all of which are known pathogens - possess transmembrane domains and are therefore predicted to be non-

cytoplasmic. Combined, these results suggest that ChaC enzymes may contribute to diverse facets of bacterial physiology.

We have previously shown that *F. tularensis* encodes two pathways for the catabolism of GSH [84]. While the role of the GGT pathway in providing cysteine during intracellular growth is clear, the precise role of the ChaC pathway remains unknown. As GSH is a potent antioxidant, we tested the contribution of this molecule in defense from ROS. Initially we speculated that deletion of *chaC* or *ggt* would increase survival, as higher periplasmic levels of GSH should be present in these genetic backgrounds. In contrast, we found that the enzymatic activity of ChaC is essential for survival when exposed to ROS and that the concentration of GSH did not influence survival dynamics. We still lack an explanation for these observations, but, as discussed below, we hypothesize that this phenotype is due to the interaction of ChaC with FupA.

Growth assays, as well as our unbiased genetic screen, revealed a critical role for FupA in GSH-catabolism independent of the genetic background tested. Importantly, we found that FupA is also required for optimal growth when Cys–Gly is the sole cysteine source. These results were unexpected, and the mechanism underlying them remain unclear. FupA is an outer-membrane protein that possesses high homology with FslE, an outer-membrane protein implicated in siderophore binding and uptake [104, 110, 232]. In *F. tularensis* subsp *tularensis* Schu S4 and *F. tularensis* subsp *holarctica* LVS, FupA has been demonstrated to contribute to iron uptake, although the form of iron is dependent on the strain used and the molecular details of the transport process have not been delineated. In U112, FupA is implicated in outer-membrane stability and antibiotic resistance; however, the mechanistic basis for this link is also lacking [110]. Whether the contribution of FupA to GSH catabolism is related to these phenotypes remain to be defined. I speculate that probing the link between iron and GSH uptake may be an informative future line of investigation.

Through immunoprecipitation assays we found that ChaC coimmunoprecipitates with FupA independent of the transmembrane domain of ChaC that mediates non-essential interactions. While it remains unclear if this interaction is direct, evidence suggests that the function of these two proteins is

linked. Beyond its role in GSH utilization, we found that deletion of *fupA* alleviates the sensitivity of a Δ*chaC* strain to H_2O_2. Iron levels did not affect the sensitivity of these strains highlighting a novel role for FupA in bacterial physiology.

As several components of both the GGT and ChaC remain unknown, as well as what additional pathways are required for GSH-catabolism, we set out to perform an unbiased genetic screen. We utilized transposon libraries generated in four genetic backgrounds – wild-type, Δ*ggt*, Δ*chaC* and Δ*dptA* Δ*dptB*- with the hopes of uncovering components of the two unique pathways. Growth of these libraries on either Cys or GSH allowed us to uncover the genes that are specifically required for GSH utilization in each background. Additionally, by comparing the essentiality of genes between the different genotypes, we hope to uncover novel components of the GGT and ChaC pathways. For examples, genes found to be essential specifically in the Δ*ggt* and Δ*dptA* Δ*dptB* backgrounds may represent components of the ChaC-pathway and vice versa.

The results from this screen demonstrate that few genes are critical for GSH-catabolism in the wild-type background further highlighting the redundant nature of these pathways. Consistent with our assignment of these genes to the same pathway, we obtained nearly identical results from the libraries constructed in the Δ*ggt* and Δ*dtpA* Δ*dptB* strains. Of note, significantly more genes were identified in the Δ*chaC* background as being required for growth when GSH is the sole cysteine source. As a Δ*chaC* strain has increased sensitivity to H_2O_2 and is sensitive to oxygen (data not shown), we hypothesize that these genes encode proteins critical for both GSH-catabolism as well as stress survival. Follow-up studies are needed to define the role of the genes we identified in these two important processes. In total, we believe these data highlight the critical and complex role of GSH catabolism in *F. tularensis* physiology and pathogenesis.

4.5 Materials and Methods

Mutant generation. In-frame deletion mutations in U112 were generated via allelic exchange as described previously [37]. Deletion vectors contained 1000bp of flanking regions of cloned into the

BamHI and PstI sites of the vector pEX18-pheS-km [22]. For all mutants, strains containing the modified genetic region of interested were confirmed by colony PCR and sequencing of PCR products generated from genomic DNA.

The miniTn7 system vector pMP749 was utilized for genetic complementation [187]. For *ggt*, *chaC, dptA and dptB*, the open reading frame plus the intergenic regions upstream (including the native promoter region) and downstream of the gene were amplified by PCR and cloned into the HindIII and BamHI sites of pMP749. For *fupA, chaC*-V, and *chaC*$^{-TM}$-V, the gene was cloned downstream of the *bfr* promoter. The two ChaC constructs contained C-terminal vsv-G epitope tags and in the case of ChaC-TM, the Sec-dependent signal sequence of *phoA* was placed between the promoter and residue 23 of ChaC (removing the transmembrane domain) Complementation strains were then generated using these vectors as described in [37]. Integration downstream of the *glmS* gene was confirmed by colony PCR.

Construction of Expression Plasmids. Heterologous expression in *E. coli* employed the plasmids pET28b and pET22. To enable IPTG-inducible expression of *dugP1* and ^{EC}*chaC*, the open reading frame of the gene was amplified from genomic DNA and cloned into the NcoI and XhoI sites of pET28b. To obtain soluble ChaC, residues 67-801 were amplified from U112 genomic DNA and cloned into BamHI and XhoI sites of pET22b. The use of pET22b was critical as it contains a periplasmic signal sequence that is necessary for the proper folding of ChaC. To construct catalytically inactive ChaC, residue E144 was mutated to Q through site-directed mutagenesis. For use in crystallization studies, residues 67-750 we amplified and again cloned into the BamHI and XhoI sites of pET22b.

Bioinformatics

The protein sequences of all experimentally confirmed GGCT and ChaC-enzymes were collected, and multi-sequence alignment tools were utilized to compare the substrate binding motif and active site resides. This revealed that the substrate binding domain of ChaC-enzymes is longer than in other GGCT proteins and allowed us to define the ChaC domain as GYGSL-xx-RE where the two amino acid motifs

are between 60-90 amino acids apart. We then submitted the amino acid sequence of the human, the E coli and the U112 ChaC sequences to BLASTp (https://blast.ncbi.nlm.nih.gov/Blast.cgi?PAGE=Proteins) using a non-redundant protein sequence library. Combining these results, we identified proteins that contain the new ChaC domain and collected a catalog of organisms that encode ChaC enzymes. Finally, we selected representative ChaC proteins from across the phylogenetic distribution of these enzymes and utilized these sequences to generate the alignment, and sequence logos presented in Fig 4.2B and 4.3.

To generate a phylogenetic tree of the ChaC sequences described above, we utilized Geneious version 10.0 created by Biomatters *(http://www.geneious.com*) to generate an unrooted tree. Importantly, branch lengths were modified and therefor genetic distances are not accurately depicted.

Growth Curves. To examine bacterial proliferation on different cysteine sources, the indicated strains of U112 were first grown overnight in Chamberlain's defined media (CDM) [227] with 1 mM cysteine at 37ºC with shaking followed by evaluation as previously described [84]. Briefly, cells were washed three times and resuspended in CDM lacking cysteine followed cysteine starved for 2 hrs at 37ºC with shaking. Cultures were then diluted to an OD_{600}= 0.01 in CDM with the indicated potential cysteine source at 100 μM. Cultures were transferred in triplicate to a 96-well plate and the OD_{600} of the cultures was monitored for 36hrs in a plate reader.

H_2O_2 sensitivity assays. To monitor H_2O_2 tolerance levels, the indicated strains of U112 were first grown overnight at 37ºC on CDM agar plates. The following day, cells were collected, resuspend in liquid CDM media and cultures were diluted to an OD_{600}= 0.1. The cultures were placed at 37ºC with shaking and grown to mid log (OD_{600}= 0.4-0.6). Again, cultures were diluted to an OD_{600}= 0.1 and samples were pulled for colony forming unit (CFU) quantification. The indicated concentration of H_2O_2 was then added and the cultures were placed at 37ºC with shaking. After 30min, samples were pulled in triplicate for CFU enumeration. Survival rates were calculated by comparing the CFU numbers pre and post H_2O_2 exposure.

To test the contribution of GSH, the indicated concentration of GSH was added to cultures prior to addition of H_2O_2. The role of iron in H2O2 tolerance was evaluated by testing CDM +/- iron. In order to remove trace iron levels, CDM was treated with BioChelex. Indicated strains were diluted to OD_{600}= 0.1 in CDM-iron and placed at 37ºC with shaking for 16hrs to iron stave the cells. The OD_{600} of the cultures were normalized and for the + iron conditions, 14μM FeSO4 was added 30min prior to H_2O_2 exposure.

Protein Expression and Purification. For protein expression, *E. coli* BL21 cells carrying expression plasmids were diluted in 2xYT broth and grown at 37°C until the OD_{600}=0.5. Induction was mediated by the addition of 1 mM IPTG to cultures followed by incubated for 18 hours at 18 °C with shaking. Cells collected by centrifugation were resuspended in buffer containing 20 mM Tris-HCl pH 7.5, 500 mM NaCl, 5mM imidazole, 1 mM AEBSF, 10 mM leupeptin, 1 mM pepstatin, 1 mM lysozome and 1mU benzonase. Cells were disrupted by sonication and cellular debris was removed by centrifugation at 45,000 x g for 45 min. Lysates were run over a 1 mL HisTrap FF NI-TA cartridge on an AKTA FPLC purification system to purify the His-tagged proteins. The bound proteins were eluted using a linear imidazole gradient from 5 mM to 500 mM. The purity of each protein sample was assessed by SDS-PAGE and Coomassie brilliant blue staining, and fractions with high purity concentrated using a 10kDa cutoff filter.

In order to further purify the proteins, samples were run over a Superdex 200 column equilibrated in sizing buffer (300 mM NaCl, 50 mM Tris-HCl pH 7.5, and 1 mM DTT). Again, purity of each fraction was assessed by SDS-PAGE and Coomassie brilliant blue straining. For Dug1P, fractions the highest purity were pooled, concentrated and utilized in biochemical assays. For all ChaC enzymes, high purity fractions were concentrated and then dialyzed in 200 mM NaCl, 20 mM Tris pH7.5 and 1 mM TCEP prior to use in downstream applications. Cells expressing selenomethionine containing ChaC were grown

in SelenoMethionine Medium Complete (Molecular Dimensions) using the expression conditions described above. All downstream steps were also performed as described above.

Crystallization, X-ray data collection, and structure determination. For crystallization of native ChaC and selenomethionine incorporated ChaC, dialyzed purified protein concentrated to 8mg/mL was screened against a commercially available crystallization screen (Microlytic). Crystals with high diffraction were obtained by hanging drop vapor diffusion at room temperature in a solution containing 200mM ammonium acetate, 100mM Bis-Tris pH 5.5, and 25% (v/v) PEG3350. Crystals containing selenomethionine were obtained at 4mg/mL in identical crystallization buffer. To obtain ChaC in complex with 5-oxoproline, 10mM GSH was added to protein prior to the crystallization screen. Crystals were obtained in buffer containing 100mM HEPES and 25% PEG3350. Prior to data collection, crystals were cryoprotected in buffer consisting of the above components plus 30% glycerol.

Native data were obtained at a resolution of 0.979 Å and 1 Å for ChaC and ChaC+5-oxoproline respectively. Selenomethionine-icorporated crystals were obtained at 1 Å and all crystals were obtained at 100 K temperature on the BL502 beamline (ALS, Lawrence Berkeley National Laboratory). All three crystals were monomers that displayed symmetry in the $P2_12_12_1$ space ground.

ChaC enzyme assays. To determine if purified ChaC enzymes generate Cys-Gly, a Dug1P-coupled assay was utilized a previously described [116]. Briefly, 5µg of purified protein (or buffer) was incubated with 10mM GSH in a buffer containing 50mM Tris pH8 and 5mM DTT at 37C for 30min. Reactions were terminated by heating at 98C for 5 min. To mediate Cys-Gly degradation, 5µg of Dug1P and 20µM MnCl2 were added to each reaction followed by incubation at 37C for 1 hr. Finally, cysteine levels were estimated using a ninhydrin-based method [233]. For samples that were treated with ChaC from E coli, 5ug of enzyme was added after the initial incubation at 98C, followed by an additional 30min incubation at 37C. Reaction were heat treated for 5min followed and experiments continued as above.

Immunoprecipitation Assays. To assess the interacting partners of ChaC, overnight cultures of the indicated strains were diluted 1:100 in 50mL CDM containing 100μM GSH and allowed to grow to mid log phase. Cells were harvested by centrifugation at 7,000 x G for 15 min. Pellets were resuspended in 4 mL IP buffer (20 mM Tris HCl pH 7.5, 150 mM NaCl, 2% glycerol, 1 mM AEBSF, 10 μM leupeptin, 1 μM pepstatin, 1mg/mL lysozyme, 1% Triton-X, and 1mM β-mercaptaethanol), sonicated and centrifuged at 4°C for 30 min at 40,000 x G to pellet debris. The supernatants were incubated with 30 μL αvsv-G agarose beads (Sigma Aldrich) for 2 hrs at 4°C and washed four times with 10 mL of IP buffer lacking lysozyme prior to analysis by SDS-PAGE and either western blot or Coomassie brilliant blue staining. In order to identify all possible ChaC interacting partners, a portion of the αvsv-G beads were reserved for MS analysis.

Identification of ChaC interacting partners by mass spectrometry. The samples described above were resuspended in 100ng trypsin diluted in 20mM ammonium bicarbonate and placed at 37°C for 16hrs with low shaking to mediate on bead digestion. The released peptides were then collected via centrifugation and reduced and alkylated with dithiotreitol and iodoactamide, respectively. The resulting peptides were desalted with C18 spin columns (Pierce) following the manufacturer's protocol**.**

Transposon mutant library generation. To construct the transposon mutant libraries, 300 ug of transposon delivery plasmid pKL97 was used to transform the indicated genetic backgrounds of *F. novicida* as described in [37] and cells were plated on TSAC with 15 μg mL^{-1} kanamycin. Plates were incubated for 20hrs at 37°C and the resulting kanamycin-resistant colonies, approximately 100,000-300,00 per genetic background, were combined in liquid CDM lacking cysteine. As we wanted to test growth on minimal media, we then washed each library x4 in CDM-Cys prior to freezing down the aliquots totally ~10^6 CFU each.

Tn-seq screen. For each genetic background, two aliquots of the transposon libraries described above were thawed and used as the innocula for 50mL CDM lacking cysteine. Cultures were placed at 37°C with shaking for 2 hrs prior to addition of 100uM cysteine or GSH and incubation for 20hrs at 37°C with shaking. Cells were then collected via centrifugation gDNA was extracted (Qiagen). To generate sequencing libraries, DNA from each sample was sheared to ~300bp on a Covaris followed by DNA-end repair and terminal C-tailing. Transposon-specific primers were then utilized to amplify the transposon-genome junctions and add the proper adaptor sequences. The resulting libraries were pooled and sequenced using single-end 150 bp sequencing with a single read cluster kit on an Illumina MiSeq at 11 pM density with 15% PhiX.

Tn-seq analysis. Data was analyzed using the Tn-Seq Pre-Processor (TPP)component of TRANSIT as described (https://transit.readthedocs.io/en/latest/transit_overview.html). Prior to TPP reads were trimmed by a fixed amount to remove transposon sequences and junk sequence added during library generation.

4.6 Figures

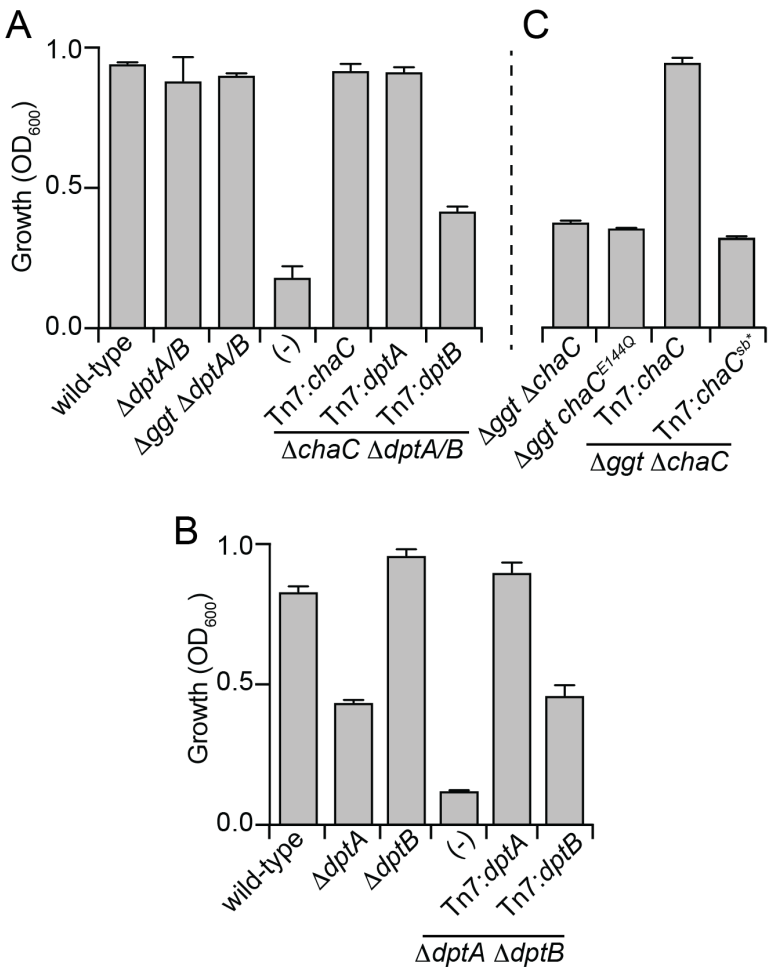

Figure 4.1. ChaC and GGT form two distinct pathways for GSH catabolism
(**A-C**) OD_{600} measurements of the indicated strains of U112 after 36hrs of growth in CDM with glutathione (A,C), or Cys–Gly (G). Data are shown as mean ± s.d.

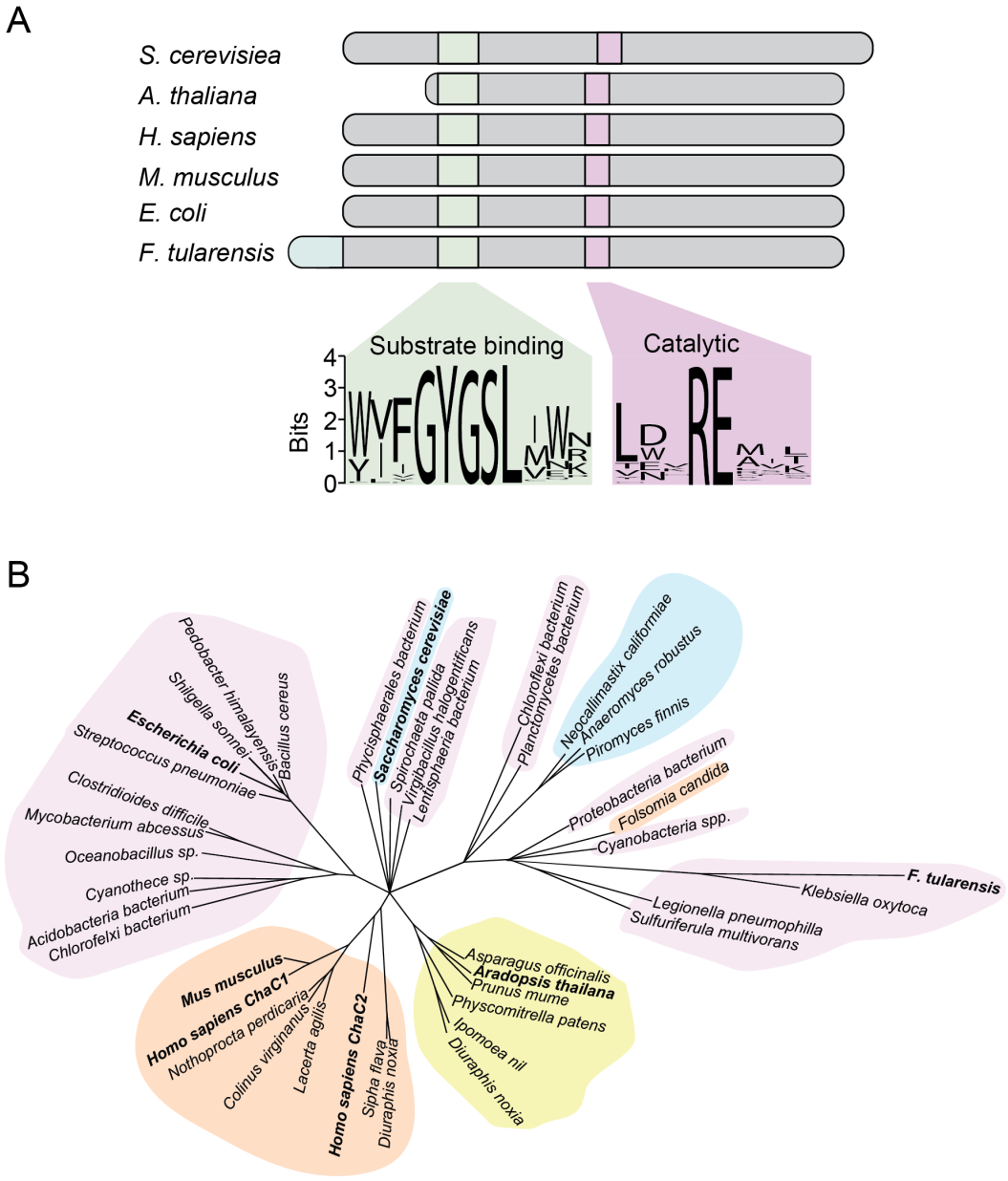

Figure 4.2. ChaC enzymes have a unique substrate binding motif and can be found throughout bacteria

(**A**) Graphical representations of experimentally confirmed ChaC proteins. Transmembrane domains (blue), substrate binding motif (green) and catalytic motifs (purple) are highlighted. Sequence logo indicates conserved motifs derived from an alignment of ChaC sequences from the species representative of the organisms shown in panel B (alignment shown in Figure 4.3). (**B**) Phylogenetic depiction of the distribution of ChaC proteins. Metazoan (orange), fungi (blue), Viridiplantae (yellow), and bacterial (purple) proteins are represented. Experimentally confirmed ChaC proteins are in bold.

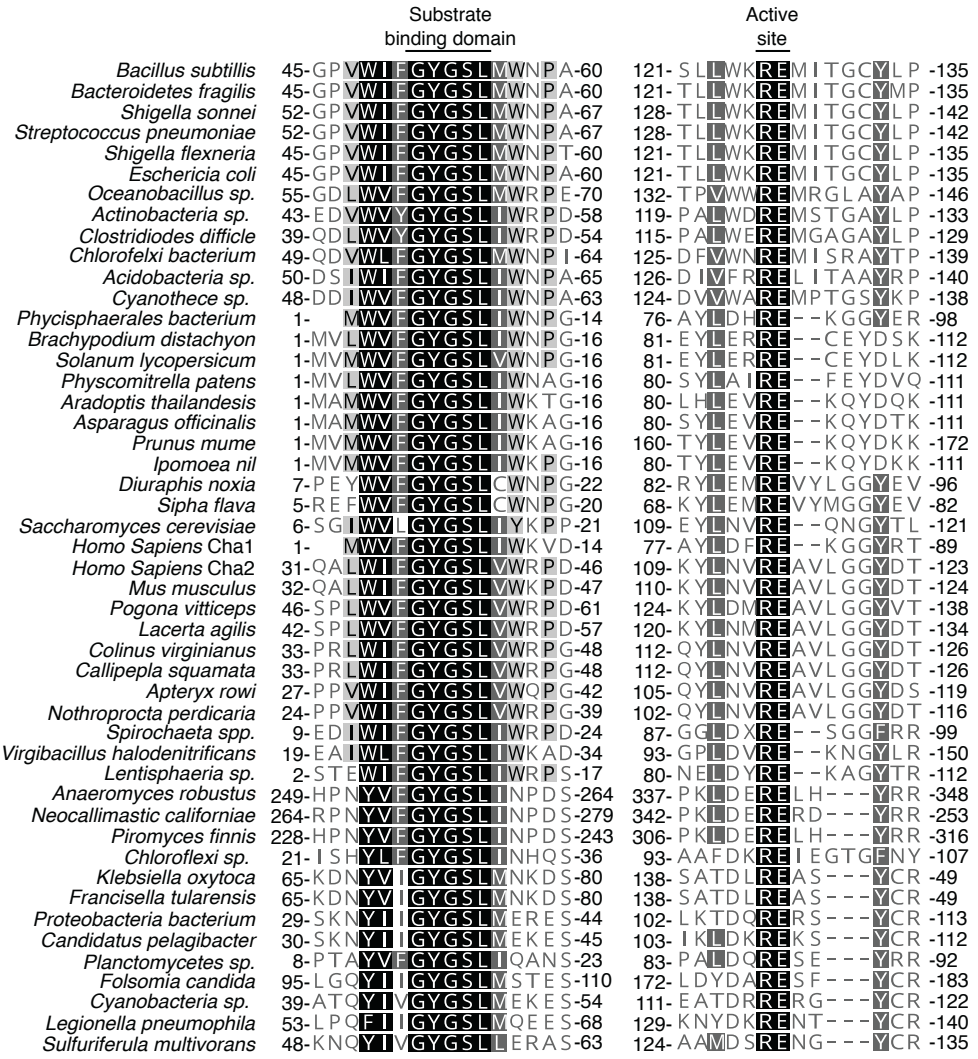

Figure 4.3. ChaC-enzymes possess two conserved amino acid motifs.
Partial alignment of ChaC sequences from species representative of each phyla we identified ChaC-homologs, highlighting the two conserved motifs (perfectly conserved residues, black; highly conserved residues, dark grey; conserved residues, light grey).

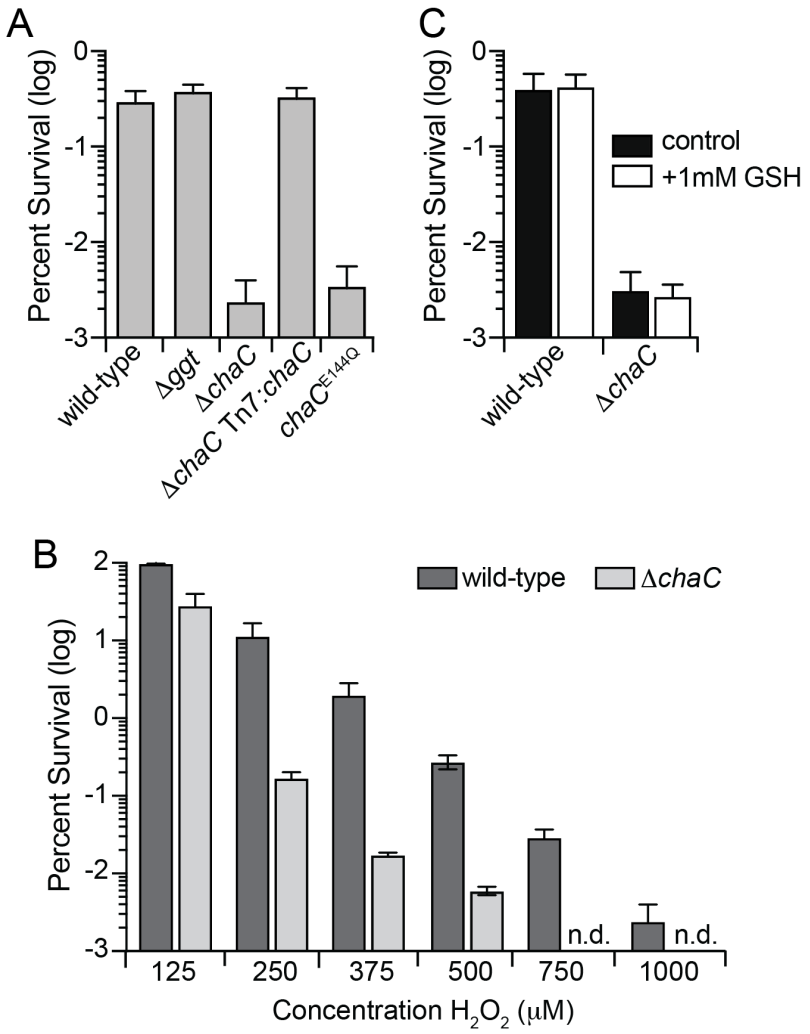

Figure 4.4. ChaC contributes to redox tolerance.
(**A-C**) Survival rates of the indicated strains following a 30 min exposure to H_2O_2. For A and C, 250 μM of $H_2O_2$was used. Data are shown as mean ± s.d.

5

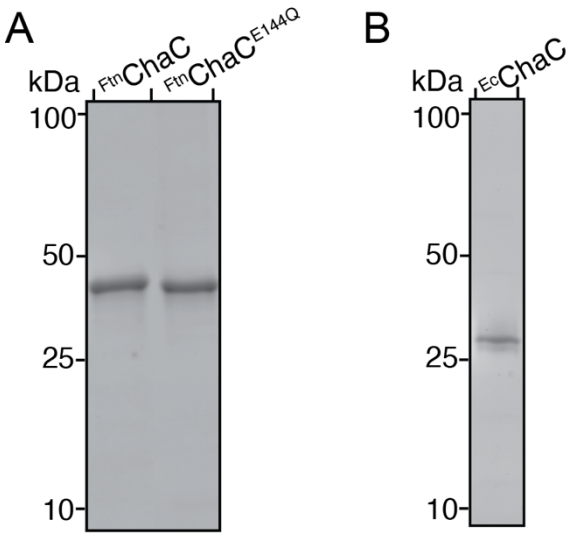

Figure 4.5. ChaC enzymes are stable and soluble post purification.
(**A**) Coomassie brilliant blue staining of purified ChaC and ChaC^{E144Q} from U112. (**B**) Coomassie brilliant blue staining of purified ChaC from *E. coli*.

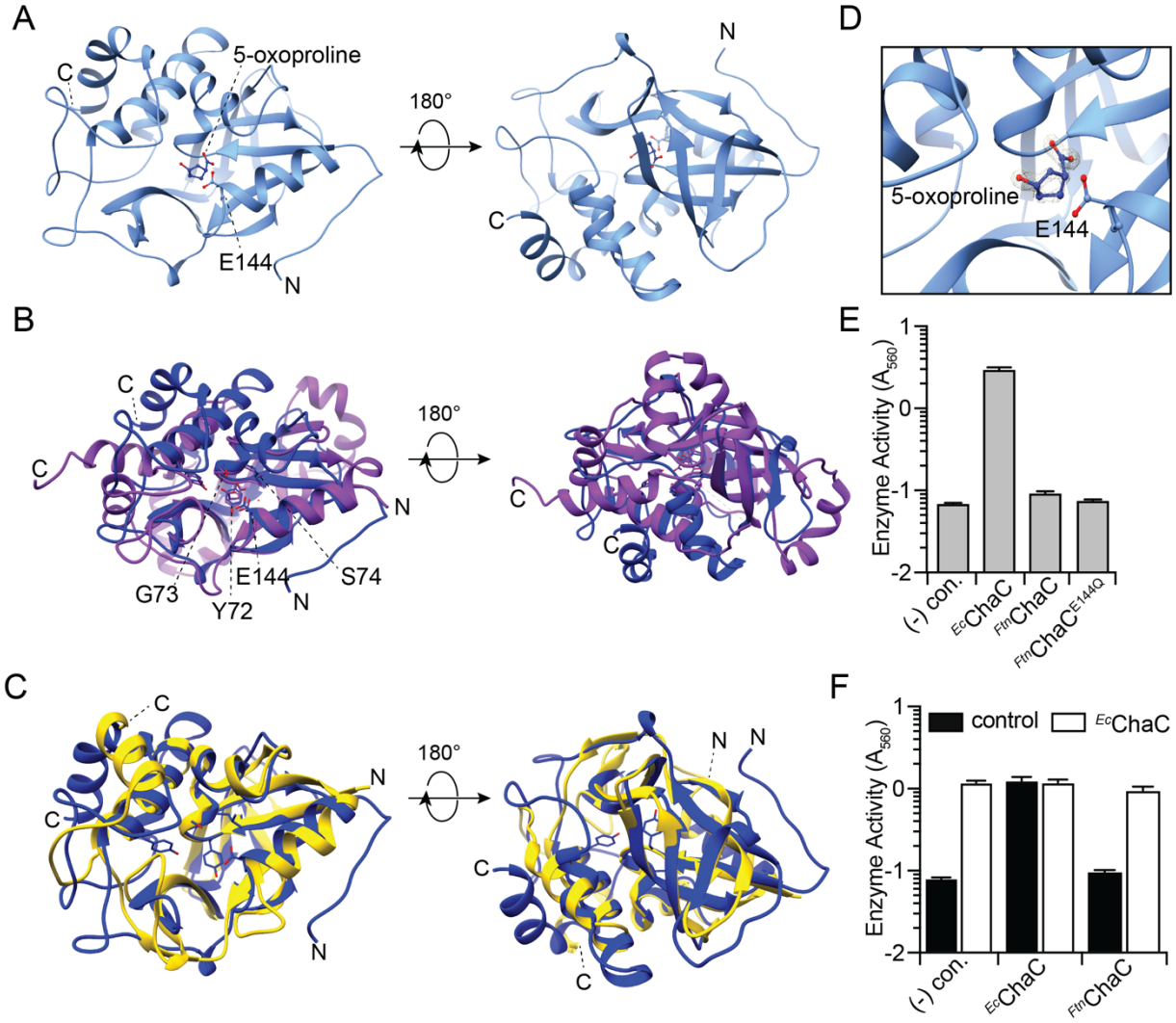

Figure 4.6. ChaC possesses the core GGCT-fold but is enzymatically inactive *in vitro*
(**A**) Ribbon diagram representation of the X-ray crystal structure of ChaC from U112 (light blue). The active residue (E144) and the byproduct 5-oxoproline are highlighted. (**B, C**) Structural alignment of U112 ChaC with ChaC from *S. cerevisiae* (B, purple) and a human GGCT (C, yellow). Critical residues for enzymatic activity are indicated. (**D**) Magnification of the active site of ChaC from U112 showing the localization of the by-product 5-oxoproline. (**E, F**) ChaC activity of the indicated proteins determined by the amounts of Cys–Gly generated from 10mM GSH. Data in E-F are shown as mean ± s.d.

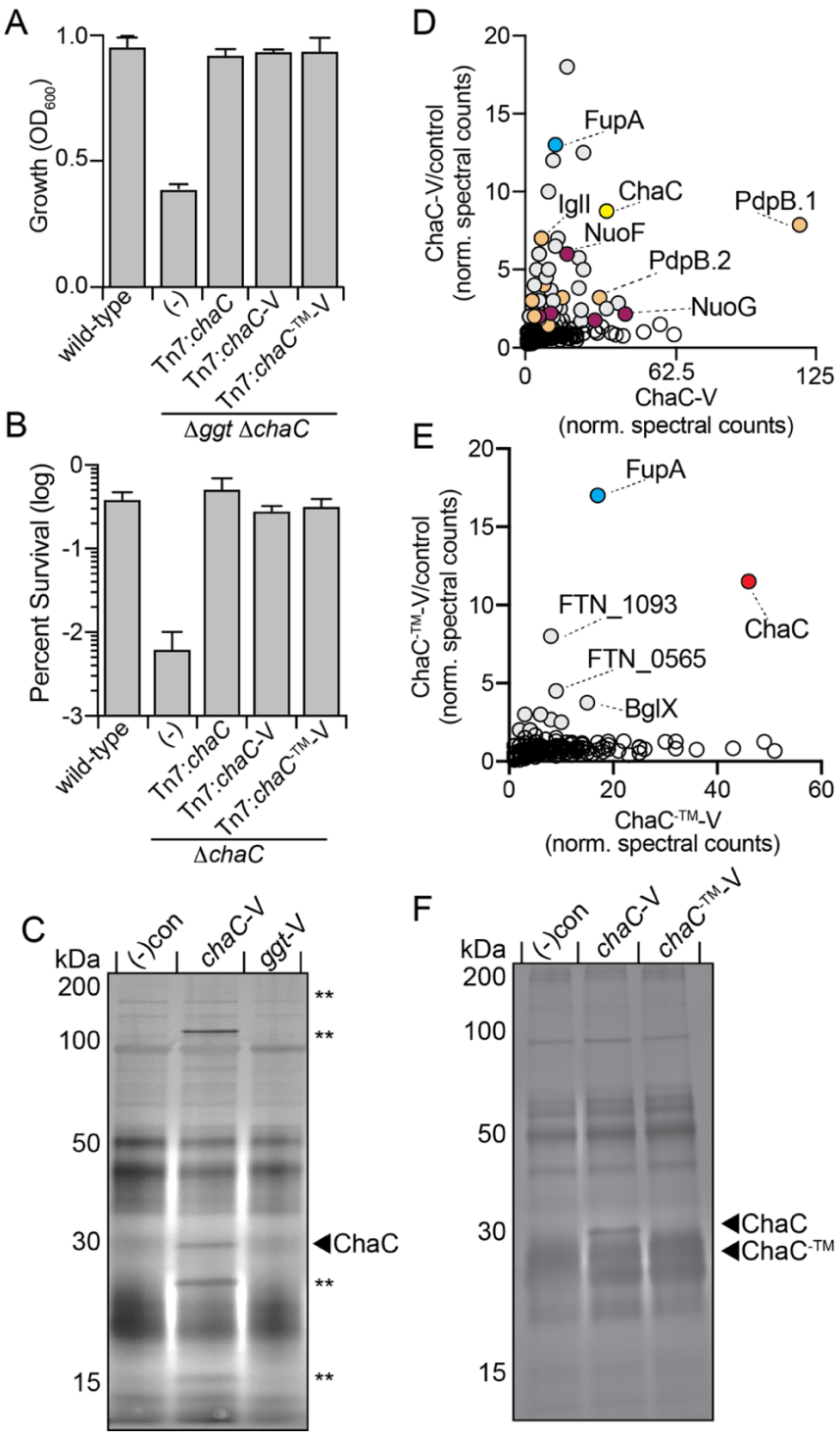

Figure 4.7. The transmembrane domain of ChaC facilitates interactions with numerous protein complexes, but not the interaction with FupA

(**A**) OD_{600} measurements of the indicated strains of U112 after 36hrs of growth in CDM with glutathione. (**B**) Survival rates of the indicated strains following a 30 min exposure to 250 μM H_2O_2. (**C**) Coomassie brilliant blue staining of αvsv-G immunoprecipitation of lysates generated from the indicated strains. ** indicate proteins present solely in the *chaC*-V samples (**D-E**) Graphical representation of the proteins

identified to co-immunoprecipitates with ChaC (D) and ChaC-TM (E). Proteins if interest are highlight. In (D) components of the T6SS (orange) and Nuo complex (maroon) are indicated. (**F**) Coomassie brilliant blue staining of αvsv-G immunoprecipitation of lysates generated from the indicated strains. Data in A and B are shown as mean ± s.d.

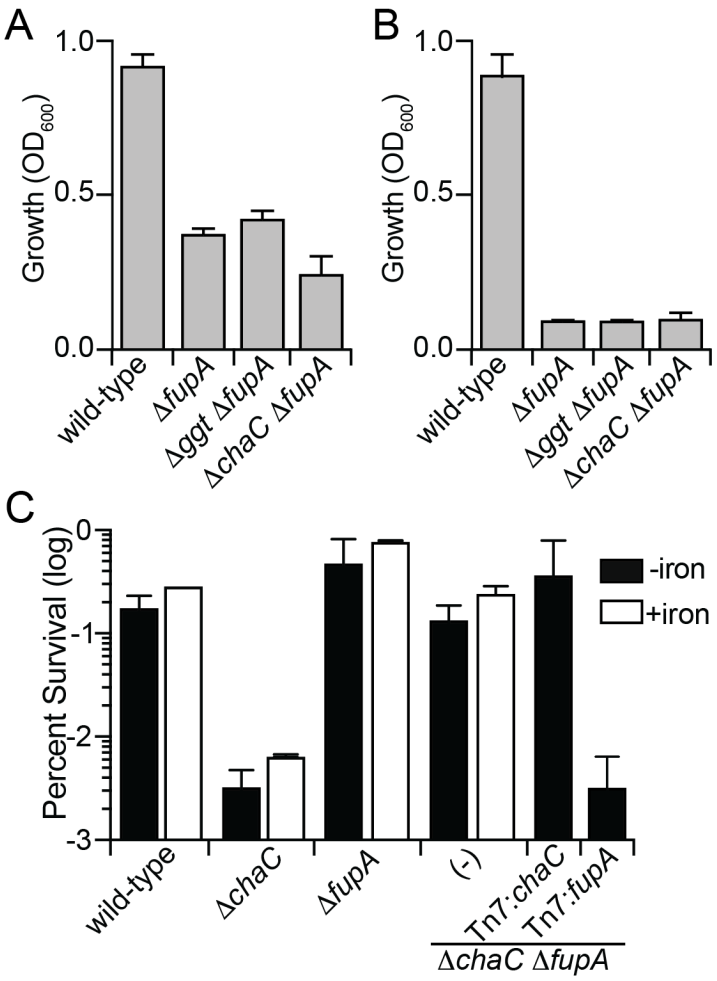

Figure 4.8. FupA contributes to GSH-catabolism and is linked to redox sensitivity
(**A-B**) OD_{600} measurements of the indicated strains of U112 after 36hrs of growth in CDM with glutathione (A) or Cys-Gly (B). (**C**) Survival rates of the indicated strains following a 30 min exposure to 250 μM H_2O_2. Data in are shown as mean ± s.d.

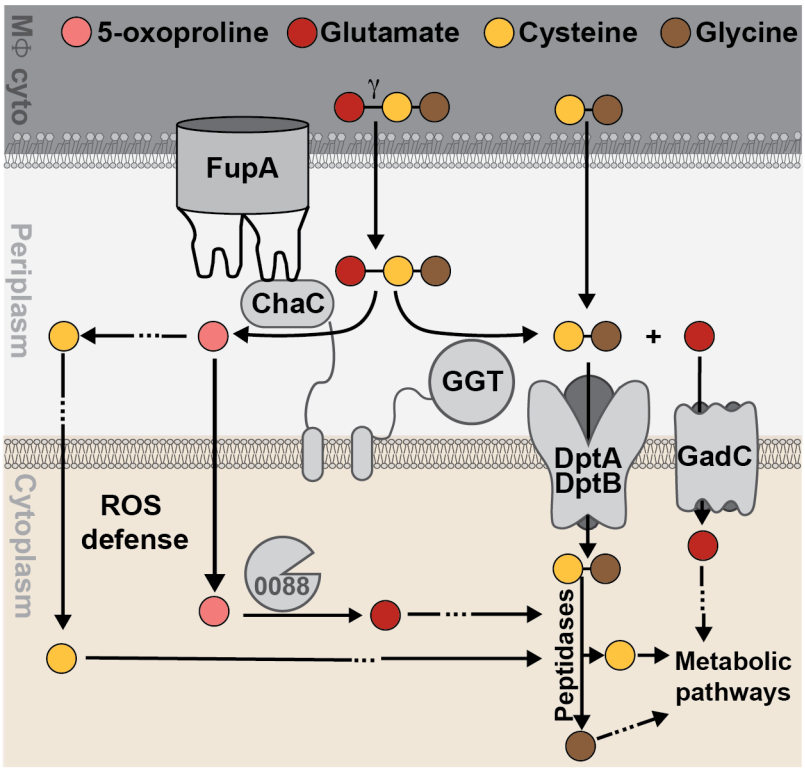

Figure 4.9. ChaC and GGT form two distinct pathways for GSH catabolism
Model depicting the localization and role of the indicated enzymes and transporters in the metabolism of GSH by *F. tularensis*. 0088 is the protein FTN_0088 which is a predicted 5-oxoprolinase.

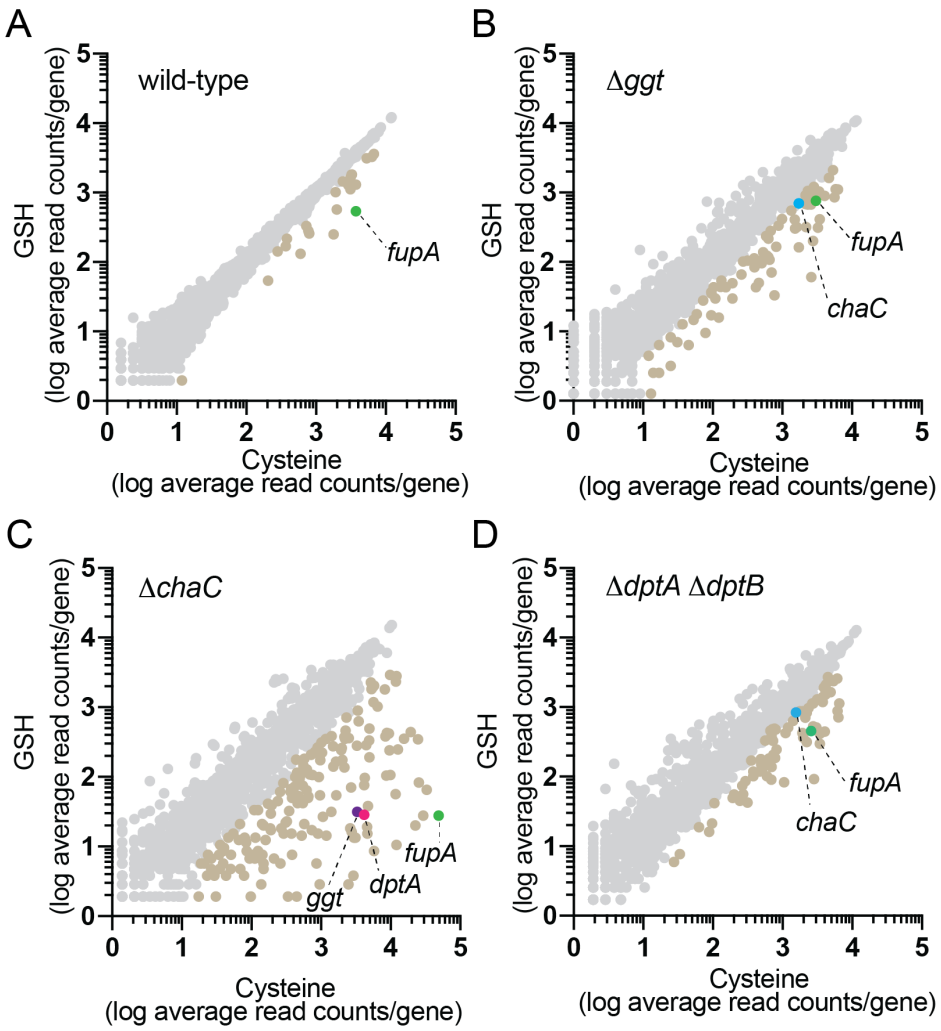

Figure 4.10. Transposon-based screen highlights the complex nature of GSH-catabolism in U112 (**A-D**) The relative abundance of mutations in each gene (average read count per gene) in the mutant pool generated in the indicated genetic background grown for 24hrs on either cysteine or GSH. Genes with at least 2-fold changed between the two conditions and at least 20 unique reads are colored in brown. Genes known to be involved in GSH metabolism are highlighted; *fupA* (green), *chaC* (blue), *ggt* (purple) *dptA* (pink).

	***F. novicida* ChaC**	***F. novicida***
	SAD peak[a]	**ChaC•pyroglutamate[a]**
PDB accession code	<tbd>	<tbd>
Data Collection		
Space group	$P2_12_12_1$	$P2_12_12_1$
Cell dimension		
a, b, c (Å)	56.56, 63.61, 66.98	56.54, 63.83, 66.97
α, β, γ (°)	90, 90, 90	90, 90, 90
Wavelength (Å)	0.9790	1.000
Resolution (Å)	35.0 – 1.70 (1.71 – 1.70)[b]	40.0 – 1.45 (1.46 - 1.45)
No. unique reflections	51094	43566
R_{merge}	0.07	0.08
$I/\sigma I$	11.7 (2.8)	37.0 (2.0)
Completeness (%)		
Total	99.7 (97.7)	99.9 (99.8)
Anomalous	99.6 (99.6)	
Redundancy	8.1 (8.0)	6.4 (4.9)
Wilson B-factor ($Å^2$)	12.7	16.1
Refinement		
Resolution (Å)	33.5 – 1.7 (1.76-1.70)	31.9 – 1.45 (1.49 – 1.45)
No. reflections	26873 (2573)	43486
Rwork/Rfree (%)	17.1 / 19.5 (20.0 / 22.5)	15.0 / 17.6 (20.4 / 22.3)
No. atoms		
Protein	1629	1668
Ligand/ion	8	13
Water	237	192
B-factors ($Å^2$)		
Protein	15.6	24.0
Ligand/ion	19.0	21.9
Water	32.1	36.8
rmsd		
Bond lengths (Å)	0.010	0.012
Bond angles (°)	1.08	1.31
Missing residues	1-34, 63, 141-143, 237-245	1-34, 237-245

[a]All data collected from a single crystal
[b]Values in parentheses are for the highest resolution shell

Table 4.1. Data collection and structure determination of ChaC

Chapter 5: Conclusions and future directions

5.1 Significance

Throughout my graduate career, our understanding of the *Francisella tularensis* lifecycle has significantly increased. We are starting to obtain insight into the mechanisms underlying phagosomal escape by this pathogen, with emphasis having been placed on characterization of the essential FPI-encoded T6SS^{ii}. There is now a better understanding of the structural composition of the secretion system, as well as what accessory proteins are necessary to mediate effector delivery [29]. Additionally, the identity of T6SS^{ii} substrates has been revealed allowing for insights into the mechanism employed by *F. tularensis* during phagosomal escape [22]. Emphasis has also been placed on determining the pathways required for cytoplasmic proliferation. This has revealed the contribution of numerous metabolic pathways during infection [83-90, 197-200]. While several virulence factors and pathways have been found to play a role in mediating the intracellular lifecycle of *F. tularensis*, further insight into the mechanisms underlying these processes is required.

My thesis was motivated by the desire to discover and characterize important mechanisms utilized by *F. tularensis* to promote intracellular growth. For these studies, I focused on the requirements for intramacrophage growth as macrophages are believed to be the primary cell type infected. The majority of my work was done with *F. tularensis* subsp *novicida* which is non-pathogenic to humans but causes a robust tularemia-like disease in mice.

During my thesis project, I discovered a novel family of phosphoinositide 3-kinases present in numerous host-associated bacteria [37]. I went on to determine that this enzyme promotes phagosomal escape thereby contributing to the lifecycle of F. *tularensis*. Additionally, I leveraged the results of genome-wide screens to uncover important metabolic pathways that play unique and critical roles during cytoplasmic replication [84]. In this chapter, I will detail how my work has contributed to the collective knowledge of not only the *F. tularensis* field, but also the conserved mechanisms utilized by intracellular pathogens in general. I will also touch on the immediate future directions for this work, and what outstanding questions remain to be answered.

5.2 Identification of the effectors secreted by T6SS^{ii}

While the T6SS^{ii} encoded by *F. tularensis* has long been recognized as the key virulence factor mediating endosomal escape, the precise mechanisms underlying this are unclear. This is due in part to conflicting publications reporting which proteins are secreted by this system [43, 44]. Additionally, structural components of T6SSs are released during secretion and therefore follow-up studies are needed to determine if secreted proteins are true effectors. Early in my graduate career, I contributed to a study where we sought to use an unbiased method to identify the substrates of this system [22]. By comparing the secretome of wild-type *F. tularensis* subsp. *novicida* (*Ftn*) and that of a strain lacking a functional T6SS^{ii}, we found seven proteins to be secreted in a T6SS^{ii}-manner. Further analysis of these proteins revealed that three play an essential role as structural components of the apparatus (IglC, VgrG and PdpA), and four are dedicated effector proteins (PdpC, PdpD, OpiA and OpiB). Due to the stringent nature of our screen, we may have missed proteins that are substrates of the system. Indeed, work by others suggest that PdpE and IglF may also be effector proteins; however, there is a lack of strong experimental evidence for these claims [42, 52].

Our screen was performed in *Ftn,* which is non-pathogenic to humans [22]. This was key as *Ftn* encodes a single copy of the T6SS^{ii} making genetic manipulation and downstream analysis manageable. Whether our results are applicable to the other, more pathogenic species, remains to be experimentally verified. However, we believe there is strong evidence to support the generalization of our work. The genes encoding the secretion system are over 98% identical between the different subspecies and therefore it is unlikely that they recognize and secrete different cargo. Additionally, the proteins we identified as effectors are all present on the genomes of the pathogenic species. There is the possibility that certain species of *F. tularensis* obtained new genes encoding proteins that can be secreted through this system. However, there is little evidence of gene acquisition by the more pathogenic strains, and instead there is an increase in the presence of pseudogenes [38].

Our work revealed that deletion of the four effectors phenocopied a strain lacking a functional secretion system, in that escape from the phagosomal compartment was minimal [22]. It remains unknown if all four proteins contribute to escape or if there are previously unrecognized roles for the secretion system cargo. There are contradictory results on the role of the T6SS^{ii} in cytoplasmic growth and therefore further mechanistic studies are needed to tease apart the function of each effector [62-64]. To date, only one of the effectors has been biochemically characterized (OpiA, see below) [37]. OpiB possesses an N-terminal cysteine protease domain and C-terminal ankyrin domains, but the targets of each of these domains are unknown [22]. PdpC and PdpD are both large, likely multidomain proteins that can only be found in *Francisella*. As these proteins possesses no previously characterized domains or motifs, studies on these proteins have been challenging. Work to reveal the mechanisms underlying the role of these two proteins is critical for understanding the *F. tularensis* lifecycle.

5.3 Discovery of a novel family of bacterial phosphatidylinositol 3-kinases

To begin unraveling the mechanisms underlying the *F. tularensis* lifecycle, I focused my attention on one effector, OpiA. We chose this effector for follow-up studies as it possesses no previously characterized domains or motifs, thereby suggesting we may have uncovered a new class of proteins. Indeed, using a hidden Markov model-based approach, we were able to identify two constellations of amino acids that are conserved throughout a group of bacterial proteins [37]. These proteins, which we termed the OpiA-family proteins (OFPs), are encoded by a diverse set of bacteria with an enrichment in host-associated species. We were excited to find that these same motifs are conserved in a family of eukaryotic kinases that act on phosphoinositides (PI), termed phosphatidylinositol-kinases (PI-kinase). PI molecules are an important class of lipids found on the cytoplasmic face of numerous eukaryotic membranes. Three positions of the inositol head group (3, 4, 5) can be phosphorylated by PI-kinases leading to the existence of eight species of PI. The different species are enriched on unique membranes and organelles, and this distinct localization is critical for their function. As these lipids play several

important roles within the cell, including protein recruitment, vesicle tethering, and immune signaling, proper regulation of these molecules is key[145].

To test if OFPs possess kinase activity, we utilized purified OpiA and the *Legionella pneumophila* OFP LegA5 in enzymatic assays that monitor the production of phosphorylated PI [37]. These experiments demonstrated that OFPs are indeed PI-kinases and follow-up studies revealed this family of enzymes specifically phosphorylates at the 3'-position of the inositol head ring. Therefore, OFPs represent a novel family of PI-3 kinases (PI3K). *L. pneumophila* has previously been demonstrated to encode a PI4K, however to the best of our knowledge my work is the first demonstration of bacteria performing PI3K activity [148]. As PI(3)P is known to be enriched within the phagosomal system we turned our attention to this stage of the *F. tularensis* life cycle [145]. Indeed, we uncovered that OpiA acts on the *Francisella* containing phagosome (FCP), prolonging the existence of PI(3)P of these vesicles. Furthermore, we demonstrated that OpiA activity likely delays phagosomal maturation thereby promoting bacterial escape into the cytoplasm [37]. This is the first demonstration of a *F. tularensis* protein that directly modulates the composition of the FCP, as well as the first biochemically defined mechanism that promotes phagosomal escape.

While we were able to show that OpiA plays a role in mediating escape, the exact mechanism underlying this remain unclear [37]. PI(3)P recruits several proteins to early endosomal membranes that are critical for interaction with other vesicles and proteins that promote maturation. Additionally, it has been demonstrated by several groups that removal of PI(3)P from early endosomal membranes is key for optimal vesicle maturation. However, why prolonged PI(3)P enrichment leads to this delay is currently undefined. Further studies on the host factors that contribute to phagosomal maturation are needed to determine the contribution of OpiA to FCP trafficking.

During the course of this study we also demonstrated that the OFP encoded by *L. pneumophila,* LegA5 possesses similar activity and substrate specificity as OpiA. While *L. pneumophila* is also an intracellular pathogen, it replicates within a membrane-bound vesicle that undergoes substantial remodeling throughout the course of infection[148]. Of note, an early feature of these structures is high

levels of PI(3)P and it is tempting to speculate that LegA5 may be responsible for this phenotype . A recent study revealed that the OFP encoded by the intracellular pathogen *Rickettsia rickettsii* contributes to virulence by modulating PI(3)P and PI(3,4,5,)P_3 levels [234]. This demonstrates that OFPs may have diverse substrate specificity as both OpiA and LegA5 are unable to generate PI(3,4,5,)P_3 [37].

We were surprised to find OFPs in several bacterial species that are not predicted to be host-associated. Few bacteria are predicted to generate PI as part of their own membranes and instead these molecules are found primarily in eukaryotic cells. It is possible that these bacteria interact with a previously unrecognized host and therefore these OFPs acts as a virulence factor. Additionally, these OFPs may reflect that these bacteria possess previously unrecognized lipids within their membrane. Finally, myo-inositol has been known to play critical roles in diverse organisms, typically as part of a secondary metabolite. Therefore, these proteins may contribute in the production of novel metabolites. Future studies are needed to determine which role these OFPs play in bacterial physiology.

5.4 Uncovering hidden components of GSH catabolism by *F. tularensis*

Macrophages are not only the first cell type infected by *F. tularensis* upon entry into a host, but they are also believed to be a major mediator of disease. Therefore, significant attention has been given to identifying the factors required for proliferation in this typically degradative cell type. In order to identify the genes required for intramacrophage growth, we generated a saturated transposon library in *F. tularensis* subsp. *holarctica* LVS [84]. We then subjected this library to growth in J774 immortalized macrophages and used high throughput sequencing to identify the transposon mutants that were depleted during infection. Due to the saturated nature of the library utilized, this screen provides the first truly comprehensive catalog of the genes required for intracellular proliferation. Our screen identified numerous genes that have been previously demonstrated to support growth and virulence, such as all 13 genes composing the purine biosynthesis pathway and the key regulatory factor PigR. Additionally, we identified numerous genes encoding uncharacterized proteins. We then characterized two of the proteins

we identified (see below), however additional studies are needed to reveal the function of the remaining of the proteins [84]. We believe these studies will lead to a better understanding of the mechanisms utilized by *F. tularensis* to promote intracellular growth.

Upon accessing the cytosol of host cells *F. tularensis* is capable of robust replication. This level of proliferation is metabolically taxing and in order conserve energy *F. tularensis* and other intracellular pathogens are known to utilizes host-derived molecules. This is clearly seen in our screen, as well as several other screens performed by other groups, which identified a large number of secondary transporters and nutrient catabolism pathways as critical for growth [83, 85-90, 197-200]. GSH is one such host-derived metabolite as it provides an essential source of cysteine to support *F. tularensis* proliferation. Prior to my work, GGT was believed to be the primary enzyme responsible for liberating cysteine from GSH. However, it was unclear how the GGT by-products are transported to the cytoplasm, as well as if there are additional roles for host derived GSH. We therefore leveraged the results of our screen to better understand the underlying mechanisms and functions of GSH-catabolism during infection. From this work, we were able to identify and characterize a Cys–Gly transporter, DptA, that is essential for GSH-utilization. Additionally, we revealed the existence of a second GSH-catabolizing enzyme, ChaC, which plays a unique role during infection [84].

DptA belongs to the POT family of di- and tripeptide transporters which are powered by proton motive force. To the best of my knowledge, DptA is the first POT implicated in not only GSH catabolism but also pathogenesis. The downstream transporter for the GGT byproducts is unknown in the majority of bacteria, with the exception being *Campylobacter jejuni* [217]. It is therefore tempting to speculate that DptA-homologs may play a more general role in GSH-catabolism and virulence. Further work is needed to define the role of this family of proteins in broader bacterial physiology.

The results from our screen, as well as analysis of GSH-catabolism in diverse *F. tularensis* species, led us to uncover a second enzyme, ChaC, that is capable of degrading GSH. ChaC has been identified by several groups as being critical for virulence, however the function of this protein was unknown. The ChaC family of enzymes has been studied primarily in eukaryotes where they are known

to degrade GSH, and while homologs have been identified in bacteria, little work has been done to characterize these proteins. Through growth curve analysis, we were able to demonstrate that, like in eukaryotes, ChaC is capable of GSH-catabolism. However, we found that the function of this protein is nonredundant with GGT, despite the fact that these enzymes are predicted to generate the same by-products. As discussed in more detail below, further work is needed to define the contribution of ChaC to bacterial physiology.

Through our growth curve analysis, we determined that the ChaC pathway only contributes to *in vitro* GSH catabolism in some subspecies of *F. tularensis (*in *Ftn* but not *Fth*). We were unable to identify any obvious explanation for this as ChaC was expressed under *in vitro* conditions in both species. Additionally, the proteins encoded by the two organisms are nearly identical (98.5%), and any differences are not found within the critical regions of the proteins. Follow-up studies in *Ftn* also revealed that this species utilizes a secondary Cys–Gly transporter that did not contribute to GSH-catabolism in *Fth*. It is unclear what is underlying these differences and more extensive comparison of the two species is necessary.

5.5 Defining the physiological roles of GSH catabolism by *F. tularensis*

As mentioned above, ChaC enzymes have not been studied in bacteria and additionally, the work done on the eukaryotic homologs is minimal. We therefore turned out attention to the ChaC enzyme encoded by *Ftn* as we know the ChaC pathway is active *in vitro* in this species. From this work, we determined that the activity of ChaC contributes to redox tolerance independent of the levels of intracellular GSH. Additionally, we found that ChaC interacts with the outer membrane protein FupA and that this interaction is linked to the role of ChaC in redox stress. We currently lack an explanation for these findings due to the fact that this phenotype is independent from the previous functions attributed to these proteins. Additionally, it is unclear if the interaction between FupA and ChaC is direct and if so, which domains are mediating this interaction.

To better characterize the function of ChaC, we utilized purified proteins in enzymatic assays that monitor the production of Cys–Gly. We were unable to find conditions under which ChaC was enzymatically active. Through immunoprecipitation assays we determined that ChaC interacts with several other proteins, including FupA. Therefore, we hypothesize that the interaction with one or more of these proteins is required for ChaC activity. Along those lines, we began to investigate the role of FupA in GSH catabolism and unexpectedly found that this protein is required for growth under conditions where GSH or Cys–Gly is the sole cysteine source. This suggests that this protein has a previously unrecognized role in amino acid metabolism and further studies are needed to define this novel function for FupA.

In our efforts to uncover the mechanism of ChaC, we determined the X-ray crystal structure of the protein in an apo state as well as in complex with the by-product 5-oxoproline. To the best of my knowledge, this is the first time the structure of a bacterial ChaC protein has been solved. Additionally, this is the first ChaC structure to contain the by-product 5-oxoproline. These structures revealed the ChaC adopts the BtrG/GGCT fold that is characteristic of the eukaryotic ChaC proteins. Superimposition with the *S. cerevisae* ChaC homolog highlighted the conserved fold surrounding the active site pocket that primarily composed of N-terminal β-sheets. In contrast, we observed low levels of superimposition of the C-terminal α-helices and the yeast protein contain two helices that are not present in the *F. tularensis* structure. It is tempting to speculate that the C-terminal region of ChaC proteins contribute to the unique contribution of these proteins to physiology. For example, it would be interesting to investigate the role of this region in the interaction of ChaC with FupA.

There are multiple lines of evidence that ChaC proteins serve a myriad of roles in GSH metabolism dependent on the needs of the organism harboring it. The function of ChaC in the majority of bacteria is currently unclear and to begin to investigate this we sought to determine the phylogenetic distribution of these enzymes. To accomplish this, we first had to establish a ChaC domain that allowed for differentiation of these proteins from the other GGCT proteins. By comparing the sequences of

characterized ChaC and non-ChaC GGCT proteins we propose that the ChaC domain is composed of two amino acid motifs (YGSGL/RE) separated by 60-90 amino acids. Using this new domain, we conducted searches to identify the phylogenetic distribution of these proteins and were able to identify ChaC homologs in diverse organisms. Within bacteria we found that the majority of ChaC proteins are localized to the cytoplasm unlike the *F. tularensis* protein. Investigation of the role of cytoplasmic ChaC catabolism is needed to better define the function of this family of enzymes.

References

1. Kingry, L.C. and J.M. Petersen, *Comparative review of Francisella tularensis and Francisella novicida.* Front Cell Infect Microbiol, 2014. **4**: p. 35.

2. Ellis, J., et al., *Tularemia.* Clin Microbiol Rev, 2002. **15**(4): p. 631–46.

3. Oyston, P.C., A. Sjostedt, and R.W. Titball, *Tularaemia: bioterrorism defence renews interest in Francisella tularensis.* Nat Rev Microbiol, 2004. **2**(12): p. 967–78.

4. Keim, P., A. Johansson, and D.M. Wagner, *Molecular epidemiology, evolution, and ecology of Francisella.* Ann N Y Acad Sci, 2007. **1105**: p. 30–66.

5. Celli, J. and T.C. Zahrt, *Mechanisms of Francisella tularensis intracellular pathogenesis.* Cold Spring Harb Perspect Med, 2013. **3**(4): p. a010314.

6. Llewellyn, A.C., et al., *Macrophage replication screen identifies a novel Francisella hydroperoxide resistance protein involved in virulence.* PLoS One, 2011. **6**(9): p. e24201.

7. Roberts, L.M., et al., *Identification of early interactions between Francisella and the host.* Infect Immun, 2014. **82**(6): p. 2504–10.

8. Clemens, D.L., B.Y. Lee, and M.A. Horwitz, *Francisella tularensis enters macrophages via a novel process involving pseudopod loops.* Infect Immun, 2005. **73**(9): p. 5892-902.

9. Geier, H. and J. Celli, *Phagocytic receptors dictate phagosomal escape and intracellular proliferation of Francisella tularensis.* Infect Immun, 2011. **79**(6): p. 2204-14.

10. Dai, S., et al., *Fine tuning inflammation at the front door: macrophage complement receptor 3-mediates phagocytosis and immune suppression for Francisella tularensis.* PLoS Pathog, 2013. **9**(1): p. e1003114.

11. Barel, M., et al., *A novel receptor - ligand pathway for entry of Francisella tularensis in monocyte-like THP-1 cells: interaction between surface nucleolin and bacterial elongation factor Tu.* BMC Microbiol, 2008. **8**: p. 145.

12. Pierini, L.M., *Uptake of serum-opsonized Francisella tularensis by macrophages can be mediated by class A scavenger receptors.* Cell Microbiol, 2006. **8**(8): p. 1361-70.

13. Balagopal, A., et al., *Characterization of the receptor-ligand pathways important for entry and survival of Francisella tularensis in human macrophages.* Infect Immun, 2006. **74**(9): p. 5114-25.

14. Chakraborty, S., et al., *Type IV pili in Francisella tularensis: roles of pilF and pilT in fiber assembly, host cell adherence, and virulence.* Infect Immun, 2008. **76**(7): p. 2852-61.

15. Tamilselvam, B. and S. Daefler, *Francisella targets cholesterol-rich host cell membrane domains for entry into macrophages.* J Immunol, 2008. **180**(12): p. 8262-71.

16. Parsa, K.V., et al., *The tyrosine kinase Syk promotes phagocytosis of Francisella through the activation of Erk.* Mol Immunol, 2008. **45**(10): p. 3012-21.

17. Brock, S.R. and M.J. Parmely, *Francisella tularensis Confronts the Complement System.* Front Cell Infect Microbiol, 2017. **7**: p. 523.

18. Hoang, K.V., et al., *Complement Receptor 3-Mediated Inhibition of Inflammasome Priming by Ras GTPase-Activating Protein During Francisella tularensis Phagocytosis by Human Mononuclear Phagocytes.* Front Immunol, 2018. **9**: p. 561.

19. Chong, A., et al., *The early phagosomal stage of Francisella tularensis determines optimal phagosomal escape and Francisella pathogenicity island protein expression.* Infect Immun, 2008. **76**(12): p. 5488–99.

20. Checroun, C., et al., *Autophagy-mediated reentry of Francisella tularensis into the endocytic compartment after cytoplasmic replication.* Proc Natl Acad Sci U S A, 2006. **103**(39): p. 14578–83.

21. Santic, M., et al., *The Francisella tularensis pathogenicity island protein IglC and its regulator MglA are essential for modulating phagosome biogenesis and subsequent bacterial escape into the cytoplasm.* Cell Microbiol, 2005. **7**(7): p. 969-79.

22. Eshraghi, A., et al., *Secreted Effectors Encoded within and outside of the Francisella Pathogenicity Island Promote Intramacrophage Growth.* Cell Host Microbe, 2016. **20**(5): p. 573–583.

23. Nano, F.E., et al., *A Francisella tularensis pathogenicity island required for intramacrophage growth.* J Bacteriol, 2004. **186**(19): p. 6430–6.

24. Bakshi, C.S., et al., *Superoxide dismutase B gene (sodB)-deficient mutants of Francisella tularensis demonstrate hypersensitivity to oxidative stress and attenuated virulence.* J Bacteriol, 2006. **188**(17): p. 6443-8.

25. Child, R., et al., *Acid phosphatases do not contribute to the pathogenesis of type A Francisella tularensis.* Infect Immun, 2010. **78**(1): p. 59-67.

26. Mohapatra, N.P., et al., *Francisella acid phosphatases inactivate the NADPH oxidase in human phagocytes.* J Immunol, 2010. **184**(9): p. 5141-50.

27. Mohapatra, N.P., et al., *Type A Francisella tularensis acid phosphatases contribute to pathogenesis.* PLoS One, 2013. **8**(2): p. e56834.

28. Ramond, E., et al., *Glutamate utilization couples oxidative stress defense and the tricarboxylic acid cycle in Francisella phagosomal escape.* PLoS Pathog, 2014. **10**(1): p. e1003893.

29. Clemens, D.L., B.Y. Lee, and M.A. Horwitz, *The Francisella Type VI Secretion System.* Front Cell Infect Microbiol, 2018. **8**: p. 121.

30. Lauriano, C.M., et al., *MglA regulates transcription of virulence factors necessary for Francisella tularensis intraamoebae and intramacrophage survival.* Proc Natl Acad Sci U S A, 2004. **101**(12): p. 4246-9.

31. Golovliov, I., et al., *Identification of proteins of Francisella tularensis induced during growth in macrophages and cloning of the gene encoding a prominently induced 23-kilodalton protein.* Infect Immun, 1997. **65**(6): p. 2183-9.

32. Nano, F.E. and C. Schmerk, *The Francisella pathogenicity island.* Ann N Y Acad Sci, 2007. **1105**: p. 122–37.

33. Barker, J.R. and K.E. Klose, *Molecular and genetic basis of pathogenesis in Francisella tularensis.* Ann N Y Acad Sci, 2007. **1105**: p. 138-59.

34. Russell, A.B., et al., *A type VI secretion-related pathway in Bacteroidetes mediates interbacterial antagonism.* Cell Host Microbe, 2014. **16**(2): p. 227–36.

35. de Bruin, O.M., J.S. Ludu, and F.E. Nano, *The Francisella pathogenicity island protein IglA localizes to the bacterial cytoplasm and is needed for intracellular growth.* BMC Microbiol, 2007. **7**: p. 1.

36. Kumar, A., et al., *Mammalian proapoptotic factor ChaC1 and its homologues function as gamma-glutamyl cyclotransferases acting specifically on glutathione.* EMBO Rep, 2012. **13**(12): p. 1095–101.

37. Ledvina, H.E., et al., *A Phosphatidylinositol 3-Kinase Effector Alters Phagosomal Maturation to Promote Intracellular Growth of Francisella.* Cell Host Microbe, 2018. **24**(2): p. 285–295 e8.

38. Larsson, P., et al., *The complete genome sequence of Francisella tularensis, the causative agent of tularemia.* Nat Genet, 2005. **37**(2): p. 153–9.

39. Hood, R.D., S.B. Peterson, and J.D. Mougous, *From Striking Out to Striking Gold: Discovering that Type VI Secretion Targets Bacteria.* Cell Host Microbe, 2017. **21**(3): p. 286–289.

40. Klein, T.A., S. Ahmad, and J.C. Whitney, *Contact-Dependent Interbacterial Antagonism Mediated by Protein Secretion Machines.* Trends Microbiol, 2020. **28**(5): p. 387–400.

41. Clemens, D.L., et al., *Atomic structure of T6SS reveals interlaced array essential to function.* Cell, 2015. **160**(5): p. 940–51.

42. Rigard, M., et al., *Francisella tularensis IglG Belongs to a Novel Family of PAAR-Like T6SS Proteins and Harbors a Unique N-terminal Extension Required for Virulence.* PLoS Pathog, 2016. **12**(9): p. e1005821.

43. Barker, J.R., et al., *The Francisella tularensis pathogenicity island encodes a secretion system that is required for phagosome escape and virulence.* Mol Microbiol, 2009. **74**(6): p. 1459–70.

44. Broms, J.E., et al., *Unique substrates secreted by the type VI secretion system of Francisella tularensis during intramacrophage infection.* PLoS One, 2012. **7**(11): p. e50473.

45. Hernandez, R.E., R. Gallegos-Monterrosa, and S.J. Coulthurst, *Type VI secretion system effector proteins: Effective weapons for bacterial competitiveness.* Cell Microbiol, 2020. **22**(9): p. e13241.

46. Yang, X., et al., *Atomic Structure of the Francisella T6SS Central Spike Reveals a Unique alpha-Helical Lid and a Putative Cargo.* Structure, 2019. **27**(12): p. 1811-1819 e6.

47. Lindgren, M., et al., *Importance of PdpC, IglC, IglI, and IglG for modulation of a host cell death pathway induced by Francisella tularensis.* Infect Immun, 2013. **81**(6): p. 2076-84.

48. Long, M.E., et al., *Disruption of Francisella tularensis Schu S4 iglI, iglJ, and pdpC genes results in attenuation for growth in human macrophages and in vivo virulence in mice and reveals a unique phenotype for pdpC.* Infect Immun, 2013. **81**(3): p. 850–61.

49. Chou, A.Y., et al., *Generation of protection against Francisella novicida in mice depends on the pathogenicity protein PdpA, but not PdpC or PdpD.* Microbes Infect, 2013. **15**(12): p. 816–27.

50. Uda, A., et al., *Role of pathogenicity determinant protein C (PdpC) in determining the virulence of the Francisella tularensis subspecies tularensis SCHU.* PLoS One, 2014. **9**(2): p. e89075.

51. Lindgren, M., et al., *Identification of mechanisms for attenuation of the FSC043 mutant of Francisella tularensis SCHU S4.* Infect Immun, 2014. **82**(9): p. 3622–35.

52. Brodmann, M., et al., *Francisella requires dynamic type VI secretion system and ClpB to deliver effectors for phagosomal escape.* Nat Commun, 2017. **8**: p. 15853.

53. Ozanic, M., et al., *Phenotypic characterization of the Francisella tularensis ΔpdpC and ΔiglG mutants.* Microbes Infect, 2016. **18**(12): p. 768–776.

54. Read, A., et al., *Francisella genes required for replication in mosquito cells.* J Med Entomol, 2008. **45**(6): p. 1108-16.

55. Ludu, J.S., et al., *The Francisella pathogenicity island protein PdpD is required for full virulence and associates with homologues of the type VI secretion system.* J Bacteriol, 2008. **190**(13): p. 4584–95.

56. Brotcke, A., et al., *Identification of MglA-regulated genes reveals novel virulence factors in Francisella tularensis.* Infect Immun, 2006. **74**(12): p. 6642-55.

57. Shao, F., et al., *A Yersinia effector and a Pseudomonas avirulence protein define a family of cysteine proteases functioning in bacterial pathogenesis.* Cell, 2002. **109**(5): p. 575–88.

58. Al-Khodor, S., et al., *Functional diversity of ankyrin repeats in microbial proteins.* Trends Microbiol, 2010. **18**(3): p. 132–9.

59. Liu, K., et al., *Negative regulation of phosphatidylinositol 3-phosphate levels in early-to-late endosome conversion.* J Cell Biol, 2016. **212**(2): p. 181–98.

60. Rapiteanu, R., et al., *A Genetic Screen Identifies a Critical Role for the WDR81-WDR91 Complex in the Trafficking and Degradation of Tetherin.* Traffic, 2016. **17**(8): p. 940–58.

61. Ghosh, S. and T.J. O'Connor, *Beyond Paralogs: The Multiple Layers of Redundancy in Bacterial Pathogenesis.* Front Cell Infect Microbiol, 2017. **7**: p. 467.

62. Meyer, L., et al., *Microinjection of Francisella tularensis and Listeria monocytogenes reveals the importance of bacterial and host factors for successful replication.* Infect Immun, 2015. **83**(8): p. 3233–42.

63. Wu, Y.C., et al., *Massively parallel delivery of large cargo into mammalian cells with light pulses.* Nat Methods, 2015. **12**(5): p. 439-44.

64. Steele, S.P., et al., *Francisella tularensis enters a double membraned compartment following cell-cell transfer.* Elife, 2019. **8**.

65. Kinchen, J.M. and K.S. Ravichandran, *Phagosome maturation: going through the acid test.* Nat Rev Mol Cell Biol, 2008. **9**(10): p. 781-95.

66. Uribe-Querol, E. and C. Rosales, *Control of Phagocytosis by Microbial Pathogens.* Front Immunol, 2017. **8**: p. 1368.

67. Pauwels, A.M., et al., *Patterns, Receptors, and Signals: Regulation of Phagosome Maturation.* Trends Immunol, 2017. **38**(6): p. 407-422.

68. Clemens, D.L., B.Y. Lee, and M.A. Horwitz, *Virulent and avirulent strains of Francisella tularensis prevent acidification and maturation of their phagosomes and escape into the cytoplasm in human macrophages.* Infect Immun, 2004. **72**(6): p. 3204-17.

69. Forgac, M., *Vacuolar ATPases: rotary proton pumps in physiology and pathophysiology.* Nat Rev Mol Cell Biol, 2007. **8**(11): p. 917-29.

70. Santic, M., et al., *Acquisition of the vacuolar ATPase proton pump and phagosome acidification are essential for escape of Francisella tularensis into the macrophage cytosol.* Infect Immun, 2008. **76**(6): p. 2671-7.

71. Panday, A., et al., *NADPH oxidases: an overview from structure to innate immunity-associated pathologies.* Cell Mol Immunol, 2015. **12**(1): p. 5-23.

72. McCaffrey, R.L. and L.A. Allen, *Francisella tularensis LVS evades killing by human neutrophils via inhibition of the respiratory burst and phagosome escape.* J Leukoc Biol, 2006. **80**(6): p. 1224-30.

73. Mohapatra, N.P., et al., *AcpA is a Francisella acid phosphatase that affects intramacrophage survival and virulence.* Infect Immun, 2007. **75**(1): p. 390-6.

74. Lindgren, H., et al., *Resistance of Francisella tularensis strains against reactive nitrogen and oxygen species with special reference to the role of KatG.* Infect Immun, 2007. **75**(3): p. 1303-9.

75. Honn, M., et al., *Lack of OxyR and KatG Results in Extreme Susceptibility of Francisella tularensis LVS to Oxidative Stress and Marked Attenuation In vivo.* Front Cell Infect Microbiol, 2017. **7**: p. 14.

76. Binesse, J., et al., *Roles of reactive oxygen species-degrading enzymes of Francisella tularensis SCHU S4.* Infect Immun, 2015. **83**(6): p. 2255-63.

77. Alqahtani, M., et al., *Characterization of a Unique Outer Membrane Protein Required for Oxidative Stress Resistance and Virulence of Francisella tularensis.* J Bacteriol, 2018. **200**(8).

78. Ma, Z., et al., *EmrA1 membrane fusion protein of Francisella tularensis LVS is required for resistance to oxidative stress, intramacrophage survival and virulence in mice.* Mol Microbiol, 2014. **91**(5): p. 976-95.

79. Abu Kwaik, Y. and D. Bumann, *Microbial quest for food in vivo: 'nutritional virulence' as an emerging paradigm.* Cell Microbiol, 2013. **15**(6): p. 882-90.

80. Miller, C. and J. Celli, *Avoidance and Subversion of Eukaryotic Homeostatic Autophagy Mechanisms by Bacterial Pathogens.* J Mol Biol, 2016. **428**(17): p. 3387-98.

81. Gouzy, A., Y. Poquet, and O. Neyrolles, *Amino acid capture and utilization within the Mycobacterium tuberculosis phagosome.* Future Microbiol, 2014. **9**(5): p. 631-7.

82. Zhang, Y.J. and E.J. Rubin, *Feast or famine: the host-pathogen battle over amino acids.* Cell Microbiol, 2013. **15**(7): p. 1079-87.

83. Brunton, J., et al., *Identifying Francisella tularensis genes required for growth in host cells.* Infect Immun, 2015. **83**(8): p. 3015-25.

84. Ramsey, K.M., et al., *Tn-Seq reveals hidden complexity in the utilization of host-derived glutathione in Francisella tularensis.* PLoS Pathog, 2020. **16**(6): p. e1008566.

85. Ireland, P.M., et al., *Global Analysis of Genes Essential for Francisella tularensis Schu S4 Growth In Vitro and for Fitness during Competitive Infection of Fischer 344 Rats.* J Bacteriol, 2019. **201**(7).

86. Kraemer, P.S., et al., *Genome-wide screen in Francisella novicida for genes required for pulmonary and systemic infection in mice.* Infect Immun, 2009. **77**(1): p. 232–44.

87. Maier, T.M., et al., *Identification of Francisella tularensis Himar1-based transposon mutants defective for replication in macrophages.* Infect Immun, 2007. **75**(11): p. 5376–89.

88. Qin, A. and B.J. Mann, *Identification of transposon insertion mutants of Francisella tularensis tularensis strain Schu S4 deficient in intracellular replication in the hepatic cell line HepG2.* BMC Microbiol, 2006. **6**: p. 69.

89. Su, J., et al., *Genome-wide identification of Francisella tularensis virulence determinants.* Infect Immun, 2007. **75**(6): p. 3089–101.

90. Weiss, D.S., et al., *In vivo negative selection screen identifies genes required for Francisella virulence.* Proc Natl Acad Sci U S A, 2007. **104**(14): p. 6037–42.

91. Radlinski, L.C., et al., *Defining the Metabolic Pathways and Host-Derived Carbon Substrates Required for Francisella tularensis Intracellular Growth.* MBio, 2018. **9**(6).

92. Brissac, T., et al., *Gluconeogenesis, an essential metabolic pathway for pathogenic Francisella.* Mol Microbiol, 2015. **98**(3): p. 518-34.

93. Gesbert, G., et al., *Importance of branched-chain amino acid utilization in Francisella intracellular adaptation.* Infect Immun, 2015. **83**(1): p. 173-83.

94. Steele, S., J. Brunton, and T. Kawula, *The role of autophagy in intracellular pathogen nutrient acquisition.* Front Cell Infect Microbiol, 2015. **5**: p. 51.

95. Marchetti, M., et al., *Iron Metabolism at the Interface between Host and Pathogen: From Nutritional Immunity to Antibacterial Development.* Int J Mol Sci, 2020. **21**(6).

96. Powell, D.A. and J.A. Frelinger, *Efficacy of Resistance to Francisella Imparted by ITY/NRAMP/SLC11A1 Depends on Route of Infection.* Front Immunol, 2017. **8**: p. 206.

97. Brenz, Y., et al., *Nramp1 and NrampB Contribute to Resistance against Francisella in Dictyostelium.* Front Cell Infect Microbiol, 2017. **7**: p. 282.

98. Faraldo-Gomez, J.D. and M.S. Sansom, *Acquisition of siderophores in gram-negative bacteria.* Nat Rev Mol Cell Biol, 2003. **4**(2): p. 105-16.

99. Sullivan, J.T., et al., *Characterization of the siderophore of Francisella tularensis and role of fslA in siderophore production.* J Bacteriol, 2006. **188**(11): p. 3785-95.

100. Thomas-Charles, C.A., et al., *FeoB-mediated uptake of iron by Francisella tularensis.* Infect Immun, 2013. **81**(8): p. 2828-37.

101. Ramakrishnan, G., et al., *Citryl Ornithine Is an Intermediate in a Three-Step Biosynthetic Pathway for Rhizoferrin in Francisella.* ACS Chem Biol, 2019. **14**(8): p. 1760-1766.

102. Perez, N., et al., *Two parallel pathways for ferric and ferrous iron acquisition support growth and virulence of the intracellular pathogen Francisella tularensis Schu S4.* Microbiologyopen, 2016. **5**(3): p. 453-68.

103. Kiss, K., et al., *Characterization of fig operon mutants of Francisella novicida U112.* FEMS Microbiol Lett, 2008. **285**(2): p. 270-7.

104. Ramakrishnan, G., B. Sen, and R. Johnson, *Paralogous outer membrane proteins mediate uptake of different forms of iron and synergistically govern virulence in Francisella tularensis tularensis.* J Biol Chem, 2012. **287**(30): p. 25191-202.

105. Ramakrishnan, G., A. Meeker, and B. Dragulev, *fslE is necessary for siderophore-mediated iron acquisition in Francisella tularensis Schu S4.* J Bacteriol, 2008. **190**(15): p. 5353-61.

106. Crosa, L.M., J.H. Crosa, and F. Heffron, *Iron transport in Francisella in the absence of a recognizable TonB protein still requires energy generated by the proton motive force.* Biometals, 2009. **22**(2): p. 337-44.

107. Stevenson, B., E.E. Wyckoff, and S.M. Payne, *Vibrio cholerae FeoA, FeoB, and FeoC Interact To Form a Complex.* J Bacteriol, 2016. **198**(7): p. 1160-70.

108. Kim, H., H. Lee, and D. Shin, *The FeoA protein is necessary for the FeoB transporter to import ferrous iron.* Biochem Biophys Res Commun, 2012. **423**(4): p. 733-8.

109. Lindgren, H., et al., *Iron content differs between Francisella tularensis subspecies tularensis and subspecies holarctica strains and correlates to their susceptibility to H(2)O(2)-induced killing.* Infect Immun, 2011. **79**(3): p. 1218-24.

110. Nallaparaju, K.C., et al., *Evasion of IFN-gamma signaling by Francisella novicida is dependent upon Francisella outer membrane protein C.* PLoS One, 2011. **6**(3): p. e18201.

111. Lindgren, H., et al., *The 58-kilodalton major virulence factor of Francisella tularensis is required for efficient utilization of iron.* Infect Immun, 2009. **77**(10): p. 4429-36.

112. Alkhuder, K., et al., *Glutathione provides a source of cysteine essential for intracellular multiplication of Francisella tularensis.* PLoS Pathog, 2009. **5**(1): p. e1000284.

113. Forman, H.J., H. Zhang, and A. Rinna, *Glutathione: overview of its protective roles, measurement, and biosynthesis.* Mol Aspects Med, 2009. **30**(1-2): p. 1–12.

114. Ireland, P.M., et al., *A Francisella tularensis SCHU S4 mutant deficient in gamma-glutamyltransferase activity induces protective immunity: characterization of an attenuated vaccine candidate.* Microbiology, 2011. **157**(Pt 11): p. 3172–9.

115. Ren, G., M.M. Champion, and J.F. Huntley, *Identification of disulfide bond isomerase substrates reveals bacterial virulence factors.* Mol Microbiol, 2014. **94**(4): p. 926–44.

116. Kaur, A., et al., *ChaC2, an Enzyme for Slow Turnover of Cytosolic Glutathione.* J Biol Chem, 2017. **292**(2): p. 638–651.

117. Mungrue, I.N., et al., *CHAC1/MGC4504 is a novel proapoptotic component of the unfolded protein response, downstream of the ATF4-ATF3-CHOP cascade.* J Immunol, 2009. **182**(1): p. 466–76.

118. Barel, M., et al., *Francisella tularensis regulates the expression of the amino acid transporter SLC1A5 in infected THP-1 human monocytes.* Cell Microbiol, 2012. **14**(11): p. 1769-83.

119. Ramond, E., et al., *Importance of host cell arginine uptake in Francisella phagosomal escape and ribosomal protein amounts.* Mol Cell Proteomics, 2015. **14**(4): p. 870–81.

120. Steele, S., et al., *Francisella tularensis harvests nutrients derived via ATG5-independent autophagy to support intracellular growth.* PLoS Pathog, 2013. **9**(8): p. e1003562.

121. Pechous, R., et al., *Construction and characterization of an attenuated purine auxotroph in a Francisella tularensis live vaccine strain.* Infect Immun, 2006. **74**(8): p. 4452-61.

122. Pechous, R.D., et al., *A Francisella tularensis Schu S4 purine auxotroph is highly attenuated in mice but offers limited protection against homologous intranasal challenge.* PLoS One, 2008. **3**(6): p. e2487.

123. Horzempa, J., et al., *Francisella tularensis DeltapyrF mutants show that replication in nonmacrophages is sufficient for pathogenesis in vivo.* Infect Immun, 2010. **78**(6): p. 2607-19.

124. Peng, K. and D.M. Monack, *Indoleamine 2,3-dioxygenase 1 is a lung-specific innate immune defense mechanism that inhibits growth of Francisella tularensis tryptophan auxotrophs.* Infect Immun, 2010. **78**(6): p. 2723–33.

125. Brown, M.J., et al., *The contribution of the glycine cleavage system to the pathogenesis of Francisella tularensis.* Microbes Infect, 2014. **16**(4): p. 300–9.

126. Ziveri, J., et al., *The metabolic enzyme fructose-1,6-bisphosphate aldolase acts as a transcriptional regulator in pathogenic Francisella.* Nat Commun, 2017. **8**(1): p. 853.

127. Lai, X.H., I. Golovliov, and A. Sjostedt, *Francisella tularensis induces cytopathogenicity and apoptosis in murine macrophages via a mechanism that requires intracellular bacterial multiplication.* Infect Immun, 2001. **69**(7): p. 4691-4.

128. Lai, X.H. and A. Sjostedt, *Delineation of the molecular mechanisms of Francisella tularensis-induced apoptosis in murine macrophages.* Infect Immun, 2003. **71**(8): p. 4642-6.

129. Santic, M., et al., *Regulation of apoptosis and anti-apoptosis signalling by Francisella tularensis.* Microbes Infect, 2010. **12**(2): p. 126-34.

130. Schwartz, J.T., et al., *Francisella tularensis inhibits the intrinsic and extrinsic pathways to delay constitutive apoptosis and prolong human neutrophil lifespan.* J Immunol, 2012. **188**(7): p. 3351-63.

131. Schwartz, J.T., et al., *Francisella tularensis alters human neutrophil gene expression: insights into the molecular basis of delayed neutrophil apoptosis.* J Innate Immun, 2013. **5**(2): p. 124-36.

132. McCracken, J.M., et al., *Francisella tularensis Modulates a Distinct Subset of Regulatory Factors and Sustains Mitochondrial Integrity to Impair Human Neutrophil Apoptosis.* J Innate Immun, 2016. **8**(3): p. 299-313.

133. Kinkead, L.C., D.C. Fayram, and L.H. Allen, *Francisella novicida inhibits spontaneous apoptosis and extends human neutrophil lifespan.* J Leukoc Biol, 2017. **102**(3): p. 815-828.

134. Zhu, Q., et al., *Gasdermin D Promotes AIM2 Inflammasome Activation and Is Required for Host Protection against Francisella novicida.* J Immunol, 2018. **201**(12): p. 3662-3668.

135. Steele, S., et al., *Trogocytosis-associated cell to cell spread of intracellular bacterial pathogens.* Elife, 2016. **5**.

136. Wickstrum, J.R., et al., *Francisella tularensis induces extensive caspase-3 activation and apoptotic cell death in the tissues of infected mice.* Infect Immun, 2009. **77**(11): p. 4827-36.

137. Kumari, P., et al., *AIM2 in health and disease: Inflammasome and beyond.* Immunol Rev, 2020.

138. Meunier, E., et al., *Guanylate-binding proteins promote activation of the AIM2 inflammasome during infection with Francisella novicida.* Nat Immunol, 2015. **16**(5): p. 476-484.

139. Escoll, P., et al., *Targeting of host organelles by pathogenic bacteria: a sophisticated subversion strategy.* Nat Rev Microbiol, 2016. **14**(1): p. 5–19.

140. Thi, E.P., U. Lambertz, and N.E. Reiner, *Sleeping with the enemy: how intracellular pathogens cope with a macrophage lifestyle.* PLoS Pathog, 2012. **8**(3): p. e1002551.

141. Byndloss, M.X., et al., *How bacterial pathogens use type III and type IV secretion systems to facilitate their transmission.* Curr Opin Microbiol, 2017. **35**: p. 1–7.

142. Backert, S. and T.F. Meyer, *Type IV secretion systems and their effectors in bacterial pathogenesis.* Curr Opin Microbiol, 2006. **9**(2): p. 207–17.

143. Russell, A.B., S.B. Peterson, and J.D. Mougous, *Type VI secretion system effectors: poisons with a purpose.* Nature reviews. Microbiology, 2014. **12**(2): p. 137–48.

144. Kadzhaev, K., et al., *Identification of genes contributing to the virulence of Francisella tularensis SCHU S4 in a mouse intradermal infection model.* PLoS One, 2009. **4**(5): p. e5463.

145. De Craene, J.O., et al., *Phosphoinositides, Major Actors in Membrane Trafficking and Lipid Signaling Pathways.* Int J Mol Sci, 2017. **18**(3).

146. Pizarro-Cerda, J., A. Kuhbacher, and P. Cossart, *Phosphoinositides and host-pathogen interactions.* Biochim Biophys Acta, 2015. **1851**(6): p. 911–8.

147. Weber, S.S., C. Ragaz, and H. Hilbi, *Pathogen trafficking pathways and host phosphoinositide metabolism.* Mol Microbiol, 2009. **71**(6): p. 1341–52.

148. Dong, N., et al., *Modulation of membrane phosphoinositide dynamics by the phosphatidylinositide 4-kinase activity of the Legionella LepB effector.* Nat Microbiol, 2016. **2**: p. 16236.

149. Hsu, F., et al., *Structural basis for substrate recognition by a unique Legionella phosphoinositide phosphatase.* Proc Natl Acad Sci U S A, 2012. **109**(34): p. 13567–72.

150. Toulabi, L., et al., *Identification and structural characterization of a Legionella phosphoinositide phosphatase.* J Biol Chem, 2013. **288**(34): p. 24518–27.

151. Finn, R.D., et al., *HMMER web server: 2015 update.* Nucleic Acids Res, 2015. **43**(W1): p. W30–8.

152. de Felipe, K.S., et al., *Legionella eukaryotic-like type IV substrates interfere with organelle trafficking.* PLoS Pathog, 2008. **4**(8): p. e1000117.

153. Heidtman, M., et al., *Large-scale identification of Legionella pneumophila Dot/Icm substrates that modulate host cell vesicle trafficking pathways.* Cell Microbiol, 2009. **11**(2): p. 230–48.

154. Weigele, B.A., et al., *A systematic exploration of the interactions between bacterial effector proteins and host cell membranes.* Nat Commun, 2017. **8**(1): p. 532.

155. Gehrmann, T. and L.M. Heilmeyer, Jr., *Phosphatidylinositol 4-kinases.* Eur J Biochem, 1998. **253**(2): p. 357–70.

156. Sasaki, T., et al., *Mammalian phosphoinositide kinases and phosphatases.* Prog Lipid Res, 2009. **48**(6): p. 307–43.

157. Marat, A.L. and V. Haucke, *Phosphatidylinositol 3-phosphates-at the interface between cell signalling and membrane traffic.* EMBO J, 2016. **35**(6): p. 561–79.

158. Reidick, C., F. Boutouja, and H.W. Platta, *The class III phosphatidylinositol 3-kinase Vps34 in Saccharomyces cerevisiae.* Biol Chem, 2017. **398**(5-6): p. 677–685.

159. Espinet, C., et al., *An efficient method to isolate yeast genes causing overexpression-mediated growth arrest.* Yeast, 1995. **11**(1): p. 25–32.

160. Ghosh, J., et al., *Characterization of Streptococcus pyogenes beta-NAD+ glycohydrolase: re-evaluation of enzymatic properties associated with pathogenesis.* J Biol Chem, 2010. **285**(8): p. 5683–94.

161. Qiu, J. and Z.Q. Luo, *Legionella and Coxiella effectors: strength in diversity and activity.* Nat Rev Microbiol, 2017. **15**(10): p. 591–605.

162. O'Connor, T.J., et al., *Aggravating genetic interactions allow a solution to redundancy in a bacterial pathogen.* Science, 2012. **338**(6113): p. 1440–4.

163. West, T.E., et al., *Inhalation of Burkholderia thailandensis results in lethal necrotizing pneumonia in mice: a surrogate model for pneumonic melioidosis.* Trans R Soc Trop Med Hyg, 2008. **102 Suppl 1**: p. S119–26.

164. Florey, O., et al., *V-ATPase and osmotic imbalances activate endolysosomal LC3 lipidation.* Autophagy, 2015. **11**(1): p. 88–99.

165. Gaullier, J.M., et al., *FYVE fingers bind PtdIns(3)P.* Nature, 1998. **394**(6692): p. 432–3.

166. Knight, Z.A., et al., *A pharmacological map of the PI3-K family defines a role for p110alpha in insulin signaling.* Cell, 2006. **125**(4): p. 733–47.

167. Wymann, M.P., et al., *Wortmannin inactivates phosphoinositide 3-kinase by covalent modification of Lys-802, a residue involved in the phosphate transfer reaction.* Mol Cell Biol, 1996. **16**(4): p. 1722–33.

168. Pattni, K., et al., *A PtdIns(3)P-specific probe cycles on and off host cell membranes during Salmonella invasion of mammalian cells.* Curr Biol, 2001. **11**(20): p. 1636–42.

169. Hammond, G.R. and T. Balla, *Polyphosphoinositide binding domains: Key to inositol lipid biology.* Biochim Biophys Acta, 2015. **1851**(6): p. 746–58.

170. Sbrissa, D., O.C. Ikonomov, and A. Shisheva, *Phosphatidylinositol 3-phosphate-interacting domains in PIKfyve. Binding specificity and role in PIKfyve. Endomenbrane localization.* J Biol Chem, 2002. **277**(8): p. 6073–9.

171. Patki, V., et al., *A functional PtdIns(3)P-binding motif.* Nature, 1998. **394**(6692): p. 433–4.

172. Choy, C.H., B.K. Han, and R.J. Botelho, *Phosphoinositide Diversity, Distribution, and Effector Function: Stepping Out of the Box.* Bioessays, 2017. **39**(12): p. Epub ahead of print.

173. Ivetac, I., et al., *The type Ialpha inositol polyphosphate 4-phosphatase generates and terminates phosphoinositide 3-kinase signals on endosomes and the plasma membrane.* Mol Biol Cell, 2005. **16**(5): p. 2218–33.

174. Nigorikawa, K., et al., *Inositol Polyphosphate-4-Phosphatase Type I Negatively Regulates Phagocytosis via Dephosphorylation of Phagosomal PtdIns(3,4)P2.* PLoS One, 2015. **10**(11): p. e0142091.

175. Chong, A. and J. Celli, *The francisella intracellular life cycle: toward molecular mechanisms of intracellular survival and proliferation.* Front Microbiol, 2010. **1**: p. 138.

176. Guerra, F. and C. Bucci, *Multiple Roles of the Small GTPase Rab7.* Cells, 2016. **5**(3).

177. Bucci, C., et al., *Rab7: a key to lysosome biogenesis.* Mol Biol Cell, 2000. **11**(2): p. 467–80.

178. Renvoise, A., et al., *Intracellular Rickettsiales: Insights into manipulators of eukaryotic cells.* Trends Mol Med, 2011. **17**(10): p. 573–83.

179. Finsel, I., et al., *The Legionella effector RidL inhibits retrograde trafficking to promote intracellular replication.* Cell Host Microbe, 2013. **14**(1): p. 38–50.

180. Gaspar, A.H. and M.P. Machner, *VipD is a Rab5-activated phospholipase A1 that protects Legionella pneumophila from endosomal fusion.* Proc Natl Acad Sci U S A, 2014. **111**(12): p. 4560–5.

181. Harding, C.R., et al., *LtpD is a novel Legionella pneumophila effector that binds phosphatidylinositol 3-phosphate and inositol monophosphatase IMPA1.* Infect Immun, 2013. **81**(11): p. 4261–70.

182. Jank, T., et al., *Domain organization of Legionella effector SetA.* Cell Microbiol, 2012. **14**(6): p. 852–68.

183. Weber, S.S., et al., *Legionella pneumophila exploits PI(4)P to anchor secreted effector proteins to the replicative vacuole.* PLoS Pathog, 2006. **2**(5): p. e46.

184. Yeung, T., et al., *Contribution of phosphatidylserine to membrane surface charge and protein targeting during phagosome maturation.* J Cell Biol, 2009. **185**(5): p. 917–28.

185. Lu, N., et al., *Two PI 3-kinases and one PI 3-phosphatase together establish the cyclic waves of phagosomal PtdIns(3)P critical for the degradation of apoptotic cells.* PLoS Biol, 2012. **10**(1): p. e1001245.

186. Gari, E., et al., *A set of vectors with a tetracycline-regulatable promoter system for modulated gene expression in Saccharomyces cerevisiae.* Yeast, 1997. **13**(9): p. 837–48.

187. LoVullo, E.D., et al., *Single-copy chromosomal integration systems for Francisella tularensis.* Microbiology, 2009. **155**(Pt 4): p. 1152–63.

188. Zaide, G., et al., *Identification and characterization of novel and potent transcription promoters of Francisella tularensis.* Appl Environ Microbiol, 2011. **77**(5): p. 1608–18.

189. Correia, F.F., et al., *Kinase activity of overexpressed HipA is required for growth arrest and multidrug tolerance in Escherichia coli.* J Bacteriol, 2006. **188**(24): p. 8360–7.

190. Burke, D., D. Dawson, and T. Stearn, *Methods in yeast genetics : a Cold Spring Harbor Laboratory course manual*. 2000, Plainview, N.Y.: Cold Spring Harbor Laboratory Press.

191. Walters, K.A., et al., *Prior infection with Type A Francisella tularensis antagonizes the pulmonary transcriptional response to an aerosolized Toll-like receptor 4 agonist.* BMC Genomics, 2015. **16**: p. 874.

192. Sun, Q., et al., *Rubicon controls endosome maturation as a Rab7 effector.* Proc Natl Acad Sci U S A, 2010. **107**(45): p. 19338–43.

193. Palibrk, V., et al., *Promyelocytic leukemia bodies tether to early endosomes during mitosis.* Cell Cycle, 2014. **13**(11): p. 1749–55.

194. Broms, J.E., et al., *IglG and IglI of the Francisella pathogenicity island are important virulence determinants of Francisella tularensis LVS.* Infect Immun, 2011. **79**(9): p. 3683–96.

195. Meibom, K.L. and A. Charbit, *Francisella tularensis metabolism and its relation to virulence.* Front Microbiol, 2010. **1**: p. 140.

196. Ziveri, J., M. Barel, and A. Charbit, *Importance of Metabolic Adaptations in Francisella Pathogenesis.* Front Cell Infect Microbiol, 2017. **7**: p. 96.

197. Asare, R., et al., *Molecular bases of proliferation of Francisella tularensis in arthropod vectors.* Environ Microbiol, 2010. **12**(9): p. 2587–612.

198. Lindemann, S.R., et al., *Francisella tularensis Schu S4 O-antigen and capsule biosynthesis gene mutants induce early cell death in human macrophages.* Infect Immun, 2011. **79**(2): p. 581–94.

199. Moule, M.G., D.M. Monack, and D.S. Schneider, *Reciprocal analysis of Francisella novicida infections of a Drosophila melanogaster model reveal host-pathogen conflicts mediated by reactive oxygen and imd-regulated innate immune response.* PLoS Pathog, 2010. **6**(8): p. e1001065.

200. Peng, K. and D.M. Monack, *Indoleamine 2,3-dioxygenase 1 is a lung-specific innate immune defense mechanism that inhibits growth of Francisella tularensis tryptophan auxotrophs.* Infect Immun, 2010. **78**(6): p. 2723-33.

201. Goodman, A.L., M. Wu, and J.I. Gordon, *Identifying microbial fitness determinants by insertion sequencing using genome-wide transposon mutant libraries.* Nat Protoc, 2011. **6**(12): p. 1969–80.

202. Charity, J.C., et al., *Small molecule control of virulence gene expression in Francisella tularensis.* PLoS Pathog, 2009. **5**(10): p. e1000641.

203. Pritchard, J.R., et al., *ARTIST: high-resolution genome-wide assessment of fitness using transposon-insertion sequencing.* PLoS Genet, 2014. **10**(11): p. e1004782.

204. Gesbert, G., et al., *Asparagine assimilation is critical for intracellular replication and dissemination of Francisella.* Cell Microbiol, 2014. **16**(3): p. 434-49.

205. Hanes, C.S., F.J. Hird, and F.A. Isherwood, *Enzymic transpeptidation reactions involving gamma-glutamyl peptides and alpha-amino-acyl peptides.* Biochem J, 1952. **51**(1): p. 25–35.

206. Casagrande, F., et al., *Projection structure of DtpD (YbgH), a prokaryotic member of the peptide transporter family.* J Mol Biol, 2009. **394**(4): p. 708–17.

207. Daniel, H., et al., *From bacteria to man: archaic proton-dependent peptide transporters at work.* Physiology (Bethesda), 2006. **21**: p. 93–102.

208. Osawa, H., G. Stacey, and W. Gassmann, *ScOPT1 and AtOPT4 function as proton-coupled oligopeptide transporters with broad but distinct substrate specificities.* Biochem J, 2006. **393**(Pt 1): p. 267–75.

209. Solcan, N., et al., *Alternating access mechanism in the POT family of oligopeptide transporters.* EMBO J, 2012. **31**(16): p. 3411–21.

210. Bachhawat, A.K. and S. Yadav, *The glutathione cycle: Glutathione metabolism beyond the gamma-glutamyl cycle.* IUBMB Life, 2018. **70**(7): p. 585–592.

211. Oakley, A.J., M. Coggan, and P.G. Board, *Identification and characterization of gamma-glutamylamine cyclotransferase, an enzyme responsible for gamma-glutamyl-epsilon-lysine catabolism.* J Biol Chem, 2010. **285**(13): p. 9642–8.

212. Fujiwara, S., et al., *RipAY, a Plant Pathogen Effector Protein, Exhibits Robust gamma-Glutamyl Cyclotransferase Activity When Stimulated by Eukaryotic Thioredoxins.* J Biol Chem, 2016. **291**(13): p. 6813–30.

213. Mukaihara, T., et al., *Ralstonia solanacearum Type III Effector RipAY Is a Glutathione-Degrading Enzyme That Is Activated by Plant Cytosolic Thioredoxins and Suppresses Plant Immunity.* MBio, 2016. **7**(2): p. e00359–16.

214. Potter, A.J., C. Trappetti, and J.C. Paton, *Streptococcus pneumoniae uses glutathione to defend against oxidative stress and metal ion toxicity.* J Bacteriol, 2012. **194**(22): p. 6248–54.

215. Suzuki, H., et al., *The yliA, -B, -C, and -D genes of Escherichia coli K-12 encode a novel glutathione importer with an ATP-binding cassette.* J Bacteriol, 2005. **187**(17): p. 5861–7.

216. Vergauwen, B., et al., *Delineation of the Pasteurellaceae-specific GbpA-family of glutathione-binding proteins.* BMC Biochem, 2011. **12**: p. 59.

217. Vorwerk, H., et al., *Utilization of host-derived cysteine-containing peptides overcomes the restricted sulphur metabolism of Campylobacter jejuni.* Mol Microbiol, 2014. **93**(6): p. 1224–45.

218. Ganguli, D., C. Kumar, and A.K. Bachhawat, *The alternative pathway of glutathione degradation is mediated by a novel protein complex involving three new genes in Saccharomyces cerevisiae.* Genetics, 2007. **175**(3): p. 1137–51.

219. Kaur, H., D. Ganguli, and A.K. Bachhawat, *Glutathione degradation by the alternative pathway (DUG pathway) in Saccharomyces cerevisiae is initiated by (Dug2p-Dug3p)2 complex, a novel glutamine amidotransferase (GATase) enzyme acting on glutathione.* J Biol Chem, 2012. **287**(12): p. 8920–31.

220. Goodman, A.L., et al., *Identifying genetic determinants needed to establish a human gut symbiont in its habitat.* Cell Host Microbe, 2009. **6**(3): p. 279–89.

221. Brown, M.J., et al., *The contribution of the glycine cleavage system to the pathogenesis of Francisella tularensis.* Microbes Infect, 2014. **16**(4): p. 300-9.

222. Maier, T.M., et al., *Construction and characterization of a highly efficient Francisella shuttle plasmid.* Appl Environ Microbiol, 2004. **70**(12): p. 7511–9.

223. Martin, M., *Cutadapt removes adapter sequences from high-throughput sequencing reads.* EMBnet.journal, 2011. **17**(1).

224. Langmead, B., et al., *Ultrafast and memory-efficient alignment of short DNA sequences to the human genome.* Genome Biol, 2009. **10**(3): p. R25.

225. Ramsey, K.M., et al., *Ubiquitous promoter-localization of essential virulence regulators in Francisella tularensis.* PLoS Pathog, 2015. **11**(4): p. e1004793.

226. Charity, J.C., et al., *Twin RNA polymerase-associated proteins control virulence gene expression in Francisella tularensis.* PLoS Pathog, 2007. **3**(6): p. e84.

227. Chamberlain, R.E., *Evaluation of Live Tularemia Vaccine Prepared in a Chemically Defined Medium.* Appl Microbiol, 1965. **13**: p. 232–5.

228. Ramsey, K.M. and S.L. Dove, *A response regulator promotes Francisella tularensis intramacrophage growth by repressing an anti-virulence factor.* Mol Microbiol, 2016. **101**(4): p. 688–700.

229. Mortensen, B.L., et al., *Francisella tularensis RipA protein topology and identification of functional domains.* J Bacteriol, 2012. **194**(6): p. 1474-84.

230. Wang, C.K., et al., *CHAC2 is essential for self-renewal and glutathione maintenance in human embryonic stem cells.* Free Radic Biol Med, 2017. **113**: p. 439–451.

231. Oakley, A.J., et al., *The identification and structural characterization of C7orf24 as gamma-glutamyl cyclotransferase. An essential enzyme in the gamma-glutamyl cycle.* J Biol Chem, 2008. **283**(32): p. 22031–42.

232. Sen, B., A. Meeker, and G. Ramakrishnan, *The fslE homolog, FTL_0439 (fupA/B), mediates siderophore-dependent iron uptake in Francisella tularensis LVS.* Infect Immun, 2010. **78**(10): p. 4276-85.

233. Gaitonde, M.K., *A spectrophotometric method for the direct determination of cysteine in the presence of other naturally occurring amino acids.* Biochem J, 1967. **104**(2): p. 627-33.

234. Voss, O.H., et al., *Risk1, a Phosphatidylinositol 3-Kinase Effector, Promotes Rickettsia typhi Intracellular Survival.* mBio, 2020. **11**(3).

Appendix 1

Locus Tag	Locus	Protein Name	Total TAs	Fraction TAs hit	Total reads	EL-ARTIST
FTL_0001	dnaA	chromosomal replication initiation protein	153	0.02	9	E
FTL_0002	-	DNA polymerase III subunit beta	126	0.024	11	E
FTL_0003	-	hypothetical protein	66	0.97	67216	N.E.
FTL_0004	isftu1	transposase	100	1	91977	N.E.
FTL_0005	-	Na+/H+ antiporter NHAP, fragment	67	0.985	81844	N.E.
FTL_0006	-	indolepyruvate decarboxylase	145	0.979	188295	N.E.
FTL_0007	-	hypothetical protein	16	1	17779	N.E.
FTL_0008	-	peptidase	98	0.98	136606	N.E.
FTL_0009	-	outer membrane protein	38	0.974	21945	N.E.
FTL_0010	glpe	thiosulfate sulfurtransferase	52	0.962	6410	N.E.
FTL_0011	secB1	preprotein translocase subunit SecB	29	0.966	6669	N.E.
FTL_0012	recA	recombinase A	87	0.943	14600	N.E.
FTL_0013	recX	regulatory protein recX	49	0.98	42951	N.E.
FTL_0014	ssb	single-strand binding protein	48	0.042	8	E
FTL_0015	ackA	propionate kinase	122	0.975	123301	N.E.
FTL_0016	pta	phosphate acetyltransferase	212	0.991	196668	N.E.
FTL_0017	-	-	80	0.988	109580	N.E.
FTL_0018	isftu1	transposase	100	1	92331	N.E.
FTL_0019	-	sugar transferase	41	0.976	48885	N.E.
FTL_0020	aspS	aspartyl-tRNA synthetase	160	0.031	493	E
FTL_0021	-	MFS superfamily proline/ betaine transporter	134	0.993	151858	N.E.
FTL_0022	-	-	59	0.983	87829	N.E.
FTL_0023	isftu1	transposase	100	1	105855	N.E.
FTL_0024	-	serine transporter	159	0.975	80729	N.E.
FTL_0025	-	hypothetical protein	32	0.969	33253	N.E.
FTL_0026	-	3-hydroxyisobutyrate dehydrogenase	33	0.939	34343	N.E.
FTL_0027	-	3-hydroxyisobutyrate dehydrogenase	60	0.967	61972	N.E.
FTL_0028	-	aspartate carbamoyltransferase	96	0.979	100738	N.E.
FTL_0029	carB	carbamoyl phosphate synthase large subunit	303	0.98	327819	N.E.
FTL_0030	-	carbamoyl phosphate synthase small subunit	119	0.958	132034	N.E.
FTL_0031	-	acid phosphatase	114	0.991	153016	N.E.
FTL_0032	tmpT	thiopurine S-methyltransferase	85	1	87436	N.E.
FTL_0033	pyrC	dihydroorotase	111	0.829	2867	N.E.
FTL_0034	-	hypothetical protein	128	0.977	113950	N.E.
FTL_0035	-	hypothetical protein	26	1	21677	N.E.
FTL_0036	-	hypothetical protein	49	0.959	51830	N.E.
FTL_0037	-	hypothetical protein	124	0.984	169274	N.E.
FTL_0038	emrA2	HlyD family secretion protein	115	0.983	112650	N.E.
FTL_0039	-	hypothetical protein	50	0.98	58179	N.E.
FTL_0040	-	LysR family transcriptional regulator	102	1	128305	N.E.
FTL_0041	-	hypothetical protein	36	1	46123	N.E.
FTL_0042	isftu2	transposase	77	1	66766	N.E.
FTL_0043	-	chorismate mutase	54	1	56053	N.E.
FTL_0044	-	transglutaminase	313	0.981	429672	N.E.
FTL_0045	-	orotidine 5'-phosphate decarboxylase	61	0.951	20518	N.E.
FTL_0046	-	diyroorotate dehydrogenase	80	0.975	22106	N.E.
FTL_0047	-	hypothetical protein	12	1	11915	N.E.
FTL_0048	-	prephenate dehydrogenase.	71	0.972	97497	N.E.
FTL_0049	-	D-tyrosyl-tRNA(Tyr) deacylase	41	1	45213	N.E.
FTL_0050	-	hypothetical protein	91	1	111661	N.E.
FTL_0051	-	hypothetical protein	48	0.979	61396	N.E.

FTL_0052	-	hypothetical protein	65	0.969	56904	N.E.
FTL_0053	-	Beta-fructofuranosidase	98	0.99	137537	N.E.
FTL_0054	isftu1	transposase	100	1	93023	N.E.
FTL_0055	-	hypothetical protein	66	0.985	78212	N.E.
FTL_0056	-	NADH dehydrogenase	72	0.958	68746	N.E.
FTL_0057	-	hypothetical protein	77	0.935	78295	N.E.
FTL_0058	-	aromatic amino acid HAAP transporter	137	0.109	2427	E
FTL_0059	gidB	16S rRNA methyltransferase GidB	63	0.968	52160	N.E.
FTL_0060	-	hypothetical protein	71	0.944	74328	N.E.
FTL_0061	-	hypothetical protein	124	0.992	184735	N.E.
FTL_0062	-	transcriptional regulator	57	0.965	67611	N.E.
FTL_0063	-	major facilitator transporter	164	0.994	209848	N.E.
FTL_0064	-	-	55	1	53910	N.E.
FTL_0065	-	-	96	0.979	122677	N.E.
FTL_0066	-	-	26	0.962	23173	N.E.
FTL_0067	-	-	55	1	59774	N.E.
FTL_0068	-	phosphoheptose isomerase	55	0.091	588	E
FTL_0069	-	outer membrane lipoprotein	52	0.096	516	E
FTL_0070	rpsT	30S ribosomal protein S20	21	0.143	2102	E
FTL_0071	-	GTP-binding protein LepA	153	0.418	6220	E and N.E.
FTL_0072	mnmA	tRNA-specific 2-thiouridylase MnmA	92	0.054	1173	E
FTL_0073	-	hypothetical protein	102	0.941	47280	N.E.
FTL_0074	-	peptide deformylase	42	0.167	2149	E
FTL_0075	-	riboflavin synthase beta subunit (6,7-dimethl-8-ribityllumazine synthase)	41	0.073	1323	E
FTL_0076	-	riboflavin biosynthesis protein ribA/GTP-cyclohydrolase II	116	0.026	17	E
FTL_0077	-	riboflavin synthase subunit alpha	66	0.121	3592	E
FTL_0078	-	riboflavin biosynthesis protein ribD	100	0	0	E
FTL_0079	isftu2	transposase	76	1	61738	N.E.
FTL_0080	isftu1	transposase	94	1	87924	N.E.
FTL_0081	-	-	70	0.986	88762	N.E.
FTL_0082	-	B-type cytochrome	66	0.985	78519	N.E.
FTL_0083	-	-	36	0.944	33635	N.E.
FTL_0084	-	-	46	1	75380	N.E.
FTL_0085	nhaA	pH-dependent sodium/proton antiporter	131	0.977	169487	N.E.
FTL_0086	-	hypothetical protein	79	0.987	72042	N.E.
FTL_0087	-	acetyltransferase protein	81	0.975	30505	N.E.
FTL_0088	-	acetyltransferase protein	72	0.056	111	E
FTL_0089	-	ferredoxin	27	0.074	469	E
FTL_0090	-	hypothetical protein	74	0.095	1610	E
FTL_0091	-	O-methyltransferase	43	1	55099	N.E.
FTL_0092	purT	phosphoribosylglycinamide formyltransferase 2	120	0.992	159953	N.E.
FTL_0093	chiB	chitinase	234	0.991	330753	N.E.
FTL_0094	clpB	ClpB protein	249	0.988	283276	N.E.
FTL_0095	-	-	34	0.971	29942	N.E.
FTL_0096	-	-	42	1	61924	N.E.
FTL_0097	-	hypothetical protein	32	0.875	38786	N.E.
FTL_0098	trpA	tryptophan synthase subunit alpha	81	0.988	97596	N.E.
FTL_0099	-	tryptophan synthase subunit beta	97	0.979	136098	N.E.
FTL_0100	-	carboxypeptidase,fragment	166	0.976	219767	N.E.
FTL_0101	-	voltage-gated ClC-type chloride channel clcA	102	0.971	141255	N.E.
FTL_0102	-	hypothetical protein	37	0.973	47315	N.E.
FTL_0103	-	hypothetical protein	42	0.976	53003	N.E.

FTL_0104	-	hypothetical protein	40	1	43686	N.E.
FTL_0105	-	hypothetical protein	38	0.947	26935	N.E.
FTL_0106	-	-	64	0.969	80117	N.E.
FTL_0107	isftu1	transposase	100	1	106881	N.E.
FTL_0108	-	hypothetical protein	110	0.991	104005	N.E.
FTL_0109	-	hypothetical protein	40	0.975	38380	N.E.
FTL_0110	-	hypothetical protein	25	1	25067	N.E.
FTL_0111	iglA	intracellular growth locus, subunit A	46	1	59559	N.E.
FTL_0112	iglB	intracellular growth locus, subunit B	166	0.988	188156	N.E.
FTL_0113	iglC	intracellular growth locus, subunit C	75	0.987	80103	N.E.
FTL_0114	iglD	intracellular growth locus, subunit D	131	1	118023	N.E.
FTL_0115	-	hypothetical protein	89	0.966	81004	N.E.
FTL_0116	pdpC	PdpC protein	496	0.984	480989	N.E.
FTL_0117	-	hypothetical protein	101	0.99	98556	N.E.
FTL_0118	-	hypothetical protein	132	0.992	122718	N.E.
FTL_0119	-	hypothetical protein	83	1	67788	N.E.
FTL_0120	-	hypothetical protein	181	1	190690	N.E.
FTL_0121	-	hypothetical protein	61	1	68825	N.E.
FTL_0122	-	hypothetical protein	236	0.983	184565	N.E.
FTL_0123	-	hypothetical protein	53	1	53464	N.E.
FTL_0124	-	hypothetical protein	48	1	36188	N.E.
FTL_0125	pdpB	PdpB protein	447	0.984	389202	N.E.
FTL_0126	pdpA	PdpA protein	296	0.993	302793	N.E.
FTL_0127	-	formate dehydrogenase	70	1	83456	N.E.
FTL_0128	isftu1	transposase	100	1	106624	N.E.
FTL_0129	-	2-isopropylmalate synthase	80	0.975	88517	N.E.
FTL_0130	-	isopropylmalate/homocitrate/citramalate synthase family protein	25	0.96	32645	N.E.
FTL_0131	-	branched-chain amino acid aminotransferase	102	0.98	125694	N.E.
FTL_0132	-	pyruvate phosphate dikinase	242	0.988	254191	N.E.
FTL_0133	feoB	ferrous iron transport protein	241	0.983	140314	N.E.
FTL_0134	-	hypothetical protein	51	0.961	58864	N.E.
FTL_0135	isftu1	transposase	100	1	92170	N.E.
FTL_0136	-	hypothetical protein	66	0.985	62013	N.E.
FTL_0137	-	lipopolysaccharide protein	114	0.982	98345	N.E.
FTL_0138	-	ribonuclease II family protein	181	0.945	53367	N.E.
FTL_0139	-	carboxylesterase/phospholipase family protein	77	0.377	16639	E and N.E.
FTL_0140	hemC	porphobilinogen deaminase	92	0.098	1475	E
FTL_0141	-	camphor resistance protein CrcB	41	0.976	65221	N.E.
FTL_0142	-	hypothetical protein	45	0.978	71011	N.E.
FTL_0143	-	hypothetical protein	36	0.972	78205	N.E.
FTL_0144	-	hypothetical protein	15	0.933	16327	N.E.
FTL_0145	-	ABC transporter membrane protein	201	0.08	5053	E
FTL_0146	-	ABC transporter ATP-binding protein	111	0.405	90770	E and N.E.
FTL_0147	-	hypothetical protein	167	0.988	219894	N.E.
FTL_0148	-	Sodium/hydrogen exchanger (antiporter) family protein	202	0.96	29119	N.E.
FTL_0149	-	carbonic anhydrase	48	1	44400	N.E.
FTL_0150	-	lipoprotein releasing system, subunit B, outer membrane lipoprotein	84	0.155	1157	E
FTL_0151	ipk	4-diphosphocytidyl-2-C-methyl-D-erythritol kinase	98	0.102	529	E
FTL_0152	-	hypothetical protein	38	1	45330	N.E.
FTL_0153	isftu1	transposase	97	1	107890	N.E.

FTL_0154	-	-	35	0.943	26575	N.E.
FTL_0155	-	-	39	0.923	39941	N.E.
FTL_0156	-	phosphate transport protein	98	0.112	488	E
FTL_0157	-	hypothetical protein	74	0.122	662	E
FTL_0158	acpA	acid phosphatase, phospholipase C (EC:3.1.4.3)	150	0.967	177667	N.E.
FTL_0159	-	hydrolase subunit	88	0.966	97817	N.E.
FTL_0160	-	LamB/YcsF family protein	60	0.933	66403	N.E.
FTL_0161	-	-	65	0.969	61416	N.E.
FTL_0162	-	hypothetical protein	84	0.952	91894	N.E.
FTL_0163	-	MFS transporter	21	1	21481	N.E.
FTL_0164	isftu1	transposase	100	1	91544	N.E.
FTL_0165	-	dicarboxylate MFS transporter	12	1	9430	N.E.
FTL_0166	-	universal stress protein	73	0.986	85442	N.E.
FTL_0167	-	DNA/RNA helicase	298	0.97	312089	N.E.
FTL_0168	-	hypothetical protein	74	0.959	85654	N.E.
FTL_0169	-	hypothetical protein	66	0.091	1856	E
FTL_0170	-	hypothetical protein	50	0.96	66857	N.E.
FTL_0171	-	tetrapyrrole methyltransferase family protein	92	0.978	64681	N.E.
FTL_0172	murC	UDP-N-acetylmuramate--L-alanine ligase	145	0.772	7465	E and N.E.
FTL_0173	aroE	shikimate 5-dehydrogenase	76	0.961	42927	N.E.
FTL_0174	-	hypothetical protein	38	1	48174	N.E.
FTL_0175	rpmH	50S ribosomal protein L34	7	0.143	7	E
FTL_0176	-	ribonuclease P protein component	28	0.036	6	E
FTL_0177	-	hypothetical protein	28	0.429	6254	E and N.E.
FTL_0178	yidC	inner-membrane protein	174	0.017	28	E
FTL_0179	ddg	acyltransferase	91	0.022	5	E
FTL_0180	htrB	acyltransferase	99	0.051	87	E
FTL_0181	-	Type IV pili fiber building block protein	48	0.521	14181	E and N.E.
FTL_0182	-	elongation factor P	50	0.12	89	E
FTL_0183	-	oligoribonuclease	46	0.152	1620	E
FTL_0184	-	hypothetical protein	18	0.944	21316	N.E.
FTL_0185	isftu1	transposase	97	1	105247	N.E.
FTL_0186	-	hypothetical protein	146	0.973	153565	N.E.
FTL_0187	-	cyclohexadienyl dehydratase	86	0.965	75056	N.E.
FTL_0188	-	cytochrome d terminal oxidase, polypeptide subunit II	141	0.021	31	E
FTL_0189	-	cytochrome d terminal oxidase, polypeptide subunit I	163	0.031	56	E
FTL_0190	-	major facilitator transporter	149	0.987	141402	N.E.
FTL_0191	-	cytochrome O ubiquinol oxidase subunit II	91	0.978	76417	N.E.
FTL_0192	-	cytochrome O ubiquinol oxidase subunit I	196	0.985	156543	N.E.
FTL_0193	-	cytochrome O ubiquinol oxidase, subunit III	60	0.983	47492	N.E.
FTL_0194	-	cytochrome O ubiquinol oxidase subunit IV	37	1	29544	N.E.
FTL_0195	-	protoheme IX farnesyltransferase	115	0.965	76674	N.E.
FTL_0196	-	UDP-3-O-[3-hydroxymyristoyl] glucosamine N-acyltransferase	104	0.99	135842	N.E.
FTL_0197	-	hypothetical protein	69	0.971	66062	N.E.
FTL_0198	-	pyridoxal kinase	95	0.979	70611	N.E.
FTL_0199	-	hypothetical protein	54	1	47769	N.E.
FTL_0200	-	methanol dehydrogenase regulatory protein	92	0.978	126284	N.E.
FTL_0201	-	hypothetical protein	99	0.929	106530	N.E.

FTL_0202	-	hypothetical protein	53	0.981	57485	N.E.
FTL_0203	-	hypothetical protein	101	0.96	131156	N.E.
FTL_0204	-	hypothetical protein	95	0.979	133468	N.E.
FTL_0205	-	hypothetical protein	73	0.973	84034	N.E.
FTL_0206	-	hypothetical protein	180	0.972	219795	N.E.
FTL_0207	-	pyrrolidone-carboxylate peptidase	63	0.968	82281	N.E.
FTL_0208	-	putative cytochrome c-type biogenesis protein	66	0.97	73855	N.E.
FTL_0209	-	DNA polymerase III subunit chi	49	0.653	6411	E and N.E.
FTL_0210	valS	valyl-tRNA synthetase	252	0.052	137	E
FTL_0211	-	hypothetical protein	110	0.973	135379	N.E.
FTL_0212	-	hypothetical protein	110	0.991	145076	N.E.
FTL_0213	-	hypothetical protein	33	0.97	44884	N.E.
FTL_0214	-	L-lactate dehydrogenase	105	0.981	128842	N.E.
FTL_0215	-	dihydropteridine reductase	74	1	96470	N.E.
FTL_0216	-	MutT/nudix family protein	39	0.949	52851	N.E.
FTL_0217	fumC	fumarate hydratase	123	0.992	159930	N.E.
FTL_0218	gltX	glutamyl-tRNA synthetase	131	0.053	484	E
FTL_0219	-	hypothetical protein	73	0.986	93449	N.E.
FTL_0220	isftu2	transposase	86	1	74922	N.E.
FTL_0221	-	amino acid permease	147	0.986	220537	N.E.
FTL_0222	-	hypothetical protein	84	0.988	111777	N.E.
FTL_0223	-	dihydrofolate reductase type I	56	0.161	161	E
FTL_0224	rpsB	30S ribosomal protein S2	59	0.051	33	E
FTL_0225	tsf	elongation factor Ts	53	0.019	11	E
FTL_0226	pyrH	uridylate kinase	64	0.016	27	E
FTL_0227	frr	ribosome recycling factor	48	0.146	1359	E
FTL_0228	uppS	undecaprenyl pyrophosphate synthase	71	0.099	34	E
FTL_0229	cdsA	phosphatidate cytidylyltransferase	85	0.082	470	E
FTL_0230	dut	deoxyuridine 5'-triphosphate nucleotidohydrolase	39	0.077	57	E
FTL_0231	pgsA	phosphatidylglycerophosphate synthetase	64	0.047	1570	E
FTL_0232	rpsL	30S ribosomal protein S12	33	0.061	24	E
FTL_0233	rpsG	30S ribosomal protein S7	39	0.103	42	E
FTL_0234	-	elongation factor G	148	0.047	564	E
FTL_0235	rpsJ	30S ribosomal protein S10	32	0	0	E
FTL_0236	rplC	50S ribosomal protein L3	50	0.06	26	E
FTL_0237	rplD	50S ribosomal protein L4	52	0.019	2	E
FTL_0238	rplW	50S ribosomal protein L23	26	0.038	49	E
FTL_0239	rplB	50S ribosomal protein L2	80	0	0	E
FTL_0240	rpsS	30S ribosomal protein S19	20	0	0	E
FTL_0241	rplV	50S ribosomal protein L22	28	0	0	E
FTL_0242	rpsC	30S ribosomal protein S3	57	0.035	12	E
FTL_0243	rplP	50S ribosomal protein L16	32	0	0	E
FTL_0244	-	50S ribosomal protein L29	20	0	0	E
FTL_0245	rpsQ	30S ribosomal protein S17	29	0.138	38	E
FTL_0246	rplN	50S ribosomal protein L14	33	0.03	17	E
FTL_0247	rplX	50S ribosomal protein L24	32	0.031	4	E
FTL_0248	rplE	50S ribosomal protein L5	55	0.036	24	E
FTL_0249	rpsN	30S ribosomal protein S14	28	0	0	E
FTL_0250	rpsH	30S ribosomal protein S8	35	0	0	E
FTL_0251	rplF	50S ribosomal protein L6	49	0.061	24	E
FTL_0252	rplR	50S ribosomal protein L18	36	0.028	3	E
FTL_0253	rpsE	30S ribosomal protein S5	37	0.027	2	E
FTL_0254	rpmD	50S ribosomal protein L30	24	0	0	E

FTL_0255	rplO	50S ribosomal protein L15	37	0	0	E
FTL_0256	secY	preprotein translocase subunit SecY	134	0.037	23	E
FTL_0257	rpmJ	50S ribosomal protein L36	12	0.083	4	E
FTL_0258	rpsM	30S ribosomal protein S13	31	0	0	E
FTL_0259	-	30S ribosomal protein S11	36	0.056	8	E
FTL_0260	rpsD	30S ribosomal protein S4	58	0	0	E
FTL_0261	-	DNA-directed RNA polymerase subunit alpha	112	0.036	31	E
FTL_0262	rplQ	50S ribosomal protein L17	38	0.079	630	E
FTL_0263	isftu1	transposase	68	1	76849	N.E.
FTL_0264	-	-	83	1	76549	N.E.
FTL_0265	-	hypothetical protein	143	0.993	216646	N.E.
FTL_0266	isftu1	transposase	100	1	91969	N.E.
FTL_0267	htpG	heat shock protein 90	184	0.984	135595	N.E.
FTL_0268	isftu1	transposase	100	1	91696	N.E.
FTL_0269	gdh	glutamate dehydrogenase	115	0.939	21355	N.E.
FTL_0270	isftu2	transposase	84	1	62626	N.E.
FTL_0271	-	hypothetical protein	71	0.958	88246	N.E.
FTL_0272	-	diaminopimelate decarboxylase	134	0.993	160178	N.E.
FTL_0273	-	glutamate/gamma-aminobutyrate anti-porter	156	0.974	202262	N.E.
FTL_0274	-	-	23	1	28101	N.E.
FTL_0275	-	methylated-DNA--protein-cysteine methyltransferase	66	0.985	58300	N.E.
FTL_0276	-	hypothetical protein	85	0.953	87546	N.E.
FTL_0277	-	mercuric reductase protein	154	0.968	179664	N.E.
FTL_0278	-	hypothetical protein	70	0.971	75226	N.E.
FTL_0279	-	hypothetical protein	35	1	24147	N.E.
FTL_0280	-	amino acid permease	87	0.989	113880	N.E.
FTL_0281	-	heat shock protein, hsp40	72	1	82564	N.E.
FTL_0282	-	hypothetical protein	103	0.99	115603	N.E.
FTL_0283	-	aromatic amino acid HAAP transporter	146	0.979	165344	N.E.
FTL_0284	-	hypothetical protein	43	0.953	11526	N.E.
FTL_0285	-	GTP pyrophosphokinase	194	0.964	200039	N.E.
FTL_0286	-	hypothetical protein	60	1	76246	N.E.
FTL_0287	-	hypothetical protein	55	0.945	64303	N.E.
FTL_0288	-	hypothetical protein	91	1	97757	N.E.
FTL_0289	-	hypothetical protein	93	0.978	95018	N.E.
FTL_0290	xerC	integrase/recombinase XerC	95	0.968	9222	N.E.
FTL_0291	-	aromatic amino acid HAAP transporter	167	0.964	184135	N.E.
FTL_0292	-	-	114	0.956	120239	N.E.
FTL_0293	secB2	preprotein translocase subunit SecB	43	1	52582	N.E.
FTL_0294	mutS	DNA mismatch repair protein MutS	260	0.988	301871	N.E.
FTL_0295	-	acetyl-CoA carboxylase carboxyltransferase subunit alpha	79	0.114	1234	E
FTL_0296	-	hypothetical protein	43	0.907	51112	N.E.
FTL_0297	-	hypothetical protein	105	0.933	113197	N.E.
FTL_0298	-	hypothetical protein	201	0.975	234053	N.E.
FTL_0299	murQ	N-acetylmuramic acid 6-phosphate etherase	100	0.99	117604	N.E.
FTL_0300	-	hypothetical protein	41	0.976	60101	N.E.
FTL_0301	-	hypothetical protein	49	0.918	47913	N.E.
FTL_0302	isftu2	transposase	73	1	56839	N.E.
FTL_0303	-	hypothetical protein	62	0.968	57290	N.E.
FTL_0304	nhaP	Na+/H+ antiporter	155	0.974	167942	N.E.
FTL_0305	-	hypothetical protein	81	0.025	1241	E
FTL_0306	-	tryptophanyl-tRNA synthetase	97	0.052	27	E
FTL_0307	coaE	dephospho-CoA kinase	63	0.079	1305	E

FTL_0308	-	hypothetical protein	113	0.062	2562	E
FTL_0309	aceE	pyruvate dehydrogenase subunit E1	241	0.029	40	E
FTL_0310	-	dihydrolipoamide acetyltransferase	147	0.027	22	E
FTL_0311	-	dihydrolipoamide dehydrogenase	129	0.031	392	E
FTL_0312	-	transposase	11	1	8600	N.E.
FTL_0313	-	hypothetical protein	20	1	18706	N.E.
FTL_0314	isftu1	transposase	100	1	105870	N.E.
FTL_0315	-	MutT protein	78	0.974	78370	N.E.
FTL_0316	-	arsenate reductase	33	1	28382	N.E.
FTL_0317	-	hypothetical protein	23	1	25942	N.E.
FTL_0318	-	lipoprotein	18	1	30541	N.E.
FTL_0319	-	hypothetical protein	153	0.941	33917	N.E.
FTL_0320	-	aspartate aminotransferase	154	0.987	169455	N.E.
FTL_0321	-	-	33	1	44938	N.E.
FTL_0322	-	-	137	0.971	148501	N.E.
FTL_0323	-	-	97	0.979	122767	N.E.
FTL_0324	-	-	31	0.968	20774	N.E.
FTL_0325	-	OmpA family protein	143	0.671	76617	E and N.E.
FTL_0326	-	FKBP-type 16 kDa peptidyl-prolyl cis-transisomerase	37	0.162	66	E
FTL_0327	ispH	4-hydroxy-3-methylbut-2-enyl diphosphate reductase	93	0.065	4811	E
FTL_0328	-	chorismate mutase	34	0.971	23487	N.E.
FTL_0329	pssA	CDP-alcohol phosphatidyltransferase	99	0.121	3928	E
FTL_0330	-	hypothetical protein	13	1	16296	N.E.
FTL_0331	-	TolQ protein	75	0.04	12	E
FTL_0332	-	TolR protein	40	0.025	4	E
FTL_0333	-	hypothetical protein	83	0.048	58	E
FTL_0334	-	TolB protein precursor	160	0.062	1058	E
FTL_0335	-	lipoprotein	26	1	20103	N.E.
FTL_0336	-	peptidoglycan-associated lipoprotein	65	0.123	1345	E
FTL_0337	-	-	131	0.977	135141	N.E.
FTL_0338	-	N-acetyltransferase GCN5	42	1	36021	N.E.
FTL_0339	isftu1	transposase	97	1	105434	N.E.
FTL_0340	-	hypothetical protein	20	1	15193	N.E.
FTL_0341	-	deoxyribodipyrimidine photolyase	59	0.966	55638	N.E.
FTL_0342	-	deoxyribodipyrimidine photolyase	48	0.979	49255	N.E.
FTL_0343	-	hypothetical protein	156	0.987	170995	N.E.
FTL_0344	-	hypothetical protein	11	0.909	12614	N.E.
FTL_0345	-	bile acid symporter family protein	121	0.967	116808	N.E.
FTL_0346	-	hypothetical protein	60	1	54645	N.E.
FTL_0347	-	hypothetical protein	71	0.93	89676	N.E.
FTL_0348	-	-	50	1	41380	N.E.
FTL_0349	-	-	25	1	29728	N.E.
FTL_0350	-	-	68	1	61790	N.E.
FTL_0351	-	-	52	1	65278	N.E.
FTL_0352	-	hypothetical protein	53	0.962	55258	N.E.
FTL_0353	isftu1	transposase	100	1	91665	N.E.
FTL_0354	-	hypothetical protein	44	0.977	36314	N.E.
FTL_0355	ubiA	4-hydroxybenzoate polyprenyltransferase	120	0.117	8537	E
FTL_0356	ubiC	chorismate pyruvate lyase	66	0.455	2671	E and N.E.
FTL_0357	rph	ribonuclease PH	60	0.933	40984	N.E.
FTL_0358	-	hypothetical protein	31	0.968	8016	N.E.
FTL_0359	-	Type IV pili fiber building block protein	87	0.989	77712	N.E.

FTL_0360	-	heat shock protein HtpX	120	0.992	96284	N.E.
FTL_0361	-	LemA-like protein	56	0.982	52015	N.E.
FTL_0362	-	-	36	0.944	32793	N.E.
FTL_0363	-	-	60	0.967	53543	N.E.
FTL_0364	-	-	27	1	28893	N.E.
FTL_0365	-	-	70	0.957	76214	N.E.
FTL_0366	-	-	71	0.986	83342	N.E.
FTL_0367	isftu2	transposase	73	1	56468	N.E.
FTL_0368	-	-	111	0.991	113860	N.E.
FTL_0369	-	-	57	1	54619	N.E.
FTL_0370	-	arsenical restistance operon repressor	32	0.938	30336	N.E.
FTL_0371	-	hypothetical protein	77	0.961	79794	N.E.
FTL_0372	gpsA	NAD(P)H-dependent glycerol-3-phosphate dehydrogenase	98	0.929	9821	N.E.
FTL_0373	-	hypothetical protein	56	1	44782	N.E.
FTL_0374	-	DNA repair protein RadA	129	0.984	137131	N.E.
FTL_0375	-	hypothetical protein	71	0.972	70320	N.E.
FTL_0376	-	hypothetical protein	83	0.976	91785	N.E.
FTL_0377	-	chorismate synthase	91	0.11	2908	E
FTL_0378	-	hypothetical protein	83	0.952	80847	N.E.
FTL_0379	-	methionine sulfoxide reductase B	56	0.982	51280	N.E.
FTL_0380	-	superoxide dismuate (Cu-Zn) precusor	52	0.981	61398	N.E.
FTL_0381	-	hypothetical protein	83	1	81864	N.E.
FTL_0382	-	amino acid permease	158	0.962	133957	N.E.
FTL_0383	manA	mannose-6-phosphate isomerase, fragment	37	0.973	36811	N.E.
FTL_0384	-	-	33	1	52874	N.E.
FTL_0385	-	-	36	1	51681	N.E.
FTL_0386	-	-	27	0.963	34228	N.E.
FTL_0387	aspC1	aspartate aminotransferase	115	0.948	75895	N.E.
FTL_0388	-	cation transporter	105	0.952	114800	N.E.
FTL_0389	-	DNA repair protein recN	153	0.993	157072	N.E.
FTL_0390	-	Type IV pili fiber building block protein	119	0.992	160770	N.E.
FTL_0391	-	hypothetical protein	23	1	23355	N.E.
FTL_0392	-	Type IV pili fiber building block protein	11	0.727	4889	N.E.
FTL_0393	lpxE	lipid A 1-phosphatase	84	1	81231	N.E.
FTL_0394	folD	bifunctional 5,10-methylene-tetrahydrofolate dehydrogenase/ 5,10-methylene-tetrahydrofolate cyclohydrolase	78	0.064	3148	E
FTL_0395	purM	phosphoribosylaminoimidazole synthetase	91	0.978	38960	N.E.
FTL_0396	purCD	fusion protein PurC/PurD	196	0.969	98481	N.E.
FTL_0397	purN	phosphoribosylglycinamide formyltransferase	66	0.97	54583	N.E.
FTL_0398	purE	phosphoribosylaminoimidazole carboxylase,catalyic subunit	44	0.955	7261	N.E.
FTL_0399	purK	phosphoribosylaminoimidazole carboxylase ATPase subunit	94	0.074	351	E
FTL_0400	isftu2	transposase	76	1	60386	N.E.
FTL_0401	-	Sua5_yciO_yrdC family protein	50	0.98	48521	N.E.
FTL_0402	ispZ	intracellular septation protein A family protein	65	0.954	20480	N.E.
FTL_0403	-	hypothetical protein	37	0.919	35109	N.E.
FTL_0404	glk	glucose kinase	110	0.736	2216	E and N.E.
FTL_0405	ubiE	menaquinone biosynthesis methyltransferase	63	0.063	208	E
FTL_0406	-	hypothetical protein	66	0.015	2	E

FTL_0407	ubiB	2-polyprenylphenol 6-hydroxylase	157	0.089	5935	E
FTL_0408	hitA	histidine triad (HIT) family protein	34	1	27835	N.E.
FTL_0409	-	purine/pyrimidine phosphoribosyl transferase family protein	71	1	73208	N.E.
FTL_0410	-	hypothetical protein	99	0.242	6404	E
FTL_0411	-	hypothetical protein	91	0.989	63218	N.E.
FTL_0412	murB	UDP-N-acetylenolpyruvoylglucosamine reductase	98	0.102	379	E
FTL_0413	murA	UDP-N-acetylglucosamine 1-carboxyvinyltransferase	140	0.086	90	E
FTL_0414	engA	GTP-binding protein EngA	131	0.053	136	E
FTL_0415	-	hypothetical protein	53	0.887	70323	N.E.
FTL_0416	isftu2	transposase	73	1	56494	N.E.
FTL_0417	isftu1	transposase	94	1	87164	N.E.
FTL_0418	-	hypothetical protein	27	1	26229	N.E.
FTL_0419	-	oligopeptidase A	190	0.963	90936	N.E.
FTL_0420	-	hypothetical protein	38	0.079	805	E
FTL_0421	-	lipoprotein	47	0.957	36044	N.E.
FTL_0422	-	-	40	1	31612	N.E.
FTL_0423	-	hypothetical protein	50	1	38645	N.E.
FTL_0424	-	lipoprotein	49	1	36211	N.E.
FTL_0425	-	Type IV pili glycosylation protein	171	0.977	164672	N.E.
FTL_0426	-	DNA topoisomerase I	204	0.123	7256	E
FTL_0427	-	chmomosome partition protein A	58	0.966	48450	N.E.
FTL_0428	-	chromosome partition protein B	85	0.965	74407	N.E.
FTL_0429	-	glutamine amidotransferase	77	0.948	56725	N.E.
FTL_0430	-	hypothetical protein	86	0.965	54893	N.E.
FTL_0431	-	hypothetical protein	27	0.963	27867	N.E.
FTL_0432	-	hypothetical protein	21	0.952	22532	N.E.
FTL_0433	-	ribosomal large subunit methyltransferase J	57	0.965	21022	N.E.
FTL_0434	-	hypothetical protein	50	0.12	1472	E
FTL_0435	lspA	lipoprotein signal peptidase	54	0.167	2443	E
FTL_0436	ileS	isoleucyl-tRNA synthetase	240	0.054	455	E
FTL_0437	-	riboflavin biosynthesis protein RibF	99	0.091	2449	E
FTL_0438	-	malate dehydrogenase	186	0.629	3198	E and N.E.
FTL_0439	-	hypothetical protein	154	0.838	5945	E and N.E.
FTL_0440	isftu1	transposase	94	1	100275	N.E.
FTL_0441	isftu2	transposase	108	0.991	98982	N.E.
FTL_0442	-	hypothetical protein	67	1	75839	N.E.
FTL_0443	-	major facilitator transporter	150	0.973	189863	N.E.
FTL_0444	metG	methionyl-tRNA synthetase	195	0.113	4884	E
FTL_0445	-	hypothetical protein	60	0.95	61229	N.E.
FTL_0446	-	hypothetical protein	21	0.905	22822	N.E.
FTL_0447	-	hypothetical protein	134	0.963	105591	N.E.
FTL_0448	-	hypothetical protein	84	0.988	77413	N.E.
FTL_0449	pigR	pathogenicity island gene regulator	23	0.957	2788	N.E.
FTL_0450	psd	phosphatidylserine decarboxylase	97	0.062	51	E
FTL_0451	-	hypothetical protein	103	0.563	11472	E and N.E.
FTL_0452	-	bifunctional nicotinamide mononucleotide adenylyltransferase/ADP-ribose pyrophosphatase	114	0.281	3198	E and N.E.

FTL_0453	-	UDP-N-acetylglucosamine pyrophosphorylase/glucosamine-1-phosphate N-acetyltransferase	117	0.009	4	E
FTL_0454	-	glucosamine--fructose-6-phosphate aminotransferase	193	0.031	335	E
FTL_0455	-	acetyltransferase	55	0.945	59195	N.E.
FTL_0456	rpsU	30S ribosomal protein S21	16	1	14866	N.E.
FTL_0457	-	cold shock protein	17	0.941	13516	N.E.
FTL_0458	-	hypothetical protein	36	0.972	34280	N.E.
FTL_0459	-	methionine aminopeptidase	68	0.044	135	E
FTL_0460	-	hypothetical protein	87	0.011	390	E
FTL_0461	-	hypothetical protein	70	0.957	62424	N.E.
FTL_0462	-	DNA topoisomerase IV subunit A	233	0.957	72402	N.E.
FTL_0463	-	5'-methylthioadenosine/S-adenosylhomocysteine nucleosidase	65	0.077	134	E
FTL_0464	-	hypothetical protein	101	0.901	66488	N.E.
FTL_0465	-	BNR/Asp-box repeat-containing protein	129	0.977	112543	N.E.
FTL_0466	-	soluble lytic murein transglycosylase	231	0.19	1666	E
FTL_0467	-	hypothetical protein	25	1	34972	N.E.
FTL_0468	isftu2	transposase	79	1	67946	N.E.
FTL_0469	-	hypothetical protein	53	0.981	58726	N.E.
FTL_0470	-	hypothetical protein	58	0.966	41799	N.E.
FTL_0471	-	hypothetical protein	43	0.953	33681	N.E.
FTL_0472	-	DNA polymerase III subunit alpha	324	0.025	2979	E
FTL_0473	-	peptide deformylase	70	0.929	62107	N.E.
FTL_0474	-	lipoprotein releasing system, subunit C,putative membrane protein	145	0.014	6	E
FTL_0475	-	lipoprotein releasing system, subunit D, ABC transporter ATP-binding protein	68	0.103	2277	E
FTL_0476	-	lysine decarboxylase, inducable	215	0.949	202847	N.E.
FTL_0477	gcvT	glycine cleavage system aminomethyltransferase T	93	0.989	30303	N.E.
FTL_0478	-	glycine cleavage system H protein	27	0.963	9029	N.E.
FTL_0479	-	glycine dehydrogenase subunit 1	142	0.965	54877	N.E.
FTL_0480	-	glycine dehydrogenase subunit 2	139	0.971	52768	N.E.
FTL_0481	-	shikimate 5-dehydrogenase	91	0.989	73095	N.E.
FTL_0482	-	pullulonase	321	0.981	310975	N.E.
FTL_0483	glgB	glycogen branching protein	187	0.979	72914	N.E.
FTL_0484	pgm	phosphoglucomutase	146	0.062	2997	E
FTL_0485	glgC	glucose-1-phosphate adenylyltransferase	126	0.984	160000	N.E.
FTL_0486	glgA	glycogen synthase	146	0.959	34228	N.E.
FTL_0487	-	maltodextrin phosphorylase	268	0.951	205528	N.E.
FTL_0488	-	4-alpha-glucanotransferase	149	0.98	116367	N.E.
FTL_0489	glyQ	glycyl-tRNA synthetase subunit alpha	78	0.038	294	E
FTL_0490	-	UDP-N-acetylmuramoylalanyl-D-glutamate--2,6-diaminopimelate ligase	175	0.063	3975	E
FTL_0491	-	outer membrane lipoprotein	49	0.959	38137	N.E.
FTL_0492	-	UDP-N--acetylmuramoylalanyl-D-glutamyl-2,6- diaminopimelate-D-alanyl-D-alanyl ligase	133	0.06	795	E
FTL_0493	-	hypothetical protein	84	0.988	101977	N.E.
FTL_0494	-	aspartate-semialdehyde dehydrogenase	107	0.981	113520	N.E.
FTL_0495	-	-	91	0.978	98741	N.E.
FTL_0496	-	-	9	1	14232	N.E.
FTL_0497	-	-	37	0.973	37913	N.E.
FTL_0498	-	threonine synthase	130	0.992	139307	N.E.

FTL_0499	-	S-adenosylmethionine decarboxylase	48	0.917	49632	N.E.
FTL_0500	-	spermidine synthase	91	0.934	86640	N.E.
FTL_0501	-	putative arginine decarboxylase	149	0.933	152951	N.E.
FTL_0502	-	hypothetical protein	86	0.977	80337	N.E.
FTL_0503	isftu1	transposase	100	1	92264	N.E.
FTL_0504	-	beta-alanine synthase or beta-ureidopropionase	16	0.812	17079	N.E.
FTL_0505	-	carbon-nitrogen hydrolase family protein	32	1	32582	N.E.
FTL_0506	lpxH	UDP-2,3-diacylglucosamine hydrolase	72	0.056	3324	E
FTL_0507	pyrE	orotate phosphoribosyltransferase	66	0.197	869	E
FTL_0508	mpl	UDP-N-acetylmuramate--L-alanyl-gamma-D-glutamyl-meso-diaminopimelate ligase	145	0.793	6106	E and N.E.
FTL_0509	yjfH	tRNA/rRNA methyltransferase	64	0.953	51505	N.E.
FTL_0510	isftu1	transposase	100	1	92086	N.E.
FTL_0511	-	hypothetical protein	74	0.946	86238	N.E.
FTL_0512	-	BolA-like protein	31	1	24443	N.E.
FTL_0513	-	hypothetical protein	40	0.875	26058	N.E.
FTL_0514	-	hypothetical protein	66	0.955	49090	N.E.
FTL_0515	-	ABC transporter substrate-binding protein	60	0.95	71939	N.E.
FTL_0516	-	ABC transporter membrane protein	91	0.978	99564	N.E.
FTL_0517	-	ABC transporter ATP-binding protein	87	0.977	81148	N.E.
FTL_0518	minE	cell division topological specificity factor MinE	27	0.296	3268	E and N.E.
FTL_0519	minD	septum site-determining protein MinD	73	0.918	4788	N.E.
FTL_0520	minC	septum site-determining protein MinC	68	0.926	4643	N.E.
FTL_0521	rpmG	50S ribosomal protein L33	16	0.938	638	N.E.
FTL_0522	rpmB	50S ribosomal protein L28	22	0.136	32	E
FTL_0523	-	hypothetical protein	29	0.759	21933	N.E.
FTL_0524	-	ATP-dependent DNA helicase RecG	200	0.915	120124	N.E.
FTL_0525	-	fumerate hydratase	123	0.309	2954	E
FTL_0526	isftu1	transposase	68	0.985	86447	N.E.
FTL_0527	-	endonuclease	34	1	33673	N.E.
FTL_0528	-	Type III restriction enzyme	312	0.981	281871	N.E.
FTL_0529	-	uracil-DNA glycosylase	57	1	55129	N.E.
FTL_0530	-	hypothetical protein	31	1	25209	N.E.
FTL_0531	-	hypothetical protein	30	1	28080	N.E.
FTL_0532	-	hypothetical protein	52	1	58486	N.E.
FTL_0533	-	DNA gyrase subunit A	255	0.012	20	E
FTL_0534	-	1-deoxy-D-xylulose 5-phosphate reductoisomerase	109	0.046	117	E
FTL_0535	-	outer membrane protein	269	0.007	315	E
FTL_0536	-	outer membrane protein OmpH	42	0.024	2	E
FTL_0537	lpxD	UDP-3-O-[3-hydroxymyristoyl] glucosamine N-acyltransferase	113	0	0	E
FTL_0538	fabZ	(3R)-hydroxymyristoyl-ACP dehydratase	36	0.056	43	E
FTL_0539	-	UDP-N-acetylglucosamine acyltransferase	73	0	0	E
FTL_0540	lpxB	lipid-A-disaccharide synthase	133	0.038	855	E
FTL_0541	-	hypothetical protein	71	0.972	16173	N.E.
FTL_0542	-	hypothetical protein	47	0.957	62029	N.E.
FTL_0543	-	-	121	0.975	134289	N.E.
FTL_0544	ppk	polyphosphate kinase 2	81	0.926	106895	N.E.
FTL_0545	pcs	phosphatidylcholine synthase	103	0.971	73471	N.E.
FTL_0546	ispA	geranyltranstransferase	103	0.961	39290	N.E.
FTL_0547	kdtA	3-deoxy-D-manno-octulosonic-acid transferase	138	0.014	31	E

FTL_0548	rdgB	putative deoxyribonucleotide triphosphate pyrophosphatase	56	0.982	45395	N.E.
FTL_0549	proC	pyrroline-5-carboxylate reductase	100	0.94	86244	N.E.
FTL_0550	-	-	12	1	8904	N.E.
FTL_0551	-	-	90	0.978	87751	N.E.
FTL_0552	pmrA	two-component response regulator	80	0.013	2	E
FTL_0553	lepB	signal peptidase I	78	0.064	296	E
FTL_0554	rnc	ribonuclease III	58	0.931	2620	N.E.
FTL_0555	truB	tRNA pseudouridine synthase B	106	0.972	69231	N.E.
FTL_0556	rnr	ribonuclease R	235	0.983	170931	N.E.
FTL_0557	-	Delta 9 acyl-lipid fatty acid desaturase	71	0.958	69877	N.E.
FTL_0558	-	oxidoreductase	79	0.975	62677	N.E.
FTL_0559	-	hypothetical protein	58	0.966	54425	N.E.
FTL_0560	-	hypothetical protein	50	1	53383	N.E.
FTL_0561	-	cyclopropane-fatty-acyl-phospholipid synthase	99	0.96	100615	N.E.
FTL_0562	-	-	55	0.982	57624	N.E.
FTL_0563	-	-	109	0.954	115128	N.E.
FTL_0564	-	-	74	0.946	54290	N.E.
FTL_0565	-	-	41	0.976	47510	N.E.
FTL_0566	-	-	38	1	34744	N.E.
FTL_0567	-	-	16	0.938	18061	N.E.
FTL_0568	isftu2	transposase	81	1	69040	N.E.
FTL_0569	-	hypothetical protein	45	0.978	43569	N.E.
FTL_0570	-	hypothetical protein	48	1	38500	N.E.
FTL_0571	-	hypothetical protein	62	0.984	76514	N.E.
FTL_0572	-	hypothetical protein	138	0.957	156886	N.E.
FTL_0573	-	hypothetical protein	113	0.973	103083	N.E.
FTL_0574	-	hypothetical protein	147	0.966	133180	N.E.
FTL_0575	isftu2	transposase	77	1	63974	N.E.
FTL_0576	-	hypothetical protein	59	0.983	54947	N.E.
FTL_0577	-	hypothetical protein	21	1	20749	N.E.
FTL_0578	-	ornithine cyclodeaminase	80	0.988	76379	N.E.
FTL_0579	-	putative nicotinate phosphoribosyltransferase	151	0.974	154293	N.E.
FTL_0580	-	hypothetical protein	24	1	18132	N.E.
FTL_0581	-	sugar transport protein	151	0.96	128016	N.E.
FTL_0582	-	hypothetical protein	52	1	56995	N.E.
FTL_0583	-	acetyl-CoA acetyltransferase	104	1	77931	N.E.
FTL_0584	-	bifunctional 3-hydroxacyl-CoA dehydrogenase/acyl-CoA-binding protein	246	0.959	211206	N.E.
FTL_0585	fadE	acyl-CoA dehydrogenase	202	0.97	211023	N.E.
FTL_0586	-	long chain fatty acid CoA ligase	173	0.971	171558	N.E.
FTL_0587	-	arsenate reductase	38	0.947	27734	N.E.
FTL_0588	-	isocitrate dehydrogenase	201	0.035	546	E
FTL_0589	-	hypothetical protein	108	0.981	69493	N.E.
FTL_0590	-	ATp-dependent helicase	421	0.962	362920	N.E.
FTL_0591	isftu2	transposase	76	1	58410	N.E.
FTL_0592	wbtA	dTDP-glucose 4,6-dehydratase	167	0.97	66344	N.E.
FTL_0593	wbtB	galactosyl transferase	64	0.109	673	E
FTL_0594	wbtC	UDP-glucose 4-epimerase	93	0.946	29609	N.E.
FTL_0595	-	galacturonosyl transferase	127	0.173	684	E
FTL_0596	-	UDP-glucose/GDP-mannose dehydrogenase	133	0.038	26	E
FTL_0597	wbtF	NAD dependent epimerase	114	0.833	4475	N.E.
FTL_0598	wzy	membrane protein/O-antigen protein	164	0.927	32582	N.E.
FTL_0599	wbtG	glycosyl transferase family protein	141	0.05	68	E

FTL_0600	wbtH	asparagine synthase	219	0.023	13	E
FTL_0601	wbtI	sugar transamine/perosamine synthetase	129	0.031	19	E
FTL_0602	wbtJ	hypothetical protein	74	0.054	475	E
FTL_0603	wzx	O-antigen flippase	205	0.02	17	E
FTL_0604	wbtK	glycosyltransferase	93	0.075	605	E
FTL_0605	wbtL	glucose-1-phosphate thymidylyltransferase	82	0.098	2000	E
FTL_0606	wbtM	dTDP-D-glucose 4,6-dehydratase	112	0.982	26025	N.E.
FTL_0607	isftu1	transposase	100	1	106812	N.E.
FTL_0608	manC	mannose-1-phosphate guanyltransferase	140	0.279	10863	E and N.E.
FTL_0609	manB	phosphomannomutase	158	0.222	145	E
FTL_0610	rho	transcription termination factor Rho	97	0.031	379	E
FTL_0611	trx1	thioredoxin	27	0.889	3069	N.E.
FTL_0612	ppx	exopolyphosphatase	74	0.986	22122	N.E.
FTL_0613	isftu2	transposase	85	1	65973	N.E.
FTL_0614	-	-	31	0.968	26966	N.E.
FTL_0615	-	recombination factor protein RarA	88	0.932	87658	N.E.
FTL_0616	rpoA2	DNA-directed RNA polymerase subunit alpha	96	0.281	3837	E and N.E.
FTL_0617	-	hypothetical protein	44	0.909	26139	N.E.
FTL_0618	-	-	49	0.918	45614	N.E.
FTL_0619	-	-	114	0.974	124304	N.E.
FTL_0620	tatD	deoxyribonuclease	80	0.975	67361	N.E.
FTL_0621	-	-	109	0.982	90491	N.E.
FTL_0622	isftu2	transposase	79	1	65063	N.E.
FTL_0623	-	ABC transporter ATP-binding protein	89	0.955	46938	N.E.
FTL_0624	-	ABC transporter membrane protein	102	0.98	55677	N.E.
FTL_0625	gtrB	glycosyl transferase family protein	101	0.95	85000	N.E.
FTL_0626	ppnK	inorganic phosphate/ATP-NAD kinase	90	0.022	21	E
FTL_0627	rhtB	threonine efflux protein	80	0.938	61123	N.E.
FTL_0628	-	-	64	1	43267	N.E.
FTL_0629	-	-	76	0.987	51539	N.E.
FTL_0630	-	-	27	0.963	29249	N.E.
FTL_0631	isftu1	transposase	100	1	91921	N.E.
FTL_0632	-	ArsR family transcriptional regulator	28	0.964	24017	N.E.
FTL_0633	-	hypothetical protein	48	0.979	52171	N.E.
FTL_0634	-	NADH oxidase	8	1	8903	N.E.
FTL_0635	-	FAD-dependent pyridine nucleotide-disulfide oxidoreductase	62	0.952	65192	N.E.
FTL_0636	-	NADH oxidase	86	0.988	88486	N.E.
FTL_0637	-	hypothetical protein	75	0.947	89082	N.E.
FTL_0638	-	hypothetical protein	77	0.987	74735	N.E.
FTL_0639	-	oxidoreductase	62	0.984	52924	N.E.
FTL_0640	-	hypothetical protein	38	1	42669	N.E.
FTL_0641	-	hypothetical protein	37	0.946	28507	N.E.
FTL_0642	-	lipoprotein	50	0.98	51585	N.E.
FTL_0643	-	N utilisation substance protein B	48	0.729	1372	N.E.
FTL_0644	-	carbon-nitrogen hydrolase	81	0.975	65762	N.E.
FTL_0645	-	lipoprotein	55	0.964	37313	N.E.
FTL_0646	-	hypothetical protein	94	0.957	74726	N.E.
FTL_0647	-	hypothetical protein	63	0.937	48989	N.E.
FTL_0648	-	aminotransferase	59	0.983	67440	N.E.
FTL_0649	-	aspartate/tyrosine/aromatic aminotransferase family protein	52	0.962	48312	N.E.
FTL_0650	-	prolyl-tRNA synthetase	164	0	0	E
FTL_0651	-	transposase	45	0.956	37728	N.E.

FTL_0652	-	hypothetical protein	66	0.985	56850	N.E.
FTL_0653	-	hypothetical protein	46	0.022	7	E
FTL_0654	-	uroporphyrinogen III synthase	80	0.037	142	E
FTL_0655	-	hypothetical protein	117	0.957	61438	N.E.
FTL_0656	-	hypothetical protein	136	0.949	55672	N.E.
FTL_0657	-	hydroxyacylglutathione hydrolase	84	0.94	67233	N.E.
FTL_0659	-	cell division protein	62	0.177	5507	E
FTL_0660	feoA	ferrous iron transport protein A	19	0.947	6286	N.E.
FTL_0661	-	hypothetical protein	200	0.97	155078	N.E.
FTL_0662	-	prophage repressor protein	76	0.974	62234	N.E.
FTL_0663	-	hypothetical protein	48	0.958	32611	N.E.
FTL_0664	-	hypothetical protein	119	0.958	93346	N.E.
FTL_0665	gltB	hypothetical protein (glutamate synthase domain-containing 2)	138	0.971	122040	N.E.
FTL_0666	recC	exodeoxyribonuclease V subunit gamma	349	0.662	5554	E and N.E.
FTL_0667	-	hypothetical protein	64	0.953	52976	N.E.
FTL_0668	-	ATP-dependent DNA helicase	161	0.845	69231	N.E.
FTL_0669	recB	exodeoxyribonuclease V subunit beta	376	0.54	4149	E and N.E.
FTL_0670	recD	exodeoxyribonuclease V subunit alpha	205	0.756	58672	E and N.E.
FTL_0671	-	pantothenate kinase	81	0.025	1219	E
FTL_0672	panD	aspartate alpha-decarboxylase	27	0.259	175	E
FTL_0673	panC	pantoate-beta-alanine ligase	89	0.045	26	E
FTL_0674	panB	3-methyl-2-oxobutanoate hydroxymethyltransferase	81	0.173	815	E
FTL_0675	panG	hypothetical protein, putative ketopantoate reductase	69	0.246	2260	E
FTL_0676	-	DNA ligase	186	0.022	336	E
FTL_0677	-	hypothetical protein	47	1	38860	N.E.
FTL_0678	isftu1	transposase	100	1	92381	N.E.
FTL_0679	potI	ATP-binding cassette putrescine uptake system, membrane protein, subunit I	106	0.377	482	E
FTL_0680	potH	ATP-binding cassette putrescine uptake system, membrane protein, subunit H	111	0.423	552	E
FTL_0681	potG	ATP-binding cassette putrescine uptake system, ATP-binding protein	95	0.432	383	E
FTL_0682	isftu1	transposase	100	1	92178	N.E.
FTL_0683	-	-	36	0.972	37462	N.E.
FTL_0684	-	hypothetical protein	48	0.979	43623	N.E.
FTL_0685	-	NH(3)-dependent NAD(+) synthetase	71	0.028	74	E
FTL_0686	-	outer membrane efflux protein	155	0.974	74484	N.E.
FTL_0687	-	HlyD family secretion protein	108	0.972	81952	N.E.
FTL_0688	-	major facilitator transporter	164	0.957	117085	N.E.
FTL_0689	-	transcriptional regulator araC family protein	68	0.971	58678	N.E.
FTL_0690	-	Acyl-CoA synthetase (long-chain-fatty-acid--CoA ligase)	177	0.944	78544	N.E.
FTL_0691	-	proton-dependent oligopeptide transport (POT) family protein	178	0.983	125868	N.E.
FTL_0692	-	16S ribosomal RNA methyltransferase RsmE	87	0.908	67726	N.E.
FTL_0693	-	hypothetical protein	71	0.972	48748	N.E.
FTL_0694	-	hypothetical protein	83	0.988	68084	N.E.
FTL_0695	-	cell entry (mce) related family protein	85	0.976	67828	N.E.
FTL_0696	-	ABC transporter ATP-binding protein	75	0.947	64552	N.E.
FTL_0697	-	ABC transporter membrane protein	130	0.969	93634	N.E.

FTL_0698	-	hypothetical protein	91	0.945	70694	N.E.
FTL_0699	-	ribosomal large subunit pseudouridine synthase D	100	0.99	42612	N.E.
FTL_0700	-	lipoprotein	98	0.102	2773	E
FTL_0701	mreA	FAD binding family protein	165	0.988	161830	N.E.
FTL_0702	priM	hypothetical protein	168	0.994	157957	N.E.
FTL_0703	glyA	serine hydroxymethyltransferase	118	0.059	952	E
FTL_0704	-	hypothetical protein	66	0.939	35180	N.E.
FTL_0705	-	hypothetical protein	173	0.925	111662	N.E.
FTL_0706	wyz	predicted O-antigen ligase	187	0.941	42531	N.E.
FTL_0707	-	glycosyl transferase family protein	124	0.96	29675	N.E.
FTL_0708	-	hypothetical protein	117	0.897	18249	N.E.
FTL_0709	-	glycosyl transferases group 1 family protein	113	0.08	2342	E
FTL_0710	-	choloylglycine hydrolase family protein	113	0.991	95044	N.E.
FTL_0711	-	proton-dependent oligopeptide transport (POT) family protein	71	0.93	64778	N.E.
FTL_0712	-	hypothetical protein	52	0.942	51040	N.E.
FTL_0713	-	PP-loop family protein	132	0.03	172	E
FTL_0714	-	D-3-phosphoglycerate dehydrogenase	122	0	0	E
FTL_0715	thyA	thymidylate synthase	66	0	0	E
FTL_0716	-	prolipoprotein diacylglyceryl transferase	80	0.037	204	E
FTL_0717	-	ribonuclease E	227	0.026	23	E
FTL_0718	-	cysteine desulfarase	109	0	0	E
FTL_0719	-	hypothetical protein	35	0.029	22	E
FTL_0720	-	DNA repair protein recO	89	0.955	13622	N.E.
FTL_0721	-	DedA family protein	70	0.971	59538	N.E.
FTL_0722	-	DedA family protein	81	0.802	2216	E and N.E.
FTL_0723	-	hypothetical protein	30	0.767	914	N.E.
FTL_0724	-	5-formyltetrahydrofolate cyclo-ligase	80	0.925	35589	N.E.
FTL_0725	-	hypothetical protein	39	0.744	5809	N.E.
FTL_0726	-	2-octaprenyl-6-methoxyphenyl hydroxylase	103	0.019	4	E
FTL_0727	-	monooxygenase family protein	122	0.049	240	E
FTL_0728	-	hypothetical protein	44	0.909	24287	N.E.
FTL_0729	queA	S-adenosylmethionine--tRNA ribosyltransferase-isomerase	95	0.958	79137	N.E.
FTL_0730	-	haloacid dehalogenase-like hydrolase family protein	81	0.988	68299	N.E.
FTL_0731	-	YhhQ family protein	88	0.92	43223	N.E.
FTL_0732	-	lactoylglutathione lyase	42	0.976	39114	N.E.
FTL_0733	isftu1	transposase	97	1	104725	N.E.
FTL_0734	-	-	180	0.944	152857	N.E.
FTL_0735	-	-	30	1	33473	N.E.
FTL_0736	-	ribose-5-phosphate isomerase A	61	0.082	138	E
FTL_0737	-	hypothetical protein	189	0.042	56	E
FTL_0738	-	hypothetical protein	50	0.68	6582	E and N.E.
FTL_0739	-	tRNA uridine 5-carboxymethylaminomethyl modification protein GidA	190	0.021	316	E
FTL_0740	-	hypothetical protein	129	0.969	140714	N.E.
FTL_0741	-	hypothetical protein	121	0.967	147178	N.E.
FTL_0742	-	LysR family transcriptional regulator	53	0.943	47884	N.E.
FTL_0743	-	oxidoreductase, short-chain dehydrogenase family protein	58	1	54846	N.E.
FTL_0744	-	exodeoxyribonuclease I	146	0.925	100897	N.E.
FTL_0745	-	excinuclease ABC subunit B	184	0.951	161953	N.E.

FTL_0746	-	hypothetical protein	81	0.086	645	E
FTL_0747	-	glutamate racemase	94	0.021	697	E
FTL_0748	-	major facilitator transporter	136	0.963	100261	N.E.
FTL_0749	isftu2	transposase	77	0.987	57733	N.E.
FTL_0750	-	-	118	0.975	104778	N.E.
FTL_0751	-	lipoprotein	100	0.94	84188	N.E.
FTL_0752	-	hypothetical protein	189	0.937	172051	N.E.
FTL_0753	-	aminoacylase	91	0.967	89573	N.E.
FTL_0754	xseA	exodeoxyribonuclease VII large subunit	168	0.952	119071	N.E.
FTL_0755	-	hypothetical protein	13	1	5746	N.E.
FTL_0756	-	-	54	0.907	39442	N.E.
FTL_0757	-	-	51	1	43731	N.E.
FTL_0758	-	-	30	0.967	25724	N.E.
FTL_0759	-	hypothetical protein	83	0.928	72980	N.E.
FTL_0760	-	C32 tRNA thiolase	77	0.961	67699	N.E.
FTL_0761	smpB	SsrA-binding protein	44	0.159	4857	E
FTL_0762	-	hypothetical protein	35	0.086	309	E
FTL_0763	-	hypothetical protein	38	1	12843	N.E.
FTL_0764	-	lipoprotein	146	0.945	88131	N.E.
FTL_0765	-	VacJ lipoprotein	97	0.979	80744	N.E.
FTL_0766	ggt	gamma-glutamyltranspeptidase	193	0.974	174027	N.E.
FTL_0767	-	hypothetical protein	84	1	69551	N.E.
FTL_0768	-	GTP binding translational elongation factor Tu and G family protein	147	0.959	102828	N.E.
FTL_0769	-	hypothetical protein	135	0.97	106765	N.E.
FTL_0770	-	-	14	0.929	9636	N.E.
FTL_0771	-	-	56	0.982	53320	N.E.
FTL_0772	-	-	27	1	25375	N.E.
FTL_0773	-	-	23	1	26524	N.E.
FTL_0774	-	-	20	1	17994	N.E.
FTL_0775	-	-	33	0.97	35571	N.E.
FTL_0776	-	hypothetical protein	112	0.946	73186	N.E.
FTL_0777	-	hypothetical protein	19	1	12280	N.E.
FTL_0778	-	-	42	0.929	35370	N.E.
FTL_0779	-	-	79	1	67465	N.E.
FTL_0780	-	cold shock protein (DNA-binding)	52	0.981	44186	N.E.
FTL_0781	-	-	88	0.932	76933	N.E.
FTL_0782	-	-	30	0.967	25340	N.E.
FTL_0783	isftu1	transposase	100	1	91470	N.E.
FTL_0784	-	lipoprotein	183	0.962	153958	N.E.
FTL_0785	-	GTP-binding protein	77	0.091	4465	E
FTL_0786	-	N-acetylglucosamine-6-phosphate deacetylase	106	0.34	8709	E and N.E.
FTL_0787	-	glycoprotease family protein	67	0.075	1022	E
FTL_0788	-	glutamine amidotransferases class-II family protein	70	0.957	54974	N.E.
FTL_0789	-	aspartate aminotransferase	118	0.695	4588	E and N.E.
FTL_0790	era	GTP-binding protein Era	98	0.051	5691	E
FTL_0791	-	hypothetical protein	33	0.909	27247	N.E.
FTL_0792	-	-	103	0.951	97171	N.E.
FTL_0793	-	-	74	0.959	71131	N.E.
FTL_0794	-	-	85	0.953	67993	N.E.
FTL_0795	adk	adenylate kinase	66	0.061	1377	E
FTL_0796	-	hypothetical protein	111	0.964	83259	N.E.
FTL_0797	-	Type IV pili associated protein	60	0.917	49197	N.E.

FTL_0798	-	Type IV pili glycosylation protein	68	0.956	51099	N.E.
FTL_0799	-	Type IV pili lipoprotein	59	0.898	33780	N.E.
FTL_0800	-	Type IV pilin multimeric outer membrane protein	178	0.978	175022	N.E.
FTL_0801	aroK	shikimate kinase I	46	0.022	5	E
FTL_0802	aroB	3-dehydroquinate synthase	112	0.161	2689	E
FTL_0803	-	hypothetical protein	32	0.938	5308	N.E.
FTL_0804	-	hypothetical protein	34	0.118	1093	E
FTL_0805	-	bifunctional proline dehydrogenase/pyrroline-5-carboxylate dehydrogenase	411	0.968	209136	N.E.
FTL_0806	-	amino acid transporter family protein	170	0.965	65138	N.E.
FTL_0807	-	major facilitator transporter	158	0.032	732	E
FTL_0808	-	bifunctional 4'-phosphopantothenoylcysteine decarboxylase,phosphopantothenoylcysteine synthetase	149	0.047	2582	E
FTL_0809	-	-	91	0.956	60140	N.E.
FTL_0810	-	cation transport regulator	26	1	21797	N.E.
FTL_0811	-	-	17	1	13703	N.E.
FTL_0812	-	-	21	1	16323	N.E.
FTL_0813	-	-	55	0.964	62265	N.E.
FTL_0814	-	hypothetical protein	47	0.936	33433	N.E.
FTL_0815	-	PRC-barrel protein	25	0.96	24649	N.E.
FTL_0816	-	hypothetical protein	25	0.96	25186	N.E.
FTL_0817	-	-	41	0.951	31475	N.E.
FTL_0818	-	-	37	0.973	27300	N.E.
FTL_0819	-	-	54	0.944	39117	N.E.
FTL_0820	isftu2	transposase	77	1	60709	N.E.
FTL_0821	hemH	ferrochelatase	124	0.048	2280	E
FTL_0822	-	hypothetical protein	21	0.952	19392	N.E.
FTL_0823	-	hypothetical protein	49	0.918	27315	N.E.
FTL_0824	-	-	49	0.959	35310	N.E.
FTL_0825	-	-	37	0.946	39620	N.E.
FTL_0826	-	-	25	1	20695	N.E.
FTL_0827	-	Type IV pili polytopic inner membrane protein	122	0.975	97836	N.E.
FTL_0828	-	Type IV pili nucleotide binding protein, ABC transporter ATP-binding protein	168	0.97	142660	N.E.
FTL_0829	-	glycerophosphoryl diester phosphodiesterase	70	0.943	38519	N.E.
FTL_0830	-	molybdopterin binding family protein, fragment	71	0.93	65940	N.E.
FTL_0831	-	cyanophycin synthetase	281	0.982	177992	N.E.
FTL_0832	-	Mur ligase family protein	164	0.848	5438	N.E.
FTL_0833	ispF	2-C-methyl-D-erythritol 2,4-cyclodiphosphate synthase	48	0.062	3469	E
FTL_0834	-	rhodanese-like family protein	70	0.471	1736	E and N.E.
FTL_0835	-	aromatic amino acid HAAP transporter	107	0.981	82392	N.E.
FTL_0836	-	hypothetical protein	35	0.971	40051	N.E.
FTL_0837	metIQ	D-methionine binding transport protein, ABC transporter, membrane and periplasmic protein	164	0.939	26534	N.E.
FTL_0838	metN	D-methionine transport protein, ABC transporter,ATP-binding subunit	97	0.938	14232	N.E.
FTL_0839	-	hypothetical protein	70	0.029	5	E

FTL_0840	-	hypothetical protein	40	0.975	35537	N.E.
FTL_0841	-	lipoprotein	40	0.975	39314	N.E.
FTL_0842	-	transposase	27	1	17414	N.E.
FTL_0843	tgt	queuine tRNA-ribosyltransferase	93	0.978	64819	N.E.
FTL_0844	-	LysR transcriptional regulator family protein	65	0.954	51577	N.E.
FTL_0845	-	hypothetical protein	107	0.972	85667	N.E.
FTL_0846	-	isochorismatase hydrolase family protein	59	1	55870	N.E.
FTL_0847	yajC	preprotein translocase family protein	33	0.576	482	E and N.E.
FTL_0848	secD	preprotein translocase subunit SecD	205	0.834	8855	N.E.
FTL_0849	secF	preprotein translocase subunit SecF	108	0.88	8554	N.E.
FTL_0850	-	hypothetical protein	61	0.148	521	E
FTL_0851	-	RNA polymerase factor sigma-32	79	0.025	7	E
FTL_0852	-	3-phosphoshikimate 1-carboxyvinyltransferase	131	0.038	691	E
FTL_0853	-	hypothetical protein	67	0.925	34582	N.E.
FTL_0854	-	ribonuclease H	40	0.975	22223	N.E.
FTL_0855	-	L-asparaginase	108	0.963	79790	N.E.
FTL_0856	-	carbonic anhydrase	60	0.05	1839	E
FTL_0857	-	hypothetical protein	95	0.979	73020	N.E.
FTL_0858	-	hypothetical protein	100	0.97	74134	N.E.
FTL_0859	-	rubredoxin	18	0.389	1195	E and N.E.
FTL_0860	-	hypothetical protein	73	0.973	50256	N.E.
FTL_0861	isftu2	transposase	78	0.987	58679	N.E.
FTL_0862	-	hypothetical protein	155	0.974	112709	N.E.
FTL_0863	-	Sodium-dicarboxylate symporter family protein	167	0.048	1320	E
FTL_0864	-	SIS domain-containing protein	92	0.957	85559	N.E.
FTL_0865	-	major facilitator transporter	157	0.962	145977	N.E.
FTL_0866	-	IS1 transposase	31	0.935	19937	N.E.
FTL_0867	-	hypothetical protein	166	0.976	128137	N.E.
FTL_0868	isftu2	transposase	77	0.987	62077	N.E.
FTL_0869	-	hypothetical protein	28	0.929	19929	N.E.
FTL_0870	-	hypothetical protein	21	1	14831	N.E.
FTL_0871	-	Na+/H+ antiporter	36	1	34761	N.E.
FTL_0872	-	hypothetical protein	59	0.949	65556	N.E.
FTL_0873	-	-	28	0.929	27139	N.E.
FTL_0874	-	-	28	0.929	22168	N.E.
FTL_0875	ispG	4-hydroxy-3-methylbut-2-en-1-yl diphosphate synthase	112	0.045	690	E
FTL_0876	-	hypothetical protein	71	0.944	49054	N.E.
FTL_0877	-	peptidase, M24 family protein	178	0.938	13413	N.E.
FTL_0878	-	DNA/RNA endonuclease family protein, DNA/RNA endonuclease G	111	0.973	81235	N.E.
FTL_0879	-	beta-lactamase	115	0.948	89499	N.E.
FTL_0880	-	hypothetical protein	124	0.984	86174	N.E.
FTL_0881	-	hypothetical protein	37	0.973	21312	N.E.
FTL_0882	-	apolipoprotein N-acyltransferase	178	0.966	60535	N.E.
FTL_0883	-	metal ion transporter protein	90	0.911	67957	N.E.
FTL_0884	-	hypothetical protein	41	0.098	2122	E
FTL_0885	-	phoH-like protein	79	0.506	8256	E and N.E.
FTL_0886	-	(dimethylallyl)adenosine tRNA methylthiotransferase	109	0.963	16259	N.E.
FTL_0887	-	o-methyltransferase family protein	64	0.984	55658	N.E.

FTL_0888	-	-	35	1	37566	N.E.
FTL_0889	-	hypothetical protein	16	0.875	11275	N.E.
FTL_0890	-	thymidine kinase	64	0.984	57356	N.E.
FTL_0891	tig	trigger factor	104	0.798	1941	E and N.E.
FTL_0892	clpP	ATP-dependent Clp protease proteolytic subunit	63	0.905	2065	N.E.
FTL_0893	clpX	ATP-dependent protease ATP-binding subunit ClpX	123	0.821	3314	N.E.
FTL_0894	lon	DNA-binding, ATP-dependent protease La	228	0.934	21755	N.E.
FTL_0895	hupB	histone-like protein HU form B	32	0.062	306	E
FTL_0896	-	hypothetical protein	180	0.894	27274	N.E.
FTL_0897	miaA	tRNA delta(2)-isopentenylpyrophosphate transferase	85	0.118	2519	E
FTL_0898	hfq	host factor I for bacteriophage Q beta replication	35	0.571	1466	E and N.E.
FTL_0899	-	protease, GTP-binding subunit	130	0.969	87756	N.E.
FTL_0900	-	monooxygenase	43	1	43441	N.E.
FTL_0901	-	monooxygenase family protein	57	0.965	45357	N.E.
FTL_0902	-	oxidoreductase	10	0.9	4983	N.E.
FTL_0903	-	hypothetical protein	105	0.952	18164	N.E.
FTL_0904	-	hypothetical protein	102	0.912	16226	N.E.
FTL_0905	-	low molecular weight (LMW) phosphotyrosine protein phosphatase	39	0.949	23705	N.E.
FTL_0906	engB	ribosome biogenesis GTP-binding protein YsxC	62	0.274	902	E
FTL_0907	-	-	31	0.935	24509	N.E.
FTL_0908	-	-	96	0.969	96223	N.E.
FTL_0909	-	hypothetical protein	29	1	27358	N.E.
FTL_0910	-	hypothetical protein	13	1	12028	N.E.
FTL_0911	-	-	27	1	31081	N.E.
FTL_0912	-	-	92	0.967	72736	N.E.
FTL_0913	-	-	117	0.983	99294	N.E.
FTL_0914	-	-	40	1	34514	N.E.
FTL_0915	-	acetolactate synthase small subunit	32	0.875	24105	E and N.E.
FTL_0916	-	ketol-acid reductoisomerase	93	0.957	76283	N.E.
FTL_0917	-	transcription-repair coupling factor	379	0.966	260880	N.E.
FTL_0918	yccA	hypothetical protein	86	1	36371	N.E.
FTL_0919	-	hypothetical protein	182	0.126	1701	E
FTL_0920	-	hypothetical protein	50	0.9	14384	N.E.
FTL_0921	-	endonuclease III	67	0.955	29186	N.E.
FTL_0922	-	Iron-sulfur cluster-binding protein	63	0.968	9205	N.E.
FTL_0923	-	glutaredoxin	62	0.968	20079	N.E.
FTL_0924	-	proton-dependent oligopeptide transporter	38	0.947	25753	N.E.
FTL_0925	-	proton-dependent oligopeptide transport (POT) family protein	169	0.917	118437	N.E.
FTL_0926	-	Ferritin-like protein	45	1	31741	N.E.
FTL_0927	-	lipoyl synthase	87	0.046	958	E
FTL_0928	-	isoprenoid biosynthesis protein with amidotransferase-like domain	66	0.939	23193	N.E.
FTL_0929	-	hypothetical protein	60	0.933	41308	N.E.
FTL_0930	ruvC	Holliday junction resolvase	50	0.88	2141	N.E.
FTL_0931	-	major facilitator transporter	143	0.888	102513	N.E.
FTL_0932	ruvA	Holliday junction DNA helicase RuvA	66	0.712	773	E and N.E.

FTL_0933	-	DNA recombination protein RmuC family protein	151	0.96	93068	N.E.
FTL_0934	-	hypothetical protein	55	0.964	43274	N.E.
FTL_0935	-	hypothetical protein	28	0.964	21519	N.E.
FTL_0936	-	hypothetical protein	39	1	36894	N.E.
FTL_0937	-	hypothetical protein	81	0.951	51912	N.E.
FTL_0938	-	histidine decarboxylase	146	0.938	112143	N.E.
FTL_0939	-	aldolase/adducin class II family protein	83	0.952	59631	N.E.
FTL_0940	-	methylpurine-DNA glycosylase family protein	77	0.974	61987	N.E.
FTL_0941	-	hypothetical protein	50	0.96	40572	N.E.
FTL_0942	-	nicotinamide mononucleotide transport (NMT) family protein	87	0.943	71110	N.E.
FTL_0943	-	Sodium/hydrogen exchanger family protein	128	0.977	100013	N.E.
FTL_0944	-	-	43	0.953	31087	N.E.
FTL_0945	-	hypothetical protein	62	0.984	50852	N.E.
FTL_0946	-	major facilitator transporter	128	0.969	106394	N.E.
FTL_0947	-	-	85	0.965	70262	N.E.
FTL_0948	-	hypothetical protein	87	0.966	72044	N.E.
FTL_0949	-	ribose-phosphate pyrophosphokinase	84	0.036	366	E
FTL_0950	-	50S ribosomal protein L25	27	0.481	1309	E
FTL_0951	-	hypothetical protein	143	0.951	113073	N.E.
FTL_0952	-	hypothetical protein	16	0.875	8418	N.E.
FTL_0953	-	hypothetical protein	58	0.897	40482	N.E.
FTL_0954	-	hypothetical protein	37	0.946	29066	N.E.
FTL_0955	-	GTP-dependent nucleic acid-binding protein EngD	100	0.96	50133	N.E.
FTL_0956	pth	peptidyl-tRNA hydrolase	78	0.115	1967	E
FTL_0957	blaA	Beta-lactamase class A	99	0.939	64076	N.E.
FTL_0958	-	hypothetical protein	92	0.967	67031	N.E.
FTL_0959	pilD	Type IV pili leader peptidase and methylase.	100	0.96	98138	N.E.
FTL_0960	udhA	soluble pyridine nucleotide transhydrogenase	134	0.888	10306	N.E.
FTL_0961	-	potassium channel protein	92	0.935	57202	N.E.
FTL_0962	-	hypothetical protein	40	1	24791	N.E.
FTL_0963	-	proton-dependent oligopeptide transport (POT) family protein	184	0.94	159904	N.E.
FTL_0964	hslU	ATP-dependent protease ATP-binding subunit HslU	107	0.944	24106	N.E.
FTL_0965	hslV	ATP-dependent protease peptidase subunit	50	0.92	11019	N.E.
FTL_0966	-	hypothetical protein	81	0.938	48151	N.E.
FTL_0967	lplA	lipoate-protein ligase A	90	0.067	544	E
FTL_0968	tyrS	tyrosyl-tRNA synthetase	102	0.01	4	E
FTL_0969	isftu1	transposase	100	1	92529	N.E.
FTL_0970	-	L-lactate dehydrogenase	124	0.96	110429	N.E.
FTL_0971	-	FAD linked oxidase	145	0.952	95988	N.E.
FTL_0972	-	-	142	0.979	108072	N.E.
FTL_0973	-	-	123	0.927	92708	N.E.
FTL_0974	-	50S ribosomal protein L11 methyltransferase	93	0.946	84106	N.E.
FTL_0975	-	Nif3 family protein	102	0.961	93009	N.E.
FTL_0976	-	hypothetical protein	220	0.95	149078	N.E.
FTL_0977	-	hypothetical protein	48	0.958	39437	N.E.
FTL_0978	-	hypothetical protein	38	0.974	23827	N.E.
FTL_0979	-	hypothetical protein	40	0.95	20793	N.E.
FTL_0980	-	hypothetical protein	150	0.967	112465	N.E.
FTL_0981	-	DNA polymerase IV	121	0.917	89414	N.E.
FTL_0982	-	DJ-1/PfpI family protein	70	0.957	49716	N.E.

FTL_0983	-	-	99	0.949	80264	N.E.
FTL_0984	-	bifunctional gluaredoxin/ribonucleoside-diphosphate reductase subunit beta	116	0.009	847	E
FTL_0985	grxA	glutaredoxin	27	0	0	E
FTL_0986	nrdA	ribonucleotide-diphosphate reductase subunit alpha	153	0.007	3	E
FTL_0987	mdh	malate dehydrogenase	92	0.033	98	E
FTL_0988	-	hypothetical protein	66	0.955	44146	N.E.
FTL_0989	-	ubiquinone biosynthesis protein	54	0.037	22	E
FTL_0990	-	lipoprotein	58	0.983	46253	N.E.
FTL_0991	-	-	40	0.925	32783	N.E.
FTL_0992	-	-	100	1	107853	N.E.
FTL_0993	-	HesA/MoeB/ThiF family protein	24	0.875	17001	N.E.
FTL_0994	-	hypothetical protein	177	0.972	142509	N.E.
FTL_0995	-	haloacid dehalogenase	69	0.928	44683	N.E.
FTL_0996	-	AhpC/Tsa family protein	58	0.966	56313	N.E.
FTL_0997	-	hypothetical protein	56	0.964	61792	N.E.
FTL_0998	-	hypothetical protein	78	0.974	72308	N.E.
FTL_0999	-	phosphonoacetate hydrolase	25	0.92	17555	N.E.
FTL_1000	-	hypothetical protein	26	0.923	15674	N.E.
FTL_1001	-	hypothetical protein	59	0.949	51972	N.E.
FTL_1002	-	hypothetical protein	87	0.908	70850	N.E.
FTL_1003	-	DNA polymerase III subunit epsilon	80	0.087	84	E
FTL_1004	-	D-alanyl-D-alanine carboxypeptidase	43	1	31973	N.E.
FTL_1005	-	hypothetical protein	161	0.969	117201	N.E.
FTL_1006	-	-	37	0.892	28750	N.E.
FTL_1007	-	-	28	0.964	23348	N.E.
FTL_1008	-	-	19	1	18060	N.E.
FTL_1009	-	aldehyde dehydrogenase	45	0.956	41918	N.E.
FTL_1010	-	-	29	0.966	25296	N.E.
FTL_1011	-	-	17	1	8300	N.E.
FTL_1012	-	hypothetical protein	26	0.808	14668	N.E.
FTL_1013	-	hypothetical protein	92	0.967	69608	N.E.
FTL_1014	-	oxidative stress transcriptional regulator	95	0.926	58721	N.E.
FTL_1015	-	AhpC/TSA family protein	47	0.064	3175	E
FTL_1016	-	short chain dehydrogenase	63	0.952	47439	N.E.
FTL_1017	-	cytidylate kinase	72	0.069	3081	E
FTL_1018	-	phosphoserine aminotransferase	114	0.105	831	E
FTL_1019	-	hypothetical protein	40	0.95	27891	N.E.
FTL_1020	isftu1	transposase	97	1	106425	N.E.
FTL_1021	-	hypothetical protein	126	0.976	101421	N.E.
FTL_1022	-	coproporphyrinogen III oxidase	74	0.054	1411	E
FTL_1023	isftu2	transposase	134	0.993	96487	N.E.
FTL_1024	rpsF	30S ribosomal protein S6	26	0	0	E
FTL_1025	rpsR	30S ribosomal protein S18	27	0.148	315	E
FTL_1026	rplI	50S ribosomal protein L9	32	0.906	5872	N.E.
FTL_1027	-	replicative DNA helicase	142	0.028	398	E
FTL_1028	-	radical SAM superfamily protein	109	0.972	26996	N.E.
FTL_1029	-	Type IV pili lipoprotein	106	0.887	26798	N.E.
FTL_1030	-	ribosomal large subunit pseudouridine synthase B	83	0.867	6628	N.E.
FTL_1031	-	hypothetical protein	55	0.164	542	E
FTL_1032	-	ribosomal-protein-alanine acetyltransferase	58	0.897	30891	N.E.
FTL_1033	-	-	51	1	41592	N.E.
FTL_1034	cysN	sulfate adenylyltransferase	116	0.948	98350	N.E.
FTL_1035	cysC	sulfate adenylyltransferase	55	0.964	38321	N.E.

FTL_1036	-	adenylylsulfate kinase, fragment	56	0.964	60071	N.E.
FTL_1037	-	hypothetical protein	64	0.938	32161	N.E.
FTL_1038	-	hypothetical protein	48	0.896	40366	N.E.
FTL_1039	-	hypothetical protein	87	0.92	43054	N.E.
FTL_1040	-	hypothetical protein	45	0.978	30586	N.E.
FTL_1041	-	octaprenyl-diphosphate synthase	107	0.019	231	E
FTL_1042	-	FKBP-type peptidyl-prolyl cis-trans isomerase family protein	85	0.953	59021	N.E.
FTL_1043	-	C32 tRNA thiolase	81	0.951	74167	N.E.
FTL_1044	-	hypothetical protein	54	0.981	46507	N.E.
FTL_1045	-	lipoprotein	60	0.95	33020	N.E.
FTL_1046	dacB	D-alanyl-D-alanine carboxypeptidase	172	0.029	206	E
FTL_1047	rpsU	30S ribosomal protein S21	16	0	0	E
FTL_1048	-	hypothetical protein	32	0.406	208	E
FTL_1049	dnaG	DNA primase	192	0.026	486	E
FTL_1050	rpoD	RNA polymerase sigma-70 factor	175	0.006	4	E
FTL_1051	ndh	NADH dehydrogenase	150	0.947	102912	N.E.
FTL_1052	-	putative glycosidase	26	0.885	37825	N.E.
FTL_1053	-	putative alpha-xylosidase	43	1	46645	N.E.
FTL_1054	-	putative alpha-xylosidase	45	0.978	46547	N.E.
FTL_1055	-	-	100	0.96	77547	N.E.
FTL_1056	-	-	62	0.968	46803	N.E.
FTL_1057	-	-	113	0.991	90767	N.E.
FTL_1058	lipB	lipoate-protein ligase B	71	0.085	1448	E
FTL_1059	-	hypothetical protein	27	0.074	33	E
FTL_1060	dacD	D-alanyl-D-alanine carboxypeptidase	148	0.081	299	E
FTL_1061	-	inorganic pyrophosphatase	59	0.034	920	E
FTL_1062	-	3-deoxy-D-manno-octulosonate 8-phosphate phosphatase	51	0.02	3	E
FTL_1063	-	hypothetical protein	68	0.029	5	E
FTL_1064	-	hypothetical protein	97	0.072	1704	E
FTL_1065	-	ABC transporter ATP-binding protein	64	0.031	20	E
FTL_1066	-	fumarylacetoacetate hydrolase family protein	60	0.983	39045	N.E.
FTL_1067	-	hypothetical protein	172	0.82	8658	E and N.E.
FTL_1068	truA	tRNA pseudouridine synthase A	75	0.707	1259	E and N.E.
FTL_1069	-	amino acid permease	117	0.966	105996	N.E.
FTL_1070	-	hypothetical protein	30	1	21934	N.E.
FTL_1071	guaA	GMP synthase	146	0.027	41	E
FTL_1072	-	1-deoxy-D-xylulose-5-phosphate synthase	189	0.037	1591	E
FTL_1073	-	hypothetical protein	33	0.909	26718	N.E.
FTL_1074	-	GDSL-like lipase/acylhydrolase family protein	79	0.937	52216	N.E.
FTL_1075	-	hypothetical protein	67	0.955	49085	N.E.
FTL_1076	-	short chain dehydrogenase family protein	77	0.922	56150	N.E.
FTL_1077	ruvB	Holliday junction DNA helicase RuvB	93	0.634	1761	E and N.E.
FTL_1078	-	-	64	0.984	45078	N.E.
FTL_1079	-	helix-turn-helix family protein	24	0.833	12780	N.E.
FTL_1080	-	hypothetical protein	53	0.906	45636	N.E.
FTL_1081	-	hypothetical protein	51	0.882	34435	N.E.
FTL_1082	-	hypothetical protein	39	0.897	23820	N.E.
FTL_1083	-	hypothetical protein	47	0.979	36359	N.E.
FTL_1084	-	hypothetical protein	48	0.958	25843	N.E.
FTL_1085	-	hypothetical protein	27	0.963	15791	N.E.

FTL_1086	-	proton-dependent oligopeptide transporter (POT) family protein	79	0.962	66963	N.E.
FTL_1087	isftu2	transposase	77	1	62075	N.E.
FTL_1088	-	hypothetical protein	25	0.96	29227	N.E.
FTL_1089	-	choloylglycine hydrolase family protein	91	0.978	64761	N.E.
FTL_1090	-	rRNA methyltransferase	77	0.935	53685	N.E.
FTL_1091	-	-	41	1	36552	N.E.
FTL_1092	-	-	177	0.966	137089	N.E.
FTL_1093	-	bifunctional methionine sulfoxide reductase B/A protein	95	0.968	85977	N.E.
FTL_1094	-	-	105	0.971	87382	N.E.
FTL_1095	-	-	34	0.941	38461	N.E.
FTL_1096	dsbA	Disulfide bond formation protein A	121	0.983	77692	N.E.
FTL_1097	-	hypothetical protein	20	0.95	11182	N.E.
FTL_1098	-	-	53	1	49563	N.E.
FTL_1099	-	-	43	0.953	29798	N.E.
FTL_1100	-	hypothetical protein	47	0.979	26792	N.E.
FTL_1101	-	hypothetical protein	44	0.932	24738	N.E.
FTL_1102	-	-	39	0.897	25059	N.E.
FTL_1103	-	-	84	0.952	72616	N.E.
FTL_1104	-	-	96	0.958	59152	N.E.
FTL_1105	-	hypothetical protein	40	1	28264	N.E.
FTL_1106	alaS	alanyl-tRNA synthetase	249	0.02	495	E
FTL_1107	-	hypothetical protein	155	0.968	97300	N.E.
FTL_1108	-	cytosol aminopeptidase	143	0.972	113665	N.E.
FTL_1109	-	transaldolase B	101	0.96	55791	N.E.
FTL_1110	-	hypothetical protein	56	0.982	42340	N.E.
FTL_1111	-	isochorismatase hydrolase family protein	31	0.968	23440	N.E.
FTL_1112	isftu2	transposase	96	1	72045	N.E.
FTL_1113	-	hypothetical protein	94	0.968	70069	N.E.
FTL_1114	-	isochorismatase hydrolase family protein	59	0.966	39702	N.E.
FTL_1115	-	hypothetical protein	70	0.086	5495	E
FTL_1116	-	ATP-dependent DNA helicase	215	0.94	190013	N.E.
FTL_1117	-	hypothetical protein	91	0.989	73968	N.E.
FTL_1118	-	hypothetical protein	79	0.949	54105	N.E.
FTL_1119	rdgC	recombination associated protein	100	1	86049	N.E.
FTL_1120	-	hypothetical protein	28	0.929	18664	N.E.
FTL_1121	-	hypothetical protein	95	0.968	101071	N.E.
FTL_1122	-	hypothetical protein	77	0.987	50246	N.E.
FTL_1123	-	hypothetical protein	84	0.964	95519	N.E.
FTL_1124	-	hypothetical protein	48	0.979	42835	N.E.
FTL_1125	-	transcriptional regulator	137	0.956	112772	N.E.
FTL_1126	-	transcriptional regulator	25	0.96	14686	N.E.
FTL_1127	isftu1	transposase	100	1	92211	N.E.
FTL_1128	-	hypothetical protein	31	0.935	18689	N.E.
FTL_1129	-	acetyltransferase	56	0.911	40845	N.E.
FTL_1130	-	ribosomal RNA small subunit methyltransferase	47	0.872	27427	N.E.
FTL_1131	-	Sun protein	61	0.885	50843	N.E.
FTL_1132	-	inositol-1-monophosphatase	84	0.845	5107	N.E.
FTL_1133	-	hypothetical protein	124	0.952	77170	N.E.
FTL_1134	-	hypothetical protein	149	0.953	110293	N.E.
FTL_1135	-	-	71	0.972	48208	N.E.
FTL_1136	-	hypothetical protein	31	1	19288	N.E.
FTL_1137	-	3-oxoacyl-ACP synthase	116	0.026	506	E
FTL_1138	acpP	acyl carrier protein	28	0	0	E

FTL_1139	-	3-oxoacyl-(acyl-carrier-protein) reductase	65	0.046	4696	E
FTL_1140	-	malonyl CoA-acyl carrier protein transacylase	80	0.062	144	E
FTL_1141	-	3-oxoacyl-ACP synthase	82	0.012	2	E
FTL_1142	-	putative glycerol-3-phosphate acyltransferase PlsX	99	0.02	132	E
FTL_1143	rpmF	50S ribosomal protein L32	18	0	0	E
FTL_1144	-	hypothetical protein	53	0.811	32490	N.E.
FTL_1145	-	transketolase	173	0.029	24	E
FTL_1146	gapA	glyceraldehyde-3-phosphate dehydrogenase	87	0.011	2	E
FTL_1147	pgk	phosphoglycerate kinase	99	0.02	449	E
FTL_1148	pyk	pyruvate kinase	122	0.049	96	E
FTL_1149	fbaA	fructose-1,6-bisphosphate aldolase	99	0.697	1654	E and N.E.
FTL_1150	treA	Alpha,alpha-trehalase.	46	0.978	41943	N.E.
FTL_1151	-	trehalase, pseuodgene	102	0.971	71263	N.E.
FTL_1152	-	-	35	0.857	30902	N.E.
FTL_1153	isftu1	transposase	100	1	106182	N.E.
FTL_1154	-	-	110	0.991	104241	N.E.
FTL_1155	-	hypothetical protein	40	0.975	38789	N.E.
FTL_1156	-	hypothetical protein	25	1	25423	N.E.
FTL_1157	iglA	intracellular growth locus, subunit A	46	1	59768	N.E.
FTL_1158	iglB	intracellular growth locus, subunit B	166	0.988	188443	N.E.
FTL_1159	iglC	intracellular growth locus, subunit C	75	0.987	79664	N.E.
FTL_1160	iglD	intracellular growth locus, subunit D	131	1	117314	N.E.
FTL_1161	-	hypothetical protein	89	0.966	81682	N.E.
FTL_1162	-	hypothetical protein	496	0.982	482246	N.E.
FTL_1163	-	hypothetical protein	101	0.99	98940	N.E.
FTL_1164	-	hypothetical protein	132	0.992	122335	N.E.
FTL_1165	-	hypothetical protein	83	1	68701	N.E.
FTL_1166	-	hypothetical protein	181	1	190119	N.E.
FTL_1167	-	hypothetical protein	61	1	68279	N.E.
FTL_1168	-	hypothetical protein	236	0.987	184792	N.E.
FTL_1169	-	hypothetical protein	53	1	53541	N.E.
FTL_1170	-	hypothetical protein	48	0.979	36158	N.E.
FTL_1171	pdpB	PdpB protein	447	0.987	388733	N.E.
FTL_1172	pdpA	PdpA protein	296	0.997	303416	N.E.
FTL_1173	-	hypothetical protein	73	0.986	76338	N.E.
FTL_1174	-	cystathionine beta-synthase (cystein synthase)	102	0.029	287	E
FTL_1175	-	-	101	0.96	83102	N.E.
FTL_1176	-	LysR transcriptional regulator family protein	47	0.979	32381	N.E.
FTL_1177	trmE	tRNA modification GTPase TrmE	147	0.218	502	E
FTL_1178	-	hypothetical protein	28	0.821	9611	N.E.
FTL_1179	-	sigma-54 modulation protein	32	0.031	3	E
FTL_1180	-	PEP-dependent sugar PTS system family protein	54	0.13	2476	E
FTL_1181	-	SpoU rRNA methylase family protein	82	0.976	91099	N.E.
FTL_1182	rnhB	ribonuclease HII	62	0.968	53859	N.E.
FTL_1183	-	Sodium-solute symporter family protein	168	0.976	122663	N.E.
FTL_1184	-	ClpXP protease specificity-enhancing factor	49	0.98	23881	N.E.
FTL_1185	-	macrophage growth locus subunit A	66	0.394	1263	E
FTL_1186	rpsI	30S ribosomal protein S9	36	0.028	3	E
FTL_1187	rplM	50S ribosomal protein L13	41	0.049	6	E
FTL_1188	-	hypothetical protein	125	0.024	670	E
FTL_1189	mltA	membrane-bound lytic murein transglycosylase A (MLT) family protein	125	0.064	1400	E

FTL_1190	-	heat shock protein GrpE	51	0.02	90	E
FTL_1191	dnaK	molecular chaperone DnaK	168	0.03	242	E
FTL_1192	-	chaperone protein DnaJ	90	0.956	38723	N.E.
FTL_1193	-	LysR transcriptional regulator family protein	101	0.95	69459	N.E.
FTL_1194	-	pirin family protein	28	0.964	25653	N.E.
FTL_1195	isftu1	transposase	100	1	108237	N.E.
FTL_1196	-	hypothetical protein	99	0.97	97210	N.E.
FTL_1197	pheS	phenylalanyl-tRNA synthetase subunit alpha	84	0.012	4	E
FTL_1198	pheT	phenylalanyl-tRNA synthetase subunit beta	260	0.015	228	E
FTL_1199	-	regulatory protein	44	0.955	28786	N.E.
FTL_1200	-	cobalamin (vitamin B12) synthesis protein/P47K family protein	113	0.956	93371	N.E.
FTL_1201	-	ZIP metal transporter family protein	88	0.977	61055	N.E.
FTL_1202	-	hypothetical protein	124	0.944	94058	N.E.
FTL_1203	-	cardiolipin synthetase	165	0.958	105489	N.E.
FTL_1204	-	cardiolipin synthetase	168	0.935	129113	N.E.
FTL_1205	-	hypothetical protein	54	0.963	36053	N.E.
FTL_1206	-	major facilitator transporter	44	0.955	51811	N.E.
FTL_1207	-	MRP like protein	92	0.457	4459	E
FTL_1208	dcd	deoxycytidine triphosphate deaminase	53	0.962	43513	N.E.
FTL_1209	-	hypothetical protein	87	0.931	87385	N.E.
FTL_1210	-	hypothetical protein	69	0.928	27229	N.E.
FTL_1211	-	lipoprotein	69	0.928	43863	N.E.
FTL_1212	leuS	leucyl-tRNA synthetase	237	0.013	1254	E
FTL_1213	-	hypothetical protein	253	0.98	210130	N.E.
FTL_1214	-	hypothetical protein	29	1	28717	N.E.
FTL_1215	-	hypothetical protein	36	0.056	151	E
FTL_1216	-	hypothetical protein	66	0.848	5086	N.E.
FTL_1217	-	hypothetical protein	41	0.805	17323	N.E.
FTL_1218	-	hypothetical protein	129	0.961	81380	N.E.
FTL_1219	-	hypothetical protein	150	0.973	115834	N.E.
FTL_1220	-	amino-acid permease	165	0.958	169330	N.E.
FTL_1221	-	hypothetical protein	91	0.923	54532	N.E.
FTL_1222	-	hypothetical protein	36	1	32936	N.E.
FTL_1223	-	hypothetical protein	27	0.963	15615	N.E.
FTL_1224	-	thioredoxin	30	0.967	28171	N.E.
FTL_1225	-	hypothetical protein	88	0.955	61277	N.E.
FTL_1226	-	-	30	0.967	21813	N.E.
FTL_1227	-	-	28	1	27045	N.E.
FTL_1228	-	hypothetical protein	134	0.037	1714	E
FTL_1229	-	ABC transporter ATP-binding protein	65	0	0	E
FTL_1230	-	cysteine desulfurase activator complex subunit SufB	114	0.009	3	E
FTL_1231	-	hypothetical protein	49	0.041	19	E
FTL_1232	trkA	potassium transporter peripheral membrane protein	150	0.027	999	E
FTL_1233	argP	amino acid antiporter, high affinity arginine transporter	166	0.012	195	E
FTL_1234	-	hypothetical protein	62	0.984	42162	N.E.
FTL_1235	-	-	82	0.963	55236	N.E.
FTL_1236	infA	translation initiation factor IF-1	22	0.045	75	E
FTL_1237	-	hypothetical protein	101	0.95	84013	N.E.
FTL_1238	-	hypothetical protein	43	1	30709	N.E.
FTL_1239	ffh	signal recognition particle protein, Ffh	109	0.119	5276	E
FTL_1240	-	phospho-2-dehydro-3-deoxyheptonate aldolase	110	0.982	64081	N.E.

FTL_1241	isftu1	transposase	100	1	91404	N.E.
FTL_1242	-	ThiJ/PfpI family protein	27	0.963	21810	N.E.
FTL_1243	-	hypothetical protein	33	0.97	36267	N.E.
FTL_1244	-	exodeoxyribonuclease III	72	1	48066	N.E.
FTL_1245	-	short chain dehydrogenase	72	0.972	79745	N.E.
FTL_1246	-	hypothetical protein	64	0.969	63718	N.E.
FTL_1247	-	hypothetical protein	88	0.977	74605	N.E.
FTL_1248	-	glutathione reductase	151	0.934	9023	N.E.
FTL_1249	-	hypothetical protein	40	1	39906	N.E.
FTL_1250	isftu2	transposase	81	1	59015	N.E.
FTL_1251	-	proton-dependent oligopeptide transport (POT) family protein	176	0.943	28956	N.E.
FTL_1252	-	ATP-dependent RNA helicase RhlE	122	0.975	93893	N.E.
FTL_1253	folE	GTP cyclohydrolase I	58	0.069	247	E
FTL_1254	-	-	33	0.939	19233	N.E.
FTL_1255	-	-	57	0.947	35018	N.E.
FTL_1256	-	-	45	1	22943	N.E.
FTL_1257	-	-	71	1	53668	N.E.
FTL_1258	-	aldo/keto reductase	93	0.968	82479	N.E.
FTL_1259	-	-	64	0.984	57507	N.E.
FTL_1260	-	-	69	0.971	47077	N.E.
FTL_1261	-	anthranilate synthase component II	54	0.981	46836	N.E.
FTL_1262	-	chorismate binding family protein	203	0.961	147450	N.E.
FTL_1263	fadD2	AMP-binding family protein	179	0.961	122156	N.E.
FTL_1264	-	dihydroneopterin aldolase	45	0.044	8	E
FTL_1265	-	2-amino-4-hydroxy-6-hydroxymethyldihydropteridine pyrophosphokinase	146	0.062	1093	E
FTL_1266	-	lipase/esterase	102	0.941	22124	N.E.
FTL_1267	-	hypothetical protein	59	0.949	53381	N.E.
FTL_1268	-	-	11	1	14608	N.E.
FTL_1269	-	-	41	0.951	26381	N.E.
FTL_1270	-	-	60	1	41364	N.E.
FTL_1271	bioA	adenosylmethionine-8-amino-7-oxononanoate aminotransferase	145	0.972	28327	N.E.
FTL_1272	bioB	biotin synthase	103	0.515	857	E
FTL_1273	bioF	8-amino-7-oxononanoate synthase	131	0.947	12897	N.E.
FTL_1274	bioC	biotin synthesis protein BioC	88	0.932	6762	N.E.
FTL_1275	bioD	dethiobiotin synthetase	78	0.923	16756	N.E.
FTL_1276	birA	bifunctional biotin operon repressor/biotin synthetase BirA	97	0.918	61791	N.E.
FTL_1277	-	ROK family protein	85	0.941	76153	N.E.
FTL_1278	-	major facilitator transporter	147	0.932	128773	N.E.
FTL_1279	-	acetoacetate decarboxylase, fragment	59	1	52930	N.E.
FTL_1280	-	short-chain dehydrogenase	20	1	15611	N.E.
FTL_1281	-	hypothetical protein	53	0.981	46807	N.E.
FTL_1282	-	beta-glucosidase	211	0.967	139824	N.E.
FTL_1283	-	glutamate-1-semialdehyde aminotransferase	107	0.009	174	E
FTL_1284	-	glutathione synthetase	109	0.064	203	E
FTL_1285	-	methionyl-tRNA formyltransferase	105	0.029	16	E
FTL_1286	-	hypothetical protein	32	0.406	4796	E and N.E.
FTL_1287	rlmL	23S rRNA m(2)G2445 methyltransferase	217	0.954	169900	N.E.
FTL_1288	-	fatty acid hydroxylase	74	0.905	52362	N.E.
FTL_1289	-	hypothetical protein	68	0.941	44994	N.E.
FTL_1290	isftu1	transposase	100	1	91630	N.E.

FTL_1291	-	hypothetical protein	35	0.971	34401	N.E.
FTL_1292	-	hypothetical protein	58	0.948	46378	N.E.
FTL_1293	-	hypothetical protein	43	0.977	38231	N.E.
FTL_1294	-	short-chain dehydrogenase	96	0.948	74179	N.E.
FTL_1295	-	amino acid transporter	99	0.98	88640	N.E.
FTL_1296	-	amino acid antiporter	55	0.927	44221	N.E.
FTL_1297	-	hypothetical protein	109	0.982	85636	N.E.
FTL_1298	isftu1	transposase	100	1	104699	N.E.
FTL_1299	-	hypothetical protein	50	0.98	41040	N.E.
FTL_1300	-	hypothetical protein	36	0.917	32308	N.E.
FTL_1301	isftu2	transposase	78	1	60164	N.E.
FTL_1302	-	phenol hydroxylase	75	0.027	469	E
FTL_1303	rpmE	50S ribosomal protein L31	16	0.875	990	N.E.
FTL_1304	-	glutamate--cysteine ligase	166	0.06	8909	E
FTL_1305	-	virulence factor MviN	201	0.965	136871	N.E.
FTL_1306	-	hypothetical protein	107	0.963	47381	N.E.
FTL_1307	-	nucleotide-binding protein, yjeE	42	0.048	260	E
FTL_1308	-	bifunctional folylpolyglutamate synthase/ dihydrofolate synthase	133	0.045	23	E
FTL_1309	-	Acetyl-CoA carboxylase beta subunit	82	0.037	8	E
FTL_1310	ndk	nucleoside diphosphate kinase	34	0	0	E
FTL_1311	pyrG	CTP synthetase	141	0.035	1718	E
FTL_1312	-	S-transferase	88	0.955	78414	N.E.
FTL_1313	-	short-chain fatty acids transporter	80	0.988	98053	N.E.
FTL_1314	-	hypothetical protein	115	0.948	97556	N.E.
FTL_1315	-	hypothetical protein	66	0.97	50917	N.E.
FTL_1316	isftu1	transposase	100	1	106466	N.E.
FTL_1317	-	hypothetical protein	143	0.993	160804	N.E.
FTL_1318	-	-	14	1	13677	N.E.
FTL_1319	-	transposase	59	1	46116	N.E.
FTL_1320	-	hypothetical protein	65	0.969	57963	N.E.
FTL_1321	-	hypothetical protein	38	0.974	35735	N.E.
FTL_1322	-	-	41	0.976	34281	N.E.
FTL_1323	-	-	61	0.984	45433	N.E.
FTL_1324	-	-	20	1	10488	N.E.
FTL_1325	-	-	301	0.934	228350	N.E.
FTL_1326	-	hypothetical protein	47	0.957	30714	N.E.
FTL_1327	-	hypothetical protein	129	0.946	76488	N.E.
FTL_1328	fopA	OmpA family protein, outer membrane associated protein	128	0.875	32222	E and N.E.
FTL_1329	-	ferredoxin	31	0.968	30735	N.E.
FTL_1330	coaD	phosphopantetheine adenylyltransferase	52	0.077	86	E
FTL_1331	-	hypothetical protein	53	0.717	4293	E and N.E.
FTL_1332	-	hesB family protein	36	0.083	402	E
FTL_1333	-	selenocysteine lyase	119	0.025	200	E
FTL_1334	-	L-serine dehydratase 1	119	0.958	33962	N.E.
FTL_1335	-	hypothetical protein	73	0.932	47076	N.E.
FTL_1336	-	prephenate dehydratase	84	0.94	68688	N.E.
FTL_1337	-	-	142	0.972	133753	N.E.
FTL_1338	-	alanine racemase	132	0.053	2808	E
FTL_1339	-	proton-dependent oligopeptide transport (POT) family protein	166	0.976	160088	N.E.
FTL_1340	-	hypothetical protein	80	0.963	71457	N.E.
FTL_1341	-	hypothetical protein	50	0.98	52357	N.E.
FTL_1342	-	hypothetical protein	123	0.024	1109	E

FTL_1343	-	hypothetical protein	36	0.917	27172	N.E.
FTL_1344	-	hypothetical protein	38	1	31927	N.E.
FTL_1345	-	-	142	0.993	114429	N.E.
FTL_1346	-	-	27	0.963	17554	N.E.
FTL_1347	-	hypothetical protein	20	1	17948	N.E.
FTL_1348	-	transposase	74	1	57186	N.E.
FTL_1349	isftu1	transposase	94	1	87920	N.E.
FTL_1350	-	glycyl-tRNA synthetase subunit beta	225	0.022	536	E
FTL_1351	-	TatD related DNAse family protein	85	0.988	63070	N.E.
FTL_1352	-	DNA replication and repair protein RecF	135	0.941	22629	N.E.
FTL_1353	-	hypothetical protein	36	0.944	31192	N.E.
FTL_1354	-	hypothetical protein	112	0.688	3113	E and N.E.
FTL_1355	-	-	79	0.937	68222	N.E.
FTL_1356	-	-	45	0.933	43947	N.E.
FTL_1357	-	UTP--glucose-1-phosphate uridylyltransferase	85	0.988	60800	N.E.
FTL_1358	-	cation-efflux family protein	125	0.968	36376	N.E.
FTL_1359	-	hypothetical protein	68	0.971	66978	N.E.
FTL_1360	rpsU	30S ribosomal protein S21	21	1	12607	N.E.
FTL_1361	-	cold shock protein	17	0.882	11066	N.E.
FTL_1362	-	hypothetical protein	105	0.933	63486	N.E.
FTL_1363	-	hypothetical protein	115	0.974	98560	N.E.
FTL_1364	-	hypothetical protein	84	0.976	61551	N.E.
FTL_1365	-	hypothetical protein	38	1	29899	N.E.
FTL_1366	-	membrane fusion protein	38	1	34124	N.E.
FTL_1367	-	hypothetical protein	91	0.945	88860	N.E.
FTL_1368	-	hypothetical protein	80	0.95	63397	N.E.
FTL_1369	isftu1	transposase	100	1	91603	N.E.
FTL_1370	-	hypothetical protein	83	0.048	440	E
FTL_1371	-	hypothetical protein	70	0.971	75047	N.E.
FTL_1372	-	lipoprotein	144	0.993	152205	N.E.
FTL_1373	-	hypothetical protein	43	1	44131	N.E.
FTL_1374	-	organic solvent tolerance protein	228	0.974	173066	N.E.
FTL_1375	-	heat shock protein 15 (HSP15)	36	0.972	22972	N.E.
FTL_1376	-	carbohydrate kinase family protein (YjeF-related protein)	169	0.947	147203	N.E.
FTL_1377	-	hypothetical protein	74	0.959	63168	N.E.
FTL_1378	-	-	21	0.952	19363	N.E.
FTL_1379	-	-	87	0.977	62065	N.E.
FTL_1380	-	-	29	0.931	21169	N.E.
FTL_1381	-	-	37	0.946	36668	N.E.
FTL_1382	-	-	68	0.956	78785	N.E.
FTL_1383	-	glutathione peroxidase	44	0.932	31659	N.E.
FTL_1384	-	hypothetical protein	30	0.967	22468	N.E.
FTL_1385	-	hypothetical protein	55	0.945	38591	N.E.
FTL_1386	isftu2	transposase	79	1	64542	N.E.
FTL_1387	-	-	91	0.978	77347	N.E.
FTL_1388	-	L-aspartate oxidase	176	0.085	231	E
FTL_1389	-	nicotinate-nucleotide pyrophosphorylase	91	0.022	6	E
FTL_1390	-	quinolinate synthetase	88	0.011	2	E
FTL_1391	gmk	guanylate kinase	63	0.016	2	E
FTL_1392	deaD	cold-shock DEAD-box protein A	180	0.894	19823	N.E.
FTL_1393	ppiC	peptidyl-prolyl cis-trans isomerase	22	0.955	996	N.E.
FTL_1394	galP2	major facilitator superfamily galactose-proton symporter	134	0.955	152443	N.E.

FTL_1395	galP1	major facilitator superfamily galactose-proton symporter	129	0.969	39277	N.E.
FTL_1396	-	galactose-1-phosphate uridylyltransferase	90	0.944	81474	N.E.
FTL_1397	-	galactokinase	110	0.964	97345	N.E.
FTL_1398	-	hypothetical protein	47	0.957	36866	N.E.
FTL_1399	-	3-deoxy-manno-octulosonate cytidylyltransferase	71	0.056	770	E
FTL_1400	-	hypothetical protein	25	0.84	11450	N.E.
FTL_1401	-	hypothetical protein	29	1	35603	N.E.
FTL_1402	isftu1	transposase	100	1	92521	N.E.
FTL_1403	-	hypothetical protein	82	0.963	27021	N.E.
FTL_1404	rplT	50S ribosomal protein L20	39	0.051	230	E
FTL_1405	rpmI	50S ribosomal protein L35	19	0	0	E
FTL_1406	-	translation initiation factor IF-3	27	0	0	E
FTL_1407	thrS	threonyl-tRNA synthetase	170	0.006	3	E
FTL_1408	-	chitin binding protein	165	0.964	178525	N.E.
FTL_1409	-	glycine cleavage system protein H	42	0.976	32141	N.E.
FTL_1410	murG	undecaprenyldiphospho-muramoylpentapeptide beta-N-acetylglucosaminyltransferase	112	0.036	592	E
FTL_1411	-	hypothetical protein	27	0.963	2500	N.E.
FTL_1412	-	recombination protein RecR	64	1	13314	N.E.
FTL_1413	spoT	guanosine-3',5'-bis(diphosphate) 3'-pyrophosphohydrolase/(p)ppGpp synthase	225	0.036	3118	E
FTL_1414	capA	hypothetical protein	141	0.95	115828	N.E.
FTL_1415	capC	capsule biosynthesis protein CapC	71	0.986	64357	N.E.
FTL_1416	capB	capsule biosynthesis protein capB	122	0.984	108849	N.E.
FTL_1417	-	major facilitator transporter	149	0.966	179788	N.E.
FTL_1418	-	asparaginase	75	0.973	23591	N.E.
FTL_1419	-	cyanophycinase	85	0.988	67612	N.E.
FTL_1420	-	carbohydrate/purine kinase pfkB family protein	99	0.04	2222	E
FTL_1421	-	haloacid dehalogenase-like hydrolase family protein	76	0.947	63333	N.E.
FTL_1422	-	glycosyl transferases group 1 family protein	127	0.976	121196	N.E.
FTL_1423	-	glycosyl transferase family protein	131	0.977	122260	N.E.
FTL_1424	-	glycosyl transferase family protein	136	0.949	93330	N.E.
FTL_1425	-	hypothetical protein	110	0.936	70605	N.E.
FTL_1426	-	hypothetical protein	78	0.962	60473	N.E.
FTL_1427	-	hypothetical protein	151	0.954	122190	N.E.
FTL_1428	-	ABC transporter ATP-binding and membrane protein	216	0.94	204368	N.E.
FTL_1429	-	glycosyl transferases group 1 family protein	135	0.956	126962	N.E.
FTL_1430	-	UDP-glucose 4-epimerase	120	0.967	141209	N.E.
FTL_1431	-	sugar transferase	153	0.974	128428	N.E.
FTL_1432	-	D-ribulose-phosphate 3-epimerase	61	0.066	580	E
FTL_1433	-	arabinose phosphate isomerase	91	0.022	703	E
FTL_1434	-	DoxD-like family protein	66	0.97	84987	N.E.
FTL_1435	-	hypothetical protein	50	0.96	32793	N.E.
FTL_1436	-	hypothetical protein	26	0.962	23323	N.E.
FTL_1437	-	hypothetical protein	83	0.988	80808	N.E.
FTL_1438	-	hypothetical protein	25	0.96	19462	N.E.
FTL_1439	-	arylsulfatase	44	1	47016	N.E.
FTL_1440	-	beta-lactamase superfamily hydrolase	30	0.967	33219	N.E.
FTL_1441	isftu2	transposase	87	1	64345	N.E.

FTL_1442	fabI	enoyl-[acyl-carrier-protein] reductase (NADH)	81	0.037	400	E
FTL_1443	-	hypothetical protein	69	1	70889	N.E.
FTL_1444	-	hypothetical protein	31	0.968	24294	N.E.
FTL_1445	isftu2	transposase	73	1	56893	N.E.
FTL_1446	isftu1	transposase	94	1	87887	N.E.
FTL_1447	-	hypothetical protein	51	0.98	39127	N.E.
FTL_1448	uvrC	excinuclease ABC subunit C	166	0.952	133705	N.E.
FTL_1449	-	ribonuclease D	123	0.967	105186	N.E.
FTL_1450	-	major facilitator transporter	154	0.968	113925	N.E.
FTL_1451	-	hypothetical protein	28	1	29137	N.E.
FTL_1452	rpmA	50S ribosomal protein L27	24	0.042	522	E
FTL_1453	rplU	50S ribosomal protein L21	25	0	0	E
FTL_1454	-	-	36	0.972	27978	N.E.
FTL_1455	-	-	78	0.949	78728	N.E.
FTL_1456	-	-	32	0.906	31857	N.E.
FTL_1457	-	-	20	1	18066	N.E.
FTL_1458	secA	preprotein translocase subunit SecA	231	0.082	8036	E
FTL_1459	-	hypothetical protein	122	0.934	104579	N.E.
FTL_1460	-	hypothetical protein	51	0.765	7079	E and N.E.
FTL_1461	deoD	purine nucleoside phosphorylase	75	0.987	59670	N.E.
FTL_1462	isftu1	transposase	100	1	92320	N.E.
FTL_1463	isftu2	transposase	77	1	57903	N.E.
FTL_1464	-	ATP-dependent metalloprotease	183	0.071	6300	E
FTL_1465	-	hypothetical protein	24	1	12753	N.E.
FTL_1466	-	major facilitator transporter	62	0.952	37205	N.E.
FTL_1467	isftu2	transposase	77	1	57837	N.E.
FTL_1468	-	ATP-dependent metalloprotease	183	0.071	6375	E
FTL_1469	-	hypothetical protein	24	1	12610	N.E.
FTL_1470	-	major facilitator transporter	62	0.952	37156	N.E.
FTL_1471	isftu2	transposase	76	1	58062	N.E.
FTL_1472	-	hypothetical protein	51	0.98	50246	N.E.
FTL_1473	uvrA	DNA excision repair protein subunit A	264	0.966	254586	N.E.
FTL_1474	greA	transcription elongation factor GreA	48	0.896	5626	N.E.
FTL_1475	fimT	Type IV pili fiber building block protein	65	1	71783	N.E.
FTL_1476	pgi	glucose-6-phosphate isomerase	153	0.046	1636	E
FTL_1477	-	thiamine pyrophospokinase	72	0.042	108	E
FTL_1478	guaB	inosine-5-monophosphate dehydrogenase	123	0.089	2851	E
FTL_1479	pepA	cytosol aminopeptidase	142	0.958	32648	N.E.
FTL_1480	-	YjgP/YjgQ family permease	144	0.028	185	E
FTL_1481	-	YjgP/YjgQ family permease	133	0.023	571	E
FTL_1482	-	peptidase M16 family protein	140	0.957	81500	N.E.
FTL_1483	-	peptidase M16 family protein	147	0.959	67374	N.E.
FTL_1484	-	methylase	64	0.953	35828	N.E.
FTL_1485	-	hypothetical protein	79	0.975	54351	N.E.
FTL_1486	-	tRNA-(ms(2)io(6)a)-hydroxylase	60	0.983	59010	N.E.
FTL_1487	-	uridine phosphorylase	83	0.976	86198	N.E.
FTL_1488	-	cytidine deaminase	45	0.978	48195	N.E.
FTL_1489	-	FAD-binding family protein	290	0.972	238150	N.E.
FTL_1490	-	phosphoglyceromutase	153	0.013	9	E
FTL_1491	-	seryl-tRNA synthetase	122	0.025	822	E
FTL_1492	-	fructokinase	79	0.975	78799	N.E.
FTL_1493	-	polysaccharide biosynthesis protein (export protein)	152	0.072	1170	E
FTL_1494	-	hypothetical protein	51	0.98	39556	N.E.

FTL_1495	-	cysteine/glutathione ABC transporter membrane/ATP-binding protein	196	0.031	1178	E
FTL_1496	-	cysteine/glutathione ABC transporter membrane/ATP-binding protein	187	0.043	4837	E
FTL_1497	-	C4-dicarboxylate transport protein	162	0.969	144509	N.E.
FTL_1498	-	translation initiation inhibitor	43	0.953	32239	N.E.
FTL_1499	-	sulfate permease family protein	173	0.994	163345	N.E.
FTL_1500	-	transposase	57	1	49549	N.E.
FTL_1501	-	-	14	1	13803	N.E.
FTL_1502	-	major facilitator transporter	168	0.976	176877	N.E.
FTL_1503	dgt	deoxyguanosinetriphosphate triphosphohydrolase	139	0.957	119055	N.E.
FTL_1504	katG	peroxidase/catalase	186	0.968	199458	N.E.
FTL_1505	isftu1	transposase	100	1	91957	N.E.
FTL_1506	-	short-chain dehydrogenase	53	1	58205	N.E.
FTL_1507	-	3-oxoacyl-ACP reductase	40	0.925	35114	N.E.
FTL_1508	-	-	73	0.959	56564	N.E.
FTL_1509	-	D-alanyl-D-alanine carboxypeptidase/D-alanyl-D-alanine-endopeptidase	68	0.941	55043	N.E.
FTL_1510	-	glycerol-3-phosphate transporter	149	0.966	78442	N.E.
FTL_1511	-	glycerophosphoryl diester phosphodiesterase family protein	108	0.963	106716	N.E.
FTL_1512	-	hypothetical protein	88	0.955	83805	N.E.
FTL_1513	-	ABC transporter ATP-binding protein	95	0.989	94601	N.E.
FTL_1514	-	ABC transporter permease	53	0.981	47499	N.E.
FTL_1515	-	ABC transporter membrane protein	63	0.984	61822	N.E.
FTL_1516	isftu2	transposase	73	1	56630	N.E.
FTL_1517	-	hypothetical protein	38	0.947	35847	N.E.
FTL_1518	-	-	59	1	52312	N.E.
FTL_1519	-	-	25	0.96	13792	N.E.
FTL_1520	upp	uracil phosphoribosyltransferase	51	0.961	39768	N.E.
FTL_1521	-	chitinase family 18 protein	219	0.986	247745	N.E.
FTL_1522	-	2-amino-3-ketobutyrate coenzyme A ligase	114	0.307	6962	E and N.E.
FTL_1523	tdh	L-threonine 3-dehydrogenase	93	0.172	872	E and N.E.
FTL_1524	-	serine transporter	193	0.067	219	E
FTL_1525	-	2-C-methyl-D-erythritol 4-phosphate cytidylyltransferase	75	0.013	461	E
FTL_1526	-	cell division protein	35	0	0	E
FTL_1527	eno	phosphopyruvate hydratase	127	0.063	288	E
FTL_1528	-	major facilitator transporter	147	0.98	125984	N.E.
FTL_1529	-	nicotinamide mononucleotide transport (NMT) family protein	108	0.963	90190	N.E.
FTL_1530	-	-	72	0.944	71065	N.E.
FTL_1531	rumA	23S rRNA 5-methyluridine methyltransferase	139	0.971	117486	N.E.
FTL_1532	-	hypothetical protein	64	0.984	78988	N.E.
FTL_1533	-	DNA-directed RNA polymerase subunit omega	19	1	8742	N.E.
FTL_1534	-	uridine kinase	69	0.957	59258	N.E.
FTL_1535	kdsA	2-dehydro-3-deoxyphosphooctonate aldolase	67	0.03	621	E
FTL_1536	-	iron-sulfur cluster insertion protein ErpA	29	0	0	E
FTL_1537	pnp	polynucleotide phosphorylase/polyadenylase	198	0.177	1429	E
FTL_1538	rpsO	30S ribosomal protein S15	30	0	0	E

FTL_1539	ftsI	penicillin binding protein (peptidoglycan synthetase)	170	0.018	159	E
FTL_1540	-	hypothetical protein	36	0.056	234	E
FTL_1541	mraW	S-adenosyl-methyltransferase MraW	99	0.838	36455	E and N.E.
FTL_1542	-	hypothetical protein	234	0.957	33887	N.E.
FTL_1543	-	formamidopyrimidine-DNA glycosylase	102	0.941	87665	N.E.
FTL_1544	isftu1	transposase	100	1	104882	N.E.
FTL_1545	-	glutamine amidotransferase subunit PdxT	60	0.95	54495	N.E.
FTL_1546	-	pyridoxal biosynthesis lyase PdxS	66	1	81131	N.E.
FTL_1547	-	DNA gyrase subunit B	240	0.017	211	E
FTL_1548	-	hypothetical protein	76	0.961	46189	N.E.
FTL_1549	-	tRNA-dihydrouridine synthase A	112	0.973	85239	N.E.
FTL_1550	-	lipoprotein	83	0.976	78310	N.E.
FTL_1551	-	hypothetical protein	35	0.971	39327	N.E.
FTL_1552	-	hypothetical protein	218	0.972	192788	N.E.
FTL_1553	sucC	succinyl-CoA synthetase subunit beta	101	0.337	187	E
FTL_1554	sucD	succinyl-CoA synthetase, alpha subunit	87	0.31	194	E
FTL_1555	-	hypothetical protein	47	1	53931	N.E.
FTL_1556	-	hypothetical protein	131	0.962	113764	N.E.
FTL_1557	-	hypothetical protein	81	0.988	73258	N.E.
FTL_1558	-	hypothetical protein	71	0.972	66980	N.E.
FTL_1559	-	-	73	0.973	67676	N.E.
FTL_1560	-	-	46	0.978	38536	N.E.
FTL_1561	-	-	46	1	44459	N.E.
FTL_1562	-	-	70	0.986	84519	N.E.
FTL_1563	-	-	28	1	19786	N.E.
FTL_1564	-	-	23	0.957	23293	N.E.
FTL_1565	-	-	41	0.951	40387	N.E.
FTL_1566	-	CutC family protein	70	0.986	52794	N.E.
FTL_1567	-	major facilitator transporter	131	0.969	171808	N.E.
FTL_1568	-	LysR family transcriptional regulator	113	0.973	110797	N.E.
FTL_1569	-	phosphoglycolate phosphatase	79	0.949	64880	N.E.
FTL_1570	-	phospholipase D	133	0.97	111614	N.E.
FTL_1571	-	thioredoxin reductase	94	0.968	86978	N.E.
FTL_1572	isftu2	transposase	82	1	61249	N.E.
FTL_1573	-	major facilitator transporter	108	0.972	80077	N.E.
FTL_1574	-	hypothetical protein	55	0.927	55625	N.E.
FTL_1575	-	hypothetical protein	111	0.973	99656	N.E.
FTL_1576	-	DNA mismatch repair protein	176	0.983	171632	N.E.
FTL_1577	-	hypothetical protein	36	0.889	37522	N.E.
FTL_1578	-	hypothetical protein	32	1	37638	N.E.
FTL_1579	-	hypothetical protein	63	0.032	1020	E
FTL_1580	-	hypothetical protein	93	0.968	74682	N.E.
FTL_1581	-	lipoprotein	69	1	78437	N.E.
FTL_1582	potF	putrescine-binding periplasmic protein	148	0.473	9072	E
FTL_1583	gadC	glutamate:gamma-aminobutyric acid antiporter family protein, putative glutamate transporter	160	0.106	1125	E
FTL_1584	perM	PerM family protein	137	0.942	12633	N.E.
FTL_1585	-	single-stranded-DNA-specific exonuclease	176	0.949	86362	N.E.
FTL_1586	-	biotin--acetyl-CoA-carboxylase ligase	91	0.099	1740	E
FTL_1587	-	lysyl-tRNA synthetase	102	0.941	62495	N.E.
FTL_1588	-	mechanosensitive ion channel protein	80	0.988	70094	N.E.
FTL_1589	isftu2	transposase	90	1	72829	N.E.
FTL_1590	-	hypothetical protein	98	0.929	50393	N.E.

FTL_1591	accC	Acetyl-CoA carboxylase, biotin carboxylase subunit	122	0.016	355	E
FTL_1592	accB	Acetyl-CoA carboxylase, biotin carboxyl carrier protein subunit	35	0	0	E
FTL_1593	aroD	3-dehydroquinate dehydratase	55	0.564	9613	E and N.E.
FTL_1594	apaH	diadenosine tetraphosphatase	91	0.945	44359	N.E.
FTL_1595	ksgA	dimethyladenosine transferase	78	0.974	66346	N.E.
FTL_1596	surA	peptidyl-prolyl cis-trans isomerase	135	0.052	1574	E
FTL_1597	-	organic solvent tolerance protein	305	0.361	53945	E and N.E.
FTL_1598	argS	arginyl-tRNA synthetase	154	0.032	877	E
FTL_1599	-	hypothetical protein	43	0.977	64722	N.E.
FTL_1600	-	periplasmic L-asparaginase II	103	0.961	100003	N.E.
FTL_1601	-	tRNA/rRNA methyltransferase	53	0.962	50743	N.E.
FTL_1602	-	delta-aminolevulinic acid dehydratase	82	0.012	665	E
FTL_1603	-	RNA-binding protein	24	0.042	5	E
FTL_1604	-	DNA polymerase III, delta prime subunit	104	0.019	18	E
FTL_1605	-	putative periplasmic protease	111	0.486	2991	E and N.E.
FTL_1606	sspA	stringent starvation protein A	59	0.153	182	E
FTL_1607	-	anaerobic sulfite reductase subunit	33	0.121	786	E
FTL_1608	-	hypothetical protein	20	1	12030	N.E.
FTL_1609	-	dolichyl-phosphate-mannose-protein mannosyltransferase family protein	216	0.977	214446	N.E.
FTL_1610	isftu1	transposase	100	1	91925	N.E.
FTL_1611	-	glycosyl transferase family protein	97	0.979	99293	N.E.
FTL_1612	nadX	hypothetical protein, N-acetylhexosamine deacetylase	90	0.967	80021	N.E.
FTL_1613	ftsW	cell division protein FtsW	121	0.116	4823	E
FTL_1614	murD	UDP-N-acetylmuramoylalanine--D-glutamate ligase	152	0.02	165	E
FTL_1615	mraY	phospho-N-acetylmuramoyl-pentapeptide-transferase	110	0.009	3	E
FTL_1616	pckA	phosphoenolpyruvate carboxykinase	164	0.671	1769	E and N.E.
FTL_1617	glnS	glutaminyl-tRNA synthetase	145	0.021	236	E
FTL_1618	-	hypothetical protein	77	0.987	79181	N.E.
FTL_1619	-	hypothetical protein	105	0.952	81253	N.E.
FTL_1620	-	proton-dependent oligopeptide transport (POT) family protein	61	1	54843	N.E.
FTL_1621	-	ABC transporter ATP-binding	181	0.989	141110	N.E.
FTL_1622	-	multidrug transporter (tetracycline resistance protein)	131	0.962	122231	N.E.
FTL_1623	-	hypothetical protein	138	0.949	138974	N.E.
FTL_1624	-	major facilitator transporter	133	0.992	144058	N.E.
FTL_1625	-	NADH dehydrogenase subunit	90	0.967	78832	N.E.
FTL_1626	-	rRNA methylase	25	1	33643	N.E.
FTL_1627	isftu1	transposase	100	1	107329	N.E.
FTL_1628	-	hypothetical protein	73	0.973	70514	N.E.
FTL_1629	-	hypothetical protein	200	0.985	241778	N.E.
FTL_1630	isftu1	transposase	100	1	92706	N.E.
FTL_1631	-	hypothetical protein	148	0.98	149133	N.E.
FTL_1632	-	hypothetical protein	28	0.964	26271	N.E.
FTL_1633	-	hypothetical protein	94	0.968	93183	N.E.
FTL_1634	-	LysR family transcriptional regulator	113	0.965	117454	N.E.

FTL_1635	-	chitinase, fragment	226	0.987	237065	N.E.
FTL_1636	-	hypothetical protein	24	0.958	23073	N.E.
FTL_1637	-	lipoprotein	106	0.991	116906	N.E.
FTL_1638	-	3-demethylubiquinone-9 3-methyltransferase	76	0.092	331	E
FTL_1639	-	hypothetical protein	91	0.923	25371	N.E.
FTL_1640	-	amino acid transporter protein, fragment	181	0.983	186714	N.E.
FTL_1641	-	hypothetical protein	37	0.892	22872	N.E.
FTL_1642	-	hypothetical protein	32	1	26738	N.E.
FTL_1643	isftu1	transposase	99	1	108126	N.E.
FTL_1644	-	glycerol kinase	135	0.985	154866	N.E.
FTL_1645	ansP	major facilitator transporter, asparagine transporter	137	0.971	132692	N.E.
FTL_1646	-	hypothetical protein	63	0.968	51666	N.E.
FTL_1647	-	major facilitator transporter	144	0.972	139477	N.E.
FTL_1648	-	oligopeptide transporter, subunit D, ABC transporter ATP-binding protein	72	0.972	92903	N.E.
FTL_1649	-	-	56	0.946	67581	N.E.
FTL_1650	-	-	26	0.962	37242	N.E.
FTL_1651	-	-	81	0.988	84968	N.E.
FTL_1652	-	-	29	1	22368	N.E.
FTL_1653	-	peptide transport system substrate-binding protein	38	0.947	44687	N.E.
FTL_1654	-	hypothetical protein	130	0.985	133817	N.E.
FTL_1655	isftu2	transposase	76	1	63067	N.E.
FTL_1656	uvrD	DNA helicase II	227	0.974	146978	N.E.
FTL_1657	ftsY	signal recognition particle receptor FtsY	87	0.034	713	E
FTL_1658	fimV	hypothetical protein	123	0	0	E
FTL_1659	prfC	peptide chain release factor 3	121	0.983	82392	N.E.
FTL_1660	tmk	thymidylate kinase	63	0.048	157	E
FTL_1661	-	nucleoside permease NUP family protein	145	0.938	139032	N.E.
FTL_1662	nupC1	nucleoside permease NUP family protein	142	0.979	100391	N.E.
FTL_1663	deoC	deoxyribose-phosphate aldolase	68	0.971	58179	N.E.
FTL_1664	deoB	phosphopentomutase	109	0.972	91565	N.E.
FTL_1665	-	pantothenate kinase	82	1	79032	N.E.
FTL_1666	-	DNA polymerase I	263	0.7	115596	E and N.E.
FTL_1667	lpxK	tetraacyldisaccharide 4'-kinase	105	0.029	8	E
FTL_1668	msbA	lipid A transport protein ABC transporter ATP-binding protein/permease	188	0.032	37	E
FTL_1669	-	tRNA CCA-pyrophosphorylase	109	0.972	99007	N.E.
FTL_1670	dsbB	disulfide bond formation protein	60	0.917	49797	N.E.
FTL_1671	-	RND efflux transporter	132	0.985	119460	N.E.
FTL_1672	-	AcrB/AcrD/AcrF family transporter	324	0.988	308712	N.E.
FTL_1673	-	major facilitator transporter	147	0.98	158341	N.E.
FTL_1674	-	hypothetical protein	76	0.974	74144	N.E.
FTL_1675	-	-	16	0.938	11268	N.E.
FTL_1676	-	-	24	1	20477	N.E.
FTL_1677	-	-	31	1	19872	N.E.
FTL_1678	-	hypothetical protein	142	0.944	114243	N.E.
FTL_1679	-	transposase	34	0.941	24075	N.E.
FTL_1680	isftu2	transposase	79	0.987	64063	N.E.
FTL_1681	isftu1	transposase	100	1	106227	N.E.
FTL_1682	-	hypothetical protein	35	1	40295	N.E.
FTL_1683	cysS	cysteinyl-tRNA synthetase	120	0.017	1253	E

FTL_1684	-	N5-glutamine S-adenosyl-L-methionine-dependent methyltransferase	101	0.99	92986	N.E.
FTL_1685	-	major facilitator transporter	133	0.962	120238	N.E.
FTL_1686	-	acetyltransferase	57	1	51222	N.E.
FTL_1687	isftu1	transposase	100	1	107800	N.E.
FTL_1688	-	-	31	0.871	28437	N.E.
FTL_1689	-	hypothetical protein	109	0.954	109503	N.E.
FTL_1690	-	hypothetical protein	111	0.973	121795	N.E.
FTL_1691	-	hypothetical protein	27	0.963	23879	N.E.
FTL_1692	-	hypothetical protein	34	1	34941	N.E.
FTL_1693	-	hypothetical protein	49	0.939	30594	N.E.
FTL_1694	-	hypothetical protein	166	0.94	144351	N.E.
FTL_1695	-	hypothetical protein	100	0.95	108197	N.E.
FTL_1696	-	hypothetical protein	32	0.938	23515	N.E.
FTL_1697	-	metal ion transporter	55	0.945	52801	N.E.
FTL_1698	-	hypothetical protein	38	0.974	43795	N.E.
FTL_1699	-	hypothetical protein	187	0.968	223730	N.E.
FTL_1700	-	Sodium/proline permease	152	0.046	2146	E
FTL_1701	glpX	fructose 1,6-bisphosphatase II	82	0.988	64727	N.E.
FTL_1702	-	hypothetical protein	69	0.928	53158	N.E.
FTL_1703	lysP	lysine:H+ symporter	158	0.044	1592	E
FTL_1704	-	hypothetical protein	60	0.067	3265	E
FTL_1705	ftsK	cell division protein	221	0.05	48	E
FTL_1706	lolA	lipoprotein releasing system subunit A, outer membrane lipoproteins carrier	66	0.106	1131	E
FTL_1707	-	hypothetical protein	19	0.474	2383	E and N.E.
FTL_1708	tkrH	potassium uptake protein	154	0.039	43	E
FTL_1709	-	hypothetical protein	58	1	57345	N.E.
FTL_1710	-	ProP osmoprotectant transporter, fragment	68	0.971	19116	N.E.
FTL_1711	-	HsdR protein, fragment	52	0.942	45442	N.E.
FTL_1712	-	HsdR protein, fragment	83	0.988	96731	N.E.
FTL_1713	isftu1	transposase	100	1	107638	N.E.
FTL_1714	groEL	chaperonin GroEL	150	0.02	1129	E
FTL_1715	groES	co-chaperonin GroES	26	0	0	E
FTL_1716	-	hypothetical protein	56	0.964	65905	N.E.
FTL_1717	-	hypothetical protein	83	0.94	66984	N.E.
FTL_1718	isftu1	transposase	100	1	91878	N.E.
FTL_1719	-	hypothetical protein	53	1	51206	N.E.
FTL_1720	-	modification methylase	102	0.039	1141	E
FTL_1721	prfA	peptide chain release factor 1	81	0.012	6	E
FTL_1722	-	glutamyl-tRNA reductase	133	0.015	125	E
FTL_1723	-	hypothetical protein	70	0.971	63908	N.E.
FTL_1724	-	lipoprotein	155	0.987	152510	N.E.
FTL_1725	-	eflux protein	133	0.977	165746	N.E.
FTL_1726	parE	DNA topoisomerase IV subunit B	168	0.976	55923	N.E.
FTL_1727	ampD	N-acetyl-anhydromuranmyl-L-alanine amidase	51	0.804	3714	N.E.
FTL_1728	-	PAP2 family protein	88	0.943	72507	N.E.
FTL_1729	nudH	dinucleoside polyphosphate hydrolase	45	0.956	8392	N.E.
FTL_1730	-	hypothetical protein	170	0.994	157242	N.E.
FTL_1731	-	licB-like transmembrane protein	112	0.964	128654	N.E.
FTL_1732	-	acid phosphatase	67	0.94	63276	N.E.
FTL_1733	-	oxidoreductase iron/ascorbate family protein	82	1	109867	N.E.
FTL_1734	-	integrase/recombinase	83	0.904	5272	N.E.

FTL_1735	rplS	50S ribosomal protein L19	33	0.03	47	E
FTL_1736	trmD	tRNA (guanine-N(1)-)-methyltransferase	80	0.013	5	E
FTL_1737	rimM	16S rRNA-processing protein RimM	56	0.089	1845	E
FTL_1738	rpsP	30S ribosomal protein S16	21	0.048	2	E
FTL_1739	-	S-adenosylmethionine synthetase	108	0.056	3008	E
FTL_1740	-	fatty acid desaturase	133	0.331	6768	E and N.E.
FTL_1741	-	putative DNA-binding/iron metalloprotein/AP endonuclease	105	0.038	1196	E
FTL_1742	-	hypothetical protein	33	0.152	625	E
FTL_1743	-	DNA-directed RNA polymerase subunit beta	415	0.043	8884	E
FTL_1744	rpoB	DNA-directed RNA polymerase subunit beta	382	0.013	18	E
FTL_1745	rplL	50S ribosomal protein L7/L12	25	0	0	E
FTL_1746	rplJ	50S ribosomal protein L10	39	0	0	E
FTL_1747	rplA	50S ribosomal protein L1	59	0.034	6	E
FTL_1748	rplK	50S ribosomal protein L11	42	0	0	E
FTL_1749	-	transcription antitermination protein nusG	34	0	0	E
FTL_1750	secE	preprotein translocase subunit SecE	41	0.024	2	E
FTL_1751	-	elongation factor Tu	97	0.01	75	E
FTL_1752	-	helicase	122	0.959	135532	N.E.
FTL_1753	-	ion channel protein, fragment	49	0.898	3351	N.E.
FTL_1754	-	hypothetical protein	95	1	67091	N.E.
FTL_1755	glpF	glycerol uptake facilitator protein	79	0.949	129687	N.E.
FTL_1756	glpD	anaerobic glycerol-3-phosphate dehydrogenase	149	0.624	6468	E and N.E.
FTL_1757	isftu1	transposase	97	1	106837	N.E.
FTL_1758	-	hypothetical protein	34	1	41017	N.E.
FTL_1759	-	hypothetical protein	154	0.968	179420	N.E.
FTL_1760	-	hypothetical protein	59	1	92953	N.E.
FTL_1761	-	hypothetical protein	35	0.971	39893	N.E.
FTL_1762	qseC	sensor histidine kinase	143	0.993	85251	N.E.
FTL_1763	-	hypothetical protein	102	0.99	117132	N.E.
FTL_1764	-	-	116	0.948	147211	N.E.
FTL_1765	-	cytochrome oxidase bd-II subunit II	123	0.967	128186	N.E.
FTL_1766	-	hypothetical protein	69	0.986	60426	N.E.
FTL_1767	-	-	27	1	26753	N.E.
FTL_1768	-	-	16	1	14287	N.E.
FTL_1769	-	-	49	0.959	50917	N.E.
FTL_1770	-	Type IV pili nucleotide-binding protein	56	1	84602	N.E.
FTL_1771	-	twitching motility protein PilT	33	0.97	28926	N.E.
FTL_1772	-	aconitate hydratase	261	0.054	15008	E
FTL_1773	-	hypothetical protein	76	0.908	65567	N.E.
FTL_1774	-	hypothetical protein	51	0.961	48005	N.E.
FTL_1775	-	oxygen-independent coproporphyrinogen III oxidase	114	0.974	99537	N.E.
FTL_1776	-	hypothetical protein	54	1	70181	N.E.
FTL_1777	-	-	43	0.977	54447	N.E.
FTL_1778	-	-	66	1	71905	N.E.
FTL_1779	secG	preprotein translocase subunit SecG	37	0.405	2029	E and N.E.
FTL_1780	-	triosephosphate isomerase	77	0.039	13	E
FTL_1781	glmM	phosphoglucosamine mutase	122	0.008	2	E
FTL_1782	apt	adenine phosphoribosyltransferase	43	0.674	5670	N.E.
FTL_1783	sucB	dihydrolipoamide succinyltransferase component of 2-oxoglutarate dehydrogenase complex	131	0.008	3	E

FTL_1784	sucA	2-oxoglutarate dehydrogenase E1 component	269	0.007	5	E
FTL_1785	sdhB	succinate dehydrogenase iron-sulfur subunit	68	0.015	3	E
FTL_1786	-	succinate dehydrogenase, catalytic and NAD/flavoprotein subunit	151	0	0	E
FTL_1787	-	succinate dehydrogenase hydrophobic membrane anchor protein	36	0.028	19	E
FTL_1788	-	succinate dehydrogenase, cytochrome b556	40	0	0	E
FTL_1789	-	citrate synthase	109	0.009	20	E
FTL_1790	ampG	major facilitator superfamily transporter	151	0.861	8959	N.E.
FTL_1791	-	superoxide dismutase	53	0.019	522	E
FTL_1792	-	glutaredoxin-like protein	26	0.962	4149	N.E.
FTL_1793	-	hypothetical protein	327	0.976	374871	N.E.
FTL_1794	atpC	F0F1 ATP synthase subunit epsilon	39	0.308	9087	E and N.E.
FTL_1795	-	F0F1 ATP synthase subunit beta	130	0.008	419	E
FTL_1796	-	F0F1 ATP synthase subunit gamma	89	0.034	11	E
FTL_1797	-	F0F1 ATP synthase subunit alpha	128	0.039	175	E
FTL_1798	-	F0F1 ATP synthase subunit delta	52	0.019	6	E
FTL_1799	-	F0F1 ATP synthase subunit B	43	0.023	2	E
FTL_1800	-	F0F1 ATP synthase subunit C	25	0	0	E
FTL_1801	-	F0F1 ATP synthase subunit A	69	0.058	11	E
FTL_1802	-	hypothetical protein	49	0.653	4016	E and N.E.
FTL_1803	ileP	major facilitator transporter, isoleucine transporter	134	0.948	13239	N.E.
FTL_1804	-	ribosomal large subunit pseudouridine synthase C	91	0.978	75971	N.E.
FTL_1805	-	ATPase	112	0.964	46063	N.E.
FTL_1806	fptD	major facilitator transporter, member of Fpt (Francisella phagosomal transporter) subfamily	145	0.834	7555	N.E.
FTL_1807	hisS	histidyl-tRNA synthetase	124	0.016	51	E
FTL_1808	-	ribosome-binding factor A	48	0.021	2	E
FTL_1809	infB	translation initiation factor IF-2	203	0.01	11	E
FTL_1810	nusA	transcription elongation factor NusA	131	0.023	112	E
FTL_1811	-	hypothetical protein	40	0	0	E
FTL_1812	hemE	uroporphyrinogen decarboxylase	105	0.029	768	E
FTL_1813	-	-	25	0.72	9168	E and N.E.
FTL_1814	-	-	100	0.99	107974	N.E.
FTL_1815	isftu1	transposase	100	1	92002	N.E.
FTL_1816	-	-	16	0.062	673	E
FTL_1817	-	NADH dehydrogenase I subunit N	153	0.046	5815	E
FTL_1818	-	NADH dehydrogenase I subunit M	154	0.006	3	E
FTL_1819	-	NADH dehydrogenase I subunit L	211	0.009	96	E
FTL_1820	-	NADH dehydrogenase I subunit K	36	0.028	2	E
FTL_1821	-	NADH dehydrogenase I subunit J	65	0.015	2	E
FTL_1822	-	NADH dehydrogenase subunit I	46	0.022	3	E
FTL_1823	-	NADH dehydrogenase I subunit H	112	0.027	104	E
FTL_1824	-	NADH dehydrogenase subunit G	224	0.009	153	E
FTL_1825	-	NADH dehydrogenase I subunit F	114	0.018	8	E
FTL_1826	-	NADH dehydrogenase I subunit E	45	0	0	E
FTL_1827	-	NADH dehydrogenase subunit D	100	0.01	96	E
FTL_1828	-	NADH dehydrogenase I	51	0.02	2	E
FTL_1829	-	NADH dehydrogenase subunit B	42	0	0	E

FTL_1830	-	NADH dehydrogenase I subunit A	33	0	0	E
FTL_1831	fur	ferric uptake regulation protein	35	0.971	6518	N.E.
FTL_1832	fslA	hypothetical protein	198	0.99	262225	N.E.
FTL_1833	fslB	hypothetical protein	160	0.825	8172	N.E.
FTL_1834	fslC	diaminopimelate decarboxylase	131	0.977	124765	N.E.
FTL_1835	fslD	hypothetical protein	139	0.978	156485	N.E.
FTL_1836	fslE	hypothetical protein	166	0.982	214684	N.E.
FTL_1837	fslF	hypothetical protein	47	0.979	37170	N.E.
FTL_1838	-	hypothetical protein	28	0.964	49980	N.E.
FTL_1839	-	lipase/acyltransferase	61	1	62158	N.E.
FTL_1840	-	hypothetical protein	46	1	55165	N.E.
FTL_1841	gatB	aspartyl/glutamyl-tRNA amidotransferase subunit B	125	0.04	716	E
FTL_1842	gatA	aspartyl/glutamyl-tRNA amidotransferase subunit A	140	0.029	12	E
FTL_1843	-	Glu-tRNAGln amidotransferase C subunit	23	0	0	E
FTL_1844	-	secretion protein	52	0.981	80425	N.E.
FTL_1845	-	RND efflux membrane fusion protein	43	1	51056	N.E.
FTL_1846	-	hypothetical protein	57	1	49265	N.E.
FTL_1847	-	toxin secretion ABC transporter ATP-binding protein	53	0.981	68192	N.E.
FTL_1848	-	hypothetical protein	51	0.941	49398	N.E.
FTL_1849	-	hypothetical protein	63	0.937	69044	N.E.
FTL_1850	purB	adenylosuccinate lyase	114	0.088	1161	E
FTL_1851	isftu2	transposase	76	1	61603	N.E.
FTL_1852	-	hypothetical protein	49	0.98	51462	N.E.
FTL_1853	-	lipoprotein	98	0.98	116850	N.E.
FTL_1854	-	hypothetical protein	90	0.967	117617	N.E.
FTL_1855	-	-	60	0.983	71880	N.E.
FTL_1856	-	-	25	1	31905	N.E.
FTL_1857	-	-	23	0.913	27541	N.E.
FTL_1858	-	-	34	1	45064	N.E.
FTL_1859	-	-	18	1	24403	N.E.
FTL_1860	purL	phosphoribosylformylglycinamidine synthase	305	0.984	126852	N.E.
FTL_1861	purF	amidophosphoribosyltransferase	134	0.97	53533	N.E.
FTL_1862	-	hypothetical protein	17	1	18109	N.E.
FTL_1863	-	glutamate decarboxylase	84	0.976	111983	N.E.
FTL_1864	-	hypothetical protein	62	0.145	4526	E
FTL_1865	-	outer membrane protein tolC	149	0.805	23860	E and N.E.
FTL_1866	-	protein-L-isoaspartate O-methyltransferase	71	0.958	31280	N.E.
FTL_1867	-	protease yegQ	111	0.973	130256	N.E.
FTL_1868	-	multidrug resistance protein, membrane located	115	0.991	179208	N.E.
FTL_1869	-	Na+/H+ antiporter	158	0.032	3239	E
FTL_1870	-	-	29	1	27376	N.E.
FTL_1871	-	-	110	0.955	115709	N.E.
FTL_1872	-	-	39	0.923	40633	N.E.
FTL_1873	-	amino acid transporter	192	0.036	1102	E
FTL_1874	obgE	GTPase ObgE	92	0.033	17	E
FTL_1875	-	aromatic amino acid HAAP transporter	155	0.948	141653	N.E.
FTL_1876	-	outer membrane associated protein, fragment	44	0.977	64526	N.E.
FTL_1877	-	-	41	0.976	40267	N.E.
FTL_1878	-	two component sensor protein kdpD	162	0.975	191842	N.E.
FTL_1879	-	osmosensitive K+ channel His kinase sensor	108	0.991	132211	N.E.

FTL_1880	-	potassium-transporting ATPase C chain	61	0.984	60242	N.E.
FTL_1881	-	haloacid dehalogenase-like hydrolase	98	0.949	95871	N.E.
FTL_1882	-	potassium-transporting ATPase B chain	107	1	115717	N.E.
FTL_1883	-	potassium-transporting ATPase subunit A	200	0.99	305536	N.E.
FTL_1884	-	hypothetical protein	15	1	19377	N.E.
FTL_1885	isftu2	transposase	91	1	91516	N.E.
FTL_1886	isftu1	transposase	94	1	88404	N.E.
FTL_1887	-	3-isopropylmalate dehydrogenase	42	1	53281	N.E.
FTL_1888	leuD	isopropylmalate isomerase small subunit	55	0.982	53426	N.E.
FTL_1889	-	isopropylmalate isomerase large subunit	135	0.956	198257	N.E.
FTL_1890	-	-	30	1	27462	N.E.
FTL_1891	isftu1	transposase	100	1	107523	N.E.
FTL_1892	-	hypothetical protein	143	0.993	160806	N.E.
FTL_1893	-	-	14	1	13642	N.E.
FTL_1894	-	transposase	64	1	56407	N.E.
FTL_1895	-	-	26	0.962	46514	N.E.
FTL_1896	-	hypothetical protein	151	0.974	196456	N.E.
FTL_1897	-	outer membrane lipoprotein	62	0.984	70885	N.E.
FTL_1898	-	DNA polymerase III subunit delta	92	0.022	131	E
FTL_1899	-	glutamine synthetase	95	0.032	1060	E
FTL_1900	-	L-glutaminase	149	0.966	196276	N.E.
FTL_1901	-	hypothetical protein	112	0.964	120850	N.E.
FTL_1902	-	hypothetical protein	64	0.984	61128	N.E.
FTL_1903	-	lysyl-tRNA synthetase	155	0.019	312	E
FTL_1904	-	peptide chain release factor 2	75	0	0	E
FTL_1905	-	DNA polymerase III subunit gamma and tau	166	0.042	3628	E
FTL_1906	lpxC	UDP-3-O-[3-hydroxymyristoyl] N-acetylglucosamine deacetylase	76	0.026	1305	E
FTL_1907	-	cell division protein FtsZ	92	0.033	7	E
FTL_1908	-	cell division protein FtsA	120	0.042	17	E
FTL_1909	-	cell division protein FtsQ	85	0.082	2835	E
FTL_1910	-	D-alanyl-alanine synthetase A	69	0.014	6	E
FTL_1911	tadA	zinc-binding domain-containing protein (likely adenosine deaminase)	39	0.718	1175	N.E.
FTL_1912	rpsA	30S ribosomal protein S1	135	0.178	4104	E and N.E.
FTL_1913	-	Sua5/YciO/YrdC family protein	72	0.028	2387	E
FTL_1914	ripA	hypothetical protein	65	0.969	22832	N.E.
FTL_1915	-	putative acyltransferase	98	0.888	12979	E and N.E.
FTL_1916	-	competence-like protein	257	0.992	282440	N.E.
FTL_1917	-	30S ribosomal protein S6	104	0.942	111314	N.E.
FTL_1918	-	30S ribosomal protein S6 modification protein-like protein	34	0.941	36467	N.E.
FTL_1919	-	-	112	0.982	142965	N.E.
FTL_1920	-	-	53	1	68104	N.E.
FTL_1921	-	ABC transporter ATP-binding protein	73	1	85198	N.E.
FTL_1922	-	YggT family protein	70	0.914	82960	N.E.
FTL_1923	-	hypothetical protein	79	0.975	119411	N.E.
FTL_1924	-	-	61	0.967	71451	N.E.
FTL_1925	isftu1	transposase	100	1	91595	N.E.
FTL_1926	isftu2	transposase	57	1	46464	N.E.
FTL_1927	-	-	20	1	23368	N.E.
FTL_1928	-	-	76	0.987	95315	N.E.

FTL_1929	purH	bifunctional phosphoribosylaminoimidazolecarboxamide formyltransferase/IMP cyclohydrolase	127	0.961	62371	N.E.
FTL_1930	purA	adenylosuccinate synthetase	121	0.967	10393	N.E.
FTL_1931	-	hypoxanthine-guanine phosphoribosyltransferase	56	0.964	2425	N.E.
FTL_1932	-	-	18	1	20540	N.E.
FTL_1933	-	-	56	0.982	71638	N.E.
FTL_1934	-	ABC transporter permease	101	0.98	121778	N.E.
FTL_1935	-	ABC transporter ATP-binding protein	71	0.972	72760	N.E.
FTL_1936	-	periplasmic solute binding family protein	93	0.989	101194	N.E.
FTL_1937	-	-	44	0.977	44781	N.E.
FTL_1938	-	-	100	0.98	115144	N.E.
FTL_1939	-	outer membrane lipoprotein	49	0.98	68281	N.E.
FTL_1940	-	trp repressor binding protein	57	0.07	1491	E
FTL_1941	-	tRNA processing ribonuclease BN	140	0.936	147951	N.E.
FTL_1942	-	transporter	71	0.958	21275	N.E.
FTL_1943	-	primosomal protein N'	243	0.794	6861	E and N.E.
FTL_1944	isftu1	transposase	100	1	107751	N.E.
FTL_1945	-	hypothetical protein	29	0.931	28521	N.E.
FTL_1946	-	hypothetical protein	33	1	29191	N.E.
FTL_1947	-	putative ABC transporter ATP-binding protein	151	0.987	175560	N.E.
FTL_1948	-	major facilitator transporter	175	0.983	191494	N.E.
FTL_1949	-	hypothetical protein	31	0.968	22809	N.E.
FTL_1950	-	hypothetical protein	105	0.981	90286	N.E.
FTL_1951	-	amino acid transporter LysE	36	0.944	39267	N.E.
FTL_1952	-	-	39	0.974	46991	N.E.
FTL_1953	-	-	25	0.96	29453	N.E.
FTL_1954	-	hypothetical protein	50	0.98	50563	N.E.
FTL_1955	-	-	52	1	38088	N.E.
FTL_1956	pepN	aminopeptidase N	271	0.982	194385	N.E.
FTL_1957	-	heat shock protein	55	0.964	49422	N.E.
FTL_1958	-	bifunctional indole-3-glycerol phosphate synthase/phosphoribosylanthranilate isomerase	143	0.972	94604	N.E.
FTL_1959	-	hypothetical protein	19	1	27628	N.E.
FTL_1960	-	peptide methionine sulfoxide reductase MsrA	90	0.978	87657	N.E.
FTL_1961	-	hypothetical protein	33	0.97	23411	N.E.
FTL_1962	-	hypothetical protein	35	0.971	46393	N.E.
FTL_1963	-	hypothetical protein	40	0.975	38145	N.E.
FTL_1964	-	-	127	0.984	137372	N.E.
FTL_1965	-	-	81	0.988	82700	N.E.
FTL_1966	-	anthranilate synthase component I	175	0.977	165631	N.E.
FTL_1967	-	trp operon repressor	37	0.946	30691	N.E.
FTL_1968	-	ribonuclease G	169	0.97	151662	N.E.
FTL_R0001	ssrA	-	39	0.051	6	E
FTL_R0002	-	-	10	0.1	3	E
FTL_R0003	-	16S ribosomal RNA	85	0.988	122887	N.E.
FTL_R0004	tRNA-Ile1	Ile tRNA	5	1	1965	N.E.
FTL_R0005	tRNA-Ala1	Ala tRNA	1	1	1103	N.E.
FTL_R0006	-	23S ribosomal RNA	200	0.995	197419	N.E.

FTL_R0007	-	5S ribosomal RNA	6	1	4463	N.E.
FTL_R0008	tRNA-Gln1	Gln tRNA	3	0	0	E
FTL_R0009	tRNA-Glu1	Glu tRNA	3	0	0	E
FTL_R0010	rnpB	-	22	0.136	61	E
FTL_R0011	tRNA-Gly3	Gly tRNA	2	1	1199	N.E.
FTL_R0012	tRNA-Arg3	Arg tRNA	6	0	0	E
FTL_R0013	tRNA-Ser1	Ser tRNA	4	0.5	3764	N.E.
FTL_R0014	tRNA-Ser2	Ser tRNA	5	0.2	3	E
FTL_R0015	tRNA-Val1	Val tRNA	2	1	3788	N.E.
FTL_R0016	-	16S ribosomal RNA	85	0.988	122299	N.E.
FTL_R0017	tRNA-Ile2	Ile tRNA	5	1	1984	N.E.
FTL_R0018	tRNA-Ala2	Ala tRNA	1	1	1045	N.E.
FTL_R0019	-	23S ribosomal RNA	200	0.995	197656	N.E.
FTL_R0020	-	5S ribosomal RNA	6	1	4398	N.E.
FTL_R0021	tRNA-Met3	Met tRNA	7	0	0	E
FTL_R0022	tRNA-Leu1	Leu tRNA	1	1	1084	N.E.
FTL_R0023	tRNA-Asn1	Asn tRNA	3	0	0	E
FTL_R0024	tRNA-Gly1	Gly tRNA	2	0	0	E
FTL_R0025	tRNA-Cys1	Cys tRNA	2	0	0	E
FTL_R0026	tRNA-Leu2	Leu tRNA	3	0	0	E
FTL_R0027	-	-	9	1	5541	N.E.
FTL_R0028	-	16S ribosomal RNA	85	0.988	123138	N.E.
FTL_R0029	tRNA-Ile3	Ile tRNA	5	1	1928	N.E.
FTL_R0030	tRNA-Ala3	Ala tRNA	1	1	1092	N.E.
FTL_R0031	-	23S ribosomal RNA	200	0.995	197654	N.E.
FTL_R0032	-	5S ribosomal RNA	6	1	4333	N.E.
FTL_R0033	tRNA-Val2	Val tRNA	6	1	3815	N.E.
FTL_R0034	tRNA-Ser3	Ser tRNA	1	0	0	N.E.
FTL_R0035	tRNA-Leu4	Leu tRNA	2	0	0	E
FTL_R0036	tRNA-His1	His tRNA	2	0	0	E
FTL_R0037	tRNA-Arg2	Arg tRNA	4	0	0	E
FTL_R0038	tRNA-Pro1	Pro tRNA	2	0	0	E
FTL_R0039	tRNA-Phe1	Phe tRNA	2	0	0	E

FTL_R0040	tRNA-Lys1	Lys tRNA	5	0	0	E
FTL_R0041	tRNA-Val3	Val tRNA	2	0.5	2	N.E.
FTL_R0042	tRNA-Met1	Met tRNA	6	0	0	E
FTL_R0043	tRNA-Arg1	Arg tRNA	4	0.75	3190	N.E.
FTL_R0044	ffs	-	3	0	0	E
FTL_R0045	tRNA-Trp1	Trp tRNA	3	0	0	E
FTL_R0046	tRNA-Thr2	Thr tRNA	2	0	0	E
FTL_R0047	tRNA-Gly2	Gly tRNA	3	0	0	E
FTL_R0048	tRNA-Tyr1	Tyr tRNA	1	0	0	N.E.
FTL_R0049	tRNA-Leu3	Leu tRNA	2	1	79	N.E.
FTL_R0050	tRNA-Met2	Met tRNA	4	0	0	E
FTL_R0051	tRNA-Asp1	Asp tRNA	3	0	0	E
FTL_R0052	tRNA-Thr1	Thr tRNA	5	0	0	E
FTL_R0053	-	5S ribosomal RNA	4	1	5610	N.E.

Appendix 2

Locus Tag	Locus	Protein Name	# of TA sites used	MWU (p-value)	Ave. FC	log2FC	Ave Reads (ino.)	Reads (Out.)	FC < LOD ?
FTL_0010	*glpe*	thiosulfate sulfurtransferase	46.48	5.92E-08	0.26	**-1.96**	1573	403	-
FTL_0015	*ackA*	propionate kinase	119	9.13E-09	0.48	**-1.06**	32797	15737	-
FTL_0016	*pta*	phosphate acetyltransferase	209.82	9.24E-18	0.45	**-1.15**	51379	23143	-
FTL_0033	*pyrC*	dihydroorotase	66.72	1.80E-19	0.28	**-1.83**	735	206	-
FTL_0046	-	diyroorotate dehydrogenase	76.46	2.13E-10	0.37	**-1.44**	5407	1997	-
FTL_0057	-	hypothetical protein, membrane protein	71.92	2.31E-22	0.05	**-4.45**	18795	861	-
FTL_0087	*pslC*	acetyltransferase protein	78.74	4.40E-05	0.42	**-1.25**	7128	3000	-
FTL_0113	*iglC*	intracellular growth locus, subunit C	74	8.97E-06	0.50	**-1.00**	21606	10782	-
FTL_0133	*feoB*	ferrous iron transport protein	234.84	1.27E-20	0.42	**-1.24**	38086	16100	-
FTL_0148	-	Sodium/hydrogen exchanger (antiporter) family protein	189.34	9.24E-27	0.30	**-1.76**	7965	2352	-
FTL_0172	*murC*	UDP-N-acetylmuramate--L-alanine ligase	98.56	3.80E-33	0.29	**-1.78**	2195	638	-
FTL_0177	-	hypothetical protein	12	7.17E-03	0.33	**-1.58**	1775	594	-
FTL_0223	-	dihydrofolate reductase type I	8.3	1.20E-02	0.17	**-2.58**	38	6	-
FTL_0229	*cdsA*	phosphatidate cytidylyltransferase	4.8	1.31E-02	0.01	**-6.70**	105	1	*
FTL_0284	-	hypothetical protein	41	5.02E-06	0.33	**-1.58**	2821	940	-
FTL_0290	*xerC*	integrase/recombinase XerC	85.26	5.11E-14	0.45	**-1.16**	2270	1018	-
FTL_0291	-	aromatic amino acid HAAP transporter	160.92	2.10E-25	0.26	**-1.95**	47873	12357	-
FTL_0304	*nhaP*	Na+/H+ antiporter	150.72	1.83E-52	0.01	**-6.55**	42771	458	-
FTL_0325	-	OmpA family protein	89.44	8.45E-09	0.43	**-1.23**	22296	9480	-
FTL_0334	-	TolB protein precursor	6.66	1.90E-02	0.47	**-1.10**	287	133	-
FTL_0372	*gpsA*	NAD(P)H-dependent glycerol-3-phosphate dehydrogenase	88.92	5.11E-08	0.44	**-1.20**	2834	1236	-
FTL_0387	*aspC1*	aspartate aminotransferase	109	9.06E-28	0.14	**-2.81**	22904	3265	-
FTL_0393	*lpxE*	lipid A 1-phosphatase	83	1.26E-19	0.13	**-2.89**	26014	3498	-
FTL_0395	*purM*	phosphoribosylaminoimidazole synthetase	88.86	2.84E-32	0.01	**-6.70**	11981	115	-
FTL_0396	*purCD*	fusion protein PurC/PurD	189.78	2.70E-64	0.03	**-5.24**	29644	783	-
FTL_0397	*purN*	phosphoribosylglycinamide formyltransferase	64	2.94E-13	0.23	**-2.13**	17091	3908	-
FTL_0398	*purE*	phosphoribosylaminoimidazole carboxylase,catalyic subunit	41.72	1.00E-16	0.00	**-8.27**	2155	7	-
FTL_0402	*ispZ*	intracellular septation protein A family protein	61.98	1.74E-21	0.03	**-5.11**	5814	168	-
FTL_0413	*murA*	UDP-N-acetylglucosamine 1-carboxyvinyltransferase	7.68	1.07E-02	0.26	**-1.93**	28	7	-
FTL_0430	-	hypothetical protein	82.86	1.55E-19	0.22	**-2.19**	16966	3717	-

FTL_0434	-	hypothetical protein	6	1.00E-02	0.11	**-3.14**	469	53	-
FTL_0439	-	hypothetical protein	103.06	2.48E-37	0.34	**-1.55**	1864	638	-
FTL_0449	*pigR*	pathogenicity island gene regulator	20.84	7.09E-09	0.01	**-7.30**	947	6	-
FTL_0450	*psd*	phosphatidylserine decarboxylase	4.56	1.80E-02	0.04	**-4.52**	24	1	*
FTL_0466	-	soluble lytic murein transglycosylase	36.48	1.83E-09	0.39	**-1.36**	636	248	-
FTL_0483	*glgB*	glycogen branching protein	181.98	1.44E-26	0.30	**-1.72**	24633	7459	-
FTL_0508	*mpl*	UDP-N-acetylmuramate--L-alanyl-gamma-D-glutamyl-meso-diaminopimelate ligase	100.58	4.51E-17	0.31	**-1.71**	2112	645	-
FTL_0519	*minD*	septum site-determining protein MinD	62.2	3.56E-06	0.45	**-1.16**	1436	641	-
FTL_0520	*minC*	septum site-determining protein MinC	58.82	2.08E-06	0.39	**-1.36**	1390	541	-
FTL_0541	-	hypothetical protein	68.82	1.90E-18	0.17	**-2.58**	5138	857	-
FTL_0545	*pcs*	phosphatidylcholine synthase	99.84	1.44E-16	0.22	**-2.18**	22660	4988	-
FTL_0553	*lepB*	signal peptidase I	4.18	3.40E-02	0.01	**-6.49**	91	1	*
FTL_0554	*rnc*	ribonuclease III	52.12	2.90E-18	0.06	**-4.11**	812	47	-
FTL_0592	*wbtA*	dTDP-glucose 4,6-dehydratase	160.98	2.14E-58	0.01	**-6.80**	24255	217	-
FTL_0593	*wbtB*	galactosyl transferase	4.52	2.19E-02	0.00	**-7.87**	235	1	*
FTL_0594	*wbtC*	UDP-glucose 4-epimerase	87	1.27E-32	0.00	**-7.69**	10324	50	-
FTL_0595	-	galacturonosyl transferase	12.24	2.11E-02	0.25	**-1.99**	216	54	-
FTL_0597	*wbtF*	NAD dependent epimerase	84.42	2.74E-30	0.04	**-4.65**	1655	66	-
FTL_0598	*wzy*	membrane protein/O-antigen protein	149.84	5.79E-54	0.01	**-6.10**	12080	176	-
FTL_0606	*wbtM*	dTDP-D-glucose 4,6-dehydratase	108.96	6.14E-37	0.08	**-3.62**	9271	756	-
FTL_0609	*manB*	phosphomannomutase	39.38	1.34E-04	4.55	**2.19**	41	181	-
FTL_0611	*trx1*	thioredoxin	23.78	1.16E-03	0.31	**-1.69**	967	299	-
FTL_0616	*rpoA2*	DNA-directed RNA polymerase subunit alpha	25.86	2.57E-09	0.05	**-4.29**	1314	67	-
FTL_0660	*feoA*	ferrous iron transport protein A	18	1.66E-02	0.38	**-1.40**	2039	774	-
FTL_0666	*recC*	exodeoxyribonuclease V subunit gamma	160.02	1.02E-46	0.38	**-1.38**	2139	823	-
FTL_0669	*recB*	exodeoxyribonuclease V subunit beta	142.72	7.13E-44	0.25	**-2.01**	1721	427	-
FTL_0672	*panD*	aspartate alpha-decarboxylase	6	2.19E-02	0.21	**-2.28**	59	12	-
FTL_0674	*panB*	3-methyl-2-oxobutanoate hydroxymethyltransferase	10.96	5.10E-03	0.42	**-1.24**	342	144	-
FTL_0679	*potI*	ATP-binding cassette putrescine uptake system, membrane protein, subunit I	25.12	8.23E-08	0.32	**-1.64**	203	65	-
FTL_0680	*potH*	ATP-binding cassette putrescine uptake system, membrane protein, subunit H	31.78	9.28E-07	0.36	**-1.46**	213	77	-

FTL_0681	*potG*	ATP-binding cassette putrescine uptake system, ATP-binding protein	21.76	1.21E-06	0.05	**-4.20**	148	8	-
FTL_0706	*wyz*	predicted O-antigen ligase	176	3.79E-65	0.00	**-7.65**	19894	99	-
FTL_0707	-	glycosyl transferase family protein	118.94	3.41E-31	0.14	**-2.80**	13853	1991	-
FTL_0722	-	DedA family protein	56.58	4.24E-12	0.31	**-1.67**	700	220	-
FTL_0746	-	hypothetical protein	5.4	2.28E-02	0.13	**-3.00**	209	26	-
FTL_0766	*ggt*	gamma-glutamyltranspeptidase	186.86	2.68E-56	0.04	**-4.70**	60591	2333	-
FTL_0803	-	hypothetical protein	29.96	3.57E-04	0.43	**-1.21**	1640	711	-
FTL_0832	-	Mur ligase family protein	130.1	1.99E-19	0.27	**-1.89**	2171	584	-
FTL_0837	*metIQ*	D-methionine binding transport protein, ABC transporter, membrane and periplasmic protein	146.48	1.86E-48	0.02	**-5.35**	10181	250	-
FTL_0838	*metN*	D-methionine transport protein, ABC transporter,ATP-binding subunit	89.76	1.68E-31	0.01	**-6.06**	5485	82	-
FTL_0847	*yajC*	preprotein translocase family protein	15.44	5.67E-07	0.01	**-7.37**	167	1	*
FTL_0848	*secD*	preprotein translocase subunit SecD	153	1.73E-57	0.00	**-8.12**	3068	11	-
FTL_0849	*secF*	preprotein translocase subunit SecF	76.7	2.07E-16	0.41	**-1.29**	3132	1277	-
FTL_0853	-	hypothetical protein	60	2.86E-06	0.35	**-1.52**	13509	4696	-
FTL_0878	-	DNA/RNA endonuclease family protein	106.78	2.19E-07	0.44	**-1.17**	39058	17359	-
FTL_0886	-	(dimethylallyl)adenosine tRNA methylthiotransferase	101.92	1.60E-05	0.50	**-1.00**	7670	3828	-
FTL_0891	*tig*	trigger factor	69.94	9.76E-12	0.34	**-1.54**	861	296	-
FTL_0892	*clpP*	ATP-dependent Clp protease proteolytic subunit	52.66	7.00E-08	0.29	**-1.78**	1001	292	-
FTL_0893	*clpX*	ATP-dependent protease ATP-binding subunit ClpX	90.5	3.06E-17	0.25	**-2.03**	1627	399	-
FTL_0894	*lon*	DNA-binding, ATP-dependent protease La	210.46	2.66E-12	0.50	**-0.99**	9979	5008	-
FTL_0903	-	hypothetical protein	99.84	4.37E-09	0.40	**-1.33**	7992	3179	-
FTL_0904	-	hypothetical protein	91.64	4.14E-07	0.47	**-1.08**	7409	3508	-
FTL_0918	*yccA*	hypothetical protein	85	3.14E-09	0.35	**-1.50**	16380	5800	-
FTL_0930	*ruvC*	Holliday junction resolvase	41.84	1.65E-06	0.38	**-1.38**	689	264	-
FTL_0932	*ruvA*	Holliday junction DNA helicase RuvA	37.18	2.18E-08	0.23	**-2.14**	252	57	-
FTL_0959	*pilD*	Type IV pili leader peptidase and methylase.	95	2.48E-15	0.25	**-2.00**	37170	9323	-
FTL_0960	*udhA*	soluble pyridine nucleotide transhydrogenase	106.12	1.13E-22	0.28	**-1.82**	3893	1099	-
FTL_0964	*hslU*	ATP-dependent protease ATP-binding subunit HslU	100.62	5.04E-09	0.45	**-1.16**	8606	3855	-
FTL_0965	*hslV*	ATP-dependent protease peptidase subunit	46	3.76E-04	0.49	**-1.02**	3918	1931	-
FTL_1045	-	lipoprotein	56	2.57E-05	0.47	**-1.09**	11517	5397	-

FTL_1048	-	hypothetical protein, contains yqeY domain	9.78	2.99E-02	0.42	**-1.27**	66	27	-
FTL_1049	*dnaG*	DNA primase	4	3.09E-02	0.01	**-6.69**	207	2	-
FTL_1068	*truA*	tRNA pseudouridine synthase A	38.8	1.36E-08	0.34	**-1.54**	400	137	-
FTL_1096	*fipB*	Disulfide bond formation protein A	119	1.90E-41	0.02	**-5.40**	26773	636	-
FTL_1097	*fipA*	Macrophage infectivity potentiator, fragment	19	6.11E-07	0.08	**-3.61**	3956	324	-
FTL_1159	*iglC*	intracellular growth locus, subunit C	74	1.84E-06	0.46	**-1.11**	25068	11637	-
FTL_1216	-	hypothetical protein	53.9	1.92E-04	0.46	**-1.13**	1788	818	-
FTL_1251	-	proton-dependent oligopeptide transport (POT) family protein	160.64	2.02E-53	0.03	**-4.94**	10360	337	-
FTL_1263	*fadD2*	AMP-binding family protein	171.76	1.60E-50	0.06	**-4.08**	46228	2738	-
FTL_1266	-	lipase/esterase	92.92	1.44E-27	0.05	**-4.36**	8146	396	-
FTL_1271	*bioA*	adenosylmethionine-8-amino-7-oxononanoate aminotransferase	137.8	2.25E-45	0.04	**-4.49**	10352	460	-
FTL_1272	*bioB*	biotin synthase	33.24	6.70E-12	0.11	**-3.13**	273	31	-
FTL_1273	*bioF*	8-amino-7-oxononanoate synthase	120.54	5.27E-38	0.09	**-3.45**	4660	427	-
FTL_1274	*bioC*	biotin synthesis protein BioC	77.02	1.41E-26	0.03	**-5.09**	2556	75	-
FTL_1275	*bioD*	dethiobiotin synthetase	70.96	1.12E-18	0.30	**-1.75**	6242	1855	-
FTL_1286	*fvfA*	Francisella virulence factor A	11.94	5.44E-04	0.08	**-3.61**	1817	149	-
FTL_1306	*dipA*	hypothetical protein	102.92	8.49E-06	0.46	**-1.12**	17999	8280	-
FTL_1328	*fopA*	outer membrane associated protein	109.88	7.31E-19	0.23	**-2.13**	10840	2483	-
FTL_1331	-	hypothetical protein	35.1	7.28E-07	0.20	**-2.29**	1418	290	-
FTL_1335	-	hypothetical protein	68	6.03E-07	0.45	**-1.17**	15948	7104	-
FTL_1393	*ppiC*	peptidyl-prolyl cis-trans isomerase	19.4	2.24E-02	0.45	**-1.14**	303	137	-
FTL_1411	-	hypothetical protein	24.98	1.15E-03	0.37	**-1.43**	780	289	-
FTL_1414	*capA*	hypothetical protein	133.96	1.63E-37	0.09	**-3.44**	37257	3430	-
FTL_1415	*capC*	capsule biosynthesis protein CapC	70	3.95E-21	0.10	**-3.27**	20735	2142	-
FTL_1416	*capB*	capsule biosynthesis protein capB	120	2.14E-36	0.11	**-3.25**	35536	3742	-
FTL_1458	*secA*	preprotein translocase subunit SecA	15.82	2.63E-02	0.50	**-1.00**	2332	1164	-
FTL_1479	*pepA*	cytosol aminopeptidase	134.82	2.63E-13	0.39	**-1.36**	9966	3887	-
FTL_1493	-	polysaccharide biosynthesis protein (export protein)	7.24	3.33E-02	0.33	**-1.60**	414	136	-
FTL_1548	*chaC*	gamma-glutamyl cyclotransferase	72	7.63E-28	0.00	**-8.80**	14703	33	-
FTL_1553	*sucC*	succinyl-CoA synthetase subunit beta	12.9	1.06E-05	0.03	**-5.13**	36	1	*
FTL_1554	*sucD*	succinyl-CoA synthetase, alpha subunit	12.82	8.51E-06	0.02	**-5.56**	48	1	*
FTL_1584	*perM*	PerM family protein	124.98	1.73E-46	0.01	**-7.41**	4758	28	-

FTL_1593	*aroD*	3-dehydroquinate dehydratase	30.32	7.45E-05	0.23	**-2.11**	3230	749	-
FTL_1606	*sspA*	stringent starvation protein A	7.62	1.07E-02	0.37	**-1.42**	66	24	-
FTL_1613	*ftsW*	cell division protein FtsW	13.1	1.03E-02	0.23	**-2.14**	1812	410	-
FTL_1616	*pckA*	phosphoenolpyruvate carboxykinase	74.16	4.76E-07	0.49	**-1.03**	575	281	-
FTL_1670	*dsbB*	disulfide bond formation protein	55	1.59E-21	0.00	**-7.99**	13775	54	-
FTL_1701	*glpX*	fructose 1,6-bisphosphatase II	80	5.18E-22	0.11	**-3.16**	17569	1963	-
FTL_1727	*ampD*	N-acetyl-anhydromuranmyl-L-alanine amidase	38.52	7.78E-07	0.38	**-1.41**	1129	426	-
FTL_1729	*nudH*	dinucleoside polyphosphate hydrolase	42.88	1.13E-05	0.37	**-1.42**	2480	927	-
FTL_1734	-	integrase/recombinase	67.34	2.19E-12	0.31	**-1.69**	1494	464	-
FTL_1754	-	hypothetical protein	93.98	3.92E-24	0.09	**-3.54**	20408	1749	-
FTL_1779	*secG*	preprotein translocase subunit SecG	15	5.12E-03	0.31	**-1.67**	681	214	-
FTL_1790	*ampG*	major facilitator superfamily transporter	114.88	8.35E-32	0.12	**-3.06**	3050	365	-
FTL_1806	*fptD*	major facilitator transporter	102.82	9.89E-31	0.22	**-2.20**	2294	499	-
FTL_1831	*fur*	ferric uptake regulation protein	32.9	3.56E-08	0.16	**-2.61**	1875	306	-
FTL_1860	*purL*	phosphoribosylformylglycin amidine synthase	298.66	########	0.00	**-8.73**	34288	81	-
FTL_1861	*purF*	amidophosphoribosyltransferase	129.92	1.51E-45	0.03	**-5.19**	14460	395	-
FTL_1911	-	zinc-binding domain-containing protein	22.8	2.10E-07	0.15	**-2.72**	285	43	-
FTL_1914	*ripA*	hypothetical protein	60.5	1.05E-22	0.02	**-5.91**	5467	91	-
FTL_1915	-	putative acyltransferase	85.9	1.79E-24	0.21	**-2.22**	3117	669	-
FTL_1929	*purH*	bifunctional phosphoribosylaminoimidazolecarboxamide formyltransferase/IMP cyclohydrolase	120.96	2.88E-43	0.02	**-5.65**	16000	318	-
FTL_1930	*purA*	adenylosuccinate synthetase	114.16	2.28E-43	0.00	**-8.61**	3117	8	-

Appendix 3

Uniprot ID	(-)control	ChaC-V	ChaC^{-TM}-V
A0Q5F6			3
A0Q8Q2			3
A0Q455			1
A0Q4L8			1
A0Q4R3			1
A0Q8J5			1
A0Q7D4			1
A0Q6H1			1
A0Q6M1		34	
A0Q437		19	
A0Q7M9		18	
A0Q6E8		16	
A0Q6L4		10	
A0Q542		9	
A0Q5D8		8	9
A0Q5P5		7	
A0Q7M8		7	
A0Q709		7	
A0Q5H5		7	1
A0Q6M4		6	
A0Q6S5		6	
A0Q4A7		6	
A0Q4F5		6	1
A0Q6C6		5	
A0Q8N9		5	
A0Q692		5	5
A0Q4B1		4	
A0Q4Y2		4	
A0Q5I8		4	
A0Q671		4	
A0Q8G5		4	
A0Q559		4	
A0Q7V8		4	
A0Q5C3		4	
A0Q781		4	
A0Q4W9		4	2
A0Q486		4	2
A0Q708		4	1
A0Q4B3		3	
A0Q4U1		3	
A0Q5I6		3	
A0Q5D9		3	
A0Q5R5		3	
A0Q889		3	2
A0Q5Z8		3	1
A0Q539		2	
A0Q4E0		2	
A0Q4E1		2	
A0Q676		2	
A0Q8K9		2	
A0Q7C3		2	
A0Q489		2	
A0Q3U9		2	

A0Q4A1		2	
A0Q4H6		2	
A0Q524		2	
A0Q576		2	
A0Q746		2	
A0Q7S5		2	
A0Q846		2	
A0Q881		2	
A0Q8A3		2	
A0Q8H2		2	
A0Q4P0		2	
A0Q597		2	
A0Q5K0		2	
A0Q5R4		2	
A0Q6E5		2	
A0Q6W6		2	
A0Q762		2	
A0Q5Z1		2	2
A0Q7F7		2	2
A0Q691		2	2
A0Q7E3		2	2
A0Q4Q2		2	1
A0Q6F2		2	1
A0Q7R6		2	1
A0Q6I9		1	
A0Q730		1	
A0Q7I9		1	
A0Q3Z2		1	
A0Q4U3		1	
A0Q584		1	
A0Q450		1	
A0Q4D8		1	
A0Q551		1	
A0Q5A6		1	
A0Q5L3		1	
A0Q664		1	
A0Q7B7		1	
A0Q7C9		1	
A0Q7T2		1	
A0Q4B4		1	
A0Q4S2		1	
A0Q589		1	
A0Q5E6		1	
A0Q6X6		1	
A0Q725		1	
A0Q784		1	
A0Q7G9		1	
A0Q853		1	
A0Q8E2		1	
A0Q6G8		1	3
A0Q5W2		1	2
A0Q6I2		1	2
A0Q4U6		1	1
A0Q4J1		1	1
A0Q5R9		1	1
A0Q8E0		1	1

A0Q532	1	13	17
A0Q3Z3	1	3	
A0Q6A1	1	3	
A0Q6M9	1	12	
A0Q6W4	1	7	8
A0Q464	1	18	2
A0Q7U0	2	25	1
A0Q7X6	4	10	15
A0Q7J7	1		
A0Q4C3	1	2	
A0Q5H9	4	35	46
A0Q4T7	2	5	4
A0Q556	2	10	1
A0Q6W7	1	6	3
A0Q7D1	1	5	1
A0Q547	4	23	3
A0Q7H1	15	118	19
A0Q6K1	1		
A0Q711	1	6	
A0Q5E5	2	14	9
A0Q8G7	3	18	2
A0Q674	2	4	2
A0Q867	3	11	8
A0Q7X9	5	4	2
A0Q405	1		
A0Q8F4	1		
A0Q7B9	2	13	
A0Q5M7	1	10	
A0Q7V9	1	3	
A0Q772	1	2	
A0Q6A8	1	1	2
A0Q5Z7	4	11	1
A0Q7H7	2	8	2
A0Q7Y3	1		
A0Q7H8	1	7	
A0Q6F8	1	4	
A0Q638	1	2	
A0Q7M0	1	1	
A0Q7X8	1	3	2
A0Q637	1		1
A0Q6A6	1	1	1
A0Q8A8	1	1	1
A0Q6D0	3	2	3
A0Q5J9	3	5	2
A0Q7C7	6	5	2
A0Q487	5	14	2
A0Q7I6	7	10	5
A0Q678	4	5	10
A0Q582	2	6	2
A0Q7E2	2	2	2
A0Q5I7	6	23	2
A0Q757	17	21	22
A0Q3Y6	10	32	4
A0Q685	4	2	
A0Q4M5	5	9	4
A0Q8E1	6	10	5

A0Q4N5	6	15	1
A0Q8A5	14	40	9
A0Q5P9	1		
A0Q4L1	1	3	
A0Q545	1	2	
A0Q5C4	1	2	
A0Q826	1	2	
A0Q8B2	1	2	
A0Q5A4	1	1	
A0Q8B0	1	1	
A0Q5J1	2	9	6
A0Q4K8	1	3	2
A0Q4C5	1	2	2
A0Q4N7	1	2	2
A0Q8H1	3	6	5
A0Q4L5	2	4	3
A0Q5C5	2	2	3
A0Q6R2	5	8	5
A0Q419	4	7	4
A0Q7V1	2	4	2
A0Q6B4	2	3	2
A0Q518	2	2	2
A0Q4I4	1	2	1
A0Q4Q3	1	2	1
A0Q4C8	5	9	4
A0Q6D5	14	24	9
A0Q7X2	9	16	9
A0Q6R6	18	26	15
A0Q8G6	20	43	13
A0Q8G9	17	30	12
A0Q8K7	5	13	7
A0Q592	5	25	2
A0Q714	4	7	4
A0Q4I1	4	3	4
A0Q431	4	5	3
A0Q4A2	4	4	2
A0Q8A4	10	24	10
A0Q7V4	25	33	32
A0Q5L1	3	1	
A0Q5I4	3	2	4
A0Q864	3	2	2
A0Q8D9	11	10	7
A0Q6R4	11	15	8
A0Q6N5	2	6	
A0Q507	2	3	
A0Q4U9	2	1	
A0Q4J0	2	3	4
A0Q4U8	2	2	4
A0Q8J2	2	1	3
A0Q6Y7	14	35	17
A0Q6T5	4	4	4
A0Q8N2	4	4	4
A0Q880	12	8	10
A0Q4N9	2	4	1
A0Q6S8	4	3	2
A0Q5E7	2	2	1

A0Q7R0	9	11	9
A0Q5D0	16	19	13
A0Q7H0	5	16	
A0Q417	5	9	5
A0Q885	5	8	2
A0Q410	8	14	4
A0Q8N5	8	6	1
A0Q6U2	3	2	
A0Q5N7	3	1	
A0Q7D8	3	4	5
A0Q870	9	11	11
A0Q407	6	8	6
A0Q4I0	6	8	6
A0Q7U7	3	3	2
A0Q5U7	6	6	3
A0Q4Z2	3	2	1
A0Q8M1	3	2	1
A0Q6L9	7	4	2
A0Q866	12	13	8
A0Q6S0	4	12	2
A0Q8A0	4	4	2
A0Q7F0	39	37	49
A0Q8G4	5	7	5
A0Q6Y6	5	3	5
A0Q8P7	5	6	4
A0Q832	5	5	4
A0Q7M6	10	15	6
A0Q8H0	5	11	3
A0Q7Z4	5	3	2
A0Q8R0	6	12	9
A0Q6S7	12	12	14
A0Q5I9	6	8	6
A0Q4K5	6	6	5
A0Q8K1	6	6	5
A0Q4J5	6	7	4
A0Q4A9	39	58	32
A0Q6Y0	33	31	26
A0Q4A8	14	14	13
A0Q6R9	8	9	2
A0Q7B2	10	15	12
A0Q7E9	10	11	10
A0Q5Y2	13	11	11
A0Q874	56	42	23
A0Q862	21	17	14
A0Q453	28	30	25
A0Q544	2		
A0Q7Y1	2		
A0Q810	2		
A0Q4T8	1		
A0Q5H4	1		
A0Q5P2	1		
A0Q7H9	1		
A0Q7J0	1		
A0Q8B4	1		
A0Q608	2	10	
A0Q8G8	4	4	

A0Q8N6	1	3	
A0Q4E6	2	2	
A0Q673	2	2	
A0Q782	2	2	
A0Q6J9	1	1	
A0Q7H5	1	1	
A0Q4J7	2	1	
A0Q636	2	1	
A0Q8C6	2	1	
A0Q4E5	2	2	3
A0Q6Q2	2	2	3
A0Q5E1	7	7	9
A0Q6H4	4	6	5
A0Q7E8	6	7	6
A0Q599	4	4	4
A0Q5J0	4	4	4
A0Q808	4	4	4
A0Q6Y3	4	3	4
A0Q5L4	1	3	1
A0Q4I8	2	2	2
A0Q4K3	2	2	2
A0Q4T9	2	2	2
A0Q4Z0	2	2	2
A0Q5X0	2	2	2
A0Q6E2	2	2	2
A0Q7C1	2	2	2
A0Q7D3	2	2	2
A0Q869	2	2	2
A0Q8R2	2	2	2
A0Q8E7	1	2	1
A0Q5X8	1	1	1
A0Q5J2	11	12	10
A0Q7X5	9	13	8
A0Q884	16	15	14
A0Q796	7	7	6
A0Q722	11	13	9
A0Q4I6	11	11	9
A0Q8E3	4	4	3
A0Q6S6	7	7	5
A0Q6J6	7	6	5
A0Q6N1	12	8	8
A0Q7F5	6	4	4
A0Q6J7	3	2	2
A0Q7I4	14	14	8
A0Q7Y0	4	4	2
A0Q603	2	4	1
A0Q6U1	4	3	2
A0Q4J9	2	3	1
A0Q4L7	2	2	1
A0Q4N3	2	2	1
A0Q7N5	2	2	1
A0Q429	2	1	1
A0Q6Z1	2	1	1
A0Q7Y5	6	4	2
A0Q428	3	3	1
A0Q549	3	1	1

A0Q7S4	10	5	3
A0Q868	7	5	2
A0Q7K0	4	4	1
A0Q4D6	4	3	1
A0Q521	6	3	1
A0Q3X9	19	14	11
A0Q4H1	18	18	19
A0Q7Z5	13	13	14
A0Q7J6	12	9	8
A0Q5Q2	11	12	12
A0Q4T1	11	11	10
A0Q4A4	10	12	12
A0Q6N0	8	6	2
A0Q566	16	10	3
A0Q4K6	7	7	6
A0Q6I1	7	6	6
A0Q7K6	7	6	2
A0Q8C9	20	16	18
A0Q6X7	13	11	14
A0Q4J3	18	15	13
A0Q702	76	64	51
A0Q4I3	10	8	9
A0Q561	5	4	4
A0Q4S4	5	5	3
A0Q6C5	5	4	2
A0Q7Y2	5	2	2
A0Q5K5	51	51	43
A0Q7S0	30	15	12
A0Q666	21	18	13
A0Q6P0	25	20	9
A0Q4S1	29	18	18
A0Q863	24	21	19
A0Q761	8	6	6
A0Q4U4	4	6	3
A0Q478	4	3	2
A0Q4K9	8	7	3
A0Q4F8	4	4	1
A0Q684	23	16	17
A0Q5I2	11	8	5
A0Q635	7	7	5
A0Q627	31	22	21
A0Q7Z6	24	21	30
A0Q8B7	17	12	5
A0Q8F3	27	25	25
A0Q5W5	27	22	15
A0Q5E3	10	8	10
A0Q4I2	10	12	8
A0Q4E9	3	3	
A0Q5V5	3	2	
A0Q778	3	2	
A0Q4I9	12	10	10
A0Q4J6	6	5	5
A0Q522	6	5	4
A0Q517	3	3	2
A0Q7F4	3	3	2
A0Q7K1	12	9	6

A0Q593	9	10	4
A0Q4K2	9	7	4
A0Q8Q4	8	6	5
A0Q7C0	8	5	3
A0Q5I1	5	3	3
A0Q5E4	5	3	2
A0Q4K7	7	4	4
A0Q8C7	18	11	12
A0Q3Y0	47	39	36
A0Q586	2		
A0Q839	2		
A0Q468	4	3	
A0Q463	2	2	
A0Q779	2	2	
A0Q7K3	2	2	
A0Q4K1	2	1	
A0Q6S3	2	1	
A0Q6T0	2		3
A0Q6L8	8	7	7
A0Q515	8	8	6
A0Q6C3	8	8	5
A0Q835	4	5	2
A0Q4J8	4	2	2
A0Q6W1	2	2	1
A0Q760	4	2	1
A0Q838	45	22	25
A0Q4I5	7	4	1
A0Q5C0	32	19	16
A0Q565	13	8	3
A0Q8D0	16	8	10
A0Q6D9	8	6	5
A0Q7I3	19	12	2
A0Q4K0	3	2	2
A0Q5R6	7	5	2
A0Q5X1	4	1	
A0Q775	8	2	2
A0Q4L0	14	6	8
A0Q679	5		
A0Q794	11	3	4
A0Q7R5	11	4	1
A0Q7I5	6		

Appendix 4

	cysteine				GSH			
gene	chaC	dptA/B	ggt	wt	chaC	dptA/B	ggt	wt
FTN_0001	0	3.81016901	5	7.14361938	3.82001628	5.94620423	12.0347137	6.87080626
FTN_0002	3.49056284	15.240676	15	8.73109035	8.59503662	17.8386127	27.8698634	13.7416125
FTN_0003	2620.01647	4435.03672	3811	3875.81038	4047.30724	4533.556	4200.1151	3761.27566
FTN_0004	2777.0918	4445.51469	3870	4451.26861	4876.25078	4506.37335	4154.50987	4628.96033
FTN_0005	1681.75318	2454.70138	1925	2109.74892	2316.83987	2357.24525	1971.15943	2044.55563
FTN_0006	548.716479	1057.3219	874	1035.03107	823.213508	955.639965	984.946309	1186.6864
FTN_0007	439.810918	501.989767	533	361.149646	540.532303	559.792655	528.893999	352.374207
FTN_0008	1357.13083	2087.02007	1754	1814.47932	1999.77852	1974.98926	1929.98804	1701.99687
FTN_0009	80.2829454	235.277936	69	244.47053	151.845647	228.504134	95.644304	189.437944
FTN_0010	806.320017	1181.15239	1065	1434.28002	1216.67518	1168.85386	1141.39759	1495.87268
FTN_0011	361.622311	609.627041	387	537.358924	527.162246	605.663374	358.507788	621.317195
FTN_0012	518.697639	878.243956	685	1221.55891	798.383402	762.813057	632.139175	1307.41628
FTN_0013	1944.94162	2742.36914	2330	2415.33709	2672.10139	2755.64093	2327.767	2474.4718
FTN_0014	1856.97943	2809.0471	2762	2524.07885	2641.54125	2775.17846	2850.96035	2498.02885
FTN_0015	355.339298	391.494865	364	229.389556	471.77201	358.471169	356.60757	199.253382
FTN_0016	1736.90407	3163.39282	3032	2903.48441	2688.33645	3024.91904	3114.45724	3015.30241
FTN_0017	2639.56362	4016.87068	3515	4109.16861	3859.17144	4070.60152	3592.67876	3933.04581
FTN_0018	1854.8851	2838.57591	2593	2416.13082	2592.83605	2864.37152	2831.95817	2295.83084
FTN_0019	2.79245028	23.8135563	42	20.6371226	14.325061	71.3544507	31.6702993	7.85235001
FTN_0020	27.2263902	59.0576196	56	59.5301615	61.1202604	235.299796	92.477274	73.6157814
FTN_0021	1.39622514	24.7660985	19	22.2245936	3.82001628	107.031676	39.9045771	26.5016813
FTN_0022	2174.62065	2686.16915	2984	2404.22479	2966.24264	2564.51294	3085.95397	2417.54226
FTN_0023	1852.09265	2394.69122	1718	2316.91388	2224.20448	2397.16976	1883.116	2273.25533
FTN_0024	16.7547017	35.2440633	27	27.780742	14.325061	70.504993	48.772261	20.6124188
FTN_0025	810.508692	1131.62019	994	1329.50694	1082.97461	1061.82218	1017.88342	1331.95487

FTN_0026	600.376809	903.962597	946	1018.36263	891.018796	818.02781	929.839988	995.285364
FTN_0027	921.508591	1331.65407	1059	1570.00879	1251.05533	1339.59487	1069.18931	1497.83577
FTN_0028	2300.97903	3195.77925	3276	3046.3568	3435.14964	3099.67132	3281.67642	3103.64134
FTN_0029	1771.11159	2596.63018	2144	3131.28649	2393.2402	2539.87866	2188.41768	3156.64471
FTN_0030	621.320186	955.399878	858	835.803467	985.564199	905.521958	898.169689	903.020252
FTN_0031	1962.39443	2590.91492	2391	2639.96423	2515.48072	2504.20144	2435.44602	2625.62954
FTN_0032	1112.79143	1442.14897	1200	1706.5313	1603.45183	1450.87383	1180.66876	1732.42472
FTN_0033	575.942869	608.674499	820	746.111357	681.872905	569.986148	790.490671	752.844058
FTN_0034	5142.29718	7301.23636	7005	7781.78271	8019.16917	7598.39955	6895.25757	7529.42212
FTN_0035	0.69811257	9.52542252	12	6.34988389	4.77502035	39.0750564	12.0347137	12.7600688
FTN_0036	20.9433771	57.1525351	69	45.2429227	51.5702197	85.7952324	83.6095902	36.3171188
FTN_0037	519.395751	980.165977	945	885.808803	843.268593	1068.61785	963.410505	988.414558
FTN_0038	582.923995	1158.29138	916	895.333629	881.468756	1168.0044	972.911595	932.466564
FTN_0039	643.659788	981.118519	902	973.913442	1008.4843	955.639965	1010.91595	973.691402
FTN_0040	5297.27817	8838.63955	8080	8338.98502	7672.50269	8870.88725	8606.08714	8465.81486
FTN_0041	3262.28003	5633.33488	4313	5182.29899	4627.94972	5614.91571	4470.57945	5311.13324
FTN_0042	526.376877	593.433823	574	749.286299	748.72319	580.179641	594.134815	738.120901
FTN_0043	2629.79005	3447.25041	3057	3511.48579	3809.51123	3419.91689	2979.54176	3289.15311
FTN_0044	1416.4704	1834.59638	1509	1654.93849	1777.26257	1764.32374	1436.56478	1485.0757
FTN_0045	1551.20613	1934.61331	1589	1836.70392	2228.02449	1919.77451	1722.23088	1875.73011
FTN_0046	4808.59937	6234.38904	5979	6919.78597	6593.34809	6099.10662	6266.91883	6805.04283
FTN_0047	5850.88144	8533.82603	8197	8512.81309	8464.20106	8368.85772	8340.69003	8696.47764
FTN_0048	2539.73353	3734.91817	3435	3190.81666	3735.97592	3759.69999	3599.64622	3110.51215
FTN_0049	816.093593	1279.26424	1291	1044.5559	1268.2454	1207.07946	1223.74037	1100.31055
FTN_0050	2696.11074	3967.33848	3546	4234.57882	3827.65631	3913.45184	3672.48791	4373.75896
FTN_0051	832.848295	1061.13207	1056	1516.03478	1337.9607	1117.88639	1145.83143	1606.78712
FTN_0052	2274.45075	3448.20295	3447	3355.1199	3528.74004	3242.38022	3537.57243	3491.35112
FTN_0053	713.471045	804.898203	845	662.769131	1148.8699	823.124557	881.067727	769.530301

FTN_0054	485.188235	546.759252	679	888.983745	607.382588	611.609578	701.180427	871.610851
FTN_0055	1318.03653	1785.06418	1435	1758.91784	1927.19821	1733.74326	1432.76434	1646.04887
FTN_0056	409.093965	592.481281	704	395.280272	561.542393	564.889402	691.679337	390.654413
FTN_0057	2524.37505	3205.30468	3178	3111.44311	3438.01465	3069.9403	3180.33146	3077.13966
FTN_0058	2098.52638	2852.86404	2387	2717.75031	2810.57698	2784.52249	2543.75844	2745.37787
FTN_0059	2271.6583	2270.86073	2343	2377.23778	3184.93857	2259.55761	2507.6543	2374.35434
FTN_0060	671.584291	814.423625	925	857.234325	790.743369	896.177923	917.805274	901.057164
FTN_0061	2643.7523	3068.13859	3174	3398.77535	3955.62685	3104.76806	3319.04737	3485.46186
FTN_0062	2520.18637	3425.34194	3392	3424.17489	3814.28625	3377.444	3469.79799	3320.56251
FTN_0063	2220.69608	3114.81316	2977	3209.07257	3152.46843	3154.88607	3085.32056	3046.71181
FTN_0064	3411.67612	4960.84005	4309	4956.08438	4385.37869	4779.04928	4441.44278	5093.23053
FTN_0065	462.150521	554.37959	656	637.369596	697.15297	621.803071	717.648983	630.151089
FTN_0066	75.3961574	526.755865	502	424.648485	28.6501221	1781.3129	1129.99628	595.797057
FTN_0067	803.527567	914.440562	988	1112.02342	1168.92498	973.478578	984.946309	1170.00015
FTN_0068	4.88678798	0	14	1.58747097	8.59503662	1.69891549	14.5683377	0.98154375
FTN_0069	0	2.85762675	3	5.5561484	4.77502035	4.24728873	6.33405986	3.92617501
FTN_0070	108.905561	201.938957	190	236.533175	170.945728	425.578331	326.837489	244.404394
FTN_0071	2.09433771	4.76271126	8	2.38120646	1.91000814	11.8924085	7.60087184	3.92617501
FTN_0072	268.773339	19.050845	32	9.52482584	18.1450773	22.9353592	34.2039233	4.90771876
FTN_0073	2.09433771	7.62033801	11	3.96867743	4.77502035	10.193493	17.7353676	7.85235001
FTN_0074	103.32066	74.2982956	33	48.4178647	7.64003255	67.107162	27.2364574	43.1879251
FTN_0075	0	0	4	0.79373549	0.95500407	5.09674648	5.06724789	0.98154375
FTN_0076	0	0	0	0	0	0	0	0
FTN_0077	594.791909	1026.84055	645	825.484906	955.959073	1044.83303	714.481953	832.349101
FTN_0078	0	22.861014	23	15.0809742	2.86501221	237.848169	58.9067567	26.5016813
FTN_0079	4158.65657	79.0610069	103	65.0863099	76.4003255	76.4511972	137.449099	46.1325563
FTN_0080	496.358036	1168.76934	1133	1142.9791	1044.77445	1425.3901	1324.45192	1020.8055
FTN_0082	26.5282776	49.5321971	37	19.8433872	14.325061	50.9674648	34.2039233	32.3909438

FTN_0084	4091.63777	5427.58575	5667	4948.94076	5632.614	5327.79899	5890.67567	5039.24562
FTN_0085	1189.58382	1231.63713	1488	1206.47794	1353.24077	1203.68163	1328.88576	1163.12935
FTN_0086	2525.07316	3268.17247	3593	3301.14589	3633.79048	3323.07871	3663.62023	3258.72526
FTN_0087	706.48992	926.823611	1024	1003.28165	1070.55956	945.446472	1085.02445	1031.60248
FTN_0088	1366.2063	1647.8981	1835	1771.61761	1942.47828	1709.10899	1915.4197	1604.82403
FTN_0089	1002.48965	1249.73543	1279	1255.68954	1326.50065	1376.97101	1328.88576	1300.54547
FTN_0090	2874.82756	3477.73176	3746	4060.75075	3937.48178	3558.3785	3771.93265	3947.76897
FTN_0091	0	2.85762675	9	6.34988389	2.86501221	7.64511972	10.1344958	6.87080626
FTN_0092	2.09433771	10.4779648	12	19.0496517	12.4150529	27.1826479	19.0021796	14.7231563
FTN_0094	1510.7156	2130.83702	1974	2220.87189	2485.87559	2177.16021	2134.57817	2165.28552
FTN_0095	948.036868	1273.54899	1251	1311.25102	1192.80008	1251.25126	1273.14603	1192.57566
FTN_0096	3465.43079	1946.99636	2587	2120.86122	628.392677	869.844733	672.677158	1426.18307
FTN_0097	1827.65871	1121.14223	2009	2112.13013	2543.17584	1163.75711	2119.37643	2174.11941
FTN_0098	703.697469	433.406725	476	415.123659	724.848088	728.834747	1023.58407	433.842338
FTN_0099	1053.45187	1442.14897	1363	1496.98513	510.927177	1429.63739	1363.72309	1462.50019
FTN_0100	2513.20525	3773.01986	3131	2892.37211	3660.5306	3810.66745	3434.96066	2851.3846
FTN_0101	1425.54587	1859.36248	1893	1685.89417	1825.96778	1816.99012	2002.82973	1805.05896
FTN_0102	2547.41276	3994.9622	3919	4428.25028	3739.79593	4061.25749	3886.57913	4370.81433
FTN_0103	3313.24225	4891.30446	4753	4294.10898	4984.16624	4736.5764	5059.01361	4325.66331
FTN_0104	1.39622514	3.81016901	1	3.17494195	3.82001628	5.94620423	5.06724789	1.9630875
FTN_0105	20.9433771	139.071169	88	54.7677486	5.73002441	68.8060775	39.9045771	57.9110813
FTN_0106	11.1698011	35.2440633	28	2.38120646	17.1900732	48.4190916	35.4707352	0
FTN_0107	166.150791	212.416922	264	239.708117	251.16607	385.653817	419.314763	231.644325
FTN_0108	18.1509268	32.3864366	34	15.8747097	34.3801465	46.7201761	23.4360215	5.88926251
FTN_0109	942.451968	671.542287	844	813.578874	731.533117	457.008268	654.94179	722.416201
FTN_0110	83.7735083	70.4881266	9	16.6684452	11.4600488	68.8060775	17.7353676	19.630875
FTN_0111	35.603741	19.050845	22	25.3995356	10.5050448	84.9457747	23.4360215	21.5939625
FTN_0112	1.39622514	9.52542252	14	12.6997678	3.82001628	25.4837324	23.4360215	9.81543752

FTN_0113	2.09433771	37.1491478	39	35.7180969	1.91000814	125.719747	40.5379831	32.3909438
FTN_0114	2.09433771	42.8644013	62	53.9740131	1.91000814	250.590035	96.9111159	54.9664501
FTN_0115	2578.12972	3537.74192	2961	2391.52502	3799.00619	3445.40062	2953.57212	2400.85602
FTN_0116	3282.5253	3858.74866	4148	3826.59878	4473.23906	3980.559	4195.04785	3868.26393
FTN_0117	458.659958	583.9084	484	623.082357	400.146705	596.319338	435.149913	583.036989
FTN_0118	1819.97947	2139.4099	2167	2397.08117	2119.15403	2148.27864	2360.07071	2290.92312
FTN_0119	515.905188	786.7999	743	831.041054	366.721563	745.823902	791.124077	755.788689
FTN_0120	857.980347	907.772766	698	678.643841	389.64166	770.458176	540.928712	681.191364
FTN_0121	445.395819	410.54571	534	552.439899	518.567209	400.944057	505.457977	557.516851
FTN_0122	937.56518	1326.89136	1315	1133.45427	1243.4153	1358.28294	1195.8705	1230.85586
FTN_0123	527.074989	702.976182	599	774.685835	705.748007	801.038655	677.111	789.161176
FTN_0124	0	3.81016901	0	1.58747097	0.95500407	0.84945775	5.06724789	2.94463126
FTN_0125	2054.54529	2728.08101	2586	2943.96492	2749.45671	2886.45742	2647.63702	2951.50206
FTN_0126	2568.35614	3950.19272	4032	3532.91665	4292.74329	4372.15902	3961.95445	3576.74543
FTN_0127	1470.92318	2559.48103	2409	2504.23546	3052.193	2651.15763	2661.57196	2445.02549
FTN_0128	2025.22456	2481.37257	2289	2202.61597	2679.74142	2477.86825	2380.9731	2148.59927
FTN_0129	21.6414896	47.6271126	42	31.7494195	22.9200977	59.4620423	62.0737867	33.3724876
FTN_0130	1700.60222	2190.84718	1998	2229.60298	1901.4131	1976.68818	1736.16581	2371.4097
FTN_0132	1932.37559	2056.53872	2027	2401.04985	1477.39129	1463.6157	1580.34794	2356.68655
FTN_0133	376.282675	1325.93881	1069	1021.53757	671.367861	1895.14023	1508.77306	1009.02698
FTN_0134	6.98112569	15.240676	27	12.6997678	8.59503662	92.5908944	51.9392909	17.6677875
FTN_0135	10.4716885	1.9050845	44	7.14361938	5.73002441	11.0429507	43.7050131	8.83389377
FTN_0136	1024.13114	1449.76931	1097	1111.22968	1323.63564	1443.22871	1233.24146	1108.1629
FTN_0137	684.84843	998.26428	903	936.607874	911.073882	880.887684	836.095902	971.728314
FTN_0139	62.1320186	221.942345	139	167.478188	166.170708	390.750564	223.592313	176.677875
FTN_0140	399.320389	269.569457	274	223.039672	914.893898	1111.94019	1271.87922	225.755063
FTN_0141	799.338891	658.206696	815	581.808112	1120.21977	852.00612	956.44304	522.181276
FTN_0142	2996.99726	4203.56896	4239	4317.12731	4142.80765	4094.38634	4195.68125	4163.70859

FTN_0143	1317.33842	746.793125	657	856.44059	1109.71473	932.704606	884.868163	860.81387
FTN_0144	189.188506	253.376239	190	280.188627	17.1900732	215.762268	157.084685	237.533588
FTN_0145	0.69811257	10.4779648	3	11.9060323	4.77502035	11.0429507	15.8351497	4.90771876
FTN_0146	0	6.66779576	4	3.17494195	0.95500407	3.39783099	15.2017437	6.87080626
FTN_0148	1274.75355	1902.22688	1616	1914.48999	1669.34711	1873.90379	1661.4239	2059.27879
FTN_0149	1933.77182	1699.33538	1654	1789.07979	1315.99561	1086.45646	860.16533	1675.49518
FTN_0150	1532.35709	1815.54553	1493	1548.57793	1186.11505	1190.93976	825.961406	1578.32235
FTN_0151	909.640677	1051.60665	1015	981.057061	1284.48047	1086.45646	1086.92467	945.226633
FTN_0152	3465.43079	3377.71482	3490	3775.79971	4816.08552	3649.27048	3595.21238	3669.01054
FTN_0153	559.188168	856.335484	811	591.332937	888.153784	857.102867	852.564458	594.815514
FTN_0154	2696.80885	3376.76228	2930	3299.55842	3642.38552	3497.21754	2956.10574	3221.42659
FTN_0155	4026.7133	5147.53833	5392	5397.40131	5440.65818	5224.16514	5714.58881	5395.546
FTN_0156	282.037478	728.694823	886	807.22899	402.056713	326.191775	333.171549	649.781964
FTN_0157	2.79245028	3.81016901	13	0	1.91000814	7.64511972	15.2017437	3.92617501
FTN_0158	43.9810918	124.783035	114	69.0549873	51.5702197	131.665951	93.11068	70.6711501
FTN_0159	28.6226153	49.5321971	67	35.7180969	58.2552482	44.1718028	124.147573	41.2248376
FTN_0160	35.603741	9.52542252	6	4.76241292	20.0550854	22.0859014	18.3687736	11.778525
FTN_0161	17.4528142	3.81016901	9	6.34988389	1.91000814	5.09674648	7.60087184	11.778525
FTN_0162	752.565349	120.020324	77	126.997678	106.005452	75.6017395	73.4750944	105.025181
FTN_0163	0	8.57288026	13	20.6371226	3.82001628	10.193493	8.23427782	13.7416125
FTN_0164	0	5.71525351	12	8.73109035	2.86501221	13.591324	15.2017437	14.7231563
FTN_0165	49.5659924	8.57288026	81	12.6997678	48.7052075	15.2902394	68.4078465	13.7416125
FTN_0166	31.4150656	30.4813521	13	29.368213	62.0752645	35.6772254	28.5032694	31.4094001
FTN_0167	1.39622514	5.71525351	7	3.96867743	2.86501221	11.0429507	17.1019616	0.98154375
FTN_0168	2.09433771	3.81016901	5	3.96867743	8.59503662	12.7418662	20.2689916	6.87080626
FTN_0169	901.263326	1249.73543	1120	1138.21669	1140.27486	1307.31547	1188.26963	1138.59075
FTN_0170	1772.50781	2539.47764	2347	2429.62432	2401.83523	2683.43702	2493.08596	2458.7671
FTN_0171	2132.03579	2830.95557	2424	2632.82061	2764.73678	2425.20187	2015.49785	2656.05739

FTN_0172	38.3961913	36.1966056	50	35.7180969	48.7052075	52.6663803	48.138855	55.9479938
FTN_0173	0	2.85762675	3	38.0993033	0	0.84945775	13.9349317	38.2802063
FTN_0174	1001.09342	1183.05748	1200	1672.40067	1360.8808	1205.38054	1287.08096	1617.5841
FTN_0176	2820.37478	2264.19293	2446	2578.8466	3004.4428	2898.34983	3053.01685	3713.18001
FTN_0177	20.2452645	27.6237253	17	13.4935033	37.2451587	36.5266831	30.4034874	13.7416125
FTN_0178	1.39622514	1.9050845	7	10.3185613	5.73002441	5.94620423	8.23427782	4.90771876
FTN_0179	489.376911	6.66779576	12	8.73109035	655.132791	8.49457747	24.7028335	7.85235001
FTN_0180	1127.4518	1414.52524	1479	1778.76122	1443.96615	1395.65908	1437.83159	1791.31735
FTN_0181	1225.18756	1658.37606	1590	1812.09812	2606.2061	1647.09857	1830.5433	1793.28043
FTN_0182	879.621837	1162.10155	866	995.3443	1619.6869	1153.56362	855.098082	1003.13771
FTN_0183	4437.20349	1523.11506	1200	1602.55195	284.591213	1333.64866	1248.4432	1453.6663
FTN_0184	2005.67741	2809.99964	2693	3249.55308	2887.9323	3063.14464	2971.30748	3094.80745
FTN_0185	1085.56504	1600.27098	1629	1712.08744	1343.69073	1581.69032	1504.97262	1639.17807
FTN_0186	1401.11193	1600.27098	1315	1450.15473	31.5151343	1490.79835	2284.06199	1307.41628
FTN_0187	1854.8851	2667.1183	2123	1961.32039	2246.16957	2583.20101	1993.96205	1859.04387
FTN_0188	384.660025	462.935534	575	503.228298	432.616843	602.265543	585.267132	565.369201
FTN_0189	510.320288	377.206732	413	272.251272	445.031896	498.631697	505.457977	301.333932
FTN_0190	2051.05473	2714.74542	2512	2524.07885	3047.41798	2683.43702	2703.37675	2569.68154
FTN_0191	785.37664	1134.47782	827	761.192331	1077.24459	1173.10115	949.475574	775.419564
FTN_0192	1089.75372	1299.26763	897	1101.70486	2398.97022	3353.65918	1999.6627	1042.39946
FTN_0193	1133.73481	1272.59645	1142	1355.70021	2927.08747	3552.4323	2773.05141	1186.6864
FTN_0194	1329.90444	2798.56914	2620	2783.63035	1060.05452	3112.41318	2820.55686	2856.29232
FTN_0195	736.50876	1318.31848	1397	1876.39069	313.241335	1421.99227	1411.86194	1969.95831
FTN_0196	1274.05544	2613.77594	2623	2671.71365	393.461676	2685.13594	2600.76498	2772.8611
FTN_0197	453.075057	899.199886	594	790.560544	114.600488	836.715881	522.559939	801.921245
FTN_0198	148.697977	491.511802	458	278.601156	80.2203418	565.738859	483.288768	304.278563
FTN_0199	511.716513	1331.65407	1428	1461.26703	339.026445	1518.83045	1574.64728	1541.02369
FTN_0200	1326.41388	1756.48791	1886	1762.09278	1590.08177	1682.7758	1923.02057	1662.73512

FTN_0201	804.923792	1089.70834	956	769.129686	1080.1096	1173.95061	988.113339	788.179633
FTN_0202	1164.45176	1725.05402	1613	1769.2364	1437.28112	1689.57146	1620.25251	1735.36935
FTN_0203	887.999188	1127.81003	1217	1097.73618	1135.49984	1256.34801	1327.61895	1107.18135
FTN_0204	1632.18719	1862.2201	1699	1621.6016	1719.00732	1699.76495	1528.40865	1596.97168
FTN_0205	1165.14988	1579.31505	1385	1746.21807	1432.5061	1506.08859	1203.47137	1738.31398
FTN_0206	819.584156	992.549026	876	908.033396	842.313589	895.328465	862.698954	850.016889
FTN_0207	1412.97984	1158.29138	1569	1676.36935	1482.16632	1194.33759	1313.05061	1639.17807
FTN_0208	1668.48904	2328.96581	1967	2350.25078	1880.40301	2268.90164	1793.17235	2190.80565
FTN_0209	1091.14995	1542.16591	1487	1285.05775	1478.3463	1529.02394	1136.96375	1358.45655
FTN_0210	3202.94047	3657.76225	3658	4121.86838	3723.56087	3642.47482	3270.27511	3995.86461
FTN_0211	959.904782	1213.53883	1081	1266.0081	1104.93971	1164.60657	1031.18495	1168.03706
FTN_0212	841.923758	924.918526	1088	1186.63455	1073.42457	889.382261	974.178407	1188.64948
FTN_0213	252.018637	107.637274	193	241.295588	174.765745	82.3974015	164.052151	239.496675
FTN_0214	0.69811257	12.3830493	26	13.4935033	13.370057	21.2364437	41.1713891	10.7969813
FTN_0215	880.319949	1419.28795	1311	1427.1364	1414.36103	1486.55106	1447.96609	1426.18307
FTN_0216	651.339027	906.820224	684	746.905093	634.122702	929.306775	784.790017	762.659495
FTN_0217	1560.9797	1809.83028	1857	2152.61064	2125.83906	1834.82873	1817.87518	2117.18987
FTN_0218	955.716107	1241.16255	1151	1131.07307	1366.61082	1235.96102	1271.24581	1117.97833
FTN_0219	466.339196	596.29145	606	491.322266	753.49821	597.168796	644.173888	485.864157
FTN_0220	2139.71502	2328.01326	2560	2856.65402	3122.86331	2412.46	2652.70427	2920.09266
FTN_0221	54.4527804	33.3389788	63	46.0366582	139.430594	49.2685493	68.4078465	44.1694688
FTN_0222	1779.48894	2497.56578	2096	1969.25774	2440.9904	2586.59884	2292.29627	1828.61601
FTN_0223	3660.2042	4728.41974	4322	5381.5266	4995.62629	4949.79029	4405.97204	5241.44363
FTN_0225	672.980516	1334.51169	1160	1682.71923	1512.72645	1546.86256	1206.6384	1709.84922
FTN_0226	9.77357596	13.3355915	27	2.38120646	14.325061	22.9353592	31.0368933	0.98154375
FTN_0227	0.69811257	1.9050845	1	0	0	2.54837324	8.86768381	0.98154375
FTN_0228	0	2.85762675	9	3.96867743	1.91000814	1.69891549	5.70065388	0
FTN_0229	9.07546339	1.9050845	1	10.3185613	1.91000814	7.64511972	12.0347137	2.94463126

FTN_0230	19.5471519	27.6237253	28	5.5561484	8.59503662	33.9783099	57.0065388	4.90771876
FTN_0231	0.69811257	0	3	1.58747097	3.82001628	5.09674648	10.7679018	2.94463126
FTN_0232	2.09433771	1.9050845	3	2.38120646	0.95500407	5.94620423	9.5010898	3.92617501
FTN_0233	0	1.9050845	1	1.58747097	0	0	1.90021796	0
FTN_0234	9.07546339	60.0101619	15	31.7494195	18.1450773	62.8598733	19.0021796	31.4094001
FTN_0235	0.69811257	0.95254225	0	0	0	2.54837324	5.06724789	3.92617501
FTN_0236	0	0.95254225	2	5.5561484	2.86501221	2.54837324	5.06724789	0
FTN_0237	0.69811257	6.66779576	10	7.14361938	4.77502035	5.94620423	12.6681197	6.87080626
FTN_0238	0	0	0	1.58747097	0	3.39783099	2.53362395	0
FTN_0239	0	0.95254225	2	1.58747097	0.95500407	2.54837324	2.53362395	0.98154375
FTN_0240	0	0	2	0.79373549	0.95500407	1.69891549	2.53362395	1.9630875
FTN_0241	0	0	0	0	0.95500407	0	2.53362395	0
FTN_0242	0.69811257	3.81016901	2	2.38120646	0	0	5.06724789	1.9630875
FTN_0243	0	0.95254225	1	0	0	3.39783099	1.90021796	3.92617501
FTN_0244	0	0	3	1.58747097	0	0	0.63340599	0
FTN_0245	0.69811257	0	1	5.5561484	0.95500407	1.69891549	5.06724789	1.9630875
FTN_0246	0	0	1	0	0	0	3.80043592	0.98154375
FTN_0247	0	1.9050845	0	0	0	0	1.26681197	1.9630875
FTN_0248	0	1.9050845	1	0	0	0	3.16702993	0
FTN_0249	0	0	3	0.79373549	0	2.54837324	2.53362395	0.98154375
FTN_0250	0	0	1	0.79373549	0	0.84945775	3.16702993	1.9630875
FTN_0251	0.69811257	2.85762675	2	4.76241292	0	3.39783099	8.23427782	0.98154375
FTN_0252	0	2.85762675	2	2.38120646	0	0.84945775	0.63340599	0
FTN_0253	0	0	1	0	0	0	2.53362395	2.94463126
FTN_0254	0	1.9050845	1	1.58747097	0.95500407	0	3.80043592	0.98154375
FTN_0255	0	0	2	0.79373549	0	0	2.53362395	1.9630875
FTN_0256	0	0	0	0.79373549	0.95500407	0.84945775	3.16702993	2.94463126
FTN_0257	0	0	1	0	0	2.54837324	3.80043592	0.98154375

FTN_0258	0.69811257	0	1	1.58747097	0	0	2.53362395	1.9630875
FTN_0259	0.69811257	2.85762675	8	0.79373549	3.82001628	2.54837324	5.06724789	6.87080626
FTN_0260	0	0	0	4.76241292	0	4.24728873	2.53362395	0
FTN_0261	0	0	0	0	0.95500407	0	2.53362395	2.94463126
FTN_0262	0.69811257	0	0	0	0	1.69891549	0.63340599	2.94463126
FTN_0263	0.69811257	3.81016901	4	0	1.91000814	0.84945775	6.96746585	1.9630875
FTN_0264	0	2.85762675	5	1.58747097	1.91000814	2.54837324	12.6681197	0
FTN_0265	0	1.9050845	20	0	6.68502848	1.69891549	13.9349317	0
FTN_0266	2098.52638	3291.98602	3059	3501.16723	2992.02775	2652.00709	2407.57615	3410.86454
FTN_0267	508.924063	592.481281	600	623.876092	732.488121	593.770965	639.740046	671.375926
FTN_0269	2768.01634	3497.73515	3844	3052.70668	3859.17144	3714.67873	3858.70927	3102.6598
FTN_0270	9.07546339	40.0067746	16	8.73109035	17.1900732	48.4190916	17.1019616	16.6862438
FTN_0271	0	1.9050845	3	0	0	0	5.70065388	0
FTN_0272	0	4.76271126	3	0.79373549	3.82001628	5.09674648	12.6681197	2.94463126
FTN_0273	2.79245028	6.66779576	19	12.6997678	29.6051261	10.193493	10.7679018	7.85235001
FTN_0274	2.79245028	17.1457605	4	4.76241292	3.82001628	13.591324	5.06724789	0.98154375
FTN_0275	4709.46739	667.732118	582	723.093028	38.2001628	180.9345	235.627027	499.60577
FTN_0276	4520.977	4062.5927	4384	4252.041	3690.13572	2489.76066	2619.13375	4152.91161
FTN_0277	103.32066	148.596591	283	59.5301615	602.607568	198.773113	319.236617	72.6342376
FTN_0278	0	14.2881338	19	3.96867743	3.82001628	36.5266831	34.2039233	2.94463126
FTN_0279	0	20.9559295	1	3.96867743	1.91000814	26.3331902	6.96746585	3.92617501
FTN_0280	487.282573	724.884654	798	546.090015	765.913263	771.307634	818.360535	663.523576
FTN_0281	791.659653	982.071061	949	1023.12504	933.038975	944.597015	871.566637	1063.99343
FTN_0282	1251.71584	1478.34557	1758	2288.33941	1626.37193	1676.82959	1722.23088	2376.31742
FTN_0284	1618.22493	2138.45735	2204	2235.15913	2250.94459	2132.9884	2282.79518	2187.86102
FTN_0285	1676.16828	2317.5353	2099	2491.53569	2209.87942	2452.38452	2180.18341	2592.25705
FTN_0286	619.923961	892.53209	694	923.908106	889.108788	952.242134	774.022115	1037.49175
FTN_0287	1076.48958	1582.17268	1319	1660.49464	1542.33157	1670.88339	1335.85323	1639.17807

FTN_0289	437.716581	189.555908	216	160.334568	176.675753	583.577472	891.835629	196.30875
FTN_0290	1157.47064	1524.0676	1267	1573.18373	1121.17478	1073.71459	1012.81617	1545.93141
FTN_0291	6.28301312	10.4779648	18	11.9060323	13.370057	64.5587888	48.138855	11.778525
FTN_0292	36.9999661	45.7220281	11	46.8303937	34.3801465	100.236014	50.6724789	46.1325563
FTN_0293	1.39622514	24.7660985	2	19.0496517	7.64003255	24.6342747	3.16702993	39.2617501
FTN_0294	69.1131443	51.4372816	42	61.9113679	4.77502035	24.6342747	29.7700814	52.0218188
FTN_0295	51.6603301	95.2542252	81	24.6058001	57.3002441	92.5908944	58.9067567	34.3540313
FTN_0296	513.810851	1001.12191	913	846.915764	1084.88462	2059.93504	1451.76652	848.053801
FTN_0297	5673.56085	1441.19643	1329	1762.09278	1187.07006	1126.38097	979.245655	1600.89786
FTN_0298	12129.0078	2120.35905	2595	2736.79996	2817.262	2059.93504	2554.52634	2499.01039
FTN_0299	1368.30063	2878.58268	2741	2871.73499	4094.10244	4304.2024	4058.23216	2940.70508
FTN_0300	2961.39352	4785.57227	4941	5162.4556	3904.05663	5031.33823	4878.49291	5214.94195
FTN_0301	2261.18661	3152.91485	3096	3182.8793	2950.96257	3184.61709	3011.84547	3212.5927
FTN_0302	310.660093	343.867753	358	426.235956	393.461676	347.428218	342.039233	396.543676
FTN_0303	1871.6398	2407.07427	2529	2441.53036	2660.64134	2498.25523	2629.26825	2535.32751
FTN_0304	3161.05371	4008.29779	4197	3848.02964	4754.01026	3971.21497	4488.31482	3886.91326
FTN_0307	2370.79028	2729.03355	2936	3029.68835	2642.49626	2531.38409	2806.62193	2952.48361
FTN_0308	3868.93986	4810.33837	5127	4718.75747	4716.7651	4490.23365	4774.61433	4851.77076
FTN_0309	4576.12789	5711.44334	5694	5251.35398	5813.10977	5786.50617	5513.16571	5237.51746
FTN_0310	7.67923826	1.9050845	6	48.4178647	5.73002441	5.09674648	11.4013078	42.2063813
FTN_0311	2292.60168	1946.99636	2126	1944.65194	1871.80798	1942.70987	1806.47387	1944.43817
FTN_0312	365.112873	1629.79979	1424	1530.32202	1440.14614	2307.9767	1958.49131	1578.32235
FTN_0313	608.056047	724.884654	721	758.811125	847.088609	743.275529	765.154432	791.124264
FTN_0314	439.112806	537.23383	418	405.598834	588.282507	536.857296	458.585934	423.045357
FTN_0315	887.999188	1096.37613	918	855.646854	1153.64492	1089.85429	995.080805	848.053801
FTN_0316	2026.62079	2560.43357	2940	3328.13289	2955.73759	2584.89992	3134.09282	3465.83099
FTN_0317	2594.88442	2890.01319	3099	3015.40111	3382.62441	2934.87652	3198.06683	2944.63126
FTN_0318	271.565789	372.44402	426	336.543846	390.596664	384.804359	438.316943	393.599044

FTN_0319	3441.69496	3759.68427	3910	3881.36653	4712.94508	3876.92516	4041.7636	4044.9418
FTN_0320	513.810851	873.481245	670	936.607874	108.870464	922.511113	774.022115	977.617577
FTN_0321	3.49056284	23.8135563	4	3.17494195	5.73002441	11.8924085	10.1344958	1.9630875
FTN_0322	1297.79127	1533.59303	1621	1655.73222	683.782913	1667.48556	1501.17219	1601.8794
FTN_0323	302.980855	453.410112	576	537.358924	377.226607	420.481585	642.907076	598.741689
FTN_0324	224.094135	520.088069	446	367.49953	91.6803906	544.502416	473.154272	437.768513
FTN_0325	418.169429	717.264315	749	885.015067	72.5803092	761.114141	775.922333	846.090714
FTN_0326	626.905087	903.962597	1038	885.015067	127.970545	981.973155	994.447399	907.92797
FTN_0327	1032.50849	1429.76592	1670	1394.59325	223.470952	1553.65822	1545.51061	1413.423
FTN_0328	534.056115	1194.48798	1057	1150.91646	113.645484	1255.49855	965.944129	1133.68303
FTN_0329	85.867846	65.7254154	113	26.1932711	8.59503662	64.5587888	80.4425603	12.7600688
FTN_0330	51.6603301	139.071169	163	178.590484	32.4701383	258.235155	197.622668	198.271838
FTN_0331	67.0188066	254.328781	245	232.564498	64.9402767	434.072909	304.66828	217.902713
FTN_0332	6.98112569	44.7694858	65	37.3055679	12.4150529	87.4941479	81.0759663	45.1510126
FTN_0333	0	0.95254225	1	0	0	0	3.80043592	5.88926251
FTN_0334	272.962014	450.552485	385	534.183982	368.631571	432.373993	303.401468	544.756782
FTN_0335	2385.45065	2980.50471	2850	3036.03824	3009.21782	3061.44572	3094.18824	3024.1363
FTN_0336	706.48992	786.7999	995	1019.15636	924.443939	807.834317	919.072086	1112.08907
FTN_0337	23.0377148	51.4372816	82	5.5561484	35.3351506	53.5158381	106.412206	16.6862438
FTN_0338	1283.1309	1919.37264	1543	2105.78025	1883.26802	2030.20402	1948.35681	2110.31907
FTN_0339	399.320389	337.199957	361	240.501852	480.367047	336.385268	413.614109	255.201375
FTN_0340	291.811054	290.525387	314	382.580504	416.381774	302.406958	348.373293	399.488307
FTN_0341	367.207211	404.830457	604	442.904401	471.77201	417.933211	623.271491	449.547038
FTN_0342	2186.48857	2566.14883	2846	2516.93523	3149.60342	2600.19016	2995.37691	2423.43152
FTN_0343	2687.73339	3327.23009	3158	2711.40042	3548.79512	3303.54118	3176.53102	2694.3376
FTN_0344	2633.97872	2845.24371	3200	3768.65609	3567.8952	2939.1238	3277.87598	3632.69342
FTN_0345	2056.63963	2774.75558	2652	2327.23245	2773.33182	2848.23183	2816.12302	2366.50199
FTN_0346	1455.56471	1596.46081	1438	1581.91482	1689.4022	2210.28906	1877.41534	1509.61429

FTN_0347	0	1.9050845	3	6.34988389	0.95500407	3.39783099	9.5010898	4.90771876
FTN_0348	0.69811257	30.4813521	19	46.8303937	21.9650936	132.515409	122.247355	53.0033626
FTN_0349	14.6603639	63.8203309	124	129.378884	62.0752645	561.491571	710.048111	144.286931
FTN_0350	100.52821	65.7254154	89	106.360555	44.8851912	69.6555352	91.843868	109.9329
FTN_0351	108.905561	164.78981	135	24.6058001	133.70057	135.063782	137.449099	24.5385938
FTN_0352	0.69811257	12.3830493	13	3.17494195	2.86501221	11.8924085	8.86768381	8.83389377
FTN_0353	0	46.6745703	19	11.1122968	1.91000814	59.4620423	24.7028335	13.7416125
FTN_0354	4.88678798	99.0643942	70	61.1176325	1.91000814	141.009986	80.4425603	52.0218188
FTN_0355	58.6414558	587.718569	411	350.831085	18.1450773	705.04993	550.429802	346.484944
FTN_0356	1168.64044	355.29826	242	345.274937	348.576485	309.20262	246.394929	332.743332
FTN_0357	39.7924164	308.62369	185	284.157304	23.8751017	378.008697	314.802775	312.130913
FTN_0358	1934.46993	1698.38283	1722	1298.55126	2239.48454	1897.68861	2033.86662	1185.70485
FTN_0359	1142.11216	1251.64052	1249	1512.0661	1573.84671	1250.4018	1309.25017	1464.46328
FTN_0360	247.131849	293.383014	190	217.483523	396.326689	291.364007	170.38621	238.515132
FTN_0361	2168.33764	2245.14209	2336	2736.79996	2791.47689	2364.89037	2287.22902	2879.84937
FTN_0362	2580.92217	2690.93186	2630	2628.0582	3266.11392	2883.90905	2587.46345	2761.08257
FTN_0363	1383.65911	1763.15571	1677	1947.82688	2025.56363	1815.29121	1779.23742	1960.14287
FTN_0364	956.414219	1312.60322	1364	1467.61691	1301.67055	1430.48685	1412.49535	1635.25189
FTN_0365	1553.99858	1936.5184	1687	1680.33802	2099.09894	2032.75239	1808.37409	1614.63947
FTN_0367	2035.69625	2496.61324	2840	2372.47537	3088.48316	2477.86825	2999.81075	2484.28724
FTN_0368	615.037173	744.888041	749	706.424583	879.558748	664.275958	735.38435	725.360832
FTN_0369	50.9622175	52.3898238	31	42.8617163	91.6803906	67.9566198	44.971825	53.9849063
FTN_0370	668.093728	763.938886	955	961.213674	948.319041	802.737571	1036.8856	941.300458
FTN_0371	1267.77242	1610.74895	1691	1521.59093	1879.44801	1754.13025	1727.29813	1641.14115
FTN_0372	278.546915	403.877915	509	261.932711	431.661839	401.793514	475.05449	262.072182
FTN_0373	2065.71509	2901.4437	2437	3184.46677	3031.18292	3029.16633	2367.03817	3111.49369
FTN_0374	361.622311	295.288098	311	346.068672	379.136615	304.955331	332.538143	363.171188
FTN_0375	1188.18759	1436.43372	1395	1871.62828	1712.3223	1458.51895	1506.87284	1893.3979

FTN_0378	2666.0919	2794.75897	2803	3020.16353	3604.18536	2951.01621	2728.07958	3001.56079
FTN_0379	398.622277	602.959245	503	409.567511	496.602116	609.061205	425.015417	483.90107
FTN_0381	940.35763	966.830385	955	600.064028	1182.29504	919.96274	943.141514	579.110813
FTN_0382	2057.33774	2878.58268	2625	3425.76236	3054.10301	2944.22055	2740.7477	3484.48032
FTN_0384	622.716411	782.989731	905	940.576551	881.468756	758.565768	885.501569	957.005158
FTN_0385	134.037613	254.328781	276	163.50951	183.360781	296.460754	306.568497	186.493313
FTN_0386	0	5.71525351	4	5.5561484	3.82001628	14.4407817	13.9349317	4.90771876
FTN_0387	326.716682	702.976182	613	799.291635	423.066803	1072.01568	687.245495	775.419564
FTN_0388	106.811223	155.264387	143	161.128304	50.6152157	98.5370986	82.3427782	177.659419
FTN_0390	1639.86642	1967.95229	1825	2153.40437	2237.57453	1986.88167	1904.0184	2191.7872
FTN_0391	749.772899	1083.99308	1049	592.920408	972.194142	1056.72544	1123.02881	619.354107
FTN_0392	1148.39518	1645.04047	1538	1334.26935	1699.90724	1867.10813	1790.63872	1377.10588
FTN_0393	1971.46989	1965.09467	2139	2344.69463	2217.51945	2160.17105	2166.88188	2381.22514
FTN_0394	3644.84572	4500.76214	4613	4425.86907	4180.05281	4428.22323	4360.36681	4269.71532
FTN_0395	450.282607	578.193147	494	548.471221	594.012531	538.556212	527.627187	572.240007
FTN_0396	1137.22537	1051.60665	1359	1826.38535	1592.94679	1096.64995	1355.48881	1912.04723
FTN_0397	1498.84769	3.81016901	9	19.0496517	1839.33784	153.751852	33.5705173	17.6677875
FTN_0398	738.603098	710.59652	810	669.119015	944.499024	704.200472	740.451598	711.61922
FTN_0399	2321.22429	2503.28104	2781	2458.1988	3178.25354	2571.3086	2797.75424	2508.82583
FTN_0400	849.602996	1067.79986	1121	1159.64755	1303.58055	1535.81961	1558.81213	1187.66794
FTN_0401	1393.43269	1581.22014	1708	1608.1081	2065.6738	1721.85085	1871.71469	1611.69484
FTN_0402	41.8867541	94.3016829	73	185.734104	53.4802279	146.95619	98.8113339	171.770157
FTN_0403	849.602996	1243.06764	1303	985.025739	1082.97461	1635.20616	1770.36973	942.282002
FTN_0404	1156.77253	1223.06425	1200	1149.32898	1373.29585	1022.74713	869.033013	1105.21826
FTN_0405	1069.50846	927.776153	1101	1304.90114	1237.68527	887.683346	1152.7989	1292.69312
FTN_0406	919.414253	1168.76934	1276	1677.16308	1381.89089	1263.99313	1303.54952	1564.58074
FTN_0407	2030.80946	3084.33181	3124	3206.69136	3693.00074	3194.81059	3391.25565	3016.28395
FTN_0409	3345.35543	2202.27769	2379	2820.93592	2145.89414	2197.54719	2268.22684	2796.41815

FTN_0410	79.5848328	1607.89132	1154	1238.22736	76.4003255	2638.41576	2011.06401	1328.0287
FTN_0411	1725.73427	2206.08785	2073	2153.40437	2396.10521	2305.42833	2202.98602	2226.14123
FTN_0412	2582.31839	2637.58949	3188	3089.21851	3434.19463	2829.54375	3196.80001	3128.17994
FTN_0413	2645.14852	3314.84704	3175	3292.4148	3658.62059	3348.56244	3428.6266	3367.67661
FTN_0414	616.433398	924.918526	849	961.213674	841.358585	836.715881	811.393069	982.525295
FTN_0415	1941.45105	443.884689	441	387.342917	243.526038	457.857726	454.152092	372.005082
FTN_0416	2032.9038	1629.79979	1726	1808.12944	174.765745	1940.16149	2090.87316	1844.32071
FTN_0417	17.4528142	54.2949083	49	3.17494195	47.7502035	107.881134	79.8091543	7.85235001
FTN_0418	141.716851	301.955894	259	300.825749	407.786737	744.124986	696.746585	354.337294
FTN_0419	0	4.76271126	7	11.1122968	4.77502035	13.591324	12.0347137	5.88926251
FTN_0420	0.69811257	3.81016901	21	10.3185613	2.86501221	28.8815634	20.2689916	5.88926251
FTN_0421	9.77357596	34.2915211	53	46.0366582	15.2800651	253.138409	147.583595	52.0218188
FTN_0422	0	7.62033801	4	1.58747097	0.95500407	15.2902394	6.96746585	6.87080626
FTN_0423	26.5282776	11.430507	26	96.0419939	17.1900732	4.24728873	16.4685556	86.3758501
FTN_0424	511.716513	556.284675	635	619.907415	730.578113	519.018683	671.410346	588.926251
FTN_0425	1504.43259	2428.0302	2215	2566.14683	4096.96746	3251.72426	2869.32912	2723.78391
FTN_0426	372.093999	340.057584	322	523.071686	66.8502848	417.933211	414.880921	537.885976
FTN_0427	1310.35729	1150.67104	975	1054.08073	1174.655	751.770106	713.848547	982.525295
FTN_0428	673.678629	884.911752	824	658.800454	967.419122	898.726296	869.666419	772.474933
FTN_0429	953.621769	796.325322	632	810.403932	2.86501221	476.545796	216.624847	734.194726
FTN_0430	859.376572	1474.53541	1025	1049.31831	5.73002441	993.016106	708.781299	977.617577
FTN_0431	3154.7707	3430.10465	3186	3096.36213	4641.31978	2849.93074	2710.34422	3044.74872
FTN_0432	77.4904951	147.644049	109	152.397213	85.9503662	221.708472	140.616129	157.047
FTN_0433	258.999763	468.650788	418	473.06635	61.1202604	118.074627	43.0716071	427.953076
FTN_0434	193.377182	596.29145	460	819.928757	64.9402767	101.085472	50.0390729	731.250095
FTN_0435	381.867575	1050.6541	774	1123.13571	49.6602116	83.2468592	32.9371113	1063.99343
FTN_0436	309.961981	1022.07784	1002	978.675855	838.493573	830.769676	591.601191	1010.00852
FTN_0437	684.84843	967.782928	995	862.790474	1070.55956	1003.2096	971.011377	860.81387

FTN_0438	222.697909	479.128753	602	785.004396	409.696746	516.47031	641.640264	837.25682
FTN_0439	427.244892	118.115239	32	74.6111357	99.3204232	62.8598733	43.0716071	60.8557126
FTN_0440	78.1886077	18.0983028	11	5.5561484	3.82001628	13.591324	5.70065388	2.94463126
FTN_0441	0.69811257	5.71525351	10	13.4935033	4.77502035	15.2902394	32.3037053	7.85235001
FTN_0442	2.79245028	16.1932183	7	5.5561484	16.2350692	17.8386127	13.9349317	5.88926251
FTN_0443	22.3396022	76.2033801	136	11.9060323	33.4251424	84.9457747	138.082505	17.6677875
FTN_0444	48620.0499	2571.86408	2804	3731.35052	27.695118	453.610437	742.985222	538.86752
FTN_0445	2037.09248	2276.57598	2524	2399.46238	2223.24947	1976.68818	1442.89884	2215.34425
FTN_0446	0.69811257	27.6237253	13	8.73109035	1.91000814	35.6772254	18.3687736	8.83389377
FTN_0447	34.9056284	16.1932183	17	19.0496517	4.77502035	15.2902394	31.0368933	14.7231563
FTN_0448	26.5282776	16.1932183	30	17.4621807	6.68502848	16.9891549	17.7353676	9.81543752
FTN_0449	3262.97815	1142.09816	1202	1176.31599	279.816192	1052.47815	1081.22402	1271.09916
FTN_0450	46.0754295	69.5355844	49	46.8303937	15.2800651	81.5479437	57.0065388	44.1694688
FTN_0451	2599.07309	3409.14872	3371	3762.30621	2718.89658	3009.6288	3427.35979	3708.27229
FTN_0452	2899.95961	3352.94873	3131	3354.32617	3962.31188	3484.47568	3310.17969	3426.56924
FTN_0453	2307.96015	3168.15553	2387	3466.24287	3232.68877	3226.24052	2380.9731	3663.12128
FTN_0454	1843.71529	2224.18616	2343	2368.50669	2456.27047	2206.04177	2423.4113	2597.16477
FTN_0455	3949.2228	4186.4232	4140	4726.69482	5405.32303	4330.53559	4313.49477	4593.62476
FTN_0456	3088.45	3720.63003	4118	3977.40852	4317.5734	3912.60238	4351.49913	3955.62132
FTN_0457	1038.09339	1284.9795	1116	1242.98977	1620.64191	1209.62783	1162.29999	1245.57902
FTN_0458	365.112873	379.111816	404	445.285608	525.252238	407.739719	442.750785	401.451394
FTN_0459	117.981024	158.122014	185	124.616471	130.835557	155.450768	200.789698	142.323844
FTN_0460	0.69811257	2.85762675	3	1.58747097	0	4.24728873	8.86768381	2.94463126
FTN_0461	0	5.71525351	1	0	3.82001628	0	10.1344958	1.9630875
FTN_0462	286.924266	561.999928	602	693.724815	2565.14093	1737.99055	1231.34124	686.099082
FTN_0463	618.527736	549.616879	487	850.090706	272.17616	561.491571	497.857105	884.37092
FTN_0464	4969.16526	271.474542	150	177.796749	191.955818	56.0642113	107.679018	159.991632
FTN_0465	2014.75287	2042.25059	2119	1920.04614	1772.48755	2033.60185	2097.20722	1948.36435

FTN_0466	897.772763	1181.15239	1259	1460.47329	1322.68064	1128.07989	1294.68184	1419.31226
FTN_0467	2706.58243	3513.92837	3674	3740.08161	3866.81148	3716.37764	3856.17565	3622.87799
FTN_0468	64.2263563	124.783035	48	65.8800454	141.340602	126.569204	67.7744406	48.0956438
FTN_0471	961.99912	1061.13207	1442	1385.86216	1331.27567	1105.99399	1477.10276	1407.53374
FTN_0472	234.565823	316.244028	259	265.901388	212.010903	374.610866	259.696454	280.721513
FTN_0475	298.792179	1008.74224	886	869.934093	419.246786	1251.25126	1094.52554	888.297095
FTN_0476	7.67923826	26.671183	30	32.5431549	14.325061	32.2793944	47.505449	36.3171188
FTN_0477	1093.9424	1052.55919	1085	1038.20602	1655.02205	1164.60657	1193.33688	1181.77868
FTN_0478	1188.8857	1303.0778	1440	1185.04708	1635.92197	1342.14324	1530.30886	1234.78204
FTN_0479	875.433161	1112.56935	1385	1268.38931	1199.48511	1137.42392	1549.31104	1334.8995
FTN_0480	255.5092	491.511802	464	795.322957	0	150.354021	101.978364	258.146007
FTN_0481	0	5.71525351	2	7.14361938	0.95500407	10.193493	11.4013078	1.9630875
FTN_0482	124.96215	149.549134	181	234.151968	71.6253052	177.536669	155.817873	275.813794
FTN_0483	21.6414896	23.8135563	18	33.3368904	13.370057	52.6663803	65.8742226	27.483225
FTN_0484	0.69811257	10.4779648	10	10.3185613	2.86501221	10.193493	15.2017437	6.87080626
FTN_0485	20.9433771	8.57288026	25	21.4308581	23.8751017	21.2364437	32.9371113	9.81543752
FTN_0486	616.433398	663.921949	654	473.860085	816.528479	643.888972	668.243316	519.236645
FTN_0487	52.3584427	204.796584	181	69.0549873	93.5903988	176.687211	148.217001	72.6342376
FTN_0488	96.3395345	319.101654	281	451.635492	153.755655	293.062923	264.763702	421.082269
FTN_0489	487.282573	508.657562	426	611.176325	660.862816	501.180071	392.711712	605.612495
FTN_0490	0	2.85762675	0	0.79373549	1.91000814	3.39783099	5.70065388	0
FTN_0491	12.5660262	12.3830493	7	4.76241292	43.9301872	7.64511972	5.70065388	2.94463126
FTN_0492	166.150791	84.7762604	81	69.0549873	123.195525	95.9887254	95.644304	87.3573939
FTN_0493	89.3584088	68.5830421	33	23.8120646	116.510496	67.9566198	45.605231	35.3355751
FTN_0494	659.716378	1169.72189	1068	946.1327	879.558748	1393.1107	1396.02679	1049.27027
FTN_0495	1412.97984	1688.85741	1564	2136.73593	1506.04142	2069.27907	1906.55202	2132.89457
FTN_0496	528.471215	3217.68773	2754	3096.36213	14.325061	447.664233	201.423104	1120.92296
FTN_0497	1088.35749	1214.49137	1290	1341.41297	1539.46656	1260.5953	1295.94865	1383.97669

FTN_0499	41.1886416	44.7694858	28	111.916704	69.715297	46.7201761	44.971825	125.6376
FTN_0500	873.338824	1185.9151	981	803.260312	1288.30049	1194.33759	1026.7511	826.459839
FTN_0501	14.6603639	63.8203309	81	0	70.6703011	50.9674648	74.7419064	1.9630875
FTN_0502	0.69811257	16.1932183	12	15.8747097	5.73002441	18.6880704	29.1366754	8.83389377
FTN_0503	12.5660262	26.671183	65	44.4491872	26.7401139	39.9245141	54.4729148	62.8188001
FTN_0504	3166.63861	3848.2707	3852	4324.27093	4269.82319	3815.7642	3992.99134	4308.97707
FTN_0505	2272.35641	2021.29466	1853	1708.11877	2237.57453	2410.76109	2244.15741	1582.24853
FTN_0506	802.131342	516.2779	685	434.967047	741.083158	585.276388	819.627347	437.768513
FTN_0507	1766.2248	2579.48442	2488	2651.87026	3030.22791	2761.58714	2584.29642	2582.44161
FTN_0508	1655.2249	2601.39289	2560	2470.10483	2792.4319	2968.85483	2800.92127	2483.30569
FTN_0509	4742.27868	5514.26709	5704	6384.01452	3196.39862	3914.3013	4692.27155	6364.32969
FTN_0510	698.112569	806.803287	1240	1065.98676	1142.18487	861.350155	1148.36505	1170.9817
FTN_0511	874.735049	1282.12187	1322	1031.0624	1381.89089	1326.00354	1411.86194	1126.81223
FTN_0512	5687.5231	6062.93143	6404	6878.51172	6186.51636	5775.46322	5995.18766	6637.19885
FTN_0513	161.264003	314.338943	464	429.410898	409.696746	362.718458	285.6661	397.525219
FTN_0514	5288.90082	4463.61299	4460	4113.93103	1821.19276	2711.46913	3021.97996	4067.51731
FTN_0515	2446.18644	2491.85053	2467	2674.09485	3890.68658	2300.33158	2443.04689	2553.97684
FTN_0516	15.3584765	241.945732	311	225.420878	155.665663	1313.26168	1047.0201	268.942988
FTN_0517	3431.92139	4207.37913	4447	4496.51153	5494.13841	4685.60893	5212.29786	4591.66167
FTN_0518	1498.14957	1712.67097	1839	1689.06912	2361.72506	1809.345	2052.2354	1653.90122
FTN_0519	0.69811257	4.76271126	5	7.14361938	3.82001628	1.69891549	5.06724789	5.88926251
FTN_0520	134.735726	14.2881338	19	52.3865421	6.68502848	19.5375282	36.7375472	47.1141001
FTN_0521	656.225815	715.359231	816	812.785138	839.448577	773.00655	881.067727	828.422926
FTN_0522	68.4150317	43.8169436	79	15.8747097	21.0100895	30.5804789	63.9740046	16.6862438
FTN_0523	1577.03629	1832.69129	2065	2279.60832	2081.90887	1967.34414	2069.33736	2194.73183
FTN_0524	1876.52658	1836.50146	2368	2494.71063	2600.47608	1862.86084	2349.3028	2618.75873
FTN_0525	4182.3924	4230.24014	4250	4119.48717	5695.64427	4417.18028	4183.64654	4132.29919
FTN_0526	1725.03616	1795.54214	1805	1881.94684	2277.6847	1871.35542	1881.84919	1836.46836

FTN_0527	1569.35705	2037.48788	2143	1576.35868	2475.37055	2074.37582	2090.23976	1503.72503
FTN_0528	39.0943039	48.5796548	57	92.8670519	47.7502035	67.107162	70.9414705	104.043638
FTN_0529	0.69811257	2.85762675	5	2.38120646	2.86501221	4.24728873	5.06724789	5.88926251
FTN_0530	4574.03355	2113.69126	2191	2041.48767	19.1000814	704.200472	319.236617	2095.59591
FTN_0531	1683.84752	1450.72185	1497	1510.47863	1279.70545	1388.01396	1413.76216	1500.7804
FTN_0532	1696.41354	1854.59976	1892	1825.59162	1974.94841	1811.89337	1924.28739	1908.12105
FTN_0533	2065.01698	2194.65735	2210	2252.62131	2802.93694	2208.59014	2369.5718	2253.62445
FTN_0534	1769.71536	2366.11495	2799	2268.49602	2780.97185	2592.54504	3062.51794	2291.90466
FTN_0535	1440.90434	1782.20655	1722	2323.26377	1121.17478	1806.79663	1616.45208	2244.79056
FTN_0536	309.263868	1016.36258	1317	1448.56726	21.9650936	1569.79792	1292.78162	1283.85923
FTN_0537	2202.54515	3121.48096	3013	2743.94358	3506.77494	3207.55245	3011.21206	3012.35777
FTN_0538	2595.58253	3086.2369	2918	3613.87767	3682.49569	3251.72426	3025.7804	3876.11628
FTN_0539	9.77357596	34.2915211	22	6.34988389	38.2001628	37.3761409	32.3037053	4.90771876
FTN_0540	272.962014	1384.99643	1648	1586.67724	674.232873	2978.19886	4091.16927	1704.9415
FTN_0541	30.716953	12.3830493	18	19.8433872	1.91000814	16.1396972	10.1344958	8.83389377
FTN_0542	159.169666	23.8135563	18	19.0496517	12.4150529	32.2793944	28.5032694	19.630875
FTN_0543	127.056488	93.3491407	125	61.9113679	99.3204232	90.0425212	93.744086	57.9110813
FTN_0544	3355.82712	1245.92527	1172	1463.64824	891.9738	885.98443	718.915795	1277.96996
FTN_0545	1091.84806	1162.10155	866	1337.44429	471.77201	1320.05734	723.983043	1242.63439
FTN_0546	9793.82123	3646.33174	4349	3797.23057	2928.04248	2313.9229	2431.64558	3767.16492
FTN_0547	164.056454	323.864366	180	187.321575	54.4352319	245.493289	203.956728	164.89935
FTN_0548	0	0.95254225	1	1.58747097	5.73002441	5.94620423	5.06724789	0
FTN_0549	3.49056284	5.71525351	5	3.96867743	0.95500407	2.54837324	11.4013078	9.81543752
FTN_0550	9.07546339	14.2881338	28	15.0809742	2.86501221	29.7310211	29.7700814	20.6124188
FTN_0551	0	2.85762675	6	3.17494195	0	4.24728873	6.33405986	4.90771876
FTN_0552	5.58490055	29.5288098	55	23.0183291	58.2552482	89.1930634	58.9067567	34.3540313
FTN_0553	4.88678798	20.9559295	3	0	14.325061	20.3869859	6.33405986	2.94463126
FTN_0554	622.716411	686.782963	605	714.361938	869.053703	658.329754	679.011218	748.917883

FTN_0555	1512.80994	1897.46417	2066	2173.24776	2030.33865	1941.01095	2220.08798	2229.08586
FTN_0557	3.49056284	20.9559295	21	6.34988389	10.5050448	30.5804789	25.9696454	11.778525
FTN_0558	20.2452645	83.8237181	82	126.203942	13.370057	186.031247	76.6421244	105.025181
FTN_0559	29.3207279	15.240676	71	19.0496517	3.82001628	13.591324	33.5705173	17.6677875
FTN_0560	215.716784	1123.04731	1257	1146.94778	134.655574	919.96274	965.310723	1090.49511
FTN_0561	1.39622514	27.6237253	42	30.955684	8.59503662	282.86943	130.481633	46.1325563
FTN_0562	0	11.430507	4	9.52482584	0	42.4728873	15.8351497	3.92617501
FTN_0563	1.39622514	0.95254225	0	3.17494195	0	5.09674648	0	0.98154375
FTN_0564	6.98112569	12.3830493	15	19.0496517	14.325061	16.9891549	21.5358035	22.5755063
FTN_0565	2536.94108	981.118519	1122	1008.04407	848.043613	918.263824	976.078625	978.59912
FTN_0566	1743.8852	1919.37264	1979	2200.23477	2555.59089	2025.10727	1978.1269	2157.43317
FTN_0567	274.35824	657.254154	661	543.708808	1082.97461	1117.03694	1364.9899	558.498395
FTN_0568	45.377317	281.952506	268	377.024356	38.2001628	552.996993	302.134656	389.672869
FTN_0569	564.074956	1530.7354	1412	1412.84917	517.612205	2056.53721	1356.75562	1417.34918
FTN_0570	469.829759	682.020252	824	660.387925	53.4802279	981.973155	958.976664	684.135995
FTN_0571	71.9055946	367.681309	340	335.750111	86.9053703	1821.23741	1477.10276	398.506763
FTN_0572	131.943276	112.399986	81	136.522504	220.60594	162.24643	107.045612	158.028544
FTN_0573	1283.82901	1300.22017	1822	1274.73919	1622.55191	1332.7992	1910.35246	1368.27199
FTN_0574	219.207347	46.6745703	78	34.1306259	91.6803906	63.709331	110.212642	41.2248376
FTN_0575	5.58490055	23.8135563	99	6.34988389	5.73002441	30.5804789	80.4425603	7.85235001
FTN_0576	1250.31961	991.596484	1306	963.59488	957.869081	1044.83303	1349.15475	1051.23336
FTN_0577	2957.20484	3068.13859	3226	3098.74334	3691.09073	3099.67132	3256.34018	3064.37959
FTN_0578	2176.71499	2437.55562	2611	3163.03591	2908.94239	2708.92075	2648.90384	3247.92827
FTN_0579	2064.31887	2809.99964	2569	2866.17884	2691.20147	2718.26479	2599.49817	3155.66316
FTN_0580	26.5282776	39.0542323	67	39.6867743	20.0550854	27.1826479	78.5423423	44.1694688
FTN_0581	1691.52675	1840.31163	1775	1960.52665	2547.95086	1941.86041	2035.76684	1893.3979
FTN_0582	867.753923	1089.70834	1092	1323.95079	1497.44638	1337.89595	1285.81415	1385.93978
FTN_0583	1872.33791	2071.7794	2215	2435.18047	2541.26583	2247.6652	2291.66286	2398.89293

FTN_0584	2731.71448	2976.69454	3021	3376.55076	3714.96583	3150.63878	3063.15135	3283.26385
FTN_0585	899.168989	793.467696	1009	972.325971	1215.72018	937.801353	1121.762	908.909514
FTN_0586	596.188134	724.884654	844	916.764487	887.19878	780.651669	863.33236	872.592395
FTN_0587	1836.03606	2347.06411	2117	2461.37374	2491.60562	2410.76109	2134.57817	2433.24696
FTN_0588	1584.01742	1595.50827	1767	1880.35937	1919.55818	1584.2387	1759.60183	1979.77375
FTN_0589	2545.31843	2620.44373	2544	3097.9496	3378.8044	2667.29733	2840.19244	3054.56416
FTN_0590	1951.92274	2247.04717	2424	2239.12781	2714.12156	2386.12681	2505.75408	2269.32915
FTN_0591	1639.86642	2317.5353	2217	1993.06981	2379.87014	2338.55718	2333.46765	1997.44153
FTN_0592	735.112535	1049.70156	914	956.451261	1164.14996	1114.48856	906.403967	892.22327
FTN_0593	18.8490394	60.0101619	59	73.0236647	41.065175	131.665951	79.1757483	60.8557126
FTN_0594	23.0377148	54.2949083	108	97.6294648	46.7951994	145.257275	99.4447399	90.3020252
FTN_0595	233.867711	3892.08764	3398	3478.1489	213.920911	3528.64748	3247.47249	3496.25884
FTN_0597	980.150047	1122.09477	1182	1179.49093	1321.72563	1122.98314	1216.7729	1207.29881
FTN_0598	1674.07394	2178.46413	2419	2482.01087	2098.14394	2499.10469	2906.70007	2569.68154
FTN_0599	18.1509268	1301.17272	1725	2097.04916	13.370057	775.554923	697.379991	1956.2167
FTN_0600	20.9433771	9.52542252	33	31.7494195	36.2901546	16.9891549	38.0043592	40.2432938
FTN_0601	6.28301312	862.050738	1026	892.158687	2.86501221	1184.99356	1204.73819	1109.14444
FTN_0602	16.0565891	764.891428	879	562.75846	38.2001628	941.199184	1016.61661	681.191364
FTN_0603	1352.24405	1664.09131	1646	1614.45798	1950.11831	1743.0873	1829.90989	1640.15961
FTN_0604	2178.11121	2121.31159	1799	1585.8835	904.388853	2569.60968	2148.51311	1428.14616
FTN_0605	319.735557	365.776225	473	413.536188	378.181611	675.318909	919.705492	431.879251
FTN_0606	46.7735421	0.95254225	11	6.34988389	13.370057	1.69891549	7.60087184	5.88926251
FTN_0607	286.226153	42.8644013	47	88.104639	81.1753459	28.0321056	22.8026155	85.3943064
FTN_0608	0	0.95254225	0	0.79373549	0	1.69891549	6.33405986	4.90771876
FTN_0609	11.1698011	20.0033873	58	30.955684	4.77502035	59.4620423	82.9761842	23.55705
FTN_0610	2.09433771	2.85762675	25	17.4621807	1.91000814	2.54837324	3.16702993	19.630875
FTN_0611	192.679069	779.179562	657	737.380267	0.95500407	186.031247	107.679018	542.793695
FTN_0612	79.5848328	433.406725	453	319.875401	383.911636	512.223021	347.106481	403.414482

FTN_0613	8.37735083	27.6237253	40	22.2245936	25.7851099	46.7201761	18.3687736	53.0033626
FTN_0615	1050.65942	1280.21679	1302	1293.78884	1525.1415	1240.20831	1370.69055	1392.81058
FTN_0616	2234.65833	2117.50143	2863	2574.08418	2512.61571	2575.55589	3756.73091	2728.69163
FTN_0617	1789.96063	1416.43033	1265	1304.90114	1935.79325	1786.40964	1508.77306	1344.71494
FTN_0618	1674.77205	1405.95236	1429	1856.5473	1664.57209	1898.53806	1912.25267	1812.91131
FTN_0620	3040.97835	2809.0471	2791	2793.15518	2900.34736	2684.28648	2586.19664	2781.69499
FTN_0621	143.811189	9.52542252	16	7.14361938	7.64003255	12.7418662	18.3687736	3.92617501
FTN_0622	23.0377148	0.95254225	2	5.5561484	3.82001628	2.54837324	1.26681197	4.90771876
FTN_0623	59.3395683	60.9627041	46	3.17494195	46.7951994	63.709331	66.5076286	6.87080626
FTN_0624	2117.37542	2216.56582	2271	2307.38906	3467.61977	2680.88865	2553.25953	2594.22014
FTN_0625	1726.43238	1457.38965	1450	1791.46099	2676.87641	1766.02266	1529.04205	1830.5791
FTN_0626	1551.90424	1546.92862	1719	1334.26935	2487.7856	1884.09728	1899.58455	1387.90286
FTN_0627	3864.75118	3886.37239	4416	5137.05607	5259.20741	4040.02104	4231.15199	5113.84295
FTN_0628	542.433466	561.047386	664	690.549873	688.557934	566.588317	761.987402	688.06217
FTN_0629	200.358307	780.132104	1073	882.633861	271.221156	773.00655	1252.24364	908.909514
FTN_0630	277.15069	253.376239	360	368.293266	424.021807	287.966176	366.742066	400.469851
FTN_0631	1723.63993	2564.24374	2352	2147.84823	2601.43108	2403.96542	2177.01638	2171.17478
FTN_0632	1368.99875	1368.80322	1688	1293.78884	1973.99341	1534.97015	1900.21796	1458.57402
FTN_0633	2176.01688	2794.75897	2814	2762.99323	3438.96965	3064.84355	2966.24023	2928.92656
FTN_0634	1181.20647	1536.45065	1734	1704.94382	1891.86306	1573.19575	1902.11818	1673.5321
FTN_0635	1183.99892	1666.94894	1859	1777.96749	1243.4153	1988.58059	1774.80357	1776.59419
FTN_0636	2193.46969	2699.50474	2476	2779.66167	2938.54752	2766.68388	2451.28117	2888.68326
FTN_0637	1482.7911	1734.57944	1633	1739.86819	1978.76843	1724.39923	1745.03349	1705.92304
FTN_0638	3024.22365	3208.1623	3193	2984.44543	4155.2227	3405.47611	3145.49413	3077.13966
FTN_0639	338.584596	479.128753	391	469.097672	468.906998	476.545796	376.243156	516.292013
FTN_0640	2409.88459	2605.20306	2397	2256.58999	3219.31872	2591.69559	2584.29642	2211.41807
FTN_0641	133.339501	211.46438	181	207.958697	201.505859	536.857296	537.761683	157.047
FTN_0642	29.3207279	100.016936	118	123.822736	63.0302686	452.760979	357.874382	100.117463

FTN_0643	716.263496	435.311809	617	756.429919	651.312775	389.901106	587.167349	640.94807
FTN_0644	203.150758	264.806746	183	209.546168	283.636209	271.826479	197.622668	167.843982
FTN_0645	82.3772831	87.6338872	127	65.0863099	106.005452	66.2577043	78.5423423	61.8372564
FTN_0646	1198.65928	1347.84729	1628	1476.348	1545.19658	1354.88511	1784.93807	1549.85758
FTN_0647	16.7547017	5.71525351	45	96.8357293	29.6051261	8.49457747	42.4382011	131.526863
FTN_0648	1.39622514	7.62033801	7	3.96867743	3.82001628	16.9891549	13.3015257	6.87080626
FTN_0649	738.603098	2994.79284	2823	3023.33847	2628.1712	2943.37109	2401.24209	2978.00374
FTN_0651	591.301346	912.535477	871	561.964724	852.818634	1002.36014	974.178407	682.172907
FTN_0652	1399.7157	1668.85402	1453	1409.67422	1619.6869	1774.51723	1383.99208	1378.08743
FTN_0653	1031.81038	975.403266	1237	907.239661	1218.58519	975.177493	1329.51917	969.765227
FTN_0654	1052.75375	1131.62019	1615	1361.25636	1504.13141	1232.56319	1625.31976	1408.51528
FTN_0655	238.056386	460.077908	487	419.886072	462.221969	620.104155	653.041572	424.026901
FTN_0656	861.47091	1576.45743	1632	1589.05844	1745.74744	2192.45044	2005.99676	1665.67975
FTN_0657	774.206839	1327.8439	1329	1318.39464	1385.7109	1781.3129	1605.05077	1394.77367
FTN_0658	2.09433771	2.85762675	27	10.3185613	4.77502035	5.94620423	27.2364574	15.7047
FTN_0659	0	5.71525351	8	20.6371226	5.73002441	14.4407817	24.0694275	8.83389377
FTN_0660	1411.58361	1196.39307	1512	1410.46796	383.911636	506.276817	916.538462	1093.43974
FTN_0661	14.6603639	73.3457534	63	7.93735486	23.8751017	101.93493	64.6074106	19.630875
FTN_0662	0.69811257	11.430507	3	1.58747097	11.4600488	32.2793944	10.7679018	3.92617501
FTN_0663	11.8679137	20.0033873	17	11.1122968	11.4600488	27.1826479	23.4360215	3.92617501
FTN_0664	472.622209	738.220245	773	874.696506	481.322051	1121.28423	805.059009	765.604126
FTN_0665	28.6226153	36.1966056	26	35.7180969	18.1450773	32.2793944	15.2017437	36.3171188
FTN_0666	3096.12924	3783.49782	4138	3801.99298	4760.69528	4025.58026	4295.7594	3712.19847
FTN_0667	2615.8278	2914.77929	3039	3380.51944	3537.33507	2882.21014	3010.57865	3568.89308
FTN_0668	101.226322	194.318619	108	164.303246	193.865826	240.396542	195.089044	141.3423
FTN_0669	2170.43198	1019.22021	965	972.325971	1334.14068	942.898099	1014.71639	889.278639
FTN_0670	221.301684	145.738965	241	230.183291	356.216518	202.170944	272.364574	246.367482
FTN_0671	1382.26289	1693.62012	1870	2037.51899	1851.75289	1806.79663	1943.92297	2158.41471

FTN_0672	207.339433	243.850816	144	94.4545229	181.450773	217.461183	139.349317	78.5235001
FTN_0673	632.489987	610.579583	756	936.607874	935.903988	680.415655	777.822551	904.001795
FTN_0674	1171.43289	1344.03712	1320	1173.93478	1722.82734	1426.23956	1435.93137	1083.6243
FTN_0675	0	1.9050845	0	0.79373549	0	0	1.26681197	0
FTN_0676	2.79245028	6.66779576	0	0	12.4150529	6.79566198	5.70065388	0
FTN_0677	284.829928	266.71183	427	265.107652	364.811554	263.331902	395.878742	215.939625
FTN_0678	1066.01789	2461.36918	3109	2544.71597	3172.52352	3010.47826	3862.50971	2422.44998
FTN_0679	1829.75304	2238.47429	2020	1646.2074	2306.33483	2280.79405	2349.3028	1712.79385
FTN_0680	2512.50714	2660.45051	2940	2592.3401	3250.83385	2598.49125	2962.4398	2651.14967
FTN_0681	1095.33862	1225.92188	1135	1523.1784	1583.39675	1267.39096	1226.9074	1593.04551
FTN_0682	138.924401	313.386401	123	246.058001	2.86501221	42.4728873	15.8351497	170.788613
FTN_0683	194.773407	381.016901	259	368.293266	39.1551668	118.074627	65.8742226	168.825525
FTN_0684	555.697605	677.257541	652	543.708808	831.808544	746.67336	694.846367	522.181276
FTN_0685	1547.01745	1959.37941	2182	2154.99185	2099.09894	1943.55932	2458.24863	2199.63955
FTN_0686	1107.20653	1142.09816	1178	1189.80949	1434.41611	1242.75668	1318.75126	1264.22835
FTN_0687	1187.48948	1606.93878	1960	2239.92154	2439.08039	1845.87168	2277.72793	2213.38116
FTN_0688	1216.11209	1315.46085	1470	1395.38699	2824.90204	1731.19489	1803.94025	1515.50355
FTN_0689	16.7547017	157.169472	188	67.4675163	14.325061	123.171373	180.520706	53.9849063
FTN_0690	291.112941	2259.43022	2277	1967.67027	357.171522	2076.92419	2204.88624	1892.41635
FTN_0691	0	6.66779576	0	0.79373549	14.325061	19.5375282	6.96746585	2.94463126
FTN_0692	1.39622514	60.0101619	62	40.4805098	11.4600488	397.546226	124.147573	63.8003439
FTN_0693	1.39622514	54.2949083	84	42.0679808	21.9650936	304.105873	151.384031	36.3171188
FTN_0694	16.0565891	306.718605	289	166.684452	185.270789	1528.17449	593.501409	158.028544
FTN_0695	1787.16818	1906.98959	1947	2063.71226	2260.49463	1962.2474	2084.5391	2133.87612
FTN_0696	813.301143	874.433787	960	823.103699	1172.745	898.726296	1016.61661	891.241727
FTN_0697	231.07526	272.427084	424	420.679808	348.576485	327.89069	478.22152	411.266832
FTN_0698	408.395853	363.87114	340	593.714144	625.527665	378.008697	388.27787	580.092357
FTN_0699	2060.8283	1900.32179	2310	2417.71829	2831.58706	2036.15022	2343.60215	2577.53389

FTN_0700	1611.94192	1720.29131	1845	1650.17608	2179.31929	1885.7962	1831.17671	1495.87268
FTN_0701	1079.28203	1343.08457	1230	1404.91181	1570.02669	1418.59444	1325.08532	1486.05724
FTN_0702	2165.54519	2189.89464	2484	2233.57166	2959.55761	2330.0626	2723.01234	2375.33588
FTN_0703	808.414355	920.155815	931	1125.51692	1285.43548	963.285085	955.176228	1137.60921
FTN_0704	2617.22402	2628.06407	2852	2701.08186	3179.20855	2292.68646	2692.60885	2679.61444
FTN_0705	872.640711	1065.89478	1088	948.513906	1279.70545	933.554064	1070.45612	978.59912
FTN_0706	393.735489	370.538936	305	234.151968	509.017169	394.997852	331.271331	181.585594
FTN_0707	1540.73444	1615.51166	1507	1506.50995	1970.17339	1452.57275	1494.83813	1462.50019
FTN_0708	242.943174	295.288098	266	365.912059	419.246786	310.052078	252.728989	396.543676
FTN_0709	906.848227	1063.9897	1162	916.764487	1379.02588	1149.31633	1330.15257	961.912877
FTN_0710	2164.84708	3672.05038	3388	3325.75169	2970.06265	4221.805	3846.04115	3247.92827
FTN_0711	620.622074	948.732083	1044	811.991403	1001.79927	999.811768	1046.38669	803.884333
FTN_0712	263.886551	274.332168	296	231.770762	406.831733	276.073768	357.240976	210.050363
FTN_0713	970.376471	4349.30792	3106	2724.10019	1260.60537	4875.88747	3103.68933	2818.01211
FTN_0716	594.093796	593.433823	532	486.559853	891.018796	688.060775	635.306204	555.553763
FTN_0717	2402.20535	3224.35552	3023	2747.91225	3691.09073	3141.29475	3007.41162	2823.90137
FTN_0718	1364.81007	1392.61677	1135	1336.65056	2077.13385	1464.46516	1164.83361	1288.76695
FTN_0719	397.924164	393.39995	533	429.410898	602.607568	434.922366	631.505769	464.270195
FTN_0720	502.64105	767.749055	989	817.547551	1256.78535	880.887684	972.278189	793.087351
FTN_0721	1262.18752	1664.09131	1449	1109.64221	1742.88243	1737.14109	1556.91191	1220.05888
FTN_0722	333.697808	844.904977	895	1065.98676	1314.0856	1408.40094	1391.59295	1041.41792
FTN_0723	106.811223	160.979641	107	108.741762	140.385598	155.450768	105.7788	101.099006
FTN_0724	336.490258	421.976217	463	503.228298	556.767372	471.44905	497.857105	548.682957
FTN_0725	208.037546	199.081331	178	256.376562	247.346054	221.708472	216.624847	247.349025
FTN_0727	855.886009	937.301576	1179	927.876784	1307.40057	974.328036	1207.90522	934.429652
FTN_0728	1859.07377	2026.05737	2269	1693.03779	2434.30537	2125.34328	2332.20084	1642.1227
FTN_0729	1091.84806	970.640554	1240	1376.33733	424.976811	601.416085	833.562278	1344.71494
FTN_0730	3235.75176	3471.06397	4042	3294.00227	4300.38332	3535.44314	4129.80703	3210.62961

FTN_0731	1500.24391	2257.52514	2567	2239.92154	3376.89439	2613.78149	2933.93653	2266.38452
FTN_0732	249.226187	336.247415	220	118.266587	394.416681	422.1805	302.134656	147.231563
FTN_0733	328.81102	410.54571	511	348.449879	522.387226	485.040373	599.835469	393.599044
FTN_0734	1041.58395	1545.02353	1725	1027.09372	1745.74744	1642.85128	1914.7863	1202.3911
FTN_0735	1272.65921	1320.22356	1273	927.083048	1428.68609	1376.12155	1480.26979	991.359189
FTN_0736	7.67923826	12.3830493	41	93.6607874	26.7401139	19.5375282	57.0065388	137.416125
FTN_0737	27.2263902	16.1932183	18	14.2872388	60.1652563	42.4728873	38.0043592	13.7416125
FTN_0738	26.5282776	9.52542252	13	14.2872388	57.3002441	42.4728873	53.8395089	15.7047
FTN_0739	16.0565891	6.66779576	16	8.73109035	21.9650936	43.3223451	36.7375472	16.6862438
FTN_0740	360.226085	410.54571	367	531.00904	560.587389	385.653817	360.408006	544.756782
FTN_0741	2603.95988	2843.33862	3279	2359.7756	3704.46078	3231.33727	3298.77838	2511.77046
FTN_0742	538.942903	896.342259	757	804.847783	1235.77527	1044.83303	1145.83143	758.73332
FTN_0743	122.1697	42.8644013	29	46.8303937	145.160618	38.2255986	48.138855	46.1325563
FTN_0744	959.20667	1262.11848	1268	965.182351	1332.23068	1236.81048	1314.95083	1018.84241
FTN_0745	1170.03667	1031.60326	1162	1212.03409	1290.2105	1126.38097	1342.82069	1171.96324
FTN_0746	974.565146	1706.95571	1639	1785.90484	172.855736	1011.70418	859.531924	1536.11597
FTN_0747	2797.33706	1766.96588	1860	1594.61459	3213.58869	1902.78535	1904.0184	1691.19988
FTN_0748	0	24.7660985	9	21.4308581	0.95500407	349.976592	148.217001	25.5201375
FTN_0749	809.81058	923.013442	1023	1162.02875	1207.12514	1042.28466	1230.07443	1269.13607
FTN_0750	1415.77229	1150.67104	1377	944.545229	595.922539	1489.09943	1597.4499	822.533664
FTN_0751	0.69811257	10.4779648	7	3.17494195	3.82001628	5.94620423	9.5010898	11.778525
FTN_0752	0	3.81016901	3	1.58747097	0.95500407	3.39783099	7.60087184	1.9630875
FTN_0753	2.79245028	8.57288026	4	2.38120646	0.95500407	11.0429507	6.33405986	4.90771876
FTN_0754	14.6603639	1.9050845	17	1.58747097	11.4600488	5.94620423	2.53362395	0
FTN_0755	641.565451	774.416851	717	710.39326	758.273231	904.6725	724.616449	788.179633
FTN_0756	4907.73136	1098.28122	1348	1674.78188	333.29642	424.728873	549.16299	1489.00187
FTN_0757	1017.15001	4579.82315	4762	5004.50224	310.376322	3392.73424	1923.02057	4807.6013
FTN_0758	1197.26306	1512.6371	1502	1599.37701	1672.21212	1587.63653	1592.38265	1574.39618

FTN_0759	477.508997	641.060935	624	473.06635	640.80773	682.964029	642.907076	444.63932
FTN_0760	958.508557	912.535477	815	881.04639	1169.87998	965.833458	879.800915	860.81387
FTN_0761	1277.546	1373.56593	1285	1709.70624	1851.75289	1353.18619	1254.14385	1741.25862
FTN_0762	340.678934	239.088105	288	313.525517	387.731652	232.751423	260.963266	316.057088
FTN_0763	626.206974	868.718534	720	966.769822	900.568837	917.414367	887.401787	941.300458
FTN_0764	438.414693	381.969443	294	421.473543	562.497397	372.911951	279.33204	379.857432
FTN_0765	1376.67799	1719.33876	1475	1835.91018	2024.60863	1794.90422	1527.14183	1833.52373
FTN_0766	759.546475	894.437174	932	969.151029	1086.79463	959.887254	1043.21966	994.30382
FTN_0767	2954.41239	3352.94873	3265	3781.35586	3985.23198	3575.36766	3528.70475	3671.95518
FTN_0768	1525.37596	935.396491	1090	1227.11506	1267.2904	703.351014	822.794376	1180.79713
FTN_0769	1151.88574	1162.10155	1078	1596.9958	1558.56664	1264.84259	1181.30216	1624.45491
FTN_0770	2333.0922	2565.19628	3087	2930.47142	3668.17063	2917.0379	3286.11026	2994.68999
FTN_0771	242.245061	215.274549	212	259.551504	226.335964	163.945345	203.323322	231.644325
FTN_0772	148.697977	56.1999928	53	70.6424583	5.73002441	22.9353592	14.5683377	48.0956438
FTN_0773	1551.90424	1733.6269	1596	2070.85588	2021.74361	1811.04392	1727.29813	2024.92476
FTN_0774	497.056149	535.328745	573	503.228298	631.25769	649.835176	683.445059	536.904432
FTN_0775	427.244892	640.108393	699	464.33526	761.138243	659.179212	721.449419	505.495032
FTN_0776	3280.43096	3500.59277	3754	3900.41618	4774.06534	3605.94814	3832.10622	4020.40321
FTN_0777	513.112738	564.857555	643	696.106022	521.432222	520.717599	561.197704	722.416201
FTN_0778	33.5094033	20.0033873	43	63.4988389	11.4600488	24.6342747	51.3058849	62.8188001
FTN_0779	12686.1016	2929.06742	2560	2631.23314	248.301058	2542.42704	2496.8864	2648.20504
FTN_0780	2496.45055	2493.75561	2566	2913.00924	3451.38471	2668.99624	2777.48525	2751.26714
FTN_0781	29.3207279	573.430435	654	605.620176	281.7262	1076.26297	1122.39541	746.954795
FTN_0782	725.338959	977.30835	903	947.720171	1118.30976	1139.9723	912.738027	993.322277
FTN_0783	421.659992	466.745703	553	348.449879	621.707649	518.169226	628.972145	433.842338
FTN_0785	615.037173	687.735506	705	627.051034	867.143695	740.727155	812.659881	691.988345
FTN_0786	34.2075159	70.4881266	55	81.7547551	27.695118	55.2147535	62.7071927	59.8741689
FTN_0787	1621.7155	2329.91835	2269	2208.96586	838.493573	1581.69032	1483.43682	2194.73183

FTN_0788	998.300973	1199.25069	1215	827.866112	1249.14532	1283.53066	1309.88358	806.828964
FTN_0789	860.772797	1110.66427	1018	1028.68119	1079.1546	1015.10201	860.798736	1069.88269
FTN_0790	1344.56481	1491.68117	1824	1477.93548	1795.40765	1546.0131	2009.7972	1481.14952
FTN_0791	404.90529	342.915211	403	396.074008	539.577299	359.320627	423.115199	403.414482
FTN_0792	709.980482	698.21347	675	983.438268	1018.98934	742.426071	803.158791	966.820595
FTN_0797	587.810783	745.840583	964	982.644532	827.033524	776.404381	1167.36723	1064.97497
FTN_0798	1574.94196	2948.11827	2978	2883.64102	2261.44964	3118.35939	3388.08862	3068.30577
FTN_0799	507.527838	771.559224	792	727.855441	735.353133	810.382691	810.759663	775.419564
FTN_0800	1523.28163	2011.76924	2170	1719.23106	2437.17038	2040.39751	2254.29191	1881.61937
FTN_0801	377.6789	391.494865	337	603.23897	622.662653	408.589176	427.549041	634.077264
FTN_0802	50.264105	45.7220281	59	41.2742453	4.77502035	24.6342747	17.7353676	32.3909438
FTN_0803	10.4716885	14.2881338	12	11.1122968	6.68502848	23.7848169	19.0021796	2.94463126
FTN_0804	106.811223	11.430507	13	8.73109035	113.645484	17.8386127	23.4360215	6.87080626
FTN_0805	12.5660262	31.4338943	22	13.4935033	27.695118	34.8277676	25.9696454	12.7600688
FTN_0806	899.168989	2051.77601	2233	2035.93152	2687.38145	2768.3828	2877.5634	2412.63454
FTN_0807	1111.39521	933.491407	1263	927.083048	1586.26176	975.177493	1293.41502	854.924608
FTN_0808	924.301041	936.349033	1160	1092.97376	1249.14532	1006.60743	1274.41284	1068.90115
FTN_0809	2028.01701	2746.17931	2277	2079.58697	2753.27673	2977.3494	2358.17049	2205.52881
FTN_0810	1264.97997	799.182949	1165	866.759151	1752.43247	929.306775	1231.97464	823.515208
FTN_0811	1075.09336	1096.37613	1138	1431.10508	1410.54101	1054.17706	1336.48663	1411.45991
FTN_0812	9.77357596	608.674499	809	675.468899	5.73002441	863.049071	841.16315	748.917883
FTN_0813	16.0565891	769.654139	858	730.236647	2.86501221	1011.70418	1053.98756	846.090714
FTN_0814	30.716953	1561.21675	2067	1881.1531	16.2350692	2040.39751	2342.33534	2127.00531
FTN_0815	4.88678798	175.267774	144	178.590484	9.55004069	751.770106	247.661741	167.843982
FTN_0816	64.9244689	1625.98962	2040	1900.99649	63.0302686	2139.78406	2206.78646	2180.99022
FTN_0817	964.093458	1025.88801	1137	700.868434	1386.66591	1030.39225	1211.07225	749.899426
FTN_0818	63.5282438	1391.66423	1629	1219.97144	24.8301058	1959.69902	1962.29175	1394.77367
FTN_0819	25.1320525	10.4779648	36	7.93735486	36.2901546	16.1396972	49.4056669	12.7600688

FTN_0820	0	1.9050845	2	3.96867743	2.86501221	1.69891549	4.43384191	6.87080626
FTN_0821	29.3207279	603.911788	524	364.324588	19.1000814	2115.99925	1963.55856	479.974895
FTN_0822	1179.11213	2508.04375	2224	2011.32572	1781.08259	3029.16633	3014.37909	2006.27543
FTN_0823	330.207245	576.288062	695	750.87377	491.827096	751.770106	811.393069	734.194726
FTN_0824	2288.413	2433.74545	2201	2709.01922	3281.39398	2353.84742	2499.42002	2735.56244
FTN_0825	11915.3853	1550.73879	1603	1269.97678	2328.29992	1478.05648	1596.18309	1179.81559
FTN_0826	1838.13039	1551.69133	1634	1813.68559	2177.40928	1658.14152	1646.22216	1823.70829
FTN_0827	1410.8855	1444.05405	1227	1933.53964	1869.89797	1651.34586	1420.09622	1879.65628
FTN_0828	124.264037	280.999964	153	285.744775	33.4251424	389.901106	202.689916	303.297019
FTN_0829	929.187829	1169.72189	1155	915.177016	1273.02042	1085.607	1194.60369	947.18972
FTN_0830	1.39622514	3.81016901	18	3.17494195	0.95500407	7.64511972	27.8698634	2.94463126
FTN_0831	1275.45166	1690.7625	1673	1465.23571	1729.51237	1757.52808	1644.95535	1521.39282
FTN_0832	4154.4679	26.671183	4327	3251.14055	28.6501221	22.9353592	4056.33194	1814.8744
FTN_0833	730.225747	663.921949	649	588.157995	1054.32449	773.00655	735.38435	618.372564
FTN_0834	1496.05523	112.399986	86	105.56682	140.385598	62.8598733	72.8416884	97.1728314
FTN_0835	999.697199	1140.19308	1258	1139.80416	1477.39129	1234.26211	1206.005	1225.94815
FTN_0836	1066.01789	1431.671	1270	1062.01808	1368.52083	1410.09986	1278.84669	1051.23336
FTN_0837	975.961371	1221.15917	1278	1502.54128	1334.14068	1151.01525	1281.38031	1512.55892
FTN_0838	938.263292	983.976146	934	1110.43595	1377.11587	880.038226	860.798736	1163.12935
FTN_0839	1840.92284	2083.2099	2125	2434.38674	2334.02994	2273.14893	2090.87316	2506.86274
FTN_0840	871.244486	972.545639	1080	912.795809	1231.95525	1004.90851	1029.28473	918.724952
FTN_0841	741.395548	887.769379	939	1013.60022	1154.59992	892.780092	995.714211	1099.329
FTN_0842	22.3396022	29.5288098	56	14.2872388	14.325061	218.310641	96.2777099	20.6124188
FTN_0843	1.39622514	0	3	8.73109035	1.91000814	19.5375282	19.0021796	3.92617501
FTN_0844	277.848802	463.888077	592	240.501852	478.457039	556.394824	711.314923	261.090638
FTN_0845	1611.24381	1669.80657	1695	1322.36332	1895.68308	1606.3246	1761.50205	1224.9666
FTN_0846	9.07546339	10.4779648	15	0	4.77502035	11.0429507	20.2689916	0.98154375
FTN_0847	1937.96049	2249.9048	1905	1632.7139	2163.08422	2188.20316	1901.48477	1776.59419

FTN_0848	611.54661	662.016865	732	838.978409	2080.95387	1353.18619	1450.49971	857.869239
FTN_0849	43.2829793	21.9084718	31	26.1932711	24.8301058	67.9566198	64.6074106	28.4647688
FTN_0850	0.69811257	1.9050845	5	3.17494195	1.91000814	1.69891549	6.33405986	0.98154375
FTN_0851	0	1.9050845	6	1.58747097	1.91000814	9.34403522	5.06724789	0
FTN_0852	0	0.95254225	3	11.9060323	0	0	2.53362395	11.778525
FTN_0853	23.7358273	51.4372816	36	57.9426905	51.5702197	42.4728873	29.7700814	66.7449751
FTN_0854	1006.67832	1092.56596	1268	870.727829	1228.13523	1174.80006	1387.15911	947.18972
FTN_0855	1149.09329	1302.12526	1267	1101.70486	1374.25086	1234.26211	1263.01154	1160.18471
FTN_0856	275.754465	417.213506	393	230.183291	367.676567	411.987007	407.913455	205.142644
FTN_0858	513.112738	425.786386	529	479.416234	674.232873	352.524965	538.395089	514.328926
FTN_0859	982.942497	1083.04054	1522	1068.36796	1351.33076	1145.06904	1548.67764	1161.16626
FTN_0860	1895.37562	2463.27426	2283	1974.02015	2812.48698	2622.27606	2340.43512	2132.89457
FTN_0861	2059.43208	1786.01672	1876	1916.8712	2859.28218	1907.03264	1975.59327	2064.18651
FTN_0862	1144.90461	1286.88458	1463	1294.58258	1617.77689	1268.24042	1435.93137	1392.81058
FTN_0863	593.395683	608.674499	725	538.15266	663.727828	632.846021	739.184786	605.612495
FTN_0864	132.641388	105.73219	140	99.2169358	225.38096	137.612155	190.655202	105.025181
FTN_0865	303.678967	446.742316	475	443.698137	412.561758	473.997423	545.99596	455.436301
FTN_0866	897.772763	399.115203	421	377.818092	265.491131	494.384409	596.668439	392.617501
FTN_0867	6.28301312	0	1	1.58747097	2.86501221	6.79566198	6.96746585	2.94463126
FTN_0869	2414.07326	3470.11142	3273	3589.27187	3447.56469	3609.34597	3700.35777	3784.83271
FTN_0870	9.77357596	9.52542252	26	9.52482584	19.1000814	25.4837324	27.8698634	8.83389377
FTN_0871	600.376809	644.871104	871	786.591867	622.662653	620.104155	770.22168	762.659495
FTN_0872	1708.97957	1754.58283	1996	1931.15844	2461.04549	1876.45216	2110.50875	2067.13114
FTN_0873	23.7358273	506.752478	604	524.659156	13.370057	310.052078	380.676998	527.088995
FTN_0874	6.98112569	45.7220281	24	75.4048712	4.77502035	21.2364437	26.6030514	77.5419564
FTN_0875	1609.14947	1470.72524	1612	1900.20275	2078.08885	1591.88382	1617.71889	1810.94822
FTN_0876	1908.63976	2048.91838	1827	2431.21179	2623.39618	2106.65521	1932.52166	2446.00703
FTN_0877	1422.0553	1680.28453	1582	1958.14544	2056.12376	1736.29163	1706.39573	1985.66301

FTN_0878	1392.73457	1676.47436	1614	1267.59557	1945.34329	1664.08773	1651.28941	1393.79213
FTN_0879	950.131206	851.572773	720	1229.49627	1414.36103	957.338881	831.028654	1231.83741
FTN_0880	1154.67819	1428.81338	1080	1300.13873	1536.60155	1495.04563	1076.15677	1367.29045
FTN_0881	365.112873	421.976217	324	229.389556	489.917087	383.105444	352.173728	248.330569
FTN_0882	2.79245028	8.57288026	10	7.14361938	4.77502035	21.2364437	25.3362395	10.7969813
FTN_0883	2.79245028	1.9050845	3	2.38120646	1.91000814	2.54837324	8.23427782	1.9630875
FTN_0884	1316.6403	1878.41332	1504	1586.67724	1998.82352	1984.3333	1605.68418	1707.88613
FTN_0885	2562.07313	2825.24032	3285	3123.34914	3452.33971	2845.68345	3402.02355	3085.97356
FTN_0886	2072.69622	2338.49123	2486	2272.4647	3113.31327	2401.41705	2712.87784	2393.00367
FTN_0887	1205.64041	1168.76934	1492	1646.2074	1708.50228	1215.57404	1619.61911	1723.59083
FTN_0888	1103.01786	1726.00656	1448	1123.13571	1413.40602	1602.92677	1465.06805	1193.5572
FTN_0889	223.396022	160.027098	253	105.56682	177.630757	116.375711	228.659561	102.08055
FTN_0890	629.697537	781.084646	743	567.520873	806.978438	829.920219	803.158791	625.24337
FTN_0891	543.131579	355.29826	478	398.455214	545.307323	524.964888	513.692255	461.325563
FTN_0892	670.886179	709.643977	931	527.834098	887.19878	748.372275	1031.18495	569.295376
FTN_0893	1092.54617	981.118519	1111	883.427596	1352.28576	951.392677	1260.47791	900.07562
FTN_0894	851.697334	983.976146	955	729.442912	1163.19496	1082.20917	1091.35851	717.508482
FTN_0895	491.471248	499.13214	440	473.860085	654.177787	591.222592	445.284409	494.698051
FTN_0896	20.9433771	35.2440633	28	65.0863099	40.1101709	54.3652958	44.971825	44.1694688
FTN_0897	0.69811257	5.71525351	10	6.34988389	5.73002441	6.79566198	15.2017437	2.94463126
FTN_0898	2619.31836	3128.14875	2934	2855.06654	3563.12018	3187.16547	2945.33784	2999.59771
FTN_0899	101.924435	33.3389788	35	53.9740131	114.600488	112.128423	86.7766201	37.2986626
FTN_0900	331.60347	245.755901	235	200.021343	467.951994	453.610437	514.325661	193.364119
FTN_0901	562.67873	735.362618	585	413.536188	818.438487	734.780951	571.3322	383.783607
FTN_0902	7.67923826	8.57288026	2	2.38120646	7.64003255	15.2902394	6.96746585	4.90771876
FTN_0903	76.09427	44.7694858	39	51.5928066	54.4352319	35.6772254	29.1366754	52.0218188
FTN_0904	2.09433771	3.81016901	4	3.17494195	4.77502035	5.09674648	5.06724789	6.87080626
FTN_0905	0	2.85762675	3	4.76241292	0.95500407	3.39783099	5.06724789	5.88926251

FTN_0906	9.77357596	20.9559295	32	46.0366582	11.4600488	23.7848169	27.8698634	61.8372564
FTN_0907	65.6225815	24.7660985	36	27.780742	12.4150529	43.3223451	39.9045771	15.7047
FTN_0908	0.69811257	0.95254225	0	0.79373549	6.68502848	3.39783099	2.53362395	0.98154375
FTN_0909	70.5093694	72.3932111	16	38.0993033	72.5803092	85.7952324	20.9023976	36.3171188
FTN_0910	2787.56349	2965.26403	3277	3298.76468	3812.37624	3243.22968	3520.47047	3333.32258
FTN_0911	2955.1105	2809.99964	3454	3006.67002	3756.031	2917.88736	3620.54862	3041.80409
FTN_0912	1255.90451	1388.8066	1287	1001.69418	1713.2773	1463.6157	1375.1244	1111.10753
FTN_0913	0.69811257	3.81016901	1	4.76241292	3.82001628	4.24728873	8.23427782	5.88926251
FTN_0914	1.39622514	3.81016901	0	6.34988389	3.82001628	8.49457747	22.1692095	3.92617501
FTN_0915	0.69811257	2.85762675	2	0	2.86501221	5.94620423	3.80043592	2.94463126
FTN_0916	0	0	1	0	0	0.84945775	3.16702993	0
FTN_0917	2619.31836	223.847429	126	240.501852	18.1450773	145.257275	121.613949	192.382575
FTN_0918	1054.84809	845.857519	864	843.740822	889.108788	734.780951	829.761842	821.55212
FTN_0919	1099.5273	814.423625	861	727.061706	1055.2795	718.641254	914.638244	759.714864
FTN_0920	1058.33865	1244.97272	1028	1221.55891	1478.3463	1314.11113	1164.2002	1196.50183
FTN_0921	666.697503	950.637167	898	970.7385	488.962083	1042.28466	1021.05045	971.728314
FTN_0922	1.39622514	12.3830493	5	9.52482584	0	37.3761409	12.0347137	5.88926251
FTN_0923	471.924097	372.44402	544	432.58584	657.0428	372.911951	552.963426	407.340657
FTN_0924	535.45234	611.532126	714	505.609505	833.718552	635.394395	804.425603	570.27692
FTN_0926	1188.8857	1469.77269	1590	1933.53964	1483.12132	1525.62611	1604.41736	1995.47845
FTN_0927	2360.3186	2978.59962	3064	2743.14984	3031.18292	3196.5095	3250.63952	2759.11949
FTN_0928	1072.99902	1361.18288	1071	1238.22736	1426.77608	1336.19704	1177.50173	1256.376
FTN_0929	1717.35692	2333.72852	2326	2543.1285	2568.00594	2470.22313	2635.60231	2622.6849
FTN_0930	1378.07421	1521.20998	1422	1624.77654	1846.97787	1594.43219	1606.31758	1578.32235
FTN_0931	1112.79143	1444.05405	1235	1554.92782	1405.76599	1476.35756	1375.1244	1466.42637
FTN_0932	2996.99726	3458.68092	3500	3697.2199	4073.09235	3904.95726	3926.48371	3692.56759
FTN_0933	307.16953	385.779612	506	380.199298	530.982262	469.750134	547.896178	365.134276
FTN_0934	833.546407	955.399878	1100	1484.28536	1384.7559	971.779662	1235.77508	1538.07906

FTN_0935	2288.413	2879.53523	3048	2333.58233	3325.32417	3007.08042	3248.1059	2428.33924
FTN_0936	1868.14923	2321.34547	2121	2024.02549	2697.8865	2299.48212	2289.76264	2039.64792
FTN_0937	1261.48941	1670.75911	1583	2017.67561	1780.12758	1867.10813	1788.1051	2171.17478
FTN_0938	238.754499	348.630464	429	226.214614	346.666477	372.062493	437.683537	291.518494
FTN_0940	254.112975	321.006739	203	212.72111	400.146705	300.708042	217.891659	215.939625
FTN_0943	398.622277	447.694858	447	295.269601	527.162246	496.083324	481.38855	326.854069
FTN_0944	20.9433771	0.95254225	0	2.38120646	17.1900732	1.69891549	9.5010898	0.98154375
FTN_0945	72.6037072	120.020324	142	112.710439	89.7703825	187.730162	240.694275	105.025181
FTN_0946	307.867643	582.955858	714	627.051034	384.86664	1083.05863	1230.07443	650.763507
FTN_0947	430.037342	711.549062	738	802.466577	317.061351	1159.50982	1131.26309	825.478295
FTN_0948	25.1320525	31.4338943	88	13.4935033	25.7851099	48.4190916	114.646484	10.7969813
FTN_0949	12.5660262	67.6304999	72	65.8800454	13.370057	52.6663803	36.1041412	87.3573939
FTN_0950	0	0.95254225	1	1.58747097	0.95500407	1.69891549	3.80043592	0
FTN_0951	0	0	2	0.79373549	1.91000814	0	1.90021796	0
FTN_0953	20.9433771	3.81016901	10	15.0809742	32.4701383	7.64511972	17.1019616	9.81543752
FTN_0954	2159.96029	2368.97258	2132	2974.9206	3049.32799	2386.97627	2354.37005	3049.65644
FTN_0955	9.77357596	13.3355915	9	12.6997678	20.0550854	4.24728873	25.9696454	9.81543752
FTN_0956	40.490529	27.6237253	59	0.79373549	28.6501221	28.8815634	65.2408166	7.85235001
FTN_0957	661.112603	556.284675	810	752.461241	942.589016	631.996564	754.38653	737.139358
FTN_0958	508.22595	432.454182	550	481.003705	683.782913	465.502845	561.197704	478.993351
FTN_0959	525.678764	1028.74563	1276	806.435254	1082.97461	1115.33802	1414.39557	877.500114
FTN_0960	1399.01759	1539.30828	1714	1536.6719	1963.48837	1664.93718	1982.56074	1461.51865
FTN_0961	273.660127	321.006739	259	566.727137	378.181611	343.18093	293.266972	603.649407
FTN_0962	894.980313	1031.60326	1018	990.581887	1375.20586	1163.75711	1035.61879	1048.28873
FTN_0963	2724.73336	3086.2369	3150	2852.68534	3700.64077	3247.47697	2989.04285	3002.54234
FTN_0964	1793.45119	1989.86076	2416	1608.1081	2504.02067	2090.51552	2571.62831	1702.97841
FTN_0965	1896.77185	1806.97265	1671	1929.57097	2524.07575	1856.91463	1726.03131	2012.16469
FTN_0966	3168.03484	2935.73522	3128	2746.32478	3292.85403	2402.26651	2427.21174	2834.69835

FTN_0967	2483.18641	688.688048	700	773.098364	2.86501221	90.0425212	70.3080645	279.739969
FTN_0968	0	0.95254225	2	0.79373549	1.91000814	5.09674648	10.7679018	4.90771876
FTN_0969	2367.29972	2416.59969	2576	2674.09485	3204.99366	2578.95372	2738.21408	2576.55235
FTN_0970	311.358206	381.969443	395	403.217627	452.671929	434.922366	383.210622	410.285288
FTN_0971	308.565755	441.979605	496	389.724124	441.21188	431.524535	579.566478	368.078907
FTN_0972	2839.22382	3035.75216	3459	3017.78232	3847.71139	3204.15462	3916.34921	3094.80745
FTN_0973	409.792078	795.37278	929	781.035719	933.038975	977.725867	1028.65132	855.906151
FTN_0974	617.131511	1092.56596	1225	757.223654	1152.68991	1104.29507	1407.4281	794.068895
FTN_0975	2921.6011	2940.49793	3212	2988.41411	3141.96339	2928.93031	3019.44634	2907.33259
FTN_0976	820.282268	966.830385	1092	928.670519	1331.27567	1163.75711	1377.65802	1025.71322
FTN_0977	612.942835	552.474506	670	577.839434	879.558748	576.78181	782.889799	546.71987
FTN_0978	1.39622514	3.81016901	2	3.17494195	0	7.64511972	15.2017437	2.94463126
FTN_0979	529.86744	849.667688	798	792.148015	843.268593	949.693761	800.625167	794.068895
FTN_0980	21.6414896	101.922021	116	88.8983745	7.64003255	636.243852	516.225879	76.5604126
FTN_0981	0	1.9050845	7	2.38120646	1.91000814	1.69891549	12.6681197	15.7047
FTN_0982	0	0	0	0	0	1.69891549	1.26681197	0
FTN_0983	0.69811257	9.52542252	21	0.79373549	10.5050448	9.34403522	22.1692095	4.90771876
FTN_0984	1917.01711	1970.80992	1980	2033.55032	2640.58625	2057.38666	2282.16177	1984.68147
FTN_0985	672.282404	710.59652	606	636.57586	903.433849	653.233007	635.306204	682.172907
FTN_0986	1687.33808	2051.77601	2058	2374.85658	2492.56062	2202.64394	2246.69103	2363.55735
FTN_0987	1740.39463	1509.77947	1845	1752.56795	2311.10985	1646.24911	1909.08564	1683.34753
FTN_0988	1480.69676	1616.4642	1754	1469.20439	2045.61872	1834.82873	1892.61709	1499.79885
FTN_0989	1864.65867	2103.21329	2353	2338.34474	2565.14093	2211.13852	2496.8864	2428.33924
FTN_0990	3637.16648	3824.45714	3910	4086.15028	4978.43621	4002.6449	4124.73978	4143.09618
FTN_0991	1651.03623	1740.29469	1721	1720.0248	2270.99968	2016.61269	1670.29159	1835.48682
FTN_0992	2.09433771	3.81016901	2	22.2245936	2.86501221	11.8924085	12.0347137	39.2617501
FTN_0993	2.09433771	11.430507	33	1.58747097	3.82001628	22.9353592	39.9045771	4.90771876
FTN_0994	770.018163	1066.84732	1061	1046.93711	1085.83963	1005.75797	840.529744	1005.1008

FTN_0995	374.886449	341.010126	515	553.233634	191.000814	327.89069	379.410186	538.86752
FTN_0996	901.263326	867.765991	1039	1040.58722	600.697559	861.350155	843.696774	1007.06389
FTN_0997	2917.41242	3261.50467	3546	3168.59206	4017.70212	3544.78718	3638.28399	3190.99874
FTN_0999	14.6603639	81.9186336	128	95.2482584	26.7401139	285.417803	243.227899	73.6157814
FTN_1000	696.018231	1334.51169	1078	1168.37864	640.80773	1314.11113	1118.59497	1248.52365
FTN_1001	2157.16784	1406.90491	1682	1321.56958	375.316599	1051.62869	984.946309	1475.26026
FTN_1002	971.772696	1006.83716	1055	1080.274	1293.07551	1106.84344	1055.88778	1102.27363
FTN_1003	47.4716547	8.57288026	71	61.9113679	74.4903174	24.6342747	81.0759663	83.4312189
FTN_1004	1457.65904	786.7999	994	839.772145	1050.50448	867.29636	1115.42794	795.050439
FTN_1005	448.188269	718.216858	775	653.244305	768.778276	816.328895	818.360535	687.080626
FTN_1006	1683.1494	2500.42341	2271	2336.75727	2377.96013	1997.07516	1535.37611	2604.03557
FTN_1007	36.9999661	2.85762675	45	46.0366582	54.4352319	5.09674648	25.9696454	46.1325563
FTN_1008	1.39622514	32.3864366	5	25.3995356	16.2350692	37.3761409	12.0347137	31.4094001
FTN_1009	1135.13104	1278.3117	1231	1054.87446	1574.80171	1341.29378	1495.47153	1062.03034
FTN_1010	2053.84718	2037.48788	2772	2172.45403	3064.60806	2398.86868	3125.85854	2279.14459
FTN_1011	2170.43198	2832.86066	2598	2855.06654	136.565582	92.5908944	60.1735687	2999.59771
FTN_1012	935.470842	1257.35577	1146	1247.75218	1422.00106	1382.06775	1299.11568	1341.77031
FTN_1013	2250.71492	1647.8981	2225	1781.93617	2115.33401	1715.90465	2217.55436	1834.50527
FTN_1014	1763.43235	1847.93197	2098	1890.67793	2093.36892	1946.95716	2317.6325	1932.65965
FTN_1015	769.320051	739.172787	868	1072.33664	961.689098	792.544078	972.278189	1112.08907
FTN_1016	994.112298	711.549062	671	728.649176	879.558748	704.200472	734.750944	735.17627
FTN_1018	1273.35733	1694.57267	1608	1456.50462	1582.44174	1874.75325	1827.37627	1487.03878
FTN_1019	1320.82898	1846.97943	1930	1984.33872	2034.15867	2018.31161	2279.62815	1991.55227
FTN_1020	1065.31978	1080.18291	772	1104.8798	1305.49056	1169.70332	955.809634	1273.06225
FTN_1021	1067.41412	676.304999	998	1008.8378	778.328316	677.017824	1067.92249	1114.05216
FTN_1022	77.4904951	143.83388	174	184.146633	371.496583	536.007838	551.063208	209.068819
FTN_1023	937.56518	1248.78289	1431	1128.69186	1465.93125	1314.96059	1648.75578	1129.75686
FTN_1024	1628.69662	2118.45397	2097	2367.71296	2129.65907	2282.49297	2197.91877	2365.52044

FTN_1025	205.943208	215.274549	167	249.232943	152.800651	396.696768	208.39057	227.71815
FTN_1026	1185.39514	1296.41	1148	1327.91947	1569.07169	1467.86299	1212.97246	1440.90623
FTN_1027	534.754228	358.155887	462	365.912059	500.422132	464.653388	577.032854	412.248376
FTN_1028	124.264037	374.349105	342	284.95104	8.59503662	366.965747	225.492531	334.706419
FTN_1029	83.7735083	426.738929	488	525.452892	310.376322	1090.70375	939.341078	543.775238
FTN_1030	2.09433771	1.9050845	3	25.3995356	4.77502035	4.24728873	11.4013078	29.4463126
FTN_1031	487.282573	589.623654	525	670.706486	601.652563	619.254698	552.963426	660.578945
FTN_1032	3456.35533	3712.05715	3950	3352.73869	4601.2096	3965.26876	4081.03477	3519.81589
FTN_1033	127.7546	145.738965	127	122.235265	320.881367	286.267261	224.225719	142.323844
FTN_1034	154.98099	60.0101619	92	107.948026	324.701383	261.632986	259.063048	99.1359189
FTN_1035	196.169632	547.711795	562	452.429227	756.363223	1117.88639	1054.62097	404.396026
FTN_1036	45.377317	119.067781	116	106.360555	79.2653377	461.255557	365.475254	132.508406
FTN_1037	10.4716885	42.8644013	69	82.5484906	31.5151343	215.762268	304.66828	100.117463
FTN_1038	1343.16858	1151.62358	1266	953.276319	1281.61546	1337.89595	1378.29143	942.282002
FTN_1039	4030.20386	5141.82307	4776	4762.41292	6464.42254	5526.5721	5197.72953	4972.50065
FTN_1040	1251.01772	1274.50153	1334	1228.70253	1296.89553	1212.1762	1309.25017	1204.35418
FTN_1041	571.754194	457.220281	745	737.380267	689.512938	421.331042	784.790017	690.025257
FTN_1042	3045.16703	2755.70473	3229	2978.88928	3935.57177	2810.00623	2868.69571	3180.20176
FTN_1043	3329.29884	3261.50467	3164	3133.6677	3799.00619	3403.77719	2928.23588	3123.27222
FTN_1044	3639.26082	3276.74535	3895	3324.95795	4461.77901	3535.44314	4034.79613	3370.62124
FTN_1045	13.2641388	29.5288098	26	20.6371226	7.64003255	35.6772254	32.3037053	32.3909438
FTN_1046	6.28301312	146.691507	190	63.4988389	14.325061	219.160099	264.130296	67.7265189
FTN_1047	9.07546339	254.328781	258	250.026678	10.5050448	303.256416	235.627027	251.2752
FTN_1048	6.98112569	284.810133	217	202.402549	16.2350692	382.255986	231.826591	202.198013
FTN_1049	1862.56433	1935.56586	2083	1699.38768	2373.18511	2104.9563	2248.59125	1718.68311
FTN_1050	1881.41337	1588.84048	1944	1691.45032	2016.96859	1669.18447	1992.69523	1510.59583
FTN_1051	61.4339061	60.9627041	41	31.7494195	50.6152157	78.9995705	140.616129	28.4647688
FTN_1052	44.6792044	73.3457534	46	52.3865421	89.7703825	78.1501127	45.605231	71.6526939

FTN_1053	268.075226	269.569457	283	225.420878	234.931001	349.127134	390.178088	216.921169
FTN_1054	0.69811257	0.95254225	0	0	0.95500407	0.84945775	4.43384191	0.98154375
FTN_1055	2011.26231	2047.0133	2331	2400.25611	1080.1096	1969.89252	1665.85774	2385.15132
FTN_1056	252.018637	465.793161	684	706.424583	195.775834	536.857296	447.184626	659.597401
FTN_1057	123.565925	222.894887	305	384.167975	79.2653377	259.084613	219.791877	381.820519
FTN_1058	194.075294	295.288098	339	319.875401	161.395688	363.567916	313.535963	295.444669
FTN_1059	784.678527	949.684625	930	1302.51993	1135.49984	1049.92978	925.406146	1244.59748
FTN_1060	1087.65938	1418.33541	1253	1449.361	1451.60618	1570.64737	1235.77508	1401.64448
FTN_1061	1172.131	1576.45743	1523	1755.7429	1889.95305	1757.52808	1565.7796	1698.07069
FTN_1062	1044.3764	1072.56258	1055	931.051726	1262.51538	1162.90766	1019.78364	969.765227
FTN_1063	839.131308	200.033873	192	130.17262	408.741742	308.353162	259.063048	144.286931
FTN_1064	79.5848328	15.240676	14	34.9243614	13.370057	7.64511972	9.5010898	33.3724876
FTN_1065	575.942869	25.7186408	69	7.93735486	21.0100895	16.1396972	39.2711712	5.88926251
FTN_1066	9611.61385	1885.08112	1968	2002.59463	240.661025	1127.23043	1088.19148	1967.01368
FTN_1067	25314.2599	4870.34853	3381	3751.19391	83.085354	1633.50725	1036.8856	3273.44841
FTN_1068	585.716445	686.782963	567	459.572847	814.618471	739.877698	597.301845	546.71987
FTN_1069	4134.22263	4720.7994	4842	5054.50758	5712.83434	4938.74734	5059.01361	5062.80267
FTN_1070	2106.20562	2437.55562	2360	2506.61667	3123.81831	2570.45914	2456.34842	2523.54899
FTN_1071	2200.45082	2669.97593	2647	2586.78395	3360.65932	2831.24267	2849.69353	2744.39633
FTN_1072	1456.96093	1752.67774	1633	1646.2074	2181.22929	1704.01224	1660.7905	1676.47673
FTN_1073	1996.60195	1646.94555	1963	2066.88721	2217.51945	1788.10856	2075.03801	2176.0825
FTN_1074	1510.01749	1461.19981	1489	1659.7009	2426.66534	1935.06475	1936.3221	1727.517
FTN_1075	903.357664	910.630393	850	752.461241	1023.76436	1089.85429	910.837809	741.065533
FTN_1076	11.1698011	38.1016901	6	5.5561484	20.0550854	45.8707183	12.0347137	5.88926251
FTN_1077	1153.28196	1210.6812	1379	1392.21204	1619.6869	1269.93933	1420.09622	1375.1428
FTN_1079	2436.41287	2838.57591	3171	2863.0039	3710.19081	3196.5095	3334.88252	2873.9601
FTN_1080	1178.41402	1503.11167	1482	1366.01877	1817.37274	1629.25996	1409.96173	1394.77367
FTN_1081	166.150791	1872.69807	2019	1906.55264	225.38096	1839.92548	1902.75158	1812.91131

FTN_1082	2268.86585	2098.45058	2518	2189.12247	2561.32091	2049.74154	2258.72575	2161.35934
FTN_1083	1026.22548	1268.78628	1128	1074.71785	1303.58055	1230.01482	1154.69911	1077.73504
FTN_1084	0	7.62033801	0	0	0.95500407	4.24728873	1.26681197	1.9630875
FTN_1085	1073.69713	1151.62358	1277	981.850797	1558.56664	1200.2838	1373.85758	1073.80886
FTN_1086	1049.9613	1392.61677	1489	1193.77817	2568.00594	1029.54279	1239.57552	1343.7334
FTN_1087	1172.131	1449.76931	1489	1185.04708	495.647112	861.350155	628.338739	1089.51356
FTN_1088	2009.16797	1850.78959	1846	2464.54869	2165.94923	1718.45302	1731.09856	2344.90802
FTN_1089	260.395988	445.789774	328	361.943382	301.781286	454.459895	438.950349	353.355751
FTN_1090	717.659721	738.220245	820	688.962402	209.145891	207.26769	165.318962	764.622583
FTN_1091	6.28301312	53.3423661	39	91.2795809	4.77502035	135.063782	62.7071927	55.9479938
FTN_1092	4.18867541	11.430507	4	6.34988389	15.2800651	10.193493	8.23427782	6.87080626
FTN_1093	84.4716208	53.3423661	61	82.5484906	94.5454028	69.6555352	92.477274	95.2097439
FTN_1094	163.358341	119.067781	35	94.4545229	105.050448	130.816493	43.0716071	92.2651127
FTN_1095	39.0943039	55.2474506	40	14.2872388	8.59503662	62.8598733	36.7375472	17.6677875
FTN_1096	0	13.3355915	5	8.73109035	0	20.3869859	3.16702993	6.87080626
FTN_1097	1191.67815	1198.29815	1331	1536.6719	1563.34166	1287.77794	1391.59295	1652.91968
FTN_1098	1635.67775	1923.18281	1942	1604.13942	2323.5249	1875.60271	1966.72559	1630.34417
FTN_1099	1269.86676	1442.14897	1418	1249.33966	1740.01741	1423.69118	1554.37829	1217.11425
FTN_1100	1172.131	1523.11506	1369	1339.8255	1457.33621	1483.15323	1477.10276	1260.30218
FTN_1101	1453.47037	1786.01672	1462	1898.61528	1977.81343	1758.37754	1374.49099	1909.1026
FTN_1103	1397.62136	1240.21001	1513	1335.06309	1588.17177	1331.10029	1431.49753	1396.73676
FTN_1104	844.716208	845.857519	1038	909.620867	1107.80472	921.661655	984.946309	996.266908
FTN_1105	5.58490055	4.76271126	19	6.34988389	6.68502848	2.54837324	24.0694275	2.94463126
FTN_1106	1264.97997	1656.47098	1497	1910.52132	1694.17722	1650.4964	1587.3154	1897.32407
FTN_1107	2179.50744	3109.09791	2916	2610.59601	3443.74467	3112.41318	2905.43326	2747.34096
FTN_1108	1767.62102	2529.95222	2703	2345.48836	3220.27372	2789.61924	3051.11664	2567.71845
FTN_1109	6.98112569	26.671183	32	30.1619485	9.55004069	61.1609578	63.3405986	31.4094001
FTN_1110	94.9433094	63.8203309	113	44.4491872	114.600488	97.6876409	104.511988	52.0218188

FTN_1111	34.2075159	6.66779576	9	15.8747097	7.64003255	6.79566198	25.9696454	10.7969813
FTN_1112	9388.21783	6697.32457	6995	6612.61034	418.291782	5976.78471	5897.00973	6659.77436
FTN_1113	1017.84813	1060.17953	1110	1159.64755	1228.13523	1085.607	972.278189	1163.12935
FTN_1114	561.282505	767.749055	892	1070.74917	769.73328	778.952754	939.974484	1171.96324
FTN_1115	1544.92311	1710.76588	1713	2295.48303	2402.79024	3011.32771	2793.3204	2334.11104
FTN_1116	1377.3761	1565.02692	1780	1542.22805	1995.0035	2725.06045	2536.15757	1533.17134
FTN_1117	1386.45156	1479.29812	1669	1656.52596	1893.77307	1602.07731	1675.99224	1602.86095
FTN_1118	321.131782	319.101654	441	519.103008	486.097071	357.621711	468.72043	490.771876
FTN_1119	309.961981	451.505027	581	380.993033	443.121888	445.965317	615.670619	487.827245
FTN_1120	28.6226153	87.6338872	20	24.6058001	67.8052889	86.6446902	37.3709532	45.1510126
FTN_1121	1695.71543	1906.03705	1550	1776.38002	2190.77933	1960.54848	1671.5584	1887.50863
FTN_1122	577.339094	883.95921	508	900.096042	860.458666	846.059916	474.421084	981.543752
FTN_1123	441.905256	443.884689	672	517.515537	612.157608	453.610437	592.234597	553.590676
FTN_1124	364.414761	438.169436	443	431.792105	513.792189	434.072909	366.742066	474.085632
FTN_1125	1783.67761	2598.53526	2344	2058.94985	2463.9105	2497.40578	2287.86242	2163.32243
FTN_1126	201.754532	202.8915	202	146.047329	295.096257	222.55793	203.323322	190.419488
FTN_1127	1948.43218	1899.36925	1821	1773.99881	2302.51481	1928.26909	1843.21142	1810.94822
FTN_1128	4.88678798	11.430507	25	9.52482584	23.8751017	9.34403522	8.23427782	11.778525
FTN_1129	113.792349	201.938957	193	189.702781	13.370057	55.2147535	29.7700814	168.825525
FTN_1130	2644.45041	2662.35559	2934	2831.25448	4048.26225	3217.74595	3212.00176	2784.63962
FTN_1131	1182.60269	2156.55566	2538	2201.0285	1282.57046	5535.06668	5715.85562	2229.08586
FTN_1132	4.88678798	7.62033801	27	11.9060323	5.73002441	62.8598733	86.7766201	31.4094001
FTN_1133	142.414964	86.6813449	56	85.7234325	21.0100895	40.7739719	33.5705173	89.3204814
FTN_1134	263.188438	407.688084	540	281.776098	445.9869	453.610437	569.431982	295.444669
FTN_1135	2.79245028	22.861014	31	15.8747097	16.2350692	170.741007	79.8091543	16.6862438
FTN_1136	0	2.85762675	5	0.79373549	0.95500407	0.84945775	4.43384191	0.98154375
FTN_1137	2611.63912	2727.12847	2859	2592.3401	3903.10163	4666.92086	4440.17597	2653.11276
FTN_1138	339.282708	627.725344	470	749.286299	604.517576	1108.54236	715.115359	657.634314

FTN_1139	654.82959	710.59652	636	721.505557	1126.9048	1156.11199	1107.82707	736.157814
FTN_1140	763.037038	942.064287	841	739.761473	1152.68991	1442.37925	1426.43028	680.20982
FTN_1141	1308.96107	1468.82015	1727	1705.73756	2037.02368	2452.38452	2745.81495	1699.05223
FTN_1142	18.8490394	39.0542323	40	19.8433872	17.1900732	56.0642113	32.3037053	15.7047
FTN_1143	4199.1471	4665.55195	4664	4458.41223	5724.29439	4804.53302	5074.21536	4486.63649
FTN_1144	785.37664	1016.36258	918	1012.80648	1043.81945	1050.77923	974.811813	1004.11926
FTN_1145	128.452713	81.9186336	151	3.17494195	117.4655	64.5587888	114.646484	2.94463126
FTN_1146	54.4527804	128.593204	185	147.6348	87.8603744	720.340169	644.807294	152.139282
FTN_1147	747.678561	1180.19985	1028	1482.69789	1427.73108	1500.99184	1230.07443	1547.8945
FTN_1148	60.0376809	15.240676	9	4.76241292	83.085354	28.0321056	18.3687736	7.85235001
FTN_1149	91.4527465	148.596591	201	296.063336	318.971359	273.525395	318.603211	332.743332
FTN_1150	76.7923826	114.30507	34	86.517168	129.880553	108.730592	42.4382011	89.3204814
FTN_1151	2162.75274	2633.77933	2549	2795.53638	3448.51969	4269.37464	3826.40556	2794.45506
FTN_1152	2684.24283	2792.85388	2951	2606.62734	3026.40789	2611.23311	3011.21206	2632.50034
FTN_1153	749.074786	808.708372	770	1050.90578	1034.26941	823.124557	884.868163	1070.86423
FTN_1154	2186.48857	2368.97258	2479	2462.16748	2686.42645	2302.03049	2399.34188	2474.4718
FTN_1155	4299.67531	4136.891	4372	4471.11199	5442.56819	4025.58026	4447.77684	4554.36301
FTN_1156	2151.58294	2611.87085	3048	2589.16516	3282.34899	2612.08257	3222.76966	2645.26041
FTN_1157	2215.11118	1932.70823	1987	2085.93686	354.30651	1900.23698	1677.25905	2105.41135
FTN_1158	890.791638	1089.70834	1151	1004.07539	1412.45102	1208.77837	1201.57116	973.691402
FTN_1159	3292.29887	3371.99957	40	3220.18487	31.5151343	5098.4454	79.1757483	1804.07742
FTN_1160	1479.99865	1450.72185	1773	1608.90183	2356.95004	1415.19661	1943.28957	1604.82403
FTN_1161	1413.67795	1923.18281	1885	1732.72457	2298.69479	2080.32202	1957.2245	1709.84922
FTN_1162	416.075091	109.542359	145	115.885381	295.096257	199.622571	253.995801	112.877531
FTN_1163	12.5660262	3.81016901	10	1.58747097	2.86501221	17.8386127	13.3015257	0.98154375
FTN_1164	69.8112569	42.8644013	91	131.760091	84.0403581	45.8707183	96.2777099	139.379213
FTN_1165	1399.01759	1428.81338	1648	1520.79719	1799.22767	1591.88382	1568.31322	1502.74348
FTN_1166	2263.28095	2158.46074	2327	2532.80994	3063.65305	2248.51466	2292.92967	2654.0943

FTN_1167	116.584799	198.128788	187	239.708117	125.105533	219.160099	176.72027	257.164463
FTN_1168	2442.69588	2435.65054	2752	2401.84358	3288.07901	2481.26608	2936.47015	2434.2285
FTN_1169	1998.69628	2199.42006	2344	2077.9995	2872.65224	2356.39579	2548.82569	2200.62109
FTN_1170	2806.41253	2890.01319	3099	2985.23916	3506.77494	2849.08128	2907.33348	3060.45342
FTN_1171	1187.48948	1714.57605	1642	1888.29672	2059.94378	1835.67819	1716.53022	1901.25025
FTN_1172	1869.54546	1966.99975	2537	1945.44568	2893.66233	2138.93461	2596.33114	1893.3979
FTN_1173	2002.88496	2437.55562	2896	2538.36609	2883.15728	2566.21185	2577.96237	2603.05403
FTN_1174	2696.11074	90.4915139	55	120.647794	70.6703011	95.9887254	126.681197	132.508406
FTN_1175	545.225916	292.430471	103	108.741762	42.020179	85.7952324	43.0716071	107.969813
FTN_1176	2638.86551	3384.38262	3441	3400.36282	4871.47576	3268.71341	3085.95397	3379.45514
FTN_1177	1166.5461	1555.5015	1570	1119.16704	2142.07413	1788.95802	1985.09436	1130.7384
FTN_1178	1006.67832	1026.84055	1073	977.088384	1378.07087	1078.81134	1150.26527	950.134352
FTN_1179	1621.01738	1998.43364	2637	1581.12109	2308.24483	1931.66692	2800.28787	1528.26362
FTN_1180	969.678358	1810.78282	1393	1712.08744	1345.60073	1857.76409	1233.24146	1830.5791
FTN_1181	1032.50849	1554.54895	1569	1766.85519	1315.99561	1385.46559	1570.84685	1813.89285
FTN_1182	26.5282776	13.3355915	15	21.4308581	4.77502035	22.0859014	27.2364574	20.6124188
FTN_1183	11.8679137	2.85762675	16	5.5561484	0.95500407	4.24728873	7.60087184	5.88926251
FTN_1184	2.79245028	9.52542252	20	15.0809742	15.2800651	16.9891549	30.4034874	9.81543752
FTN_1185	4.18867541	0.95254225	10	6.34988389	7.64003255	11.8924085	6.96746585	5.88926251
FTN_1186	3189.67633	2624.2539	2745	2866.97258	2647.27128	2402.26651	2482.31806	2922.05575
FTN_1187	1085.56504	784.894815	907	797.704164	1129.76981	801.888113	1041.31944	866.703133
FTN_1188	30.716953	6.66779576	14	25.3995356	32.4701383	8.49457747	13.3015257	16.6862438
FTN_1189	0	0	3	0	0.95500407	0.84945775	1.90021796	0
FTN_1190	3.49056284	0	1	0	0	0	0.63340599	0.98154375
FTN_1191	2.09433771	1.9050845	7	7.93735486	5.73002441	6.79566198	17.1019616	2.94463126
FTN_1192	2874.82756	2789.99626	2868	2724.89392	3769.40106	2984.14506	3061.88454	2827.82755
FTN_1193	641.565451	982.071061	1015	730.236647	1073.42457	1032.94062	1014.08298	807.810508
FTN_1194	223.396022	261.949119	219	434.173311	300.826282	300.708042	229.292967	408.322201

FTN_1195	71.9055946	17.1457605	17	15.0809742	33.4251424	20.3869859	11.4013078	12.7600688
FTN_1196	198.962082	276.237253	285	322.256607	176.675753	269.278106	309.735527	315.075544
FTN_1197	1169.33855	1043.98631	1066	879.458919	1474.52628	1163.75711	1115.42794	921.669583
FTN_1198	35.603741	19.050845	84	34.9243614	129.880553	39.9245141	85.5098082	30.4278563
FTN_1199	3431.22328	3630.13852	3668	2914.59671	1376.16086	2753.09256	3049.84982	2691.39297
FTN_1200	2016.84721	1880.3184	2013	2081.96818	897.703825	1460.21787	1829.90989	1840.39453
FTN_1201	2724.03524	2358.49462	2417	2785.21782	1170.83499	1756.67862	1968.62581	2583.42315
FTN_1202	1318.73464	2924.30471	2942	2971.74566	1091.56965	2602.73854	2685.00798	2878.86782
FTN_1208	3543.6194	1572.64726	1401	1571.59626	1838.38283	1271.63825	1153.4323	1590.10088
FTN_1209	981.546272	1531.68794	1683	1939.88953	1724.73735	1963.09685	1923.65398	2009.22006
FTN_1210	57.9433432	33.3389788	26	113.504175	524.297234	113.827338	79.8091543	101.099006
FTN_1211	1043.67829	1346.89474	1435	1073.13038	1362.79081	1280.98228	1382.72527	1150.36928
FTN_1212	1782.28139	2617.58611	2607	2154.19811	2636.76623	1485.7016	1685.49333	2134.85766
FTN_1213	1506.52692	2712.84033	2943	2695.52571	2621.48617	1559.60442	1859.67998	2828.80909
FTN_1214	1211.22531	2749.98948	2599	2002.59463	1813.55273	1129.7788	1029.28473	2278.16305
FTN_1215	1259.39507	3123.38604	2841	2566.94056	2236.61953	1287.77794	1202.20456	2870.03393
FTN_1216	1099.5273	1768.87096	1717	2195.47236	1710.41229	867.29636	756.920154	2408.70837
FTN_1217	1510.01749	3932.09441	4427	3806.75539	3629.01546	1911.27993	1911.61927	4201.9888
FTN_1218	2387.54499	2970.02674	3050	2570.1155	3596.54532	2042.94588	2220.08798	2477.41643
FTN_1219	2382.6582	3101.47757	3466	3644.03962	3679.63068	2267.20273	2280.89496	3744.58941
FTN_1220	1238.4517	1823.16587	2011	1951.00183	1540.42156	2469.37367	2448.11414	2013.14623
FTN_1221	1.39622514	7.62033801	4	4.76241292	0.95500407	11.8924085	10.1344958	6.87080626
FTN_1222	5796.42866	3428.19956	3239	3732.93799	8.59503662	296.460754	311.002339	1298.58238
FTN_1223	1782.28139	2108.92855	2045	2314.53268	2399.92523	2176.31075	2067.43714	2327.24024
FTN_1224	820.980381	968.73547	1062	1339.03177	1209.99016	1072.86513	1100.8596	1402.62602
FTN_1225	1510.7156	2006.05398	1994	1489.04777	2058.03377	2111.75196	2102.90788	1483.11261
FTN_1226	299.490292	300.050809	274	193.671459	367.676567	303.256416	310.368933	204.1611
FTN_1227	1125.35746	1283.07441	1058	1283.47028	1516.54646	1410.09986	1150.89868	1351.58575

FTN_1228	0	1.9050845	3	3.96867743	0	4.24728873	3.16702993	0.98154375
FTN_1229	898.470876	1271.64391	1161	1389.0371	1634.96697	1549.41093	1580.34794	1368.27199
FTN_1230	1072.30091	944.921914	1115	1115.19836	654.177787	1087.30592	1330.78598	1012.95315
FTN_1231	590.603233	969.688012	959	900.889777	937.813996	1003.2096	1041.95285	1017.86087
FTN_1232	1068.81034	1084.94562	1232	1318.39464	1310.26558	1107.6929	1331.41938	1347.65957
FTN_1233	1150.48951	1448.81676	1645	1291.40764	2096.23393	1541.76581	1807.10728	1377.10588
FTN_1234	1507.22504	1719.33876	2095	2281.19579	2252.8546	1752.43133	2108.60853	2196.69492
FTN_1235	402.810952	559.142302	598	663.562867	572.047437	585.276388	622.004679	676.283645
FTN_1236	80.2829454	22.861014	52	64.2925744	106.005452	62.8598733	84.8764022	58.8926251
FTN_1237	2.09433771	3.81016901	12	7.93735486	0.95500407	9.34403522	12.6681197	7.85235001
FTN_1238	71.207482	184.793197	166	150.016007	55.390236	206.418233	117.813513	143.305388
FTN_1239	1373.88554	1083.04054	1309	1366.81251	1029.49439	1059.27381	1221.20674	1357.47501
FTN_1240	166.848904	64.7728731	141	104.773084	0.95500407	39.0750564	69.6746585	66.7449751
FTN_1241	21.6414896	28.5762675	9	4.76241292	26.7401139	12.7418662	10.7679018	5.88926251
FTN_1242	1984.03592	1211.63374	1602	954.070055	901.523841	1014.25255	1118.59497	1027.67631
FTN_1243	1047.16885	1293.55238	1454	1343.79418	1634.01196	1422.84173	1612.01824	1481.14952
FTN_1244	2.79245028	0.95254225	17	0.79373549	14.325061	7.64511972	20.2689916	1.9630875
FTN_1245	3.49056284	4.76271126	14	5.5561484	18.1450773	23.7848169	19.6355856	1.9630875
FTN_1246	0.69811257	7.62033801	14	8.73109035	5.73002441	14.4407817	30.4034874	13.7416125
FTN_1247	0.69811257	2.85762675	4	6.34988389	2.86501221	8.49457747	7.60087184	3.92617501
FTN_1248	0	1.9050845	2	7.14361938	2.86501221	5.09674648	7.60087184	3.92617501
FTN_1249	0	5.71525351	4	6.34988389	2.86501221	11.8924085	17.1019616	16.6862438
FTN_1250	5.58490055	10.4779648	8	7.14361938	9.55004069	8.49457747	17.1019616	6.87080626
FTN_1251	3067.50663	3240.54874	3856	3388.45679	3948.94183	3351.96027	3732.02807	3449.14474
FTN_1252	1762.73424	2227.99633	2081	1968.46401	2446.72042	2290.13809	2047.80155	1991.55227
FTN_1253	32925.7812	4037.8266	4068	3104.29949	64.9402767	445.965317	892.469035	1616.60256
FTN_1254	9912.50036	2737.60643	2141	2086.73059	106.005452	530.061634	686.612089	1981.73683
FTN_1255	6452.65447	3771.11477	3662	4275.05933	1020.89935	1181.59573	1658.89028	4269.71532

FTN_1256	8209.1057	3773.01986	3759	3105.09322	1800.18267	1398.20745	1863.48041	3263.63297
FTN_1257	1789.26251	2201.32514	2311	1732.72457	2211.78942	2074.37582	2450.64776	1928.73347
FTN_1258	203.84887	641.060935	589	496.084679	317.061351	814.629979	777.189145	540.830607
FTN_1259	20.2452645	2.85762675	11	8.73109035	25.7851099	6.79566198	34.2039233	5.88926251
FTN_1260	2877.62001	2850.95896	3180	3078.89995	3787.54614	2971.4032	3404.55718	3136.03229
FTN_1261	3727.92112	3552.03006	4369	3547.99762	3236.50879	2497.40578	2542.49163	3646.43504
FTN_1262	2902.05395	2827.1454	3037	3179.70436	4018.65712	2836.33942	2959.27277	3306.8209
FTN_1263	39.0943039	99.0643942	117	54.7677486	72.5803092	69.6555352	91.843868	56.9295376
FTN_1264	1298.48938	1126.85748	1111	956.451261	876.693735	1915.52722	2317.6325	877.500114
FTN_1265	1008.77266	1466.91507	1087	1504.92248	1324.59064	1365.0786	1086.29127	1458.57402
FTN_1266	1907.24354	2690.93186	2433	2516.14149	2042.7537	2101.55847	1793.17235	2538.27214
FTN_1267	1128.84802	1746.96249	1935	1658.11343	1265.38039	1264.84259	1319.38467	1682.36599
FTN_1268	956.414219	1518.35235	1645	1639.06378	1026.62937	1156.96145	1176.23492	1624.45491
FTN_1269	994.112298	1453.57948	1446	1608.90183	1132.63483	1131.47772	1012.81617	1660.77203
FTN_1270	919.414253	1011.59987	1223	1164.40996	1179.43003	1060.97273	1128.72947	1225.94815
FTN_1271	933.376504	1171.62697	1082	1032.64987	1125.9498	1280.13282	1211.70565	1069.88269
FTN_1272	2885.29925	6.66779576	3498	2960.63336	4284.14825	11.8924085	3603.44666	2929.9081
FTN_1273	578.037207	1651.70826	1767	1519.20972	425.931815	1140.82175	972.278189	1404.58911
FTN_1274	1066.01789	961.115132	1039	1126.31066	26.7401139	1045.68249	1030.55154	1078.71658
FTN_1275	4612.42974	3863.51137	4166	3331.30784	15.2800651	4337.33126	5654.41524	3274.42996
FTN_1276	2984.43123	2657.59288	2739	2782.04288	13.370057	2808.30731	3574.30998	2674.70672
FTN_1277	2750.56352	2549.00307	2202	1717.64359	16.2350692	2377.63223	2607.73245	1754.01868
FTN_1278	5.58490055	59.0576196	49	42.8617163	14.325061	329.589606	111.479454	34.3540313
FTN_1279	685.546543	742.982956	647	977.882119	918.713914	722.039085	661.909256	1034.54711
FTN_1280	966.885908	1188.77273	1178	1035.82481	1328.41066	1200.2838	1110.36069	1010.00852
FTN_1281	1098.82918	1398.33203	1355	1298.55126	1768.66754	1318.35842	1357.38903	1367.29045
FTN_1282	999.697199	1315.46085	1343	1367.60624	1553.79162	1387.1645	1427.69709	1326.06561
FTN_1283	552.207042	1216.39646	956	1013.60022	289.366233	1257.19747	819.627347	1097.36591

FTN_1284	7.67923826	21.9084718	28	9.52482584	7.64003255	34.8277676	24.0694275	9.81543752
FTN_1285	8.37735083	4.76271126	11	5.5561484	2.86501221	2.54837324	9.5010898	2.94463126
FTN_1286	40.490529	80.0135491	54	179.38422	9.55004069	216.611725	46.238637	120.729881
FTN_1287	5.58490055	14.2881338	14	11.1122968	4.77502035	12.7418662	30.4034874	7.85235001
FTN_1288	0.69811257	0.95254225	4	0.79373549	0	0	1.26681197	0.98154375
FTN_1289	0	0	0	1.58747097	1.91000814	0	3.16702993	0
FTN_1290	9.07546339	53.3423661	59	119.854058	19.1000814	78.9995705	67.7744406	110.914444
FTN_1291	435.622243	691.545675	976	660.387925	657.0428	798.490282	1048.28691	701.803782
FTN_1292	2227.67721	2549.95561	2796	2285.9582	3215.4987	2683.43702	2982.70879	2454.84092
FTN_1293	965.489683	1160.19646	1060	1434.28002	1308.35557	1139.9723	1130.62969	1493.90959
FTN_1294	781.886077	1234.49476	1360	1327.12573	1577.66672	1340.44432	1766.5693	1222.02197
FTN_1295	20.2452645	26.671183	90	106.360555	76.4003255	62.0104155	100.711552	87.3573939
FTN_1296	0	3.81016901	4	2.38120646	0.95500407	22.9353592	13.9349317	4.90771876
FTN_1297	67.0188066	203.844042	129	153.984684	150.890643	256.53624	163.418745	155.083913
FTN_1298	342.075159	368.633851	408	273.838743	530.982262	926.758402	1218.67312	273.850707
FTN_1299	147.301752	142.881338	123	204.783755	219.650936	135.063782	125.414385	212.01345
FTN_1300	1324.31954	1712.67097	1455	1528.73455	1791.58763	1769.42049	1567.67982	1462.50019
FTN_1301	2278.63942	2704.26745	2718	2881.25982	3049.32799	2765.83442	2780.65228	2943.64971
FTN_1302	289.716716	695.355844	603	638.957067	15.2800651	382.255986	122.880761	388.691326
FTN_1303	1251.71584	1341.17949	1082	1269.18304	1831.6978	1423.69118	1202.83797	1374.16125
FTN_1304	9.07546339	34.2915211	41	26.9870065	15.2800651	43.3223451	51.3058849	38.2802063
FTN_1305	321.131782	989.691399	897	842.153351	403.011717	1291.17578	1094.52554	908.909514
FTN_1308	224.792247	320.054197	254	265.107652	195.775834	366.965747	254.629207	276.795338
FTN_1309	4421.1469	6524.91442	6751	6728.49572	7225.56079	6690.32921	7122.65032	6926.75426
FTN_1310	5327.29701	7665.1075	7648	6784.0572	8068.82938	7835.39826	7555.26661	7184.90026
FTN_1311	422.358104	570.572809	582	644.513215	634.122702	537.706754	608.703153	645.855789
FTN_1312	487.980686	694.403301	658	693.724815	742.038162	645.587888	762.620808	713.582307
FTN_1313	2140.41314	3048.13521	2895	2628.0582	3231.73377	3112.41318	3088.48759	2976.04066

FTN_1314	1096.73485	960.16259	1020	882.633861	1001.79927	836.715881	939.341078	919.706495
FTN_1315	3161.05371	2856.67421	3386	3052.70668	3013.03784	2575.55589	3144.22732	3025.11784
FTN_1316	1359.92328	1161.149	1190	1245.37098	1327.45566	1065.22001	1141.39759	1231.83741
FTN_1317	1583.31931	1876.50824	1886	2014.50066	2213.69943	1865.40921	1909.71905	2179.02713
FTN_1318	1148.39518	1575.50488	1652	1573.18373	1881.35802	1597.83002	1708.92935	1765.79721
FTN_1319	5154.1651	7236.46349	6697	6413.38273	7340.16127	7307.885	6976.96694	6861.97237
FTN_1320	728.131409	950.637167	984	903.270984	1077.24459	945.446472	995.080805	924.614214
FTN_1321	1261.48941	1520.25743	1485	1704.94382	1698.95224	1535.81961	1524.60821	1604.82403
FTN_1322	1823.47003	2043.20313	1964	1612.87051	1974.94841	1743.0873	1742.49987	1555.74685
FTN_1323	3850.78893	3525.35887	4068	4019.4765	4429.30887	3042.75765	3467.89778	4033.16328
FTN_1324	795.848328	724.884654	706	992.169358	949.274045	601.416085	660.642444	969.765227
FTN_1325	5934.65495	7579.3787	7309	8251.67412	7743.17299	7688.44207	7408.31642	8375.51283
FTN_1326	1863.96056	3066.23351	2875	2527.25379	3072.24809	3322.22925	2876.92999	2702.18995
FTN_1328	1842.31907	1899.36925	2054	1808.12944	2453.40545	1886.64566	2139.01202	1855.11769
FTN_1329	806.320017	144.786422	242	262.726446	2638.67624	415.384838	375.60975	248.330569
FTN_1330	71.207482	20.9559295	15	23.0183291	60.1652563	53.5158381	23.4360215	24.5385938
FTN_1331	0.69811257	2.85762675	2	10.3185613	1.91000814	20.3869859	12.6681197	5.88926251
FTN_1332	1.39622514	3.81016901	5	3.96867743	2.86501221	12.7418662	15.2017437	6.87080626
FTN_1333	4.18867541	19.050845	17	16.6684452	6.68502848	33.1288521	26.6030514	12.7600688
FTN_1334	2312.84694	1185.9151	1284	841.359616	712.433036	1094.10158	1391.59295	859.832326
FTN_1335	0	0	2	0.79373549	0	0	0.63340599	0
FTN_1336	2.79245028	9.52542252	6	7.14361938	0	16.9891549	8.23427782	8.83389377
FTN_1337	0	3.81016901	6	4.76241292	1.91000814	4.24728873	8.86768381	1.9630875
FTN_1338	1.39622514	1.9050845	3	3.96867743	2.86501221	4.24728873	10.7679018	3.92617501
FTN_1339	13.9622514	20.0033873	4	13.4935033	3.82001628	16.9891549	12.6681197	14.7231563
FTN_1340	1.39622514	0	1	1.58747097	0.95500407	0	1.26681197	0.98154375
FTN_1341	0	6.66779576	6	1.58747097	4.77502035	7.64511972	10.1344958	3.92617501
FTN_1342	324.622344	381.969443	248	229.389556	406.831733	375.460324	231.193185	214.958082

FTN_1343	930.584054	1135.43036	1326	869.934093	1319.81562	1218.12241	1361.18946	787.198089
FTN_1344	2185.09234	2128.93193	2313	2538.36609	2934.7275	2203.4934	2382.87332	2813.10439
FTN_1345	2171.13009	2397.54885	2220	2304.21412	2833.49707	2461.72855	2111.77556	2356.68655
FTN_1346	27.9245028	97.1593097	83	76.1986067	58.2552482	524.964888	741.71841	63.8003439
FTN_1347	835.640745	1656.47098	1529	1597.78953	1477.39129	2154.22485	2057.93605	1519.42973
FTN_1348	2226.97909	1485.01337	1548	1513.65357	1609.18186	1474.65865	1648.12238	1383.97669
FTN_1349	1089.05561	1063.03715	1134	1393.79951	1640.69699	1092.40266	1358.65584	1425.20153
FTN_1350	3.49056284	4.76271126	12	11.1122968	5.73002441	17.8386127	18.3687736	7.85235001
FTN_1351	956.414219	1197.34561	1198	758.017389	1437.28112	1255.49855	1231.34124	837.25682
FTN_1352	1503.03636	1884.12857	1776	2015.2944	2048.48373	2011.51594	1847.64526	2043.57409
FTN_1353	1336.18746	1644.08793	1260	1690.65659	1825.96778	1635.20616	1285.18075	1682.36599
FTN_1354	390.244926	508.657562	485	680.231312	522.387226	424.728873	448.451438	687.080626
FTN_1355	1436.01755	1520.25743	1360	1432.69255	1492.67136	1676.82959	1483.43682	1482.13107
FTN_1356	1106.50842	1787.92181	1559	1536.6719	1489.80635	2132.13894	1884.38281	1554.7653
FTN_1357	477.508997	1276.40662	1426	1008.8378	635.077706	1986.88167	1637.98788	1041.41792
FTN_1358	810.508692	1096.37613	1032	877.077712	1104.93971	1246.15451	935.540642	897.130989
FTN_1359	559.88628	1241.16255	1342	1086.62388	808.888446	1991.97842	1828.00968	1194.53875
FTN_1360	2274.45075	2369.92512	2288	1927.18976	2964.33263	2417.55675	2344.86896	2060.26033
FTN_1361	1246.13094	1177.34222	1320	1294.58258	1302.62555	1617.36755	2071.23758	1297.60084
FTN_1362	534.754228	692.498217	617	699.280964	780.238324	732.232578	711.314923	719.47157
FTN_1363	277.15069	1277.35916	1236	1160.44128	887.19878	1299.67035	1088.19148	1232.81895
FTN_1367	3485.67606	3717.77241	3902	4307.60248	3111.40326	3524.40019	3545.80671	4504.30428
FTN_1368	9.77357596	13.3355915	14	15.0809742	4.77502035	47.5696338	27.2364574	39.2617501
FTN_1369	4234.75084	368.633851	247	504.022034	96.455411	284.568345	152.650843	573.221551
FTN_1370	1100.92352	1612.65403	1028	1177.10973	987.474207	1394.80962	927.306364	1144.48001
FTN_1371	1956.80953	2155.60312	1918	1909.72758	1779.17258	2152.52593	1881.21578	1951.30898
FTN_1372	2364.50727	2809.99964	3079	2827.2858	2151.62417	2764.98497	3031.48105	2803.28895
FTN_1373	6.28301312	56.1999928	8	7.93735486	1.91000814	48.4190916	8.23427782	4.90771876

FTN_1374	1.39622514	1.9050845	3	5.5561484	1.91000814	8.49457747	5.70065388	0.98154375
FTN_1376	1308.96107	1260.2134	1346	1440.62991	1668.39211	1305.61656	1352.32178	1396.73676
FTN_1377	11.8679137	30.4813521	41	22.2245936	19.1000814	32.2793944	53.2061029	37.2986626
FTN_1378	1442.99868	1604.08115	1951	2134.35472	1866.07795	1600.3784	1962.29175	2127.98685
FTN_1380	2638.1674	3080.52164	2918	2605.03987	3469.52978	2907.69387	2754.04923	2625.62954
FTN_1382	763.73515	1004.93208	1150	989.788152	1173.7	956.489423	1218.03971	968.783683
FTN_1383	2019.63966	1749.82012	1737	1790.66726	1652.15704	1606.3246	1491.03769	1824.68983
FTN_1384	6.98112569	24.7660985	64	41.2742453	17.1900732	37.3761409	101.344958	36.3171188
FTN_1385	680.659755	766.796513	690	765.954744	847.088609	789.995705	712.581735	801.921245
FTN_1386	515.207076	471.508415	608	519.103008	575.867454	442.567486	583.366914	473.104088
FTN_1387	673.678629	894.437174	686	788.973073	924.443939	948.844303	760.087184	757.751776
FTN_1388	751.867237	729.647365	742	767.542215	985.564199	704.200472	692.312743	739.102445
FTN_1389	1560.9797	1905.0845	1768	1966.87654	1902.36811	1963.94631	1562.61257	1905.17642
FTN_1390	1801.82854	2313.72513	2606	1817.65426	2347.4	2382.72898	2612.79969	1868.8593
FTN_1391	3367.69503	3909.2334	3411	4439.36258	4284.14825	3922.79588	3614.21456	4493.5073
FTN_1392	642.961676	786.7999	827	814.372609	832.763548	832.468592	902.603531	795.050439
FTN_1393	368.603436	327.674535	476	316.700459	479.412043	338.933641	489.622828	357.281926
FTN_1394	524.980652	622.962633	567	660.387925	754.453215	602.265543	609.969965	680.20982
FTN_1395	1743.8852	1941.28111	2277	2262.93987	2325.43491	1976.68818	2282.16177	2117.18987
FTN_1396	1226.58378	1556.45404	1455	1278.70787	1741.92742	1575.74412	1591.74924	1269.13607
FTN_1397	5650.52313	6845.92116	6799	6907.0862	7621.88748	6805.85547	7054.24247	6810.93209
FTN_1398	415.376978	726.789738	629	342.89373	594.967535	727.135831	706.881081	349.429576
FTN_1399	812.60303	955.399878	1117	920.733164	1152.68991	945.446472	1064.75546	888.297095
FTN_1400	915.225578	896.342259	992	910.414603	1166.05997	964.134543	1064.75546	939.33737
FTN_1401	57.2452306	521.993154	604	660.387925	489.917087	1289.47686	1458.10058	781.308826
FTN_1402	2.79245028	2.85762675	13	8.73109035	3.82001628	5.94620423	17.7353676	6.87080626
FTN_1403	1965.88499	2060.34889	2038	2300.24544	1792.54264	1997.07516	1789.37191	2129.94994
FTN_1404	725.338959	2673.7861	2620	2671.71365	3438.01465	2888.15634	2586.19664	2798.38124

FTN_1405	416.075091	1471.67778	1419	2033.55032	1862.25793	1531.57232	1473.93573	1936.58582
FTN_1406	743.489886	1009.69479	925	1019.9501	965.509114	967.532374	833.562278	966.820595
FTN_1407	871.942598	940.159202	635	854.853119	1184.20505	892.780092	651.77476	923.63267
FTN_1408	1307.56484	1859.36248	1570	1714.46865	1439.19113	1774.51723	1556.91191	1620.52873
FTN_1409	3267.16682	4505.52485	4531	4044.0823	4563.00944	4617.65231	4544.68795	4118.55758
FTN_1410	788.867203	800.135491	870	554.027369	987.474207	825.67293	918.43868	636.040351
FTN_1412	9.07546339	13.3355915	42	35.7180969	13.370057	17.8386127	32.9371113	48.0956438
FTN_1413	1854.8851	2324.20309	2200	2020.05681	2251.89959	2257.85869	2246.69103	2020.99858
FTN_1414	223.396022	728.694823	728	627.84477	2535.5358	1500.99184	1013.44958	657.634314
FTN_1415	259.697876	104.779648	154	88.104639	5.73002441	41.6234296	43.0716071	69.6896064
FTN_1416	5.58490055	1.9050845	9	7.14361938	0.95500407	4.24728873	12.6681197	10.7969813
FTN_1417	22717.2811	6331.54835	5596	6284.79758	20.0550854	714.393965	855.731488	3254.79908
FTN_1418	24625.2228	6135.32464	5804	5294.21569	344.756469	878.33931	1112.26091	3105.60443
FTN_1420	1484.18732	2588.0573	2581	2328.81992	1735.24239	1193.48813	972.911595	2775.80573
FTN_1421	2803.62008	5364.71796	5348	4252.041	3956.58186	2364.89037	2094.6736	4544.54757
FTN_1422	1587.50798	2662.35559	2761	2397.08117	1429.64109	1128.07989	1076.79018	2761.08257
FTN_1423	1926.09258	2345.15902	2144	2362.95054	1495.53637	970.080747	913.371433	2766.97184
FTN_1424	4661.99573	4192.13845	3906	3621.81502	3882.09154	2099.85955	2427.84515	3976.23374
FTN_1425	209.433771	525.803323	647	519.896744	661.81782	665.974874	606.169529	444.63932
FTN_1426	5524.16476	4144.51134	4694	3700.39484	1923.3782	1523.07774	1623.41954	3752.44176
FTN_1427	2872.73322	2219.42345	2314	2107.36772	1290.2105	828.221303	1052.08734	2258.53217
FTN_1428	1638.4702	1558.35912	1671	1518.41599	1107.80472	835.866423	1004.58189	1616.60256
FTN_1429	1113.48955	828.711759	900	1121.54824	843.268593	626.899817	693.579555	1149.38773
FTN_1430	3985.52466	2009.86415	2006	2061.33106	3368.29935	1574.89466	1849.54548	1955.23515
FTN_1431	5774.08906	4149.27405	4000	2984.44543	2045.61872	1610.57189	1771.63654	2938.74199
FTN_1432	6072.18312	6515.389	6428	5995.08413	7453.80676	6306.37431	6392.96662	6062.01421
FTN_1433	2546.01654	2326.10818	2369	2787.59903	2254.76461	1934.21529	1977.49349	2913.22185
FTN_1434	8.37735083	25.7186408	47	23.0183291	21.0100895	55.2147535	56.3731328	14.7231563

FTN_1435	27.9245028	254.328781	332	261.138975	295.096257	631.996564	780.356175	275.813794
FTN_1436	3128.24242	3351.99618	3460	3014.60738	4075.00236	3495.51863	3377.95413	3040.82254
FTN_1437	4849.78802	5190.40273	5023	5595.04144	5624.01896	5250.49833	4889.89422	5570.26079
FTN_1438	4430.22236	5312.32814	5467	5252.14771	6197.97641	5440.77687	5648.08118	5022.55938
FTN_1439	1738.3003	2224.18616	2455	1728.75589	2468.68552	2357.24525	2536.15757	1648.01196
FTN_1440	1241.94226	1605.03369	1767	1339.8255	1581.48674	1632.65779	1699.42826	1329.99178
FTN_1441	2774.99746	2378.498	2795	2747.11852	3142.91839	2435.39536	2731.88002	2883.77554
FTN_1442	251.320525	446.742316	300	341.306259	397.281693	442.567486	297.067408	340.595682
FTN_1443	2574.63915	2843.33862	2916	2994.76399	3362.56933	2936.57543	2901.63282	2964.26213
FTN_1444	1290.11203	1520.25743	1553	1886.70925	2008.37356	1786.40964	1897.05093	1919.89958
FTN_1445	1180.50835	1474.53541	1749	1397.76819	1527.05151	1928.26909	2132.67796	1414.40455
FTN_1446	2776.39369	3248.16908	3364	3223.35981	3368.29935	3206.70299	3460.2969	3252.83599
FTN_1447	2402.20535	2549.95561	2480	2708.22548	3119.04329	2657.95329	2489.91893	2717.89465
FTN_1448	2788.95971	3288.17585	3158	3659.91433	3837.20635	3052.10168	2945.33784	3403.01219
FTN_1449	1442.30057	1617.41674	1765	1308.86982	1843.15785	1622.4643	1677.25905	1375.1428
FTN_1450	885.206737	1079.23037	1353	1054.87446	1237.68527	1118.73585	1322.5517	1088.53202
FTN_1451	948.734981	1136.38291	1376	1668.43199	1177.52002	1142.52067	1287.08096	1719.66465
FTN_1452	1190.28193	1701.24046	1853	1620.80786	894.838813	1629.25996	1618.3523	1582.24853
FTN_1453	1592.39477	2136.55227	2254	2382.00019	1240.55029	2210.28906	2327.767	2357.66809
FTN_1454	3160.3556	3668.24021	3446	3603.55911	3712.10082	3656.9156	3458.39669	3720.05082
FTN_1455	1477.90431	1623.132	1466	1802.57329	1747.65745	1605.47514	1445.43246	1804.07742
FTN_1456	666.697503	950.637167	1022	981.850797	772.598292	1030.39225	881.701133	1004.11926
FTN_1457	645.056014	892.53209	839	681.818783	283.636209	886.833888	919.705492	716.526939
FTN_1458	820.282268	1089.70834	874	1113.61089	229.200977	1034.63954	914.638244	1153.31391
FTN_1459	862.867135	1107.80664	982	1240.60857	1343.69073	1182.44518	1045.75328	1237.72667
FTN_1460	1338.28179	1766.96588	1664	1581.91482	1792.54264	1773.66778	1525.87502	1602.86095
FTN_1461	4199.84521	4342.64013	4617	4506.83009	3781.81611	4240.49307	4703.67286	4556.3261
FTN_1462	2374.97896	1547.88116	1358	1252.5146	1709.45728	1687.87254	1769.10292	1223.00351

FTN_1463	491.471248	56.1999928	23	17.4621807	94.5454028	94.2898099	41.8047951	21.5939625
FTN_1464	3.49056284	1.9050845	5	4.76241292	0	3.39783099	7.60087184	8.83389377
FTN_1465	0.69811257	2.85762675	3	3.17494195	1.91000814	6.79566198	6.33405986	3.92617501
FTN_1466	2056.63963	2626.15899	2481	3305.11457	2637.72124	2554.31944	2408.20956	3253.81754
FTN_1467	1513.50805	2157.5082	1882	2224.84057	2180.27429	2065.03178	1864.11382	2187.86102
FTN_1468	787.470978	842.999893	925	910.414603	940.679008	834.167507	979.245655	872.592395
FTN_1469	3.49056284	97.1593097	95	203.99002	0.95500407	21.2364437	17.1019616	53.9849063
FTN_1470	173.131917	357.203344	307	339.718788	41.065175	526.663803	475.687896	404.396026
FTN_1471	608.056047	1978.43026	1668	1867.6596	638.897722	1627.56104	1608.85121	1998.42308
FTN_1472	640.169226	928.728695	738	758.811125	1096.34467	866.446902	653.674978	748.917883
FTN_1474	1762.03612	2027.96245	1962	2774.10552	2608.11611	2102.40792	2133.31136	2873.9601
FTN_1475	735.810648	875.386329	585	767.542215	858.548658	909.769247	611.870183	851.979976
FTN_1476	688.338993	59.0576196	138	171.446865	108.870464	48.4190916	106.412206	136.434581
FTN_1477	23.0377148	14.2881338	16	9.52482584	60.1652563	16.9891549	14.5683377	7.85235001
FTN_1478	0.69811257	4.76271126	6	7.93735486	0.95500407	2.54837324	10.1344958	9.81543752
FTN_1479	0	0	2	2.38120646	0	5.09674648	3.16702993	2.94463126
FTN_1480	2.09433771	16.1932183	14	7.14361938	4.77502035	16.1396972	13.3015257	7.85235001
FTN_1481	0	2.85762675	5	1.58747097	0.95500407	7.64511972	6.96746585	0.98154375
FTN_1482	1.39622514	10.4779648	15	16.6684452	5.73002441	32.2793944	29.7700814	26.5016813
FTN_1483	1.39622514	6.66779576	8	7.14361938	0	9.34403522	14.5683377	5.88926251
FTN_1484	9.77357596	21.9084718	53	32.5431549	1.91000814	21.2364437	44.3384191	32.3909438
FTN_1485	3010.95951	3855.89103	3640	4029.00133	3906.92165	3937.23666	3567.34252	4042.97871
FTN_1486	844.716208	1066.84732	854	1082.6552	1277.79544	1037.18791	806.325821	1058.10416
FTN_1487	3267.86493	3934.95204	3789	4086.94402	4284.14825	3061.44572	3538.83925	4039.05254
FTN_1488	1401.81004	1550.73879	1695	1835.91018	2066.62881	1593.58273	1814.70815	1879.65628
FTN_1489	1329.90444	1732.67436	1620	1737.48698	1673.16713	1709.10899	1869.18107	1734.38781
FTN_1490	913.829353	1245.92527	1532	1250.92713	1501.2664	1276.73499	1613.28505	1350.6042
FTN_1492	3.49056284	15.240676	19	38.0993033	3.82001628	16.9891549	27.2364574	39.2617501

FTN_1493	0.69811257	4.76271126	8	4.76241292	4.77502035	14.4407817	13.9349317	6.87080626
FTN_1494	5.58490055	3.81016901	14	19.8433872	8.59503662	24.6342747	22.1692095	14.7231563
FTN_1495	26.5282776	26.671183	74	66.6737809	21.9650936	34.8277676	79.1757483	54.9664501
FTN_1496	18.8490394	31.4338943	16	55.561484	27.695118	51.8169226	32.9371113	39.2617501
FTN_1499	2.09433771	3.81016901	7	3.96867743	1.91000814	8.49457747	13.3015257	4.90771876
FTN_1500	13.2641388	28.5762675	33	19.0496517	29.6051261	32.2793944	44.3384191	18.6493313
FTN_1501	3134.52543	3727.29783	3907	4206.79808	3675.81066	3656.9156	3802.33614	3989.97535
FTN_1502	1322.22521	1812.6879	2082	1500.9538	1895.68308	1805.09771	2178.28319	1596.97168
FTN_1503	851.697334	957.304963	1378	1288.23269	1207.12514	937.801353	1470.13529	1200.42801
FTN_1504	233.867711	1533.59303	1411	1483.49162	2389.42018	2094.7628	1864.74722	1515.50355
FTN_1505	1901.65864	3371.99957	3285	3286.85865	4148.53768	5919.87104	5016.57541	3384.36286
FTN_1506	1022.0368	1407.85745	1367	1395.38699	1745.74744	2332.61097	2226.42204	1382.0136
FTN_1507	392.339264	571.525351	478	629.432241	712.433036	1000.66123	840.529744	592.852426
FTN_1508	3.49056284	18.0983028	32	10.3185613	32.4701383	37.3761409	64.6074106	22.5755063
FTN_1509	4379.95826	5260.89086	5190	5651.39666	6069.05086	5315.90658	5508.09846	5426.9554
FTN_1510	874.036936	1113.52189	749	1274.73919	912.028886	1004.05906	787.957047	1324.10252
FTN_1511	381.867575	1483.10829	1784	1666.84452	1910.00814	2174.61183	2420.24427	1765.79721
FTN_1512	210.829996	1696.47775	1506	1921.63361	2278.63971	3631.43187	2746.44836	1987.6261
FTN_1513	501.942937	592.481281	644	670.706486	308.466314	619.254698	544.729148	718.490026
FTN_1514	1098.13107	1685.04724	1781	1385.06842	1477.39129	1653.89423	1556.27851	1473.29717
FTN_1515	2069.90377	2650.92509	2464	2297.0705	2939.50252	2671.54461	2534.25735	2300.73855
FTN_1516	674.376741	723.932111	932	706.424583	909.163874	763.662514	940.60789	744.991708
FTN_1517	509.622175	654.396527	566	636.57586	871.918715	1004.05906	742.985222	618.372564
FTN_1518	8426.91682	3895.89781	4605	3877.39785	381.046624	3594.90518	6634.2943	3551.22529
FTN_1519	374.886449	263.854204	316	167.478188	15.2800651	73.902824	104.511988	173.733244
FTN_1520	129762.372	6093.41278	7215	6953.12286	2931.86249	2574.70643	4557.35607	6212.1904
FTN_1521	2144.60181	2430.88783	2531	2819.34845	2639.63125	2405.66434	2537.42438	2812.12285
FTN_1522	802.131342	1356.42017	1072	1266.80184	1013.25932	1409.2504	861.432142	1242.63439

FTN_1523	1716.65881	2237.52175	2038	2077.20577	2455.31546	2196.69773	2229.58907	2186.87948
FTN_1524	545.924029	770.606682	691	622.288621	679.007893	726.286374	722.082825	570.27692
FTN_1525	1300.58372	1581.22014	1343	1373.16239	1994.0485	1568.94846	1271.24581	1324.10252
FTN_1526	2719.84657	3115.76571	2808	3231.29717	3275.66396	3163.38065	2781.91909	3158.60779
FTN_1527	1471.6213	1789.82689	1906	1818.448	1840.29284	1709.95844	1756.4348	1799.1697
FTN_1528	681.357867	822.043963	696	778.654512	901.523841	857.102867	656.842008	782.29037
FTN_1529	3490.56284	4371.21639	4349	4618.7468	4579.24451	4091.83797	3903.68109	4579.88315
FTN_1530	2576.03538	3594.89446	3085	2988.41411	3698.73076	3519.30345	2991.57647	3076.15812
FTN_1531	1281.73468	1774.58621	1698	1863.69092	1745.74744	1754.97971	1712.09638	1815.85594
FTN_1532	651.339027	271.474542	255	192.877723	49.6602116	163.095887	140.616129	171.770157
FTN_1533	2202.54515	3034.79961	2235	3178.11689	2935.68251	2962.90862	2064.27011	3169.40477
FTN_1534	340.678934	682.972794	444	396.074008	627.437673	720.340169	375.60975	376.912801
FTN_1535	2110.3943	1727.91164	1801	2086.73059	2345.48999	1742.23784	1771.63654	2006.27543
FTN_1536	2555.092	2602.34543	2971	2581.2278	3320.54915	2824.44701	3002.97778	2648.20504
FTN_1537	1718.05503	2295.62683	2070	2400.25611	2431.44036	2319.01965	2005.36335	2349.81574
FTN_1538	71.9055946	56.1999928	112	123.029	62.0752645	51.8169226	114.646484	110.914444
FTN_1539	0	5.71525351	7	21.4308581	2.86501221	8.49457747	10.7679018	9.81543752
FTN_1540	1144.2065	1370.7083	1480	1012.80648	1521.32148	1381.2183	1620.25251	920.688039
FTN_1542	1087.65938	1608.84386	1403	1327.12573	1596.7668	1824.63524	1724.7645	1243.61593
FTN_1543	634.584325	723.932111	750	941.370287	992.249228	916.564909	1074.25655	887.315552
FTN_1544	8.37735083	101.922021	96	94.4545229	7.64003255	601.416085	245.761523	64.7818876
FTN_1545	1.39622514	0	11	11.1122968	1.91000814	15.2902394	10.1344958	15.7047
FTN_1546	1.39622514	7.62033801	6	22.2245936	3.82001628	16.9891549	24.7028335	10.7969813
FTN_1547	11800.8949	3444.39278	3457	2901.1032	56.3452401	413.685923	412.980703	1277.96996
FTN_1548	19326.5484	6530.62968	6292	6775.32611	438.346868	1128.07989	1109.72729	3616.00718
FTN_1549	1771.8097	2730.93864	2986	3709.91966	2181.22929	2537.33029	2721.11212	3434.42159
FTN_1550	49.5659924	16.1932183	46	69.0549873	25.7851099	21.2364437	43.0716071	63.8003439
FTN_1551	3115.67639	608.674499	508	722.299293	13.370057	151.203479	95.644304	329.798701

FTN_1552	2258.39416	2308.00988	1879	1811.30438	2505.93068	2012.3654	1893.8839	1801.13278
FTN_1553	334.39592	554.37959	571	861.996738	102.185435	636.243852	461.752964	846.090714
FTN_1554	3118.46884	4264.53166	3927	3774.21224	4411.16379	4479.1907	4257.12164	3890.83943
FTN_1555	2106.20562	2648.06746	2819	3022.54473	2891.75232	2722.51208	2772.418	3242.03901
FTN_1556	1136.52726	1303.0778	1298	1348.55659	1367.56583	1341.29378	1385.8923	1408.51528
FTN_1557	1697.80977	1736.48452	2020	1884.32804	2181.22929	1770.26994	1970.52602	1763.83412
FTN_1558	469.131646	684.877879	498	700.074699	303.691294	692.308064	456.685716	719.47157
FTN_1559	2.79245028	4.76271126	6	1.58747097	1.91000814	13.591324	17.1019616	4.90771876
FTN_1560	0	8.57288026	6	10.3185613	4.77502035	10.193493	14.5683377	6.87080626
FTN_1561	6.28301312	1.9050845	34	13.4935033	8.59503662	3.39783099	32.3037053	4.90771876
FTN_1562	0.69811257	0.95254225	1	1.58747097	0	0	1.26681197	0
FTN_1563	25.1320525	34.2915211	42	29.368213	41.065175	42.4728873	61.4403807	22.5755063
FTN_1564	31.4150656	217.179633	165	156.365891	84.0403581	157.999141	162.151933	170.788613
FTN_1565	16.7547017	35.2440633	14	18.2559162	16.2350692	30.5804789	29.7700814	14.7231563
FTN_1566	0.69811257	3.81016901	2	3.96867743	0.95500407	0	4.43384191	1.9630875
FTN_1567	31.4150656	77.1559224	60	45.2429227	78.3103337	84.9457747	82.3427782	47.1141001
FTN_1568	4.18867541	17.1457605	37	36.5118324	9.55004069	26.3331902	48.772261	19.630875
FTN_1569	0	0	1	1.58747097	0	0	2.53362395	1.9630875
FTN_1570	0	0.95254225	0	4.76241292	0.95500407	2.54837324	1.90021796	0.98154375
FTN_1571	0.69811257	2.85762675	5	7.14361938	0	4.24728873	5.06724789	3.92617501
FTN_1572	0	0	0	4.76241292	0	3.39783099	3.80043592	6.87080626
FTN_1573	0	2.85762675	2	0.79373549	0.95500407	2.54837324	1.26681197	1.9630875
FTN_1574	2.09433771	0.95254225	3	3.96867743	0.95500407	0.84945775	3.16702993	3.92617501
FTN_1576	0.69811257	7.62033801	6	15.8747097	0	3.39783099	10.1344958	6.87080626
FTN_1580	2097.13016	2091.78278	2644	2209.75959	2582.331	2074.37582	2654.60449	2181.97176
FTN_1581	332.301583	1112.56935	1209	850.884441	404.921725	1065.22001	1087.55808	804.865876
FTN_1582	2259.09227	2840.48099	3023	1992.27607	464.131978	1260.5953	760.72059	1486.05724
FTN_1583	321.829894	1410.71507	1514	796.910428	22.9200977	634.544937	407.913455	623.280282

FTN_1584	48.8678798	1214.49137	1040	567.520873	20.0550854	835.016965	622.004679	531.01517
FTN_1585	381.169463	2199.42006	1997	2054.18744	1342.73572	2518.64222	2259.35915	2069.09423
FTN_1586	2141.80936	3486.30464	3003	2977.30181	2788.61188	4128.36465	3847.94137	2978.98529
FTN_1587	901.263326	1070.65749	1113	1180.28467	1119.26477	1203.68163	1140.13078	1186.6864
FTN_1588	2786.86537	3221.4979	3776	4026.62012	3585.08528	3159.13336	3904.94791	3966.4183
FTN_1589	1365.50818	1625.98962	1310	2084.34939	1649.29203	1528.17449	1294.68184	1960.14287
FTN_1590	2500.63922	2771.89795	2766	2486.77328	3063.65305	2592.54504	2502.58705	2447.97012
FTN_1591	1912.13033	1860.31502	2065	2013.70693	2248.07958	1833.12982	1741.86646	1880.63783
FTN_1592	2014.05476	2043.20313	2101	2246.27143	2458.18047	1861.16192	1914.15289	2341.96339
FTN_1593	3253.90268	3521.5487	3328	3136.84264	3824.7913	3412.27177	3427.9932	3058.49033
FTN_1594	3150.58202	3527.26396	3682	3918.6721	3912.65167	3728.27005	3740.26235	3979.17837
FTN_1595	16.7547017	57.1525351	33	47.6241292	27.695118	46.7201761	28.5032694	46.1325563
FTN_1596	2.79245028	8.57288026	16	11.9060323	5.73002441	10.193493	19.6355856	13.7416125
FTN_1597	400.716614	1892.70145	1727	2164.51667	270.266152	1810.19446	1715.26341	2070.07577
FTN_1598	0	1.9050845	12	2.38120646	0	3.39783099	13.3015257	4.90771876
FTN_1599	1419.26285	2236.56921	2361	2227.22177	1713.2773	2116.84871	2464.58269	2185.89794
FTN_1600	1411.58361	2298.48445	2078	2327.23245	1855.57291	2244.26737	2091.50657	2524.53053
FTN_1601	978.055709	1033.50834	1022	1296.17005	1300.71554	1020.19875	1035.61879	1272.0807
FTN_1602	682.05598	1128.76257	938	1006.4566	1001.79927	1729.49597	1378.29143	1056.14108
FTN_1603	547.320254	730.599907	690	444.491872	432.616843	1245.30506	942.508108	420.100726
FTN_1604	2182.998	2073.68448	2160	2416.13082	1794.45265	2065.88124	2259.35915	2347.85265
FTN_1605	32.1131782	16.1932183	59	70.6424583	32.4701383	22.0859014	60.1735687	71.6526939
FTN_1606	1.39622514	10.4779648	9	19.8433872	1.91000814	11.8924085	19.6355856	17.6677875
FTN_1607	1905.1492	2500.42341	2253	2570.90924	2732.26664	2570.45914	2449.38095	2487.23187
FTN_1608	12121.3285	1917.46755	1520	1782.7299	10.5050448	423.029958	302.768062	249.312113
FTN_1609	2473.41283	2852.86404	2419	2305.80159	2397.06021	2529.68517	2178.91659	2219.27042
FTN_1610	6905.72953	6857.35167	6824	7877.03097	6868.38926	6377.72876	6292.25507	7498.01272
FTN_1611	2491.56376	2947.16573	2463	2259.76493	3513.45997	3103.91861	2665.37239	2243.80902

FTN_1612	1220.99888	1506.92184	1523	1362.84383	1685.58218	1464.46516	1575.91409	1379.06897
FTN_1613	1660.11169	2213.70819	2631	2128.79857	2586.15102	2300.33158	2664.10558	2231.04895
FTN_1615	420.263766	2762.37253	2300	2770.93058	1569.07169	3838.69956	2828.79114	2884.75709
FTN_1616	1180.50835	2960.50132	2949	2678.06353	2190.77933	3238.98239	3062.51794	2656.05739
FTN_1617	1638.4702	1841.26417	1793	1706.5313	165.215704	2124.49383	2069.33736	1829.59755
FTN_1618	1593.09288	1506.92184	1490	1578.73988	1841.24785	1521.37882	1455.56696	1659.79048
FTN_1619	913.13124	2305.15225	2388	2483.59834	728.668105	2356.39579	2422.7779	2275.21842
FTN_1620	620.622074	2161.31837	2438	2374.06284	487.052075	2415.85783	2445.58051	2026.88785
FTN_1621	1125.35746	1403.09474	1318	1547.7842	1561.43165	1331.10029	1329.51917	1560.65457
FTN_1622	1215.41398	1298.31509	1306	1201.71553	1548.0616	1435.58359	1395.39339	1186.6864
FTN_1623	78.8867203	218.132176	208	155.572155	146.115623	383.954902	254.629207	146.250019
FTN_1624	839.131308	1224.01679	1081	1408.88049	825.123516	1344.69161	1129.99628	1334.8995
FTN_1625	1197.26306	484.844006	397	540.533866	14.325061	179.235585	83.6095902	600.704776
FTN_1626	1940.05483	1851.74214	1746	2151.8169	1788.72262	1941.86041	1988.26139	2050.4449
FTN_1627	1479.99865	1613.60657	1871	1690.65659	1887.08804	1644.5502	1898.31774	1556.72839
FTN_1628	1807.41344	2594.72509	1662	2462.16748	2621.48617	2538.17975	1795.07257	2572.62617
FTN_1630	80.981058	135.261	115	138.90371	74.4903174	126.569204	96.2777099	138.397669
FTN_1631	0.69811257	1.9050845	6	11.9060323	0.95500407	6.79566198	3.80043592	5.88926251
FTN_1632	0	8.57288026	6	11.9060323	0	9.34403522	13.9349317	8.83389377
FTN_1633	1.39622514	9.52542252	15	19.8433872	8.59503662	61.1609578	24.0694275	15.7047
FTN_1634	2.09433771	4.76271126	11	11.1122968	2.86501221	9.34403522	25.3362395	10.7969813
FTN_1635	4.88678798	8.57288026	11	15.8747097	7.64003255	23.7848169	43.0716071	19.630875
FTN_1636	0	1.9050845	6	5.5561484	2.86501221	5.09674648	12.0347137	10.7969813
FTN_1637	4.18867541	3.81016901	9	8.73109035	7.64003255	12.7418662	22.8026155	13.7416125
FTN_1638	1.39622514	1.9050845	5	3.17494195	3.82001628	3.39783099	1.26681197	3.92617501
FTN_1639	0.69811257	0.95254225	7	0.79373549	3.82001628	5.09674648	3.16702993	0.98154375
FTN_1640	16.0565891	42.8644013	34	7.14361938	52.5252238	128.26812	38.6377652	17.6677875
FTN_1641	55.1508929	2213.70819	1731	1982.75124	15.2800651	313.449909	162.151933	569.295376

FTN_1642	0	2.85762675	6	5.5561484	0	4.24728873	5.70065388	1.9630875
FTN_1643	138.924401	216.227091	212	168.271923	55.390236	233.60088	330.637925	146.250019
FTN_1644	4261.27912	4968.46038	5149	5383.9078	6707.94858	7493.91624	7152.4204	5445.60473
FTN_1645	90.0565214	73.3457534	126	115.885381	140.385598	78.1501127	125.414385	107.969813
FTN_1646	4.88678798	10.4779648	7	4.76241292	4.77502035	23.7848169	29.1366754	16.6862438
FTN_1647	0	4.76271126	10	7.93735486	0	11.8924085	14.5683377	7.85235001
FTN_1648	2.09433771	5.71525351	7	6.34988389	5.73002441	16.1396972	27.2364574	11.778525
FTN_1649	1.39622514	2.85762675	2	6.34988389	0.95500407	5.94620423	15.8351497	2.94463126
FTN_1650	0.69811257	0	2	0.79373549	1.91000814	1.69891549	5.70065388	0
FTN_1651	2.09433771	0.95254225	2	0.79373549	1.91000814	0	3.80043592	4.90771876
FTN_1652	2.79245028	2.85762675	3	1.58747097	0.95500407	9.34403522	5.06724789	2.94463126
FTN_1653	15.3584765	20.0033873	23	9.52482584	37.2451587	42.4728873	82.3427782	10.7969813
FTN_1654	1969.37556	2127.97939	2240	2289.13314	3098.0332	2624.82444	2717.94509	2171.17478
FTN_1655	1060.43299	1367.85067	1311	1446.18606	1061.00952	1540.91635	1472.66892	1535.13443
FTN_1656	265.282776	1230.68459	1296	1361.25636	508.062165	1361.68077	1292.78162	1343.7334
FTN_1657	587.11267	2147.03024	2264	2246.27143	1367.56583	2433.69644	2480.41784	2363.55735
FTN_1658	4.88678798	4.76271126	16	7.93735486	5.73002441	11.8924085	37.3709532	3.92617501
FTN_1659	0	1.9050845	8	3.96867743	2.86501221	5.09674648	6.33405986	2.94463126
FTN_1660	0	12.3830493	12	11.9060323	1.91000814	16.9891549	27.2364574	12.7600688
FTN_1661	0.69811257	10.4779648	7	8.73109035	2.86501221	11.0429507	17.1019616	9.81543752
FTN_1662	0	1.9050845	6	3.17494195	1.91000814	3.39783099	0.63340599	2.94463126
FTN_1664	25.1320525	51.4372816	38	65.8800454	29.6051261	56.913669	39.2711712	84.4127626
FTN_1665	1253.11206	1498.34896	1565	1761.29904	1655.97706	1626.71159	1638.62129	1650.95659
FTN_1666	1.39622514	12.3830493	9	7.93735486	2.86501221	11.0429507	17.1019616	3.92617501
FTN_1667	71.207482	87.6338872	125	56.3552195	99.3204232	125.719747	128.581415	84.4127626
FTN_1668	0.69811257	5.71525351	7	7.14361938	2.86501221	11.0429507	12.0347137	10.7969813
FTN_1669	0	3.81016901	14	14.2872388	3.82001628	25.4837324	16.4685556	14.7231563
FTN_1670	0	1.9050845	0	2.38120646	2.86501221	1.69891549	3.80043592	1.9630875

FTN_1671	0.69811257	0.95254225	2	3.96867743	0.95500407	7.64511972	6.33405986	1.9630875
FTN_1672	0	1.9050845	5	3.17494195	0	2.54837324	2.53362395	0.98154375
FTN_1673	0	8.57288026	4	4.76241292	2.86501221	7.64511972	18.3687736	4.90771876
FTN_1674	3.49056284	2.85762675	10	10.3185613	0	15.2902394	16.4685556	5.88926251
FTN_1675	3.49056284	5.71525351	7	10.3185613	1.91000814	10.193493	14.5683377	7.85235001
FTN_1678	1.39622514	2.85762675	3	3.17494195	0	1.69891549	1.90021796	0.98154375
FTN_1679	0.69811257	1.9050845	3	2.38120646	0.95500407	3.39783099	5.70065388	0.98154375
FTN_1680	0	0.95254225	0	0.79373549	0	0	1.90021796	0
FTN_1681	19.5471519	343.867753	245	217.483523	17.1900732	513.921937	176.086864	189.437944
FTN_1682	4398.10918	4906.54514	4691	6329.24677	5942.03532	5055.97251	4810.08506	6311.32632
FTN_1683	2602.56366	3793.97579	3679	3524.9793	3858.21644	3829.35552	3908.11494	3476.62797
FTN_1684	2522.97882	3300.5589	2968	2839.98557	3437.05964	3136.198	2953.57212	2819.9752
FTN_1685	2639.56362	2947.16573	3054	3092.39345	3645.25053	2979.04832	3169.56356	3098.73362
FTN_1686	646.452239	361.966056	318	272.251272	958.824085	417.933211	371.175908	300.352388
FTN_1687	2742.88428	3803.50121	3106	3501.96097	3702.55078	3924.49479	3175.89762	3392.21521
FTN_1688	588.508895	923.965984	695	985.819474	1033.3144	944.597015	863.965766	914.798777
FTN_1689	20.9433771	13.3355915	43	53.1802776	57.3002441	11.0429507	32.3037053	59.8741689
FTN_1690	2.79245028	11.430507	12	3.96867743	3.82001628	6.79566198	12.0347137	11.778525
FTN_1691	0	1.9050845	0	4.76241292	0	1.69891549	0.63340599	0
FTN_1692	8826.23721	2105.11838	1993	2658.22014	427.841823	1991.12896	1977.49349	2434.2285
FTN_1693	15539.9858	4528.38586	4226	4624.30294	354.30651	4085.89176	4169.0782	4630.92342
FTN_1694	19.5471519	64.7728731	48	18.2559162	31.5151343	90.8919789	82.3427782	10.7969813
FTN_1695	1231.47057	1958.42687	1845	1807.3357	1669.34711	1835.67819	1920.48695	1869.84085
FTN_1696	2068.50754	2850.00642	2756	2583.60901	2635.81123	2850.7802	2881.99724	2552.01375
FTN_1697	1603.56457	2018.43703	2083	2330.40739	2321.61489	1958.00011	2136.47839	2305.64627
FTN_1698	693.923893	1140.19308	819	896.9211	1043.81945	1089.85429	850.030834	856.887695
FTN_1699	8.37735083	42.8644013	40	39.6867743	21.9650936	107.031676	37.3709532	22.5755063
FTN_1700	4.18867541	19.050845	21	22.2245936	5.73002441	114.676796	27.2364574	21.5939625

FTN_1701	1335.48934	1853.64722	1733	2385.96887	2045.61872	1965.64523	1779.23742	2351.77883
FTN_1702	6.98112569	2.85762675	20	4.76241292	6.68502848	11.0429507	19.0021796	1.9630875
FTN_1703	478.905222	253.376239	323	205.577491	100.275427	313.449909	356.60757	194.345663
FTN_1704	187.094168	180.030486	129	165.890717	18.1450773	177.536669	113.379672	179.622507
FTN_1705	1998.69628	2164.176	2441	2770.13685	2528.85077	2020.01052	2401.24209	2817.03057
FTN_1706	2607.45044	2800.47422	2245	2391.52502	2826.81204	2610.38366	2204.25283	2345.88957
FTN_1707	900.565214	42.8644013	64	46.0366582	15.2800651	50.9674648	94.377492	61.8372564
FTN_1708	2626.9976	3472.01651	3410	3804.37419	3358.74931	3418.21797	3510.33598	3711.21693
FTN_1709	34.2075159	112.399986	144	177.796749	76.4003255	497.78224	419.314763	181.585594
FTN_1710	0.69811257	4.76271126	14	7.14361938	3.82001628	27.1826479	28.5032694	9.81543752
FTN_1711	4794.63712	3913.04357	3531	3594.82802	4117.02254	3231.33727	3243.03865	3481.53569
FTN_1712	755.357799	1265.92865	1136	784.210661	1158.41994	1300.51981	1216.13949	813.69977
FTN_1714	557.791942	853.477857	1009	871.521564	968.374126	853.705036	1054.62097	871.610851
FTN_1715	8824.14287	6243.91446	5921	6440.36974	6027.03068	6040.49404	5920.44576	6052.19877
FTN_1716	885.90485	1122.09477	895	1050.11205	1204.26013	1165.45603	868.399607	1093.43974
FTN_1717	3908.03416	3847.31815	4270	4794.16234	3428.46461	3645.02319	3927.75052	4714.35464
FTN_1718	4994.99543	5163.73155	5448	5611.70989	4211.56794	4869.94126	4841.75536	5309.17015
FTN_1719	1477.2062	1906.98959	1663	2034.34405	2017.9236	1830.58144	1721.59747	1826.65292
FTN_1720	7.67923826	23.8135563	25	30.955684	19.1000814	43.3223451	49.4056669	31.4094001
FTN_1721	291.811054	961.115132	860	782.62319	387.731652	1206.23	1067.28909	849.035345
FTN_1724	228.28281	295.288098	258	256.376562	215.83092	348.277676	283.132476	296.426213
FTN_1725	2622.80892	3875.89442	3869	4440.15631	3499.13491	3840.39847	3815.00426	4180.39484
FTN_1727	1368.30063	1795.54214	1634	1813.68559	1716.14231	1723.54977	1358.65584	1820.76366
FTN_1728	2476.20528	3326.27754	2976	3195.57907	3229.82376	3262.76721	2729.3464	3048.67489
FTN_1729	1267.77242	1926.99298	1886	1793.8422	1681.76217	1936.76366	1810.90772	1674.51364
FTN_1730	2499.94111	4258.81641	3617	3470.21155	3479.07982	4137.70869	3733.92829	3177.25712
FTN_1731	1829.05493	2192.75226	2275	2231.19045	2521.21074	2191.60099	2214.38733	2282.08922
FTN_1732	1915.62089	2862.38947	2871	2461.37374	2501.15566	2745.44744	2879.46361	2471.52717

FTN_1733	1074.39524	2410.88444	2323	2127.2111	2122.97405	2543.27649	2318.26591	2258.53217
FTN_1734	398.622277	376.254189	234	602.445234	515.702197	400.944057	272.364574	571.258463
FTN_1735	483.093898	992.549026	653	759.60486	791.698373	987.069902	720.182607	752.844058
FTN_1736	924.999154	1453.57948	1306	1545.40299	1371.38584	1470.41136	1409.96173	1559.67302
FTN_1737	4204.732	3985.43678	3707	3694.04495	3275.66396	3032.56416	2550.72591	3651.34276
FTN_1738	3145.69523	4211.18929	4180	4459.9997	4105.56249	4298.2562	4291.32556	4443.44856
FTN_1739	2.09433771	39.0542323	64	32.5431549	4.77502035	289.665092	89.9436501	37.2986626
FTN_1740	16.7547017	52.3898238	101	57.148955	22.9200977	204.719317	184.321142	57.9110813
FTN_1741	501.942937	895.389717	734	866.759151	638.897722	840.963169	696.113179	829.40447
FTN_1742	1810.20589	2580.43696	2499	2047.04382	2327.34492	2608.68474	2570.9949	2006.27543
FTN_1743	4161.44902	5935.29077	5891	6169.70594	5858.94996	5924.96778	5718.38925	5956.98903
FTN_1744	3984.12843	4972.27055	4423	5164.04307	4907.76591	4937.89788	4344.53166	5041.20871
FTN_1745	2333.79032	3210.06739	2787	2557.41574	3163.92848	2992.63964	2793.3204	2532.38288
FTN_1747	30.0188405	18.0983028	56	9.52482584	42.9751831	22.9353592	60.1735687	14.7231563
FTN_1748	20.2452645	12.3830493	3	3.17494195	19.1000814	23.7848169	8.23427782	0.98154375
FTN_1749	9.07546339	1.9050845	5	3.96867743	5.73002441	2.54837324	11.4013078	5.88926251
FTN_1750	29232.0676	3050.04029	2322	1901.79023	27.695118	506.276817	670.77694	1017.86087
FTN_1751	927.093491	1224.01679	846	1265.21437	992.249228	1145.9185	908.937591	1192.57566
FTN_1752	2259.79039	2880.48777	2478	2666.1575	2817.262	2737.80232	2565.92765	2587.34933
FTN_1753	1708.97957	2304.19971	2078	2272.4647	2089.5489	2206.89123	2016.13126	2109.33752
FTN_1754	1022.73491	1743.15232	1378	1827.97283	1776.30757	1564.70117	1363.72309	1865.91467
FTN_1755	2703.09187	3914.94865	3253	4468.73079	3693.95574	3823.40932	3210.73495	4299.16163
FTN_1756	769.320051	937.301576	1024	943.751493	856.63865	952.242134	967.844347	864.740045
FTN_1757	1264.97997	1736.48452	1536	1761.29904	1800.18267	1693.81875	1665.85774	1718.68311
FTN_1758	1111.39521	1589.79302	1526	1536.6719	1696.08723	1542.61527	1625.95317	1605.80558
FTN_1759	544.527804	661.064323	637	857.234325	771.643288	668.523247	651.141354	977.617577
FTN_1760	1431.13077	2234.66412	1744	2528.84126	1961.57836	2085.41877	1721.59747	2327.24024
FTN_1762	5210.0141	4523.62315	4627	4947.35329	2268.13466	3405.47611	3631.94993	4718.28081

FTN_1763	3013.05385	3775.87749	3874	3840.09228	4142.80765	3804.72125	3597.1126	3883.96863
FTN_1764	273.660127	494.369429	361	211.927375	473.682018	494.384409	430.716071	259.12755
FTN_1765	959.904782	1518.35235	1521	1716.84986	1401.94597	1489.94889	1587.94881	1612.67638
FTN_1766	2463.63926	3219.59281	2928	2757.43708	3418.91457	3047.8544	2778.75206	2844.51379
FTN_1767	1329.90444	1925.08789	1907	1524.76587	1888.99805	1867.95759	1934.42188	1544.94987
FTN_1768	4354.8262	5697.15521	5268	5408.5136	6229.49154	5758.47407	5421.32184	5205.12652
FTN_1769	926.395379	975.403266	886	1140.59789	1122.12978	959.887254	877.900697	1154.29545
FTN_1770	13.9622514	49.5321971	68	80.9610196	19.1000814	270.127564	129.214821	64.7818876
FTN_1771	656.225815	972.545639	882	1092.18003	989.384216	972.62912	917.171868	1169.01861
FTN_1772	1296.39504	1946.04382	1586	2003.38837	1800.18267	1894.29078	1558.17873	2000.38617
FTN_1773	345.565722	519.135527	474	472.272614	514.747193	498.631697	544.095742	429.916163
FTN_1774	411.886416	559.142302	671	782.62319	598.787551	550.44862	667.60991	878.481658
FTN_1775	427.244892	641.060935	524	512.753124	544.352319	604.813916	601.102281	523.16282
FTN_1776	20.2452645	94.3016829	121	46.8303937	55.390236	375.460324	182.420924	25.5201375
FTN_1777	2.09433771	36.1966056	33	38.8930388	4.77502035	249.740578	100.078146	34.3540313
FTN_1778	2.09433771	50.4847393	64	46.0366582	6.68502848	434.072909	134.282069	54.9664501
FTN_1779	76.7923826	167.647436	153	185.734104	182.405777	292.213465	226.759343	176.677875
FTN_1782	2503.43167	3630.13852	2426	2929.67768	360.036534	2595.94287	1489.13747	2952.48361